Copyrighted Materials
Copyright © 2008 AIAA Retrieved from www.knovel.com

Nuclear Space Power and Propulsion Systems

Edited by
Claudio Bruno
University of Rome "La Sapienza"
Rome, Italy

Volume 225
PROGRESS IN
ASTRONAUTICS AND AERONAUTICS

Frank K. Lu, Editor-in-Chief
University of Texas at Arlington
Arlington, Texas

Published by the
American Institute of Aeronautics and Astronautics, Inc.
1801 Alexander Bell Drive, Reston, Virginia 20191-4344

American Institute of Aeronautics and Astronautics, Inc., Reston, Virginia

1 2 3 4 5

Copyright © 2008 by the American Institute of Aeronautics and Astronautics, Inc. Printed in the United States of America. All other rights are reserved by the copyright owner. Reproduction or translation of any part of this work beyond that permitted by Sections 107 and 108 of the U.S. Copyright Law without the permission of the copyright owner is unlawful. The code following this statement indicates the copyright owner's consent that copies of articles in this volume may be made for personal or internal use, on condition that the copier pay the per-copy fee ($2.50) plus the per-page fee ($0.50) through the Copyright Clearance Center. Inc., 222 Rosewood Drive, Danvers, Massachusetts 01923. This consent does not extend to other kinds of copying, for which permission requests should be addressed to the publisher. Users should employ the following code when reporting copying from the volume to the Copyright Clearence Center:

978-1-56347-951-9/08 $2.50 + .50

Data and information appearing in this book are for informational purposes only. AIAA is not responsible for any injury or damage resulting from use or reliance, nor does AIAA warrant that use or reliance will be free from privately owned rights.

ISBN 978-1-56347-951-9

Copyrighted Materials
Copyright © 2008 AIAA Retrieved from www.knovel.com

Preface

This book includes all contributions and some addenda to the Final Report of Study 3.2 to the International Academy of Astronautics on the perspectives of nuclear energy for application to space power generation and propulsion. The structure of the book is as follows:

Chapter 1 contains fundamental physics of nuclear energy, and sets the stage for its applications in space propulsion and for power generation, including ground power. The two main classes of space propulsion systems that may take advantage of nuclear energy (thermal and electric rockets) are briefly introduced. Chapter 2 discusses the class of nuclear *thermal* rockets (NTR), where energy is transferred directly to a propellant, similarly to what occurs in chemical rockets.

Chapters 3 and 4 deal with the other classes of systems, where thrust is produced by converting nuclear into electric power. Chapter 3 illustrates current and projected capability of nuclear-powered *electrostatic* thrusters; i.e., those based on the Coulomb force accelerating a plasma (ion thrusters, in particular gridded ion engines). Electrodynamic thrusters, those using the Lorentz force to accelerate plasma with a self-created or applied magnetic field, and arcjets, are discussed in Chapter 4.

Chapter 5 focuses on the architecture of nuclear reactors for in-space electric propulsion and for ground power generation, for instance on the surface of the moon or Mars. Chapter 6 discusses legal aspects of devices based on nuclear power and operated in space. The appendices are dedicated to the issue of radiation hazards, including a primer on fundamentals of fission-driven radiation and doses, and the official United Nations account of the Chernobyl accident.

Radioactive thermionic generators (RTG) are not included in this book. (In fact, they are the subject of an excellent paper by G.L. Bennett, AIAA Paper 2006-4191, presented in June 2006 at the International Energy Conversion Engineering Conference.) They have been, and still are, extensively used whenever solar panels were impractical; they are relatively well known, and therefore mostly representative of current rather than future technology. Besides, their power output is generally orders of magnitude lower than needed for the practical (fast) interplanetary missions of interest to this book.

Pulsed nuclear propulsion, i.e., propulsion by miniature nuclear explosions, recently revived and currently simulated by means of plasma zeta-pinch devices, is summarized in Chapter 2 but not discussed in detail. Its origin, the Orion Project (and Project Daedalus) has been the subject of recent literature, as is its resurrection in the form of the Magnetic Orion (MagOrion) and the more recent Mini-MagOrion concepts.

The authors of this book regret the lack of contributions from the former USSR. Substantive information (in Russian) on NTR finally became available through the good will and efforts of Russian colleagues only at the time of this writing, and

in the interest of time it was decided to set it aside, waiting for a more propitious opportunity to make it known in an English translation.

In closing, I want to acknowledge Rodger Williams, at AIAA, with whom, at the 2006 World Space Congress, I discussed the possibility of publishing the IAA Final Report as an AIAA book, for believing in this project, and for key input during the editing process; Heather Brennan, at AIAA, for her constant help and many practical suggestions; Nick Barber, at Techset Composition Ltd., for his patience; and lastly, G. De Flora, for her dedication, time, and patience in assemblying the IAA Final Report on which this volume is based, and making sure it was as intended.

Claudio Bruno
July 2008

Copyrighted Materials
Copyright © 2008 AIAA Retrieved from www.knovel.com

Table of Contents

Preface . . . . . **xiii**
Acronyms and Abbreviations . . . . . **xv**
Nomenclature . . . . . **xix**

Chapter 1. Nuclear Propulsion—An Introduction **1**
Claudio Bruno, *University of Rome "La Sapienza," Rome, Italy*

Introduction 1
Fundamental Physics 2
Conclusions 27
References 28

Chapter 2. Nuclear-Thermal-Rocket Propulsion Systems **31**
Timothy J. Lawrence, *U.S. Air Force Academy, Colorado Springs, Colorado*

Introduction 31
System Configuration and Operation 34
Nuclear-Thermal-Rocket Concepts 37
MagOrion and Mini-MagOrion 45
Safety 47
Conclusions 49
References 50

Chapter 3. Application of Ion Thrusters to High-Thrust, High-Specific-Impulse Nuclear Electric Missions **53**
D. G. Fearn, *EP Solutions, Hampshire, England, United Kingdom*

Introduction 53
Background 55
Gridded Ion Engines—Current Devices 69
Scaling Process 93
High-SI, High-Power Operation 101
Conclusions 115
References 118

Chapter 4. High-Power and High-Thrust-Density Electric Propulsion for In-Space Transportation 127
Monika Auweter-Kurtz and Helmut Kurtz, *University of Stuttgart, Stuttgart, Germany*

Introduction 127
Thermal Arcjets 128
Magnetoplasmadynamic Thruster 138
High-Power Hybrid ATTILA Thruster 168
Conclusions 170
References 171

Chapter 5. Review of Reactor Configurations for Space Nuclear Electric Propulsion and Surface Power Considerations 177
Roger X. Lenard, *GPS Solutions, Inc., Carson City, Nevada*

Introduction 177
Reactor Requirements 178
Reactor and Power Conversion—Mass Comparison 180
Reactor Operation Startup 200
Conclusions 202
Reference 202

Chapter 6. Nuclear Safety: Legal Aspects and Policy Recommendations 203
Roger X. Lenard, *Little Prairie Services, Edgewood, New Mexico*

Finding 1: Space Nuclear Power and Energy Have Important Historic and Pivotal Future Roles in Space Exploration 203
Finding 2: To Implement Space Nuclear Power and Propulsion It Must Be Perceived to be Safe by the General Population 205
Finding 3: Existing Policies and Procedures are Adequate for Achieving Requirements of Public Safety and Environmental Compliance 206
Finding 4: The Existing Processes for Design, Fabrication, and Test, Including Safety Analysis are Adequate for Pre-Launch Safety and Environmental Compliance 213
Finding 5: The Safety and Operations Phase for NEP or NTP Systems Should Be Developed so as to Maximize Possible Scenarios for Space Nuclear Reactor Employment 217
Finding 6: Safety Assessment for Additional Risks Posed by Lunar and Mars Base Mission Scenarios Indicates That Space Reactor Systems Can Be Used Safely and Effectively on the Surfaces of Other Celestial Bodies 221
Finding 7: Definable Surface Nuclear Power System Hazards Can Be Defined and Associated Risks Can Be Mitigated 223
Finding 8: There Appears to Be No Reason That a Space Nuclear Reactor Power System Cannot Be Safely Deployed and Operated on the Surface of Another World While Maintaining Standards of Planetary Protection 226

Finding 9: A Space Reactor System Enables Effective Design Options in Mitigating Potential Radiation Releases 227
Finding 10: A Transparent and Systematically Traceable Space-System Safety Test and Analysis Program Must Be Conducted to Ensure Crew and Public Safety 227
Finding 11: Prior Space Reactor Programs Expended Resources on Destructive Disassembly Testing for Low-Probability Incidents—System-Level Testing Should Be Reserved for More Likely Scenarios 231
Finding 12: An Integrated Approach for Performance and Safety Analysis and Testing Is Critical to a Cost-Effective Development Program 237
Finding 13: The Ultimate Objective of All Programmatic Activities Is to Obtain Launch Approval for the Space Reactor System—the Program Should Be Structured to Attain the Goal 239
Conclusions 241
References 242

Appendix A. Radioactivity, Doses, and Risks in Nuclear Propulsion 245
Alessio Del Rossi, *Technip Italy, Cinisello Balsamo, Italy*; and Claudio Bruno, *University of Rome "La Sapienza," Rome, Italy*

Introduction 245
Radioactivity 245
Radiation, Dose, and Their Units 247
Effects of Ionizing Radiation 251
Sources of Radiation Exposure 256
Conclusions 266
References 267

Appendix B. The Chernobyl Accident—A Detailed Account 269
Alessio Del Rossi, *Technip Italy, Cinisello Balsamo, Italy*; and Claudio Bruno, *University of Rome "La Sapienza," Rome, Italy*

Introduction 269
Reactor Design 269
Chernobyl Events 270
Consequences 273
Conclusions 273
References 274

Index 275

Supporting Materials 283

Copyrighted Materials
Copyright © 2008 AIAA Retrieved from www.knovel.com

Chapter 1

Nuclear Propulsion—An Introduction

Claudio Bruno*
University of Rome "La Sapienza," Rome, Italy

I. Introduction

THE very idea of using nuclear energy for propulsion goes back to R. Goddard, who mused in 1906–1907 about using radium as an energy source and realized, correctly, its emitted power was insufficient. In a conference he held in France in 1912 [1], Esnault-Pelterie concluded that nuclear energy was indispensable for space travel. Therefore, using nuclear energy for propulsion is nothing new, going back a century ago, and a number of books and articles have been written on this subject, e.g., [2–4]. Here the purpose is to illustrate the features of nuclear propulsion (NP) from the viewpoint of basic physics. In fact, having been revived by NASA's Jupiter Icy Moons Orbiter (JIMO) mission, technological as well as societal issues associated with NP are again being discussed, e.g., see [5, 6], and it is useful to review its fundamental principles. References dealing with the history of NP in the United States and in the Soviet Union can be found in [7], dealing with nuclear thermal propulsion. A still conceptual form of NP, fusion propulsion, is dealt with in [8, 9]. Radiation and its biological effects are discussed in [10]. A concise review of fission reactors technology is in Chapter 2 by Lawrence, 2007 and again in Chapter 5 by Lenard. The physics of *pulsed* nuclear propulsion, for example, propulsion by means of nuclear explosions [11–14], is also briefly mentioned here.

Most of the following ideas or concepts were clear to researchers working at Los Alamos Science Laboratories (LASL), Aerojet, Westinghouse, and the Kurchatov Institute in the 1960s. This is not necessarily so for the majority of today's propulsion scientists and engineers. Besides, misconceptions (and fears) still exist that might cloud understanding NP.

The second goal of this chapter is to explain why NP is physically inevitable if we want to explore our solar system and, perhaps, beyond.

The material presented in this chapter is updated from the paper published in Space Technology, Vol. 27, No. 1, 2007, pp. 3–21, and is reproduced with permission. Copyright © 2008 by the American Institute of Aeronautics and Astronautics, Inc. All rights reserved.

*Professor, School of Aerospace Engineering.

II. Fundamental Physics

A. Forces

There are only three forces in nature according to the standard model of physics [15]. This might change in the years to come, for example, if the nature of dark energy, or vacuum energy, fluctuations is understood. The three forces are *gravitation*, the so-called *electroweak* force (unified from electrodynamic and weak by the work done with particle accelerators since the 1960s), and the *nuclear force* binding nucleons and holding the nucleus together.

Gravitation is well known for its macroscopic effects, much less at the fundamental level [16, 17]. Of the two remaining forces, the electroweak is responsible for Coulomb attraction and repulsion among statically charged bodies, and thus for stable structures composed of electrons and nuclei (the atoms), and therefore for the existence of bonds among atoms and molecules. Electroweak force is also responsible for the Lorentz force when charges move in a magnetic field. The third force is the nuclear, or "strong," force. It acts at distances of the order of the nucleons' size, 10^{-14} m, or 1 fm, pulling together neutrons and protons and allowing nuclei to exist. This force is the strongest known force. Quantum mechanics has been very effective in clarifying the nature of the last two forces, but cannot "explain" gravitation.

A force field, in the modern sense, is the result of the exchange of mediating particles [15] (the action at a distance postulated by Newton is not part of modern physics) and is always associated with potential energy. It is this potential energy that, released and converted into kinetic energy, can eventually produce the effect we call *thrust*.

The physics assumed in what follows is based on Newton's Third Law (every action has an equal but opposite reaction) and on relativity. Both were and are still tested by physicists, but their validity will not be discussed or challenged here.

B. Potential Energy

The Theory of Special Relativity [18, 19] shows that formulating velocity (and momentum) as a four-component vector rather than via the usual three components results in the invariance of the square of its magnitude. The fourth component added by relativity theory is $c\,\mathrm{d}t/\mathrm{d}s$, where c is the speed of light and $\mathrm{d}s$ is the distance between two events [2]. This distance generalizes the concept of classical distance between two points in space by including also the effect of "motion" in time. The new resulting space-time is called Minkowski's space. In this space there is no privileged frame of reference; and the laws of physics, including the Maxwell equations of electromagnetism that are *not* invariant in this space for classical Galilean transformations (that is, for $x = x' + Vt'$, with V the *constant* relative velocity between the two frames of reference $x'y'z't'$ and $xyzt$), become invariant for the Lorentz transformations, where, for instance,

$$x = \frac{(x' + Vt)}{\sqrt{(1 - V^2/c^2)}}$$

and similarly for y and z, and where

$$t = \frac{[t' + V(x'/c^2)]}{\sqrt{(1-V^2/c^2)}}$$

Because the momentum $\boldsymbol{p} = m_0\, V/\sqrt{(1 - V^2/c^2)}$, with $\boldsymbol{V}$ now a four-component vector, and energy $E = |\boldsymbol{p}|c$, the total energy of a *rest* mass m_0 ("at rest" means with zero velocity in the frame of reference used) becomes

$$\text{Total energy} = \frac{m_0 c^2}{\sqrt{\left(1-V^2/c^2\right)}} \tag{1}$$

For a mass at rest, $V = 0$, and Eq. (1) states then that its total energy m_0c^2 is only *potential energy*, a famous result implying equivalence between mass and energy to a factor c^2. If V/c is nonzero, but still $\ll 1$, Taylor expansion of Eq. (1) yields

$$\text{Total energy} = m_0c^2 + \tfrac{1}{2}\, m_0V^2 + \cdots$$

showing that at $V \ll c$ energy can be separated into potential energy and kinetic energy. More generally, for *any* V/c, the Theory of Special Relativity states that total energy can be written as the sum of potential and kinetic energy (KE) as

$$\text{Total energy} = mc^2 + \text{KE} \tag{1a}$$

where, until 1948, Einstein called m the relativistic mass, that is, the *rest* mass m_o divided by $\sqrt{1-(V/c)^2}$ and c is the speed of light, about 3×10^8 m/s. In Newtonian mechanics mass and energy are separate quantities, each independently "conserved" in any isolated system; in Einstein mechanics they are interchangeable, with c being simply a constant. What is conserved is the total energy: if kinetic energy increases, it must be at the expense of potential. Because c^2 is "large" on the human scale, the energy *potentially* available is also "large" *if* it can be tapped. Equation (1a) states the *potential* energy available, just as thermodynamics does in classical chemistry. What *fraction* α of this energy can be actually extracted and converted in KE of various sorts will depend on the specific physical steps of conversion.

Rest mass and relativistic mass coincide for $V \ll c$, a condition invariably met in chemical propulsion. However, electric thrusters can accelerate propellant to exhaust $V = V_e$ far larger than chemical rockets. Future I_{sp} of order 10^5 s (e.g., see Chapter 3) correspond to V/c of order 1%. A self-consistent description of relativistic gasdynamics, as well as that of continuum mechanics, is still not available: "interpretations" are a source of lively discussions, but see [21]. For this and other reasons, only mass will be specified as either "rest" or "relativistic" in what follows.

The actual potential energy of a mass m of reactant(s), of any type (chemical, fissile, fusible,...) that can be converted in KE is therefore the fraction α mc^2:

$$\text{Reactant(s) potential energy} = \alpha\, mc^2 \tag{2}$$

where the type of conversion determines the actual value of α and thus the energy available per unit reactant(s) mass.

Through a sequence of steps, potential energy in Eq. (2) becomes microscopic kinetic energy of products (e.g., chemical species, photons, nuclides, neutrons, . . .). This kinetic energy might be the result of several distinct conversion steps (for instance, thermal to electric), or even a single step, such as thermodynamic expansion in a duct shaped by solid or magnetic boundaries. Whatever the conversion path taken, to produce thrust based on the Third Principle the end result must be an orderly motion of particles, ejected at exhaust speed V_e ($\equiv V$). At some stage during this chain of steps, "inert" (nonreacting) mass Mp can be added or can be present. One very good reason is to moderate temperature, but just as important for certain applications is to increase momentum of the total mass ejected and thus propulsion thrust.

How much mass converts into energy? The answer depends on the kind of potential energy tapped and thus on the particular force and its α.

Gravitational energy (according to Newtonian theory, not general relativity) is associated, for instance, with the force $\boldsymbol{F} = Gm_1m_2\,\boldsymbol{r}/r^3$ between two masses at distance r. Mutual attraction force can perform work, and so the potential energy E can be obtained from $\nabla E = -\boldsymbol{F}$, that is, $E = Gm_1m_2/r$. If masses were point-like, the energy would tend to ∞ when $\boldsymbol{r \to 0}$. **In fact the** constant $G = 6.67 \times 10^{-11}$ m^3 kg^{-1} s^{-2}, so that per pair of unit masses at unit distance the gravitational energy is exactly G, a very small number. (This specific energy is about 10^{-18} that released by combustion of 1 kg of H_2 with O_2.) The gravitational potential is detectable only when the product $m_1\,m_2$ is large enough to compensate for the very small ratio G/r. Typically, this is the case when massive bodies (stars and planets) are involved, e.g., near Earth, its mass being of order 10^{24} kg.

Instead of force between two masses carried onboard, spacecraft have used very successfully the gravitational potential associated with celestial bodies in gravity-assist maneuvers (planet swing-bys): multiple swing-bys in the solar system can achieve ΔV of order 20–35 km/s, with a corresponding decrease of the potential energy of the body-spacecraft system.

In general relativity, gravitation is caused by curvature of space-time. Accordingly, "warping" space-time would produce substantial, although speculative, propulsion effects.

The mass change Δm in converting completely gravitational potential into some other visible form of energy (that is, KE) is found by imposing

$$E = \frac{Gm_1m_2}{r} = \Delta mc^2$$

Hence $\alpha = \Delta m/m_1$, per unit m_2 and distance, is of order $G/c^2 \sim 10^{-27}$, an exceedingly small fraction. This too shows that trying to exploit onboard gravitation is impractical as a means of energy generation and propulsion.

The *electroweak force* potential drives nearly all aerospace propulsion systems. It is associated with the Coulomb force $F = k\,q_1q_2/r^2$ between two static electric charges q_1 and q_2 and with the Lorentz force when a charge moves in a magnetic field. In the International System of Units, the constant $k = 8.98 \times 10^9$ C^{-2}m^{-2}, much larger than G. The potential is in this case $k\,q_1q_2/r$. The constant k is the force, in newtons, between two point-like unit charges set at 1-m distance. The Coulomb

force is responsible for the existence of atoms and molecules, so that rearranging their electronic structures (in chemistry this is called *reacting*) can release energy because bonds (forces) and potentials change. Macroscopically, this potential is known as *chemical* potential: in propulsion applications its change corresponds to the heat (microscopic KE) released or absorbed. When in a chemical reaction the chemical potential decreases, temperature and pressure typically rise. Chemical rockets use this type of energy inside a combustion chamber.

The fraction α of the mass converted into energy by chemical reactions is much larger than in gravitation, but still very small. Its value depends on the specific reaction, but it can be approximately gauged from estimating the $\Delta m/m$ in forming an H atom from $p^+ + e^-$ (a proton and an electron, with $r \sim 10^{-10}$ m, $m_H \sim 1.6 \times 10^{-27}$ kg, $q_1 = q_2 = 1.6 \times 10^{-19}$ C) by writing

$$\Delta m/m = E\, c^2/m_H$$

That predicts $\alpha \sim 10^{-8}$. In fact bonds *among atoms* are weaker than between the electron and the proton of a H atom, and in fact reaction (combustion) between H_2 and O_2 has α of the order of 1.5×10^{-10}. The Coulomb force is strong on a human scale, as suggested by the value of the constant k but also confirmed by electrostatics experiments. Its potential is limited by the charge of the electron, "only" 1.6×10^{-19} C. Atoms contain Z electrons (Z = atomic number), but their potential energy is the sum of attraction and repulsion among *all* electrons and *all* nuclei, including those of nearby (colliding) atoms. Whatever the atom, its atomic number Z is less than 100, so that potential energy would be, at most, 10^2 that associated to a single positive and negative charge pair interacting at collision distance.

Because of the importance of electrons at the dawn of modern physics, particle energy is measured in electron volts. An *electron* of energy = 1 eV (1.602×10^{-19} J) has KE corresponding to ~11,300 K. A hydrogen *atom* of 1-eV energy has velocity lower by the ratio $\sqrt{m_p/m_e}$, where the p and e subscripts stand for proton and electron. In chemical reactions even such temperature is unusual: energy or potentials associated with electroweak forces are $<\mathcal{O}(1)$ eV. Only ionization reactions in plasmas can reach higher energies: for instance, ionizing hydrogen needs 13.8 eV.

Thus, electroweak forces have practical potential at most of order $\mathcal{O}(10)$ eV. Equation (2) quantifies the percentage mass change in chemical reactions, $\sim 10^{-10}$. For this and also for historical reasons, it is very inconvenient to use Eq. (2) in thermochemistry, that is, keeping track of energies by means of the mass change ("mass defect," if energy is being released). It is far more practical to follow the evolution of the sum of all *microscopic* KE of particles (i.e., translational, rotational, vibrational, electronic, . . .). Macroscopically, this sum becomes the more familiar formation enthalpy. This is what actually one does when using standard thermodynamics, unaware that *total* mass also changes, although very slightly. In thermodynamics what is being converted is mostly KE, for instance, microscopic into macroscopic. The *total* mass in standard thermodynamics stays constant ("mass is conserved").

In fact, Eq. (1a) says this is not so: in exothermic chemical reactions mass decreases. In fact, it is the slight mass "defect" in rocket combustion (of order 10^{-10} per unit mass of propellants) that, converted into microscopic energy, heats the combustion products and is responsible for thrust.

Chemical propulsion is very effective to produce thrust in a relatively simple way. In fact, combustion dates back to the Paleolithic period. The main drawback of chemical propulsion is its "low" I_{sp}. In fact, aside from its units, I_{sp} is equal to the exhaust velocity V_e of an ideal expansion, defined here as isentropic, one-dimensional, and reaching zero pressure. The exhaust velocity is limited because it cannot be much different from that reached by molecules and atoms in their random motion inside the combustion chamber. Inside the chamber the heat release forms molecules possessing large translational, rotational, and vibrational energy (all of them internal energy E), and very little bulk (flow) velocity V. When the hot products expand in the nozzle, collisions force all molecules to reach statistically the same orderly flow velocity V_e at the exit at the expense of internal energy, that is, $\Delta E = (1/2)\, mV_e^2$; hence, $V_e = (2\ \Delta E/m)^{1/2}$ if one ignores relativistic effects. The ratio E/m is the energy density J, so that $V_e = (2\ \mathrm{J})^{1/2}$. And because $\Delta E = \Delta m\, c^2$,

$$V_e = c(2\ \alpha)^{1/2} \tag{3}$$

Equation (3) says that chemical I_{sp} is intrinsically limited by the low α (or J) of the electroweak force. An α of order 10^{-10} means J of order 10^7 Joule/kg, or V_e of order $\mathcal{O}(10^3)$ m/s, too small to ensure "low" mass consumption, as shown by Tsiolkovski's law. Indeed, it is much too small to enable *practical* interplanetary missions, that is, within reasonable times and spacecraft mass. Here a "reasonable" time is purposely defined for human missions as approximately one year (to prevent unwanted physiological effects caused by microgravity and radiation), and three to four years for probes: longer unmanned missions tend to lose public attention and financial support, sometimes even in their proposal phase. In terms of mass, reasonable depends on the specific mission, a reasonable cap being linked to total cost, a fraction of order, say, 0.1% of the GNP. An α of order 10^{-10} is in fact too small to enable reaching LEO for less than $\mathcal{O}(10^3$–$10^4)$ \$/kg of payload. Research on high-energy-density-matter (HEDM) propellants, such as N_8, metallic H, metastable helium, mixtures of nanoparticles, or even less exotic molecules [22, 23], might well increase the energy available per unit mass, perhaps by a factor of order 10 [24, 25]; however, α will rise only to 10^{-9}, and V_e or I_{sp} will increase only by a factor 3.

The third force potential, or *nuclear potential*, is associated with the "strong" nuclear force acting among nucleons. It is this force that binds them together and prevents the nucleus from disintegrating spontaneously as a result of Coulomb repulsion among protons. Coulomb repulsion is long range, whereas the nuclear force is very short range: its intensity is about 10^2 that of Coulomb, but only when internucleon distance is of order 1 nucleon size, or 1 fm.

This force plays the same role as the chemical bond in thermochemistry, but at the scale of nuclei instead of that of atoms and molecules.

The curve of binding energy (Fig. 1) shows the energy, in mega electron volts, associated with this force and *averaged* over the A nucleons of each nucleus (each A). In fact, nucleons are bound to other nucleons each with a slightly different energy depending on A, just as electrons to the nucleus of an atom. Note that the binding energy is of order mega electron volts, not electron volts: it is an easy guess that the potential energy available in nuclear transformations will be about 10^6 larger than the electroweak (chemical) potential.

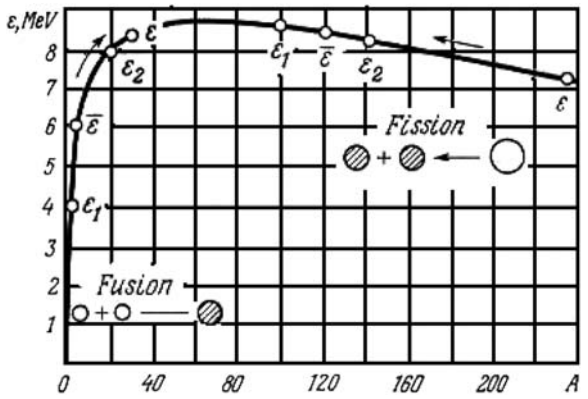


Fig. 1 Average binding energy per nucleon, MeV, as a function of the mass number A (from [26]).

The binding energy is actually the negative of the potential energy associated with the nuclear force. The larger the binding energy, the deeper the potential well. In this respect, its maximum near $A = 60$ means that near A the energy well of those nuclei is the deepest, and the binding force strongest. Before World War II this fact suggested to O. Hahn, L. Meitner, and others the possibility of extracting energy from nuclear reactions. The particular shape of the binding curve can be intuitively justified: on the left A is low, and the few nucleons imply binding energy is also low; on the right A is large: Coulomb repulsion grows with A, weakening the nuclear force. The maximum lies in between.

The binding energy, with its sign changed, plays the same role as the formation enthalpy for chemical species. If nuclei with high A (to the right of the energy peak) are broken up into several lower-A nuclei, for instance, by collisions with neutrons (*fission*), the resulting lower-A nuclei "go deeper" into the well, and the energy difference is released. For example, breaking a hypothetical $A = 240$ nucleus, composed of 240 nucleons, each with average energy 7.5 MeV, into four nuclei ("fragments") with $A = 60$, each containing 60 nucleons of average 8.5-MeV energy, releases $(240 \times 7.5 - 4 \times 60 \times 8.5) = -240$ MeV, all of this energy from a *single* nucleus.

Likewise, low-A nuclei (to the left of the energy peak) might be forced to collide, forming a higher-A nucleus (*fusion*). Note that in this case the energy change could be much larger than in fission: for instance, the binding energy of $A = 1$ (hydrogen) is much lower than that at $A = 4$ (helium), so that the net energy release per nucleon is larger. Thus in both fission and fusion the end result is a stronger binding force per nucleon.

In nuclear reactions, the original nucleus(i) plus other particles, such as neutrons, are the "reactants." The total mass of the "products" formed (lighter or heavier nuclei, plus energetic particles) can decrease or increase. If mass decreases, as stated by Eq. (1a), energy is released.

Examples of nuclear reactions are ^{235}U or ^{239}Pu reacting with neutrons and splitting into *smaller A* fragments (*fission*) and four H ions colliding and forming

He, a *higher A* element (*fusion*). Fusion processes inside stars drive the photon flux that, once captured, can power electric thrusters: solar power is the kinetic energy of products of stellar nuclear reactions. A primer on fissionable fuels is in [27].

Besides fission and fusion, a third form of nuclear energy is available from nuclei of certain isotopes. They have the same atomic and mass numbers of common nuclei, that is, the same number of electrons, protons, and neutrons, but the *spatial* arrangement of nucleons inside their nucleus is different, and so is their potential energy. (It is higher.) When these nuclei relax to their minimum energy configuration, either naturally or artificially by appropriate energy stimulation, potential energy is converted into kinetic, typically that of photons (x and gamma rays). Because no nucleons are emitted, the α of this process is lower than in fission, of order 10^{-7}. (For instance, in the case of the $^{180\,m}$Ta isotope, $\alpha = 2 \times 10^{-7}$.) Natural isotopes with this peculiarity are called *nuclear isomers*, by analogy with chemical isomers, and a *m* suffix is then attached to their mass number *A*. If more than one isomer exists, it is indicated by *m*1, *m*2,... and so on, in increasing energy order. For instance, Hf has two isomers, ^{177m1}Hf and ^{177m2}Hf. The energy available from these isomers is about 10^3 larger that of chemical reactions and about 10^3 smaller than that of fission.

Metastable nuclei can be produced by nuclear processes because most of the time they are formed in an excited state and then decay emitting beta particles (that is, electrons), gammas, or x rays. Such decay time is typically ~10^{-12} s. However, exceptionally, the decay process is slow and forms a nucleus with spin different from that of the nucleus in its ground state. This situation "hinders" gamma emission, and the nucleus might remain for a long time in its excited state, sometimes indefinitely. For instance, $^{180\,m}$Ta is an isomer that is naturally present in tantalum in a 1:8300 ratio. Theoretical considerations indicate its half-life is ~10^{15} years. When this Ta isomer is made to de-excite to ^{180}Ta, it does so by emitting a 75-keV photon. This allegedly occurs when irradiated with low-energy (~10 KeV) x rays similar to those used for dental examinations [28, 29]. In this case the energy budget is positive, hinting at possible applications as a particular HEDM, although the cost, because of scarcity, is extraordinarily high (17 M$/g) [25, 30]. A more realistic HEDM is the ^{178m2}Hf isomer, well known also because of its peculiarities: it was discovered by chance, it has a 31-year half-life and de-excites fast (instantaneous power is in the 10^{18} W range) by emitting 2.45-MeV gammas only [31]. It has been calculated that 1 g of this isomer can release 1.3 GJ. The U.S. Air Force has explored applications of this isomer for powering high-altitude reconnaissance aircraft that can stay aloft for weeks [32]. Because this isomer can be produced in nuclear reactors, it is being considered as a practical *nuclear* HEDM.

The ultimate form of nuclear energy release occurs when matter and antimatter, for instance, a proton and an antiproton, are "fused." This is actually called *annihilation*; both masses disappear, becoming energy according to Einstein's law, and $\alpha = 1$.

Once α is known, the product αc^2 is the energy/unit mass, or energy density *J*. Table 1 reports α and *J* of the energy conversion processes. Data on fission are for ^{235}U. Among many, fusion data are for reaction between deuterium (D) and tritium (T), both hydrogen isotopes containing one and two neutrons, respectively.

Table 1 Forces, conversion fractions, and energy densities

Type of force	Potential	Alpha	Energy density *J*, J/kg
Gravity	Gravitational	10^{-27}	10^{-11}[a]
Electroweak	Chemical (H_2/O_2 combustion)	1.5×10^{-10}	1.35×10^{7}
Strong force	Nuclear		
	Fission (^{235}U)	9.1×10^{-4}	8.2×10^{13}
	Fusion (D-T)	3.75×10^{-3}	3.4×10^{14}
	Metastable (^{180m}Ta)	2×10^{-7}	1.8×10^{10}
	Annihilation (p^+-p^-)	1.0	9×10^{16}

[a]Per pair of 1-kg masses at 1-m distance.

No nuclear process can produce α between $\sim 4 \times 10^{-3}$ and the theoretical 1.00 of annihilation: nuclear reactions transform mass into energy with α "limited" to a few tenths of a percent. The reason is also the limited average binding energy. Mass converts into energy when new bonds among nucleons are stronger than the old ones. Because the average bond strength per nucleon cannot be more than ~8 MeV, from Eq. (1a) α cannot be greater than $\sim 4 \times 10^{-3}$. Higher α would be possible only if binding energy *differences* among nuclei were higher than those in Fig. 1, and that is not the case in the universe we know.

Note that no nucleon is annihilated in fission/fusion reactions. Annihilation is routinely observed in particle accelerators, has been and is still investigated as an energy source, but unfortunately remains for the time being a conceptual means of propulsion.

Comparing energies in Table 1 shows that that associated with the nuclear potential via fission or fusion is about 10^6 to 10^7 times larger than chemical. The *J* from metastable nuclear isomers is smaller, but still of order 10^3 larger than chemical. Time will tell whether they can become the energy source for viable new propulsion systems.

Thus, at our stage of knowledge, besides being the only physical alternative to chemical, nuclear energy is the only means of altering the perspectives of future propulsion in the practical sense mentioned.

This statement is not meant to imply NP is the panacea propulsion solution; other propulsion concepts have been recently proposed based on sound physics, such as solar or magnetic sails, electromagnetic mass drivers, and others. However, all of these new developments suffer at present from severe limitations in thrust available or power required, so that their range of applications is likewise limited. In terms of availability, prior expertise and know-how, and overall performance, NP is a most attractive option for a broader class of interplanetary missions, including those with a human crew. It is because of this, and other, reasons that NP is among technologies given higher priority by the European Union (EU) space industry [33].

C. Propulsion

In the standard model, where gravitational mass equals inertial mass, Newton's Third Law is the only way to produce propulsive force (but some mistakenly claim

the electroweak Lorentz force capable of accelerating plasma in applied-magnetic field thrusters does not "obey" this law). Thus, relative to a frame of reference fixed to the propulsion system, something must be accelerated in the direction opposite to that of motion.

That something must possess momentum, if not mass. Chemical rockets eject matter accelerated by chemical heat release, and collimated by the solid walls of a nozzle, but propulsion by change of momentum of massless particles is also conceivable (see Sec. II.E). The difference in momenta "before and after" the acceleration is the engineers' thrust F.

1. Specific Impulse

The process changing potential energy to exhaust jet energy (also called thrust energy) can be divided into three stages.

The first stage is the conversion of potential energy into KE of particles. This is microscopic energy; in chemical rockets it corresponds to the creation of translation, vibration, rotation, and electronically excited species. In nuclear rockets this stage forms nuclear products such as fission fragments, or fused particles, nucleons, and photons (radiation). Energies vary from 160–170 MeV in the case of fission fragments (FF), to 5–15 MeV for nucleons and photons (gamma rays, mostly), and $\mathcal{O}(1)$ MeV for fused alpha particles.

In the second stage the nonequilibrium microscopic KE is redistributed via collisions among particles, tending towards statistical equilibrium. In chemical rockets this stage corresponds to an increase of rototranslational energy at the expense of the much higher electronic and vibrational excitation. In nuclear thermal (NTR) or NEP rockets this stage corresponds to the energy exchange between microscopic KE of products (neutrons, FF, fused particles, and photons) and a medium where they are made to thermalize. This medium can be fuel rods, gaseous or liquid propellants, a working fluid, or products of the nuclear reaction(s) themselves.

Finally, in the third stage the thermally equilibrated medium, with high energy density, is exploited in some way to produce thrust. This stage can take different forms, according to the specific propulsion concept chosen.

Whatever the potential energy tapped, most of the energy is conserved while going through each stage (some can be lost by radiation). Propulsion concepts differentiate only at the third stage, when deciding what to do with the microscopic kinetic energy acquired by the medium.

In this context, the main question is what is the ideal velocity V (or I_{sp}) of products after the potential energy αmc^2 has been thermalized. In general, the answer requires a relativistic energy balance. A truly rigorous balance should include the contribution of massless particles (photons and neutrinos) to the KE of products. A little simplified, here KE will include only mass contributions. Assuming no losses, the energy balance imposes the sum of potential and KE be conserved going from reactants (at $V = 0$) to products, eventually exhausted at velocity $V_e = V$:

$$m_0c^2 = (1-\alpha)m_0c^2 + \frac{1}{2}\frac{m_0(1-\alpha)V^2}{\sqrt{1-V^2/c^2}} + \frac{1}{2}\frac{Mp_0V^2}{\sqrt{1-V^2/c^2}} \tag{4}$$

where m_0 and Mp_0 are the *rest* masses of reactant and of inert propellant possibly added, respectively. On the left-hand side (LHS) energy is only potential energy: the reactant is still. Rearranging this equation, a preliminary result is

$$\frac{4\alpha^2}{(1-\alpha)^2\left[1+Mp_0/m_0(1-\alpha)\right]^2} = \frac{V^4/c^4}{1-V^2/c^2} \tag{5}$$

showing that in the limit $\alpha \to 1$ (that is, if all reactants are converted into energy, as in matter-antimatter annihilation), and when no inert mass Mp is added, the exhaust velocity V tends to the speed of light c. If inert mass is present or added, the limit velocity is less than c, as shown by the complete solution

$$\frac{V^2}{c^2} = \frac{2}{\sqrt{1+2/A}+1} \tag{6}$$

with

$$A \equiv \frac{2\alpha^2}{(1-\alpha)^2\left[1+Mp_0/m_0(1-\alpha)\right]^2} \tag{7}$$

The ratio $Mp/[m(1-\alpha)]$ might be interpreted as the dilution ratio of products; in the following, the ratio Mp_0/m_0 will be called μ.

The V/c ratio is plotted in Fig. 2 for three different $\mu = Mp_0/m_0$ ratios (1000, 10,000, and 100,000) and also for the special case $Mp_0 = 0$. For clarity, the V/c curves for $Mp_0 \neq 0$ have been magnified by a factor 10.

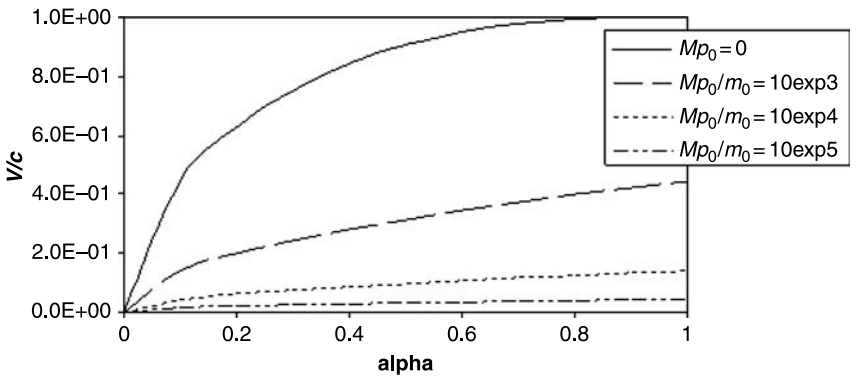


Fig. 2 Velocity acquired by nonreacted plus inert mass as a function of percentage α of mass converted into energy. The three lower curves are multiplied by a factor of 10 for clarity. Mp_0 is the rest mass of (inert) propellant added.

Equation (6) can be written as

$$I_{sp} = V = c\, f(\mu, \alpha) \tag{6bis}$$

where

$$f(\mu, \alpha) \equiv 2 \Big/ \left\lfloor \sqrt{(1 + 2/\mathrm{A})} + 1 \right\rfloor$$

showing that the exhaust velocity V, that is, the ideal I_{sp} when using its true physical units, is essentially the speed of light *scaled down* by the specific mass-conversion process (that is, by α) and by the addition of inert mass Mp_0 (that is, by μ). Only a tiny portion of the curves in Fig. 2, those closest to the left (plus the $\alpha = 1$ special case of annihilation), are in fact relevant to energy conversion and propulsion. In essence Eqs. (6) or (6bis) tell that "in principle" the exhaust speed can reach up to the speed of light. The function $f(\mu, \alpha)$ can be interpreted *as an attenuation factor*: If fuel mass is not completely converted into energy (i.e., if $\alpha \neq 1$), or if inert mass Mp is added to the conversion products, f is <1, and the specific impulse will be less than c.

The special case $Mp_0 = 0$ (top curve) is when the potential energy is completely converted to kinetic energy of products: these are ejected "as formed," with KE from $\mathcal{O}(1)$ to $\mathcal{O}(100)$ MeV, and their V is the highest possible at each α. Such a strategy has been proposed at the U.S. Lawrence Livermore National Laboratories to maximize I_{sp} in fission engines [3]. Figure 2 also shows that with α typical of fission or fusion the I_{sp} is a tiny fraction of c. However, because $c = 3 \times 10^8$ m/s, even a tiny fraction can result in I_{sp} vastly larger than that of chemical rockets.

Note that if $V \ll c$ relativistic mass and rest mass can be assumed the same, then the energy balance in Eq. (6) reduces to the well-known expression

$$I_{sp} = \sqrt{2J}$$

Equation (6) confirms why nuclear power is critical for future space missions. The square-root dependence tells that modest increases of J, for instance, using chemical HEDM, have a minor effect on I_{sp}. Only by increasing J by *orders of magnitude* can I_{sp} increase significantly. This is the case of nuclear energy, see Table 1.

2. *Thrust*

Thrust F, specific impulse (ideally V), and thrust power P satisfy the two definitions

$$F\, I_{sp} = P$$

$$F = I_{sp} \frac{\mathrm{d}m}{\mathrm{d}t}$$

where $\mathrm{d}m/\mathrm{d}t$ is the total mass consumption, equal to the sum of the mass flow rate of unreacted fuel (if ejected), and of that of the inert mass.

The reactor power P_R and the thrust power P are related by

$$P = P_R\, \eta_{tot} = \alpha \dot{m}_0\, c^2\, \eta_{tot}$$

with η_{tot} the total efficiency of energy conversion. Hence,

$$F = \left(P \frac{\mathrm{d}m}{\mathrm{d}t} \right)^{1/2}$$

Note that thrust scales with the *square root* of power. This might sound trivial, but is a key factor in nuclear propulsion because costs grow with reactor power (size) more rapidly than in chemical rockets. With the definitions given,

$$F = \{\alpha \dot{m}_0 \, c^2 \, \eta_{tot} [z(1-\alpha)\dot{m}_0 + \dot{M}_{P0}]\}^{1/2} \tag{7}$$

In Eq. (7) z is a factor either one or zero depending on whether or not unreacted fuel is ejected. Equation (7) can be rewritten in terms of the ratio μ:

$$F = \sqrt{\alpha} \cdot \dot{m}_0 \cdot c \cdot \sqrt{\eta_{tot}} \cdot \left[z \cdot (1-\alpha) \Big/ \sqrt{1-(V/c)^2} + \mu \Big/ \sqrt{1-(V/c)^2} \right]^{1/2} \tag{8}$$

In the square brackets the first term is generally much smaller than the second ($\mu \gg 1$) so that

$$F \approx \sqrt{\alpha} \cdot \dot{m}_0 \cdot c \cdot \sqrt{\eta_{tot}} \cdot \left[\frac{\mu}{\sqrt{1-(V/c)^2}} \right]^{1/2} \tag{9}$$

Equation (8) tells that if *only* fission or fusion fragments are ejected ($\mu = 0$), the thrust is of order $\sqrt{\mu}$ smaller than that in a rocket where temperature is moderated by adding mass. Because μ can be of order 10^3 to 10^6, the implications are significant.

Similarly to what is seen in discussing the specific impulse, Eq. (9) can be interpreted as specifying thrust composed of a "limit" thrust, $\sqrt{\alpha} \cdot \dot{m}_0 \cdot c$, *scaled down* by an efficiency coefficient, and that can be *scaled up* by adding mass. Adding mass lowers I_{sp} and raises F as the same time and, approximately, with the same square-root dependence. If inert mass is not added ($\mu = 0$), the maximum thrust possible is limited by $\sqrt{\alpha} \cdot \dot{m}_0 \cdot c$, just as the I_{sp} is limited by c; however, unlike I_{sp}, F increases if inert mass Mp is added. An aeronautical engineer will find an analogy with turbofan engines, where the nonreacting air passed through the fan contributes to thrust.

The nondimensional thrust $\Phi = F / [\sqrt{\alpha} \cdot \dot{m}_0 \cdot c \cdot \sqrt{\eta_{tot}}]$ is plotted vs μ in Fig. 3, showing how thrust grows with the addition of inert mass. Quite intuitively, the effect of adding mass is enhanced by increasing α and increasing power (that is, increasing rate of fuel consumption).

The scaling with $\sqrt{\alpha}$ in Eq. (9) implies that no matter what the nuclear source, metastable nuclei, fission or fusion, the effect on thrust is slight. Only annihilation makes a significant difference. Note that Eq. (8) predicts that for annihilation ($\alpha = 1$) no thrust is possible unless inert is added because reactants can be completely converted into radiation energy (that is, massless products). However, pure energy can still produce thrust (see Sec. E). The influence of η_{tot} on thrust is small.

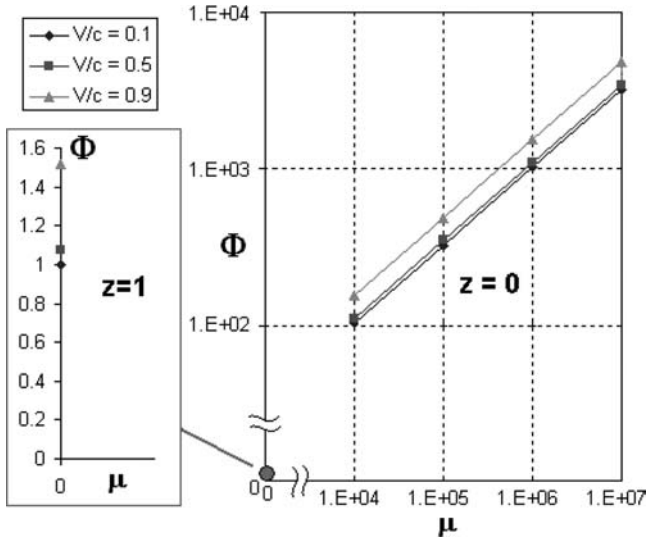


Fig. 3 Effect of inert propellant addition to nondimensional thrust Φ (case of fission, $\alpha = 9.1 \times 10^{-4}$).

Thrust can be written also as in standard rocketry textbooks to show its dependence on I_{sp} (or V). Using Eq. (6bis),

$$F = (\rho_e A_e) \cdot c^2 \left[\frac{f^2}{\sqrt{1-f^2}} \right] \tag{10}$$

depends essentially on V^2 for $V/c \ll 1$. Se and Ae are density and Area at the rocket nozzle exit. Equation (10) can be interpreted as composed of a limit thrust $(\rho_e A_e)c^2$, corresponding to a rocket with $I_{sp} = c$, scaled down by the function of V/c and μ in square brackets, always $\ll 1$. As V/c grows, relativistic effects become more and more significant, and F grows more rapidly than V^2.

3. Power

Power shapes size, complexity, and cost of nuclear reactors. In fact, at least conceptually, nuclear reactors are not power limited: they are limited by the operating temperature of fuel and structures. If heat is removed sufficiently fast to keep temperature within reasonable limits, nominal power can increase as desired. The key words are "sufficiently fast": during the Chernobyl plant accident, the 1600-MW reactor involved was being operated at only 200 MW. The sudden plunging of control rods, with the cooling system unwittingly and deliberately turned off, raised thermal power by a factor 100 in four seconds. That is, in four seconds the power became 12 times the reactor's *nominal* power. From

the engineering viewpoint, this is quite unlike chemical rockets, where power is linearly proportional to propellants' flow rate, and combustion temperature is fixed by thermodynamics. Designing compact GW-class nuclear systems is mostly a heat-transfer problem rather than a nuclear physics problem. Of course, even with adequate materials and cooling, greater power means greater fuel consumption [see Eq. (1a)].

Reactor power P_R is $1/\eta_{\text{tot}}$ of the thrust power P defined as

$$P = I_{\text{sp}}\, F \tag{11}$$

and from Eq. (10) thrust power can be written

$$P = (\rho_e A_e) \cdot c^3 \left[\frac{f^3}{\sqrt{1-f^2}} \right] \tag{12}$$

showing that for $V \ll c$ power scales with V^3, as expected. Similarly to thrust, as $V/c \to 1$ power grows faster and faster because of relativistic effects, going to infinity as V approaches c.

When power is fixed, the P = constant hyperbola on the (I_{sp}, F) plane (see Fig. 4) illustrates the power dilemma. Nuclear propulsion can raise I_{sp} by a large factor with respect to chemical, but *at fixed reactor power* thrust must decrease by the same factor, that is, as $1/I_{\text{sp}}$. Low propellant consumption goes together with low thrust, and one must choose between *either* low consumption *or* high thrust.

Generally speaking, one of the purposes of NP, and a "must" for manned missions, is to shorten mission times. To do so, spacecraft must accelerate at a significant fraction of, say, 1 *g* for longer than the few minutes of chemical rockets. This strategy shapes power requirements sharply. For instance, a 1-ton spacecraft

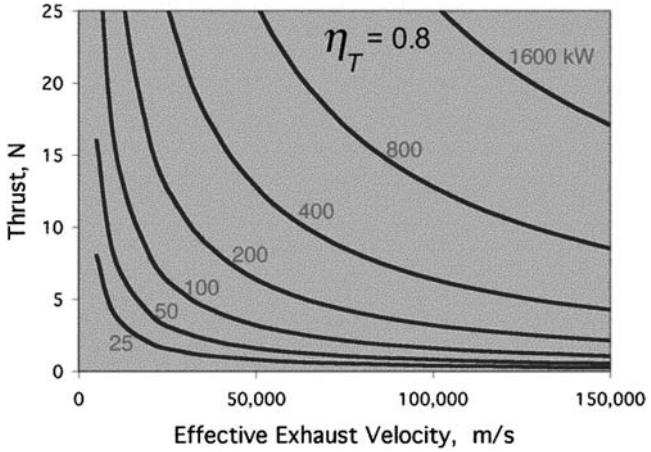


Fig. 4 Thrust vs I_{sp} at constant power P (total efficiency $\eta_{\text{tot}} = 0.8$ assumed) [34].

accelerating at 10^{-2} *g* needs a 100-N thruster. With I_{sp} = 10,000 s ($\approx 10^5$ m/s) the thrust power is of order 10 MW. This figure gives pause to any NP system designer. Note that this figure is thrust power, not reactor power. In nuclear electric propulsion it does not include total efficiency (see Sec. D.2).

4. Mass

Deriving rules to predict even preliminary mass budgets of NP systems is beyond the scope of this chapter (see instead Chapter 5). All items—engine, tanks, structure, auxiliary systems and, finally, propellant—are too intricately linked. Only *fuel* and *propellant* (inert) mass will be discussed here.

The fuel consumption rate, by definition, is

$$\dot{m}_0 = \frac{P_R}{J} = \frac{P_R}{(\alpha c^2)} \tag{13}$$

whereas that of inert propellant depends on I_{sp} (or α) and on mission time, that is, acceleration and distance, in turn a function of thrust and I_{sp}. The total instantaneous consumption is

$$\frac{\mathrm{d}m}{\mathrm{d}t} = \dot{m}_0 + \dot{M}_0 = \frac{P_R}{(\alpha c^2)}(1 + \mu)$$

and the total mass used by the propulsion system over the total mission time t is $\int_0^t (\mathrm{d}m/\mathrm{d}t)\mathrm{d}t$.

That sometimes is added to the dry mass of the spacecraft and assumed a design constraint. Doing so is not necessarily wise, even though it looks to be the easier way to constrain total mass and cost [35].

In nuclear propulsion adding inert mass M_0 is an option because a nuclear rocket can still work by ejecting only reaction products (that is, $\mu = 0$). However, moderating the nuclear reaction and cooling it can be conveniently accomplished by circulating inside the reactor a coolant that functions also as a neutron moderator: in this case it is natural to think of it as *the* propellant. In fact, if no inert mass is added ($\mu = Mp = 0$), the temperature of the mass ejected is the microscopic KE acquired by products of the first energy conversion stage, of order 5–20 MeV per particle in fusion, and correspondently higher (~160 MeV) for the heavier FF. Without appropriate measures, for example, magnetic confinement, such temperatures cannot be withstood by current or future materials: the forces keeping structural materials together are electroweak, thus with potential of order electron volts, not mega electron volts.

Thus high temperature can be lowered by adding inert mass Mp_0 to products. How much mass to add depends on maximum allowable temperature and on the specific heat of the inert Cp_M and fuel Cp_m. Assuming $V \ll c$ to simplify the reasoning, the ratio $\mu = Mp/m$ limiting the maximum temperature *rise* ΔT is equal, from a simple energy balance, to

$$\mu = \frac{[\alpha c^2/\Delta T - (1 - \alpha) Cp_m]}{Cp_M} \tag{14}$$

Because $\alpha c^2 \gg (1 - \alpha)\, Cp_M\, \Delta T$ for any reasonable structural temperature,

$$\mu \approx \frac{\alpha c^2}{(Cp_M \Delta T)} >> 1 \tag{15}$$

that is, the inert mass fraction is proportional to the ratio between energy density of fuel and enthalpy density of the inert, or to the ratio between potential energy of fuel and macroscopic KE of the inert. Equations (14) and (15) tell that constraining maximum temperature is costly in terms of mass addition: $Mp \gg m$. For instance, adding inert hydrogen to a fission rocket ($\alpha = 9.1 \times 10^{-4}$, $J = 8.2 \times 10^{13}$J/kg) to limit its temperature rise ΔT to $\approx$2500 K needs $\mu \approx 2 \times 10^3$, or carrying 2000 times more hydrogen than fissionable fuel.

The need for inert worsens with increasing α. In fact, Eq. (14), at fixed ΔT, implies the product

$$\mu/\alpha \approx \text{constant}$$

that is, the more efficient the mass conversion process, the larger the inert mass needed to moderate temperature. The extreme case is annihilation, requiring two *million* times more hydrogen than fuel (in this case proton-antiproton pairs). Such propulsion systems would be characterized by extremely large tanks (size and weight). Thus ways to insulate the exhaust products (for instance, magnetically) is a primary requirement for high-energy-density (high-α) propulsion, in that it might allow higher temperatures than bearable by structural materials. The temperature constraint explains why *solid* core nuclear thermal rockets tested in the past had I_{sp} no higher than 900 s, as shown later. It also explains the research work towards gas-core reactors.

Adding inert mass lowers I_{sp} (see Fig. 2) and, at fixed power, raises thrust. The combination I_{sp}-F is to be tailored to a specific mission. Balancing I_{sp} vs thrust *at fixed power* in planning interplanetary missions can be appreciated by calculating their effect on propellant mass and ΔV. These questions are seldom relevant to chemical propulsion, where "thrust applied for a very short time" is the real variable controlling ΔV, *not power*. These issues will become critical for future nuclear electric propulsion, where continuous thrust might have to be applied for months or even years. A simplified quantitative analysis of these issues (without relativistic effects) involves the following equations [30].

Thrust power:

$$P = I_{sp}\, F$$

I_{sp} definition ($V \ll c$ assumed):

$$\dot{M}_p = \frac{F}{I_{sp}}$$

Mass of propellant consumed at constant $\dot{M}_p$ after a time t_{acc} under power:

$$M_p = \frac{F\, t_{acc}}{I_{sp}}$$

Distance traveled at constant acceleration a:

$$d_{\text{acc}} = \tfrac{1}{2}\, a\, (t_{\text{acc}})^2$$

ΔV acquired after a time t_{acc}:

$$\Delta V = a\, t_{\text{acc}}$$

Newton's law:

$$F = M\, a$$

where M is the spacecraft mass, assuming $\gg Mp$. This set of equations models (to 0th order) propulsion performance for interplanetary missions. They have been purposely simplified to obtain an analytical solution. Part of the trajectory distance d_{acc} is assumed at constant acceleration $a = P/(I_{\text{sp}}\ M)$, positive or negative. Spacecraft mass and power (M and P) can be assumed as input. If d is the distance to the final destination, the d_{acc} should be $\leq d/2$. However, d_{acc} might turn out to be greater than $d/2$ when acceleration is modest. In this case the spacecraft *must spiral* (for instance, around a planet) until it reaches the ΔV for planetary escape. At that moment the spacecraft can start the transplanetary leg of its trajectory. The reverse procedure (constant deceleration) is assumed to orbit around the final destination.

Solving for time, mass of propellant, and ΔV [30],

$$\begin{aligned} t_{\text{acc}} &= (2 d_{\text{acc}}\, I_{\text{sp}}\, M/P)^{1/2} \\ Mp &= (2\mathrm{d}_{\text{acc}}\, P\, M/I_{\text{sp}}{}^3)^{1/2} \\ \Delta V &= [2\mathrm{d}_{\text{acc}}\, P/(I_{\text{sp}}\, M)]^{1/2} \end{aligned} \tag{16}$$

Equation set (12) shows propellant mass decreases rapidly with increasing I_{sp}. However, the effect of I_{sp} on acceleration time and on ΔV is detrimental: at fixed power, time of acceleration (and trip duration) stretches, and ΔV shrinks when I_{sp} increases. This might look rather unsettling, unless one realizes the consequences of having assumed fixed power.

It is instructive to apply the solution set (16) to a notional Earth-to-Mars mission (distance about 1.5×10^8 km), starting with a hypothetical 0.7-MW ion engine with $I_{\text{sp}} = 4000$ s and a spacecraft of mass $M = 100$ tons. Three sequential attempts are in Table 2.

Table 2 Trajectories and performance of NEP as a function of power

d_{acc}, km	P, MW	t_{acc}, days	ΔV, km/s	M_p, ton
10^7	0.7	1157	2	5
$8{\cdot}10^7$	0.7	3450	6	15
$8{\cdot}10^7$	70	33	54	135

The numbers in Table 2 show that finding a practical solution is not trivial, even with all of the simplifications made. The third attempt provides a fast mission, at the expense of much higher power than initially assumed, and violating the $Mp \ll M$ constraint. Although a solution seems within reach with further trials, xenon requirements will likely exceed current xenon worldwide production (about 59 tons/year), *unless* the thruster I_{sp} can be raised by an order of magnitude. About the spacecraft mass assumed, note that 100 tons is likely a minimum for an interplanetary *manned* mission.

The preliminary conclusion is that, for certain ambitious missions currently being discussed, for example, to Mars, short-term ion-engine technology (I_{sp} in the 4,000- to 10,000-s range), is insufficient to produce a *practical* trajectory, defined as a trajectory that is both fast and cheap [30]. Only I_{sp} of order 10 times those now available (that is, 40,000 s) can provide a satisfactory practical propulsion solution in the sense just defined. This means much more powerful nuclear reactors than those envisaged, for instance, for JIMO missions [36].

It is important to have a fast trajectory not only for technical and physiological reasons (should the mission be manned), but also because among the many motivations of space exploration there are also curiosity and adventure. Both are lived vicariously by the public, that is, the taxpayer. Public enthusiasm cannot be maintained for a mission where "nothing happens" for many months, let alone years.

D. Nuclear-Propulsion Strategies

After potential energy has gone through the second conversion stage of Sec. C.1, the choice is basically between two strategies: thermal or electric. Each has variants, briefly discussed next.

1. Nuclear Thermal Rockets

Only a brief summary of NTR features and performance is given next; more can be found in Chapter 2.

The NTR strategy consists of using heat released during the second stage of energy conversion to pressurize and eject mass. This mass might be only reaction products ($\mu = 0$, fission or fusion fragments), or inert Mp ($z = 0$, $\mu \neq 0$), or both ($z = 1$, $\mu \neq 0$). In the last two cases the ratio μ might have to be of order 10^3 to 10^6 to increase thrust and to moderate temperatures. In the third stage of conversion *micro*scopic energy becomes *macro*scopic kinetic energy of the propellant jet. This third stage occurs via collisions, for example, with the solid walls of a conventional nozzle, or by magnetic confinement inside a magnetic nozzle. (This solution is mandatory at extreme thermal loads, e.g., above $\mathcal{O}(10)$ MW/m^2 and requires an electrically conductive or ionized propellant.)

From this viewpoint, NTR work just like chemical rockets, hence, the definition "nuclear *thermal* rockets." In NTR the macroscopic KE of the jet issuing from the nozzle is of the same order of the microscopic KE acquired by particles at the end of the first or second stage, which one depends on whether only reaction products are ejected, or inert Mp is also added (see Fig. 2). In either case thrust power P differs little from reactor power P_R: nearly all of the energy from the reactor ends as kinetic energy of products and inert.

Most NTR experience is from solid-core fission types [7]. They are characterized by μ of order 10^3 and $z = 0$ (unburnt fuel stays inside fuel rods). Their most appealing feature is bulk power density, of order 1 MW/liter. During the U.S. ROVER program, the Los Alamos Science Laboratories (LASL) built the Phoebus II reactor that was tested at 4 GW for 12.5 minutes and had a power density about 1.3 MW/liter (see Fig. 5). On similar solid-core NTR the I_{sp} measured was of order 880 to 900 s.

One might ask why I_{sp} was almost twice that liquid rocket engines (LRE) if temperatures were comparable or lower. The answer is, in a chemical rocket the exhaust V (ideal I_{sp}) is close to the mean molecular speed $(8kT/\pi m)^{1/2}$ inside the combustion chamber. Although the same is true in a solid-core NTR, its propellant of choice, hydrogen, has molecular weight 2 instead of 9 or 10 typical of the combustion products of the best [LOX/LH_2] chemical rockets. Accordingly, the exhaust velocity is higher by the factor $\sqrt{9/2}$ to $\sqrt{10/2}$, about two. So, in vacuo I_{sp} might be in the 900-s range.

Variations on the NTR theme skip the second stage of energy conversion. In *gas-core* rocket concepts the fuel might be gaseous ^{235}U fissioning at 8,000–20,000 K [38, 39]. In FF rockets, the FF from a solid fuel thermalize directly *inside* the propellant.

The gas-core strategy depends on neutronics, for example, on the collisional cross section between neutrons and nuclei at high temperature. In solid-core

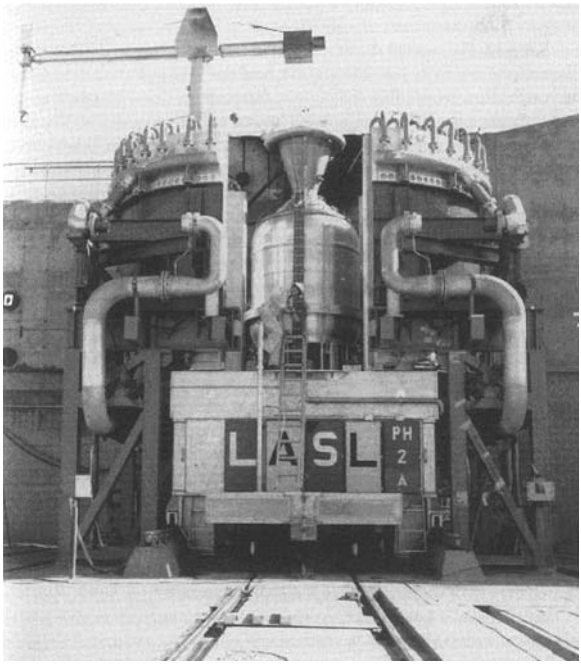


Fig. 5 Phoebus IIA solid-core nuclear reactor on its Los Alamos test stand [37].

reactors the thinner the fissioning fuel, the larger the volume of propellant injected to moderate fission kinetics and thermalize. Not much information on gas-phase neutronics exists, but see [39]. LASL has been active in the gas-core rocket for two decades, a sign that gas-core neutronics is viable. Either alone or with inert addition, fission products can be ejected at speeds that at 10,000 K, for instance, should yield I_{sp} of order 1500 s at least, and with substantial thrust [see Eqs. (9) and (10)]. I_{sp} is not especially high because ^{235}U and other high molecular weight products might be ejected together with hydrogen.

There are subvariations of the gas-core nuclear rocket: the cycle might be *open* (propellant *and* FF are ejected together, resulting in higher average molecular weight) or *closed* (the fuel is confined in a transparent chamber and heats low molecular weight propellant by radiative HT (see [38]). The complexity of such schemes has not prevented testing of hardware components.

In the *FF engine* [40], or *Rubbia engine* [41], hydrogen propellant flows in a chamber coated with a thin layer of fuel (see Fig. 6). Half of the FF from the coating is injected and thermalizes directly inside the propellant. This concept was originally proposed in [42]. Many solid-core nuclear reactor problems are bypassed in this way. This concept is capable of heating to much higher temperatures than tolerable by solid-core reactors, that is, to 6000 to 8000 K. The I_{sp} can reach 2400 to 2800 s. A rare $^{242\,m}Am$ isotope is the fuel of choice for the FF/Rubbia engine, chiefly because its neutron collision section shrinks with increasing temperature. This feature prevents loss of coolant accidents.

The radical approach to fission NTR is of course eliminating inert propellant altogether ($\mu = 0$, $z = 1$), as proposed by the Lawrence Livermore National Laboratories in the United States. The rocket can eject only the reaction products, their high momentum "undiluted" by inert mass addition. Predictably, thrust will be small [see eq. (8)]. For reference, a fission reactor ($\alpha = 9.1 \times 10^{-4}$) consumes fuel at a rate $\dot{m}_0 \approx 1.21 \times 10^{-5}$ kg/s of fuel per thermal GW. For example, the 4.1-GW Phoebus IIA reactor had $\dot{m}_0 \approx 0.05$ g/s. If operated at $\mu = 0$, its thrust would have been 40 N instead of the design 440,000 N available by adding hydrogen propellant. The tests indicate in fact that μ was 2.4×10^6 and I_{sp} "only" about 900 s.

Fusion concepts based on magnetic mirror confinement are supposed to be also operating in this mode [9]. The products are mostly fused alpha particles and unburnt fuel (e.g., D-T mixture). Cooling would be a major issue, but I_{sp} could range in the 10^4 to 10^5 s, as predicted by Eq. (6), depending also on fusion engineering strategy. In any event, the implication is that to produce F in the 10^4 N range this strategy would result in massive fusion rockets, compensating the low thrust density with sheer power and size. A detailed discussion of future fusion rockets based on open magnetic mirror confinement technology can be found in [9].

There is a third, radical way of exploiting nuclear energy for propulsion: repeated nuclear explosions astern of a spacecraft (*pulsed* nuclear propulsion is a fitting name suggested by Schmidt et al. [11]). Hardly conceivably now, this method was proposed and investigated in the 1950s by F. Dyson [12, 13] and E. Taylor, a fission bomb physicist, for single-stage-to-orbit (SSTO) launchers. A concise history of this project is in [43]; basic propulsion aspects are discussed in [1].

This propulsion technique was suggested by the results of early thermonuclear bomb testing on Eniwetok, when teams examining the ground in the aftermath of the explosion noticed that graphite-coated metal spheres hung some 30 feet from

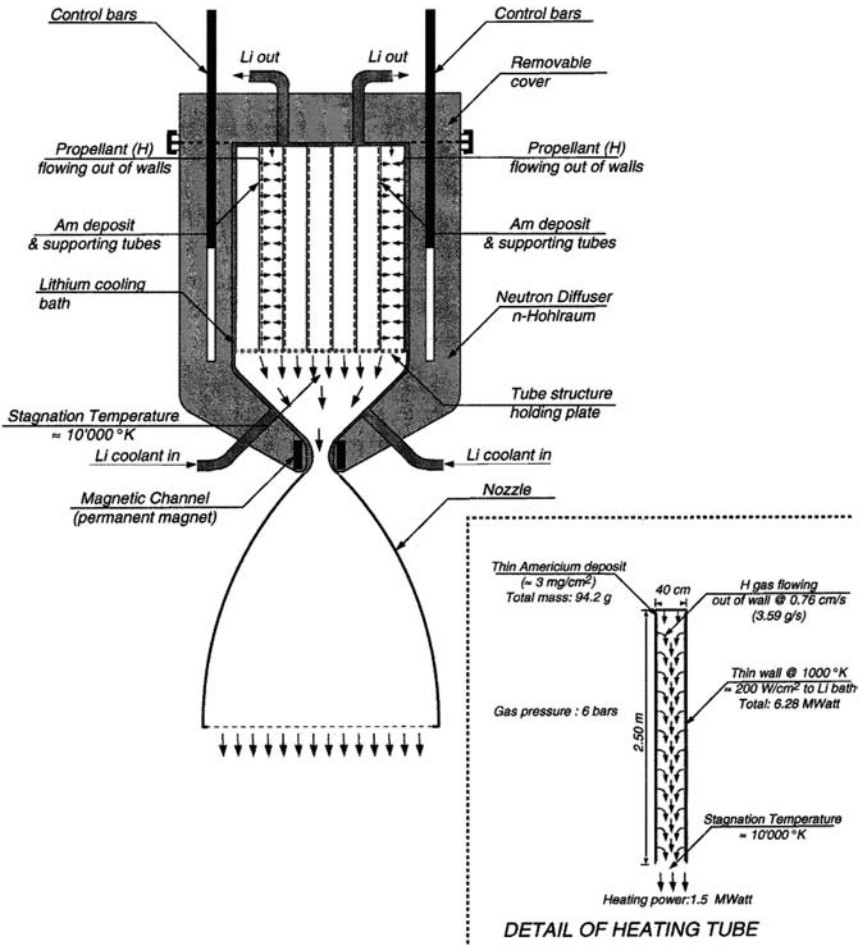


Fig. 6 Conceptual scheme of a Rubbia-type nuclear rocket engine.

ground zero were left practically unscathed. Until then, it was assumed that nothing could survive a close nuclear explosion. In fact, later testing and analyses showed ablation of a plate by an intense radiation environment could protect an underlying structure. Suitably sized and reinforced, what was then called a "thrust plate" could indeed receive and survive the impulsive force caused by shocked matter accelerated by an exploding and radiating atomic bomb. Radiation from the bomb fireball contributes to the force, for instance, by ablating a coating deposited on the thrust plate (e.g., a polymer or grease): the momentum of the ablation products ejected is equivalent to that of a rocket. Much of the information concerning this area of ablation and its physics is still classified today, but calculations and tests done with high explosives confirmed in 1959 that the concept was viable, particularly so for massive spacecraft. Such spacecraft must include also a

shock absorber to protect the crew. In the 1950s the nuclear test ban was not in existence, and so Dyson and the physicists working on this project (Project Orion) envisaged taking off from ground and accelerating to orbital speeds by sequential atomic explosions, probably the first modern SSTO proposal. Orion was eventually designed for a spaceship large enough to do a grand tour of the planets as far as Saturn, lasting about one year. The estimated mass of the spaceship for such a mission was of order 10,000 tons. Specific impulse and thrust calculations showed that both could be much higher than with chemical propulsion; in particular, I_{sp} of order 10^4 to 10^6 s were theoretically predicted. Limitations to thrust were caused by maximum allowed structural stresses, but also to the maximum acceleration that could be tolerated by the crew.

As there was no military application in sight, because of potential opposition by the public and certainly that of then Secretary of Defence McNamara, Project Orion was cancelled.

A "revisited" Orion (MagOrion and MiniMag Orion Project) has been recently revived as a space propulsion system by replacing atomic bombs with *miniature* nuclear explosions using unconventional actinide fuels; among motivations is that of reducing the mass of the spacecraft that must host this type of propulsion system. Ground testing has been carried on by substituting high-intensity electromagnetic energy pulses (theta pinch-accelerated plasma jets) for nuclear mini-explosions [14]. According to D. Andrews, at Andrews Space Company, who has led this project, the I_{sp} measured was greater than 1000 s. Calculations indicate the thrust impulse should be substantial, unlike that of any NEP thruster because the *instantaneous* power is much larger than possible by any nuclear reactor. If and when developed beyond the current stage, pulsed nuclear propulsion looks suited for powering long interplanetary missions, as it is capable of combining the best of the two classes of NP, namely, the large thrust of NTR and the high I_{sp} of NEP.

2. *Nuclear Electric Propulsion*

NEP systems are the answer to the question of how to raise I_{sp} above that of solid-core NTR. The answer consists in converting the fuel potential energy into electricity, just as in nuclear utility powerplants. This strategy involves an extra step, in which fission fragments heat a working fluid (not a propellant to be accelerated). Through a thermodynamic cycle the fluid can produce mechanical power and then electricity via an electric generator, but there are alternatives: see Bidault et al. [44] for a detailed analysis of this issue in the context of the comparison between solar-electric propulsion and NEP for a Mars mission. Conceptually, in fact, there are more direct ways of producing "large" electric power (e.g., $>$100 kW), such as magnetohydrodynamics (MHD) generators, for instance, see Smith and Anghaie [45]. However, their technology status is still immature.

Once produced, electric power can feed an electric thruster, either electrostatic (ion), or magnetohydrodynamic [Hall, PPT, magnetoplasmadynamic (MPD), and their variants, see Chapter 3 and Chapter 4 in this book]. Electrostatic thrusters rely on the electroweak Coulomb force to accelerate ions; the MHD use instead the Lorentz force caused by the simultaneous presence of electric and magnetic fields.

Electric thrusters are capable of much higher I_{sp} than any NTR because gas *acceleration is not constrained by thermodynamics*, that is, by a high-low temperature

cycle, but driven directly by the Coulomb or Lorentz forces acting on charged particles. That implies gas must be ionized and become a plasma.

The price of the NEP strategy is low overall efficiency η_{tot}. This efficiency is the product of the thermal-to-electric energy conversion efficiency η times that (electric-to-propellant kinetic energy) of the electric thruster η_E, that is, the efficiency of the conversion of electric power into thrust power. So the reactor power P_R must be $1/\eta_{tot}$ the thrust power P. Experience with large space power (above 100 kW_e) is nil, but η can be optimistically estimated of order 50% with thermodynamic cycles (actual cycles have *much lower* efficiency). The η_E are of order 70% for megawatt-class electric thrusters. This means that η_{tot} might be, at most, about 35%. The optimistic estimate is that a 1 GW of thrust power needs a reactor three times bigger. A more cautious analysis will certainly raise this figure.

Efficiency notwithstanding, experience in electric propulsion (powered by solar panels) [54] has already shown that I_{sp} can be a factor three larger than the 900–1000 s of NTR. Commercial ion thrusters [3] (Chapter 3 in this book) are routinely delivering 3000 s now and 4000 s in the near future. Higher I_{sp}, up to 8000–15,000 s, were demonstrated in the laboratory by the NEXIS and HiPEP nuclear ion thrusters planned for the JIMO mission [34, 46]. MPD thrusters are capable of even higher I_{sp} (see Auweter-Kurtz and Kurtz [47] in Bruno [48], which includes sections authored by M. Auweter-Kurtz, D. G. Fearn, H. Kurtz, T. J. Lawrence, and R. X. Lenard, and Chapter 4 in this book. In fact, with this strategy, the ideal exhaust velocity V is limited only by plasma instabilities and, eventually, by relativistic effects.

Most of the drawbacks of NEP are caused by its low η_{tot}. Waste power must be somehow disposed of. In space this can be done only by space radiators. They add extra mass to the propulsion system: a range of specific mass is 0.01 to 0.15 kg/kW for modern space radiator concepts operated at moderate temperature (~800 K). Ground-based radiators using metals (e.g., Li, or NaK eutectic) in heat exchangers are much more efficient. So the price to pay for NEP is not only a reactor with $P_R > P$, but also a heavier propulsion system. The bulk power density of NEP (power/unit mass of system) estimated by NASA might be 10^{-2} times that of NTR. These considerations are not meant to disparage NEP systems, but simply to emphasize that *practical* missions using NEP will need adequate nuclear reactor power.

Mixed ("hybrid") NTR/NEP as well as NTR/chemical systems have also been conceived and one at least has been tested (see Dujarric et al. [49], Czysz and Bruno [50], and Chapter 2 in this book).

3. *Comparison Between Chemical and NTR/NEP Systems*

Comparing different systems can yield different results depending on the choice of criteria. Here comparison is based on *specific total impulse* $I_{tot,s}$, a mission-linked parameter defined as

$$I_{tot,s} \equiv \frac{I_{sp}\, t_{operation}}{(Mp+m)}$$

where $t_{operation}$ is the mission "engine-on" total time.

Table 3 Performance index *I* of some propulsion systems (fixed P_R)

Type of propulsion	I_{sp}, s	η_{tot} (assumed)	I
Chemical	455	1	1
NTR	910	1	8
Ion NEP	3,000	0.3	65
MHD NEP	10,000	0.3	2,400

Therefore, $I_{tot,s} = I_{sp}/(dm/dt)$, and because $P = F\,I_{sp}$ and $F = I_{sp}\,(dm/dt)$,

$$I_{tot,s} = \frac{I_{sp^3}}{P} = \frac{I_{sp^3}\eta_{tot}}{P_R}$$

The dimensions of $I_{tot,s}$, distance per unit mass, classify it as a fuel economy parameter, similar to that used in stating the performance of cars (miles/gallon or kilometers/liter). The dependence on $I_{sp}{}^3$ is to be expected but still noteworthy.

The $I_{tot,s}$ normalized with respect to that of the best chemical propellants (LOX/LH_2) will be called the *mass performance index*, or simply *I*. This index is shown in Table 3.

The price of high mass performance is either low thrust, because $F\,I_{sp} = P/\eta_R$ or very high power. Thus choosing the propulsion system for a specific mission, where time might be just as important as mass consumption, should be based on solving a set of equations similar to the set in Eq. (16), although far more sophisticated.

E. Massless (Photonic) Propulsion

Because of their potential I_{sp} and public attention received, it is of interest to discuss nuclear propulsion systems not ejecting mass. These systems are often called "massless," although this word needs to be qualified.

Massless propulsion was proposed by E. Saenger in Germany [50]. His proposal was then popularized in the mid- and late 1950s in a number of European magazines.

Saenger assumed annihilation reactions (protons p – antiprotons p^-; thus, $\alpha = 1$) as the ultimate energy source maximizing *J*. Annihilation produces radiation in the form of high-energy photons (but also muons, pions, and neutrinos). Photons travel at the maximum speed known *c*. When collimated in a beam by a parabolic mirror hosting the energy source in its focus, photon emission becomes the spacecraft propulsion system. It works as such because photons emitted from the source invert their momenta when they are perfectly reflected by the mirror: the spacecraft recoil is its thrust.

If *P* is the thermal power, $E_p = h\nu$ the energy assumed *uniformly* imparted to all photons, and if *all* photons are *perfectly* reflected and collimated, the flux Φ of photons per second producing thrust *F* is

$$\Phi = \frac{P}{E_p}$$

and because the momentum of photons is $h\nu/c = E_p/c$, the thrust is

$$F = \frac{P}{c} \tag{17}$$

Note that in Eq. (17) the contribution of massive particles (pions, muons,...) has been neglected.

This thrust does not depend on photon wavelength, only on power. Equation (17) is intuitive when observing that the "exhaust" V of photons is exactly c. Alternative explanations can be cast also in terms of the Poynting vector (electromagnetic pressure), or based on $E = mc^2$: that is, a photon of energy $E = h\nu$ has a "virtual" mass $h\nu/c^2$, so that ejecting photons is the same as ejecting particles of such mass. (This mass is $\approx 9 \times 10^{-29}$ kg for a $h\nu = 5$-MeV photon, a typical fission-emitted gamma ray.)

A perfectly collimating mirror and an ideal reactor do not exist; however, photonic thrust might still be produced with some efficiency (yet to be determined). The photon momentum concept completes the discussion of thrust when $\alpha = 1$ initiated in Sec. C.1. It helps also to understand the principles of inertial confinement fusion and of pulsed nuclear propulsion.

A year later, Saenger [51] proposed gas-phase fission ($\alpha = 9.1 \times 10^{-4}$) as energy source, because matter–antimatter reactions seemed too far in the future. The performance estimated was surprisingly realistic. In Saenger, [50] the author mentions as exhaust velocity, or I_{sp}, 250 km/s, not c as one would expect based on the fact that photons move at light speed. The reason is that, in calculating I_{sp}, Saenger included also the contribution from heavy fission fragments, assumed exhausting from a duct coaxial with the mirror axis. I_{sp} is *the average* of two very different exhaust speeds, heavily weighed toward that of fission fragments. As a footnote, he added his estimate of $I_{sp} = 2.25 \times 10^6$ m/s if fusion, rather than fission, was the energy source. The ROM of both these estimates is, in fact, correct.

Quite independently, Rubbia rediscovered photonic propulsion after looking for ways of improving his fission-fragments rocket concept. He proposed *heating* a surface using a fission reactor. This surface should radiate as much as possible as a blackbody. Rubbia's concept, just like Saenger's, envisages a paraboloid mirror with the reactor at its focus. The paraboloid is much deeper than in Saenger's drawings, to capture as much as possible of the energy radiated isotropically from the reactor. The power required by an ideal 26-m-diam mirror radiating at about 3000 °C (about 0.25 eV) is about 3 GW, and thrust is 10 N.

This concept was presented at a European Science Foundation workshop held in Rome in May 2002 and to the 6th International Symposium on Propulsion for Space Transportation of the XXIst Century, organized by the Association pour l'Aeronautique et l'Astronautique Francaise (AAAF) in June of the same year in Versailles [52, 53]. It has been also evaluated under an European Space Agency (ESA) contract.

Even massless photonic propulsion consumes mass: the mass m_0 of the fuel fissioned. Precisely because of the $E = mc^2$ relationship between energy and mass,

the I_{sp} calculated by using for d(m)/dt only the fraction αm converted into energy is exactly c, the photon exhaust speed. However, *not all* fuel converts into pure radiation energy, only its fraction α. Short of recovering it and reprocessing it, the remainder fraction $(1-\alpha)$ is effectively lost to propulsion. In a solid-core fission reactor that fraction stays inside the fuel rods and cannot even work as inert propellant ($z = 0$).

Therefore, accounting for the mass of fuel consumed, the specific impulse becomes $I_{sp} = \alpha c$, a lower but still respectable 2.73×10^5 m/s when using fission. Fusion has $\alpha = (3 \text{ to } 4) \times 10^{-3}$, and I_{sp} would be in the 1×10^6 m/s range. If the fusion rocket is of the magnetic mirror type, the fuel not fused is ejected, μ is nonzero, total thrust is larger, but ideal I_{sp} is lower. Apparently, this aspect of photonic propulsion was not accounted for by Rubbia.

Thus consumption of nuclear fuel must be included when estimating performance of so-called massless photonic rockets: they should be called instead "propellantless" rockets. It must also be included in estimating performance of "conventional" nuclear-propulsion systems as well, if missions are very long. The inherently low thrust of NEP means engine-on times might be of order years. Because mass consumption is P_R/J [see Eq. (14)], it depends of course on α. Using fission, P_R/J is about 1.21×10^{-5} kg/s per GW of reactor power. A single day of operation consumes (ideally) 1.45 kg of fuel per GW. A 3-GW system, for example, like that proposed by Rubbia, would consume more than 13 tons of nuclear fuel over a 10-year mission, a reasonable time yardstick, because the ideal F is only 10 N.

III. Conclusions

The very concept and the fundamental physics of NP was established almost a century ago, and current technology is already capable of implementing it in propulsion systems. These might be NTR, where thrust can be very large, at the expense of a moderate I_{sp}, or NEP, where the reverse is typical. Mixed-mode operation appears also feasible, albeit still unproven. The choice of system depends on the mission. For manned interplanetary travel, the present technology of NTR and NEP has reached a good maturity level or will have in the next 10 to 15 years with reasonable investment in some areas, for instance, materials. In both systems the power required by fission reactors must be substantially higher, by a factor of roughly 10 to 100, than that of some interplanetary, NP-based missions being considered at this time. This conclusion is also relevant to manned and unmanned fast missions, the only ones ensuring continuing interest and financial support from the public. Among them are asteroid-threat missions, of growing importance as more and more asteroids that might cause substantial harm to Earth are discovered.

In this context, any encouraging technical solution or concept, and their offshoots or conclusions, including the present ones, must be tempered by considering also the unwanted NP effects, mainly radiation, spent fuel disposal, and their associated popular fears. Short of conveying timely and correct information, and involving the public in future decisions concerning NP, the common perception of anything nuclear, right or wrong it might be, will adversely affect future choices and prevent exploiting its immense potential.

References

[1] Federation of Atomic Scientists, http://www.fas.org/nuke/space/c02early.htm, 2005.

[2] Bussard, R. W., and DeLauer, R. D., *Nuclear Rocket Propulsion*, McGraw-Hill, New York, 1958.

[3] Lawrence, T. J., Witter, J. K., and Humble, R. W., "Nuclear Rocket Propulsion Systems," *Space Propulsion Analysis and Design*, edited by R.W. Humble, G. N. Henry, and W. J. Larsen, McGraw-Hill, New York, 1995, Chap. 8.

[4] Turner, M. J. L., *Rocket and Spacecraft Propulsion*, Springer-Praxis, Berlin, 2005, Chap. 7.

[5] Roundtable Discussion on Nuclear Propulsion and Power for Space, Special Rept., *Aerospace America*, Vol. 42, No. 11, pp. 26–39. 2004, http://boss.streamos.com/wmedia/federal/aiaa/aiaa081004.wvx.

[6] Papers presented by FGU RNZ "Kurchatov Institute," FGUP "Red Star," FGUP "Research Center M.V. Keldish," Leipunskii GNZ RF-FEI, and Korolev RKK "Energhya," *Proceedings of the International Conference Nuclear Energetics in Space 2005*, 2005 (in Russian), organized by the Int. Sci. & Techn. Center, htpp://partncistc.zu/en, Moscow, Russia.

[7] Gunn, S. V., and Ehresman, C. M., "The Space Propulsion Technology Base Established Four Decades Ago for the Thermal Nuclear Rocket is Ready for Current Applications," AIAA Paper 2003-4590, July 2003.

[8] Kammash, T., "Principles of Fusion Energy Utilization in Space Propulsion," *Fusion Energy in Space Propulsion*, edited by T. Kammash, Progress in Astronautics and Aeronautics Series, Vol. 167, AIAA, Washington, D.C., 1995, Chap. 1.

[9] Romanelli, F., Bruno, C., and Regnoli, G., "Assessment of Open Magnetic Fusion for Space Propulsion," International Astronautical Congress, Paper IAC-06-C4.6.02, Oct. 2006.

[10] Del Rossi, A., and Bruno, C., "Safety Aspects in Nuclear Space Propulsion," International Astronautical Congress, Paper IAC-04-R.4/S.7.07, Oct. 2004.

[11] Schmidt, G. R., Bonometti, J. A., and Irvine, C. A., "Project Orion and Future Prospects for Nuclear Pulsed Propulsion," *Journal of Propulsion and Power*, Vol. 18, No. 3, 2002, pp. 497–504.

[12] Dyson, F., *Disturbing the Universe*, Harper and Row, New York, 1979, Chap. 10.

[13] Dyson, G., *Project Orion*, Allen Lane – The Penguin Press, London, 2002.

[14] Lenard, R. X., "Use of MiniMag Orion and Superconducting Coils for Near-Term Interstellar Travel," International Astronautical Congress, Paper IAC-06-D2.8. – C3.5.-C4.7.02, Oct. 2006.

[15] Hooft, G., "The Making of the Standard Model," *Nature*, Vol. 448, 19 July 2007, pp. 270–273.

[16] Speake, C., "Gravity Passes a Little Test," *Nature*, Vol. 446, No. 7131, 1 March 2007, pp. 31, 32.

[17] Ciufolini, I., and Wheeler, J. A., *Gravitation and Inertia*, Princeton Univ. Press, Princeton, NJ, 1995.

[18] Einstein, A., Uber die Spezielle und allgemeine Relativitaetstheorie (Gemeinvestaendlich), Newton-Compton Publishers, Rome, 1916, Sec. 11–16.

[19] Lang, J. R., *Astrophysical Formulae: a Compendium for the Astronomer, Astrophysicist and Physicist*, 3rd ed., Springer-Verlag, Berlin, 1999, Sec. 5.5.

[20] Harwit, M., *Astrophysical Concepts*, Wiley, New York, 1973, Chap. 5.

[21] Krause, H. G. L., "Astrorelativity," NASA TR R-188, Washington, D.C., Jan. 1964.

[22] Davenas, A., Boury, D., Calabro, M., D'Andrea, B., and Mc Donald, A. J., "Solid Propulsion for Space Applications: A Roadmap," International Astronautical Congress Paper, IAA 3.3.02, Oct. 2000.

[23] Agrawal, J. P., "Recent Trends in High Energy Materials," *Progress in Energy and Combustion Sciences*, Vol. 24, No. 1, 1998, pp. 1 – 30.

[24] Perut, C., and Jacob, G., "A New Challenge, the 'High Energy Density Materials,'" *Proceedings of the 7th International Symposium on Launcher Technologies*, AAAF, Paris, 2–5 April 2007, www.launchers-symposium.org.

[25] Bruno, C., and Simone, D., "HEDM: From Basics to Exotic," Presentation at the July 11 Panel on HEDM, 43rd AIAA/ASME/SAE/ASEE Joint Propulsion Conference, July 2007.

[26] Mukhin, K. N., *Experimental Nuclear Physics – Vol. 1: Physics of Atomic Nucleus*, Mir, Moscow, 1983, Chap. 2.

[27] Sublette, C., "Nuclear Weapons Frequently Asked Questions–V.2.18," 1999, http://www.nuclearweaponarchive.org/Nwfaq/Nfqa6.html.

[28] Collins, C. B., Eberhard, C. D., Glesener, J. W., and Anderson, J. A., "Depopulation of the Isomeric State $^{180}Ta^{m}$ by the Reaction $^{180}Ta^{m}$ (γ, γ') ^{180}Ta," *Physical Review C Nuclear Physics*, Vol. 37, No. 5, 1988, pp. 2267–2269.

[29] Belic, D., Arlandini, C., Besserer, J., de Boer, J., Carrloo, J. J., Enders, J., Hartmann, T., Kaeppeler, F., Maier, J., Maser, H., Mohr, P., von Neumann-Cosel, P., Nord, A., Pitz, H. H., Richter, A., and Schurr, M., "Photoactivation of $^{180}Ta^{m}$ and Its Implications for the Nucleosynthesis of Naturally Occurring Isotope," *Physical Review Letters*, Vol. 83, No. 25, 1999, pp. 5242–5245.

[30] Czysz, P. A., and Bruno, C., *Future Spacecraft Propulsion Systems*, Springer-Praxis, London, 2006, Chap. 7.

[31] Schwarzschild, B., "Conflicting Results on a Long-Lived Nuclear Isomer of Hafnium Have Wider Implications," *Physics Today*, Vol. 57, No. 5, 2004, pp. 21–24.

[32] Hartsfield, C. R., "Analysis of the Application of a Triggered Isomer Heat Exchanger as a Replacement for the Combustion Chamber in an Off-the-Shelf Turbojet," Air Force Inst. of Technology/GAE/ENY/01M-04, M.S. Thesis, Dayton, OH, May 2001.

[33] "Space R&T Priorities for Europe – Recommendations, Technology Priorities, Technology Roadmaps Prepared by the European Space Manufacturing Industry," ASD Rept., Paris, Oct. 2005, www.eurospace.com.

[34] Andrenucci, M., "Prospective Needs and Technology Options for High Power Devices," paper presented at the Int. Symposium on Energy Conversion Fundamentals, Istanbul, 21–25 June 2004. Also, *Proceedings*, edited by M. Birkan and U. Yang, Vol. 1, pp. 1–10, U.S. Air Force, Dayton, OH.

[35] Czysz, P. A., and Bruno, C., "Interaction of the Propulsion System and System Parameters Determines the Design Space Available for Solution," International Astronautical Federation, Paper 00-S5.07, Oct. 2000.

[36] Randolph, T. M., and Polk, J. E., Jr., "An Overview of the Nuclear Electric Xenon Ion System (NEXIS) Activity," AIAA Paper 2004-3450, July 2004.

[37] Dewar, J. A., *To the End of the Solar System – The Story of the Nuclear Rocket*, Univ. Press of Kentucky, Lexington, KY, 2004.

[38] Howe, S. D., DeVolder, B., Thode, L., and Zerkle, D., "Reducing the Risk to Mars: the Gas Core Nuclear Rocket," *Space Technology and Applications International Forum-1998*, edited by Mohamed S. El-Genk, Publication CP-420, American Inst. of Physics, New York, 1998, p. 1138.

[39] Koroteev, A. S. (ed.), *Rocket Engines and Powerplants Based on Gas-Core Nuclear Reactor*, Mashinostroenie, Moscow, 2002 (in Russian).

[40] Ronen, Y., and Shwazeraus, "Ultra Thin ^{242m}Am Fuel Elements in Nuclear Reactors," *Nuclear Instruments and Methods in Physical Research A*, Vol. 455, 2000, pp. 442–451; also http://rense.co./general6/earthom.htm.

[41] Augelli, M., Bignami, G., Bruno, C., Calligarich, E., De Maria, G., Mulas, M., Musso, C., Pellizzoni, A., Piperno, W., Piva, R., Procacci, B., Rosa-Clot, M., and Rubbia, C., "Report of the Working Group on a Preliminary Assessment of a New Fission Fragment Heated Propulsion Concept and Its Applicability to Manned Missions to the Planet Mars (Project 242)," ASI Internal Rept., Rome, March 15, 1999 (proprietary).

[42] Shepherd, L. R., and Cleaver, A. V., "The Atomic Rocket-2 and -3," *Journal of the British Interplanetary Society*, Vol. 7, No. 6, 1948, pp. 237–240; also Vol. 8, No. 1, 1949, p. 30 also Bussard, R. W. and DeLauer, R. D., *Nuclear Rocket Propulsion*, McGraw-Hill, New York, 1958, p. 319.

[43] Flora, M., "Project Orion," 2005, www.islandone.org/Propulsion/ProjectOrion.html.

[44] Bidault, C., Bond, R., and Sweet, D., "Assessment of Electric Propulsion Systems for Exploration Missions: Comparison Between Solar-Electric and Nuclear-Electric Propulsion Systems," AURORA Final Rept. to European Space Agency, ESTEC Center, Noordwijk, The Netherlands, July 15, 2004.

[45] Smith, B., and Anghaie, S., "Gas Core Reactor with Magnetohydrodynamic Power System and Cascading Power Cycle," *Nuclear Technology*, Vol. 145, No. 3, 2004, pp. 311–318.

[46] Oleson, S., and Katz, I., "Electric Propulsion for Project Prometheus," AIAA Paper 2003-5279, July 2003.

[47] Auweter-Kurtz, M., and Kurtz, H., "High Power Plasma Propulsion for in-Space Transportation," 56th International Astronautical Congress, Paper IAC-05-C3.5-C4.7.05, Fukuoka, Japan, Oct. 17–21, 2005.

[48] Bruno, C., "IAA Position Paper on Nuclear Power and Propulsion," IAC Paper 06-D2.8. – C3.5.C4.7.01, Oct. 2006. Includes Sections individually authored by M. Auweter-Kurtz, D.G. Fearn, H. Kurtz, T.J. Lawrence, R.X. Lenard.

[49] Dujarric, C., Fratacci, G., and Valentian, D., (2000), "Hybridisation of Chemical, Nucleothermal and Electric Rocket Propulsion Principles: A Possible Way to Increase Rocket Specific Impulse?," International Astronautical Congress, Paper IAF-00-S.6.02, Oct. 2000.

[50] Saenger, E., "Die Erreichbarkeit der Fixsterne," *Rendiconti del VII Congresso Internazionale Astronautico,* (*Proceedings of the VII International Astronautical Congress*), Associazione Italiana Razzi, Rome 1956, pp. 97–113; See also *Mitteilungen der Landesgruppe Nordbayern der DGRR*, Vom. 13.05.1958.

[51] Saenger, E., "Zur Flugmechanik der Photonenraketen," *Acta Astronautica*, Vol. 3, No. 2, 1957, pp. 89–99.

[52] Szames, A., "La Fusée Photonique à l'Épreuve de la Critique," *Air et Cosmos*, No. 1850, 5 July 2002, pp. 34, 35.

[53] Rubbia, C., "Nuclear Space Propulsion with a Pure Electro-Magnetic Thrust," Rept. CERN-SL-2002-006 (ECT), CERN, Geneva, Feb. 2002.

[54] Rossetti, P., Saverdi, M., and Biagioni, L., "Electric-Propulsion Systems," *Advanced Propulsion Systems and Technologies, Today to 2020*, edited by C. Bruno and A. Accettura, Progress in Astronautics and Aeronautics, Vol. 223, AIAA, Reston, VA, 2008.

Copyrighted Materials
Copyright © 2008 AIAA Retrieved from www.knovel.com

Chapter 2

Nuclear-Thermal-Rocket Propulsion Systems

Timothy J. Lawrence*
U.S. Air Force Academy, Colorado Springs, Colorado

I. Introduction

THIS chapter does not want to revisit history or deal with the engineering challenges and technologies of nuclear thermal rockets (NTRs) investigated in the past or proposed. In fact, a number of excellent reviews have already appeared, for instance, on the history of the ROVER and NERVA programs that developed nuclear thermal rockets in the United States [1–3] and in the former Soviet Union [4–8]. [Note: This paper [6] has a picture of famous "three K" (Korolev, Kurchatov, and Koldysh). These Russian Scientists worked together to develop nuclear thermal rockets. Also, Chapter 1 in [7] contains a short history of the nuclear rocket engine ("ARD" in Russian). Reactors developed in the former Soviet Union are discussed in Chapter 3.] Engineering and science of NTRs have been covered extensively in [9–12]. The main goal instead is of illustrating some of their engineering, main issues, technology, and their current, although conceptual, evolution.

Most rockets are thermally driven gas devices in which energy is added in the form of heat. This heat energy ejects propellant from the engine, giving us the required momentum exchange or thrust. Energy can come from any number of sources. In chemical propulsion, the propellant releases energy through combustion. In a nuclear rocket, the propellant heats up when energy releases from the controlled fission of uranium or other fissionable material; see Chapter 1.

Fission involves the absorption of neutrons in a material such as uranium (other materials can fission, e.g., see [13]). This absorption excites the uranium atom until it splits into fragments and releases, on average, two new nuclei and one to three free neutrons. The fission fragments have high kinetic energy from the release of nuclear binding energy. This energy becomes thermal energy through collisions and interactions with other atoms. The neutrons also give up kinetic

The material presented in this chapter is updated from the paper published in *Space Technology*, Vol. 27, No. 1, 2007, pp. 23–26, and is reproduced with permission. Copyright © 2008 by the American Institute of Aeronautics and Astronautics, Inc. All rights reserved.

*Professor, Department of Astronautics.

energy and slow down so that they can be absorbed into the other fuel material. This process occurs more readily in lighter materials such as carbon, hydrogen, and beryllium because of their cross sections [14]. If each fission results in one other fission event, the core is said to be critical. Neutrons can either be absorbed by other engine materials or can leak from the reactor. The neutrons that leak out are lost from the cycle. Two or three neutrons are usually released in each fission event to ensure that at least one is absorbed by the fuel and causes another fission event. The accurate calculation of neutron fluxes inside matter, their absorption by nuclei, and their losses to the outside of a reactor (e.g., by the shield) are key to the reactor design and are performed by specialized codes [15].

The thermal energy produced from fission transfers to the coolant or propellant. For nuclear rockets using a solid fissionable material, we refer to the solid (e.g., uranium) as the fuel and to the gas, such as hydrogen or ammonia, as the coolant or propellant. Conduction across the fuel material and convection into the coolant can heat the coolant gas to high temperatures (3000 K), limited only by the requirement to keep the fuel system below the fuel's melting point.

In fact, the nuclear rocket as a simple cold-gas thruster with a heat source added can be envisioned. As the propulsion system "fires" to generate thrust, acceleration, and velocity change, it consumes large quantities of propellant. To compare the efficiency of different systems, the specific impulse is used as a yardstick; see Chapter 1. To increase specific impulse, the gas must have either a higher exit temperature or lower propellant molecular mass. Nuclear propulsion offers an

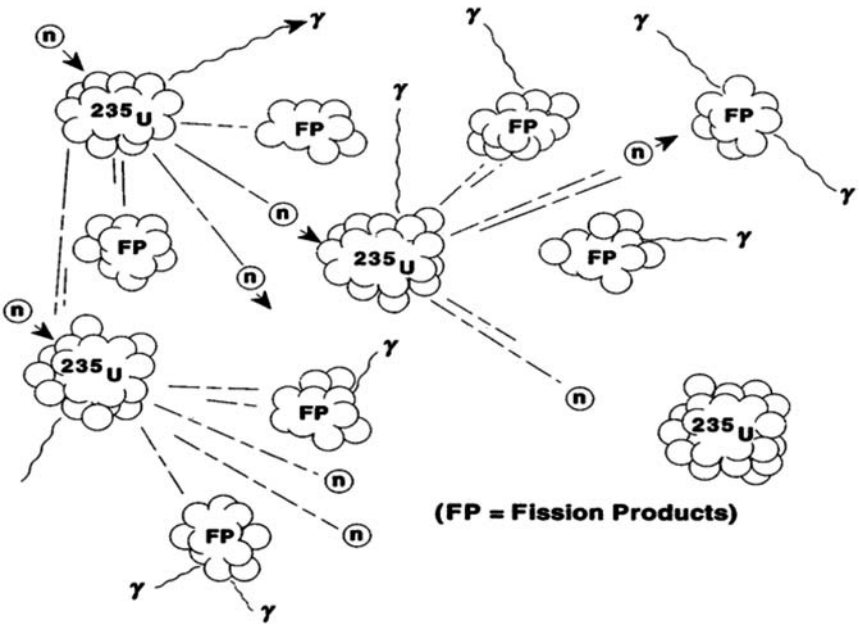


Fig. 1 Fission chain reaction [16].

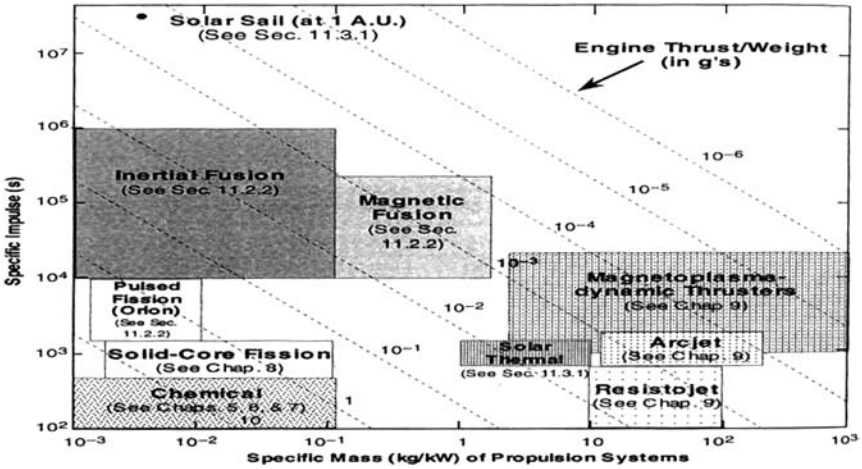


Fig. 2 Performance of propulsion systems. Fission rockets have better specific impulse than chemical rockets at equivalent thrust-to-weight and specific mass ratios [17].

advantage over chemical systems because we can choose the propellant with the lowest molecular mass. Large quantities of thermal energy can still be imparted to get high exit velocity without worrying about the combustion properties, as is instead the case of chemical rocket engines.

Nuclear-fission rockets can have a specific impulse double that of chemical rockets. To get this advantage, a lightweight gas, such as hydrogen, is usually chosen as the reactor coolant/propellant, but we can use higher-density propellants, such as methane, whenever storage volume is limited. Figure 2 shows fission rockets can produce high thrust levels (low specific mass) with good specific impulse. Having high specific impulse, high thrust, and high thrust-to-weight ratio is a tremendous advantage for a propulsion system. Systems with high specific impulse but high specific mass and low thrust, such as those using electric propulsion, require trip times of hundreds of days to go from low Earth orbit (LEO) to geosynchronous-Earth orbit (GEO). But nuclear-propulsion systems need only hours. Interplanetary missions, such as a manned mission to Mars, would be likewise shortened.

Taken as an example of the potential of NTRs, a manned mission to Mars has various ΔV requirements. A long mission (that is, hundreds of days) requires a ΔV of approximately 3.5 km/s from LEO to Mars. A 40-day transfer from LEO to Mars requires 85 km/s. Note that, for a longer-duration mission, galactic radiation makes such space travel hazardous. In addition, humans suffer physical and mental difficulties in a constant free-fall environment (microgravity), and so we must achieve the shortest possible trip time. Table 1 assesses total radiation exposure in relation to trip time for two hypothetical Mars missions, using chemical and nuclear propulsion. For both cases, the stay time on Mars's surface is 30 days. But because of the shorter length of the mission, reduced radiation exposure is actually achieved by using nuclear propulsion, as compared with a mission using a conventional chemical rocket.

Table 1 Comparison of radiation exposure for nuclear and chemical systems[a]

Radiation source	433-Day Mars mission using a chemical rocket	316-Day Mars mission using a nuclear rocket
Van Allen belts	2 rem[b]	2 rem
Mars surface	1	1
Galactic radiation	31	22
Solar flares	26	15
Reactor	——	5
Mission total	60 rem	45 rem

[a]Nuclear systems can reduce overall radiation exposure by reducing the trip duration. This shorter trip time occurs because the high specific impulse of nuclear rockets allows higher ΔV for a given mission [18].
[b]A rem (from roentgen equivalent man) is a measure of radiation dosage based on the type of radiation an individual receives.

Nuclear thermal propulsion systems can use any working fluid as a propellant and reactor coolant (e.g., see [19]). Hydrogen, ammonia, methane, octane, carbon dioxide, water, and nitrogen have been considered as propellants. Because their molecular mass is higher, specific impulse is lower than for hydrogen. However, these working fluids can offer certain advantages for long missions, in which storability is an issue, or for interplanetary missions, in which propellants could be acquired (mined or synthesized) from a planet, moon, or asteroid.

II. System Configuration and Operation

A nuclear thermal rocket's configuration is similar to that of a chemical system, except that it requires a nuclear reactor as a heat source. Figure 3 shows a typical nuclear propulsion system, which consists of a propellant tank, shielding, feed system (configured depending on type of engine cycle), reactor, and nozzle. The tank and feed system are very similar to those in chemical systems. The liquid chemical rocket requires a combination of oxidizer and fuel (each with its own feed system) for combustion to a hot gas. The nuclear rocket works the same way, except that only one propellant feeds through the core, where the reactor heats it to produce thrust. The main difference is engine control because the exhaust gas thermodynamic conditions are coupled to the reactor and its unique requirements: unlike chemical rockets, reactor operation (and its safeguards) need sophisticated and continuous active control [20].

Figure 4 shows a schematic of a reactor for nuclear propulsion. The reactor is complicated by various components needed to keep the fission reaction under control (for details see [21, 22]). The major reactor components that differ from those of a chemical system are discussed briefly next: the neutron reflector, the pressure vessel, the moderator, the fuel element (rod, or pin) assembly, and the fuel control rods.

1) **Radial reflector**—On the outside of the core is a radial reflector. To have a controlled chain reaction (that is, steady-state operation, when neutrons produced equal neutrons used) and to reduce the size of the core, a reflector made of a material with particular nuclear properties prevents neutrons produced in the chain

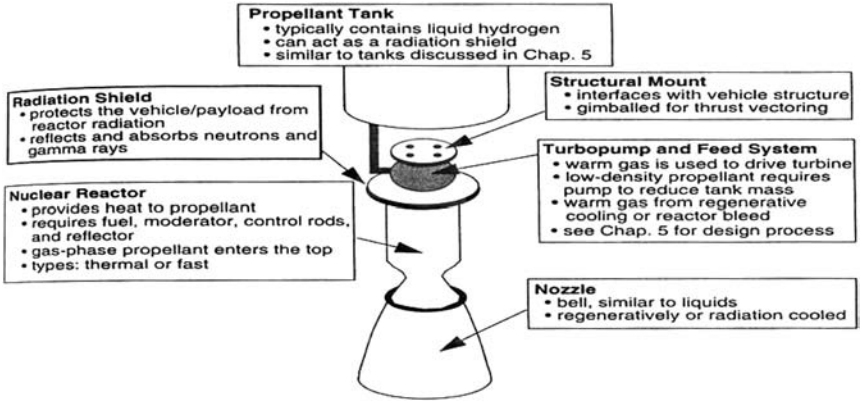


Fig. 3 Schematic of a nuclear thermal rocket. A NTR operates as a monopropellant liquid rocket system, with the nuclear reactor as a heat source.

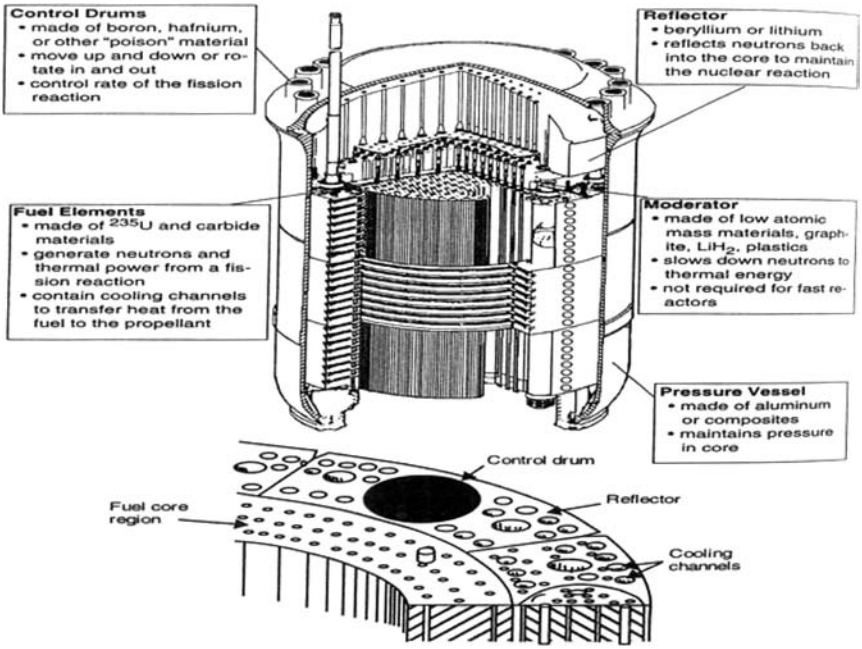


Fig. 4 Schematic of a reactor in a nuclear propulsion system. All elements work together to control the neutron population and the energy level of individual neutrons. This control makes sure we have a reliable source of heat energy [17].

reaction from escaping the reactor, that is, "reflects" neutrons back into the core. Neutrons must be prevented from leaking out of the system in a large enough quantity to destroy the steady-state neutron balance: that would cause the reactor to shut itself down. The reflector is usually made of beryllium.

2) **Reactor pressure vessel**—The reactor vessel is needed to maintain reactor pressure (3 to 8 MPa). It is typically made of aluminum or composite material to withstand the high radiation, heat flux, and pressure from the reactor. The vessel might require cooling to withstand the heat flux in some reactor designs.

3) **Moderator**—Reactors are said to be either thermal or fast, depending on the neutron energy with which most of the fissions take place. In a *thermal* reactor, most of the fissions are caused by neutrons having an energy less than 1 eV. Most neutrons produced from a nuclear-fission reaction have energies much higher than 1 eV, up to 10–15 MeV. To slow the neutrons down, a so-called moderator assembly, made of a material with a low atomic mass (beryllium, plastics, lithium hydride, graphite) is used. In a *fast* reactor, the energy range in which most of the fissions take place is much wider, extending from 100 keV to the top range of the fission spectrum (15 MeV). To build a fast reactor, one should avoid light elements (moderating materials) and have no moderator. Some reactors effectively mix moderating material with fuel material to limit the system size and mass.

4) **Fuel-element assembly**—The fuel-element assembly (sometimes referred to as the rod or pin) contains the fuel and propellant/coolant flow channels. The fuel produces the heat to be transferred to the propellant flowing past the fuel. Different configurations of a fuel element can take advantage of surface area to better transfer heat and to make sure some kind of barrier contains the fission products. The reflector, control rods, and moderator are placed around the fuel to maintain the proper flow and control of neutrons.

5) **Control rods or drums**—The control rods or drums contain certain materials (usually boron) that absorb neutrons, to decrease the neutron population. The rods control the reaction rate and can shut the reactor down. This material is also known as a "poison" because it lowers the number of fission reactions when inserted in the core. The rods are dispersed around the core to ensure the neutron population can be properly controlled and adjusted to meet engine power level requirements. The control rods can be inserted into the reactor axially or rotated. For the axial insertion, the depth of the rods controls the amount of neutrons captured. For the rotation insertion, one side of the rod contains boron, whereas the other side contains beryllium. When the boron side is rotated into place, neutrons are absorbed. When the beryllium side is rotated, neutrons are reflected back into the core.

6) **Coolant flow paths**—Coolant piping cools components while doubling as the propellant gas needed to generate thrust from the reactor. To avoid thermal shocking and boiling issues, propellant needs to be completely vaporized before it enters the reactor core.

Because a basic understanding of most of the components associated with the reactor has been achieved, the operation of the core can be examined. The engine core of a spacecraft sits inside the launcher on the launchpad with the control poison fully inserted. With the control poison in this position, the core produces no power and has negligible radioactivity (only the natural radioactivity of the fuel). This condition allows workers to handle the reactor with no protective

shielding. Once in orbit, when the spacecraft mission requires thrust, the control poison is withdrawn (either lifted vertically or rotated outward), and a neutron source is put into the reactor to provide the initial neutrons for fissioning. With the control poison now withdrawn, fissioning causes the thermal power to increase exponentially to the desired power level. When the poison is removed, the feed system immediately supplies gas to the core for cooling and thrust production. When the reactor reaches the desired full-power level, the position of the control poison is adjusted to keep the power at a steady state (number of neutrons produced equal number of neutrons used). This is a delicate balance.

At the mission's end, the control poisons are inserted back into the core, and the power decays exponentially. However, the reactor still needs to cool down for some time, depending on how long the core was at full power, and it might or might not need active cooling. This cooling might be necessary because of delayed neutrons and residual heat production that result from radioactive decay of byproducts from the fission process ("fission products," that is, *new* nuclear species formed by the fissioning fuel). This cooling-down process is not exponential, but obeys a somewhat slower power law (see [23]).

III. Nuclear-Thermal-Rocket Concepts

The following section briefly discusses nuclear thermal propulsion systems that have been developed or proposed for propulsion applications in space. For lack of detailed information on English on Russian work, the focus is on U.S. activities. Many alternative concepts are theoretically possible (18 concepts were proposed by NASA in the past [17]), but the following are the most likely candidates for near- to midterm missions.

A. NERVA Derivative or Enabler

The NERVA (Nuclear Engine for Rocket Vehicle Applications) derivative is a modified design of the reactor designed during the ROVER/NERVA program (NERVA-1); see [1–3] for details. Briefly, the NERVA program started in 1947 under U.S. Air Force and Atomic Energy Commission sponsorship with the purpose to design a reactor that could propel intercontinental ballistic missiles. In 1958, NASA took control of NERVA as part of their space-exploration program. NASA, with LASL help, ran the R&D program until 1972, with LASL developing reactors and fuels, and NASA funding experimental engine construction by Westinghouse and Aerojet, using LASL-developed reactors. (A recent report on the work done at Aerojet is in [24].) Achievements include 28 full-power tests with restarts; up to 30-min test duration, for a 90-min total life; reactors ranging from 300 to 200,000 MW; design of a hydrogen flow system; development of a way to contain affluents (propellant exhaust gases) for safe ground testing (used only in later tests); development of a high-temperature fuel (5500°F); solution to the problem of fuel erosion from hot hydrogen; specific impulse as high as 835 s; thrust as high as 890,000 N; and thrust-to-weight ratios of 3 to 4.

In all, 23 tests were conducted at the Nevada test site, the Nuclear Rocket Development Station (NRDS). Figure 5 shows one of the NERVA engine reactors built by Westinghouse undergoing testing.



Fig. 5 Test of the XE nuclear rocket engine at the Engine Test Stand (ETS) at the Nevada test site. The engine had a thrust of 75,000 lb and was down firing mounted under a 75,000-gal tank of liquid hydrogen. The exhaust fired down into a "steam trench." The ETS was constructed only of aluminum to reduce the amount of long-lived radioactivity in structural materials induced by the neutrons coming from the engine.

Born from the need for carrying the heavy thermonuclear warhead of the early 1950s, the U.S. nuclear thermal rocket program found itself without a military mission as soon as smaller warheads and larger intercontinental ballistic missile (ICBM) came on line. Reorienting its goals toward space applications under NASA management took time, whereas budget limitations at the time of the Vietnam war, and preliminary studies on what was to become the shuttle, suggested in the early 1970s that NTR were no longer needed and in any case too expensive [3]. This spelled the demise of high-power NTR in the United States, while work continued in the Soviet Union, where two engines, RD 0410 and RD 0411, were in fact developed and tested. However, after the United States reduced the scope and magnitude of its NTR work, even in the Soviet Union funding and activities declined; for instance, see [7, 8].

At this time the only full-size NTR experience is therefore based on the NERVA-derived U.S. engines (the NRX family built by Westinghouse and Aerojet) and on the two soviet union engines, for which detailed information (still in Russian) is slowly becoming available.

Table 2, from the report whose cover is shown in Fig. 6, is a summary of the main accomplishments near the end of the ROVER program. A concise account of their problems and technical developments is reported in [2], whereas [3] is a day-to-day account of the history and politics of ROVER. The technical reports concerning the rocket prototypes developed under NERVA by industry is in [25].

The reactor developed for the NERVA program in the United States contains approximately 300 hexagonally shaped, graphite fuel elements in which uranium-carbide fuel particles coated with pyrocarbon are evenly distributed (see Fig. 7). The fuel particles provide the heat source while the graphite matrix serves both as the moderator and as structural component of the fuel elements. Niobium-carbide or zirconium-carbide coatings protect the surfaces of the fuel elements from the

Table 2 NERVA: Reactor and engine systems tests

Name	Date
Phoebus 1B (one-power test)	Feb. 1967
Phoebus 2 (cold-flow tests)	July 1967–Aug. 1967
NRX-A6 (one-power test)[a]	Dec. 1967
XECF (cold-flow tests)	Feb. 1968–April 1968
Phoebus-2A (three-power tests)	Jun. 1968–July 1968
Pewee-1 (two power tests)	Nov. 1968–Dec. 1968
XE (28 starts)	Dec. 1968–Aug. 1969

[a]Operated 60 min at full power (1,100 MW).

hydrogen propellant. Twelve rotary drums in the radial reflector control the core. The drums have boron plates that rotate in toward the core or out toward the perimeter, as required, to absorb and control the neutron population. A shield containing boron carbide, aluminum, and titanium hydride is at the top of the reactor. This shield limits nuclear-radiation heating of the engine assembly's nonnuclear components, including the propellant in the storage tank.

A recent description of NERVA-derived engine (including its possible cycles) is in [26, 27]. In recent years the so-called bimodal NTR has been the subject of

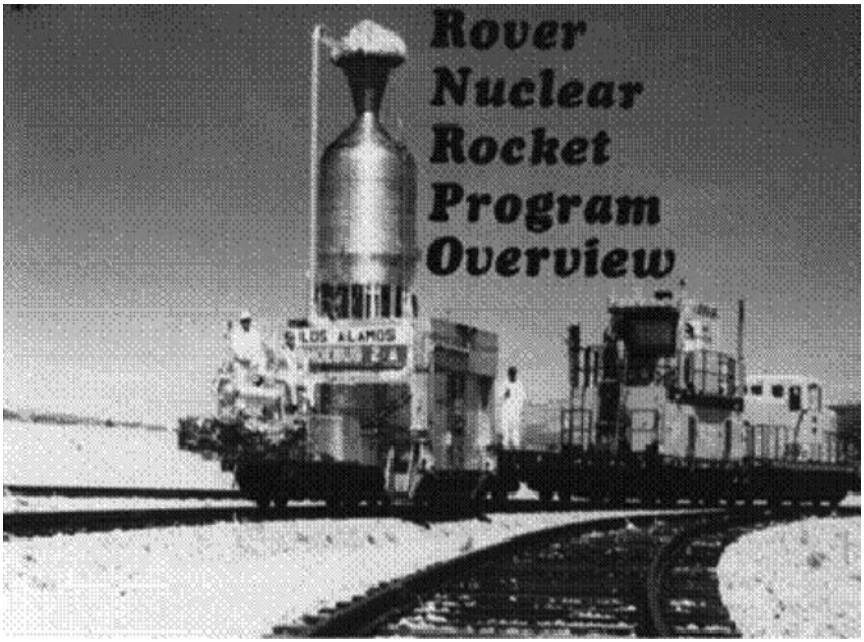
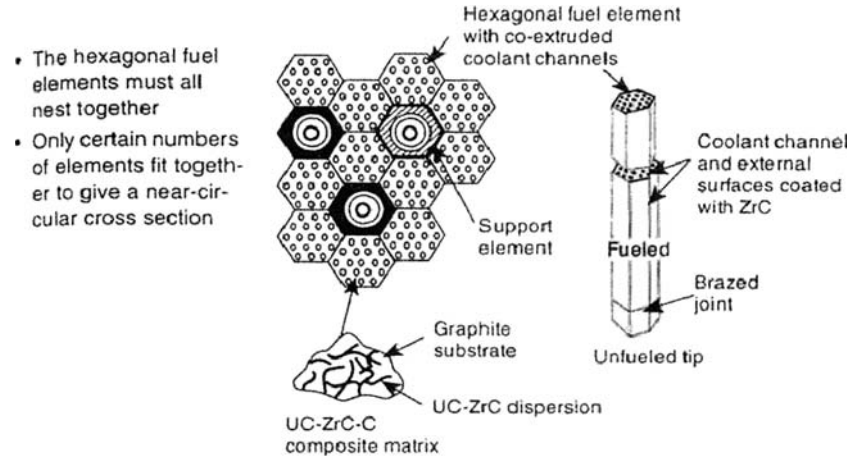


Fig. 6 Handling of experimental rocket reactors at the NRDS in Nevada was accomplished by rail. Here the reactor XECF is being moved to the static test site.



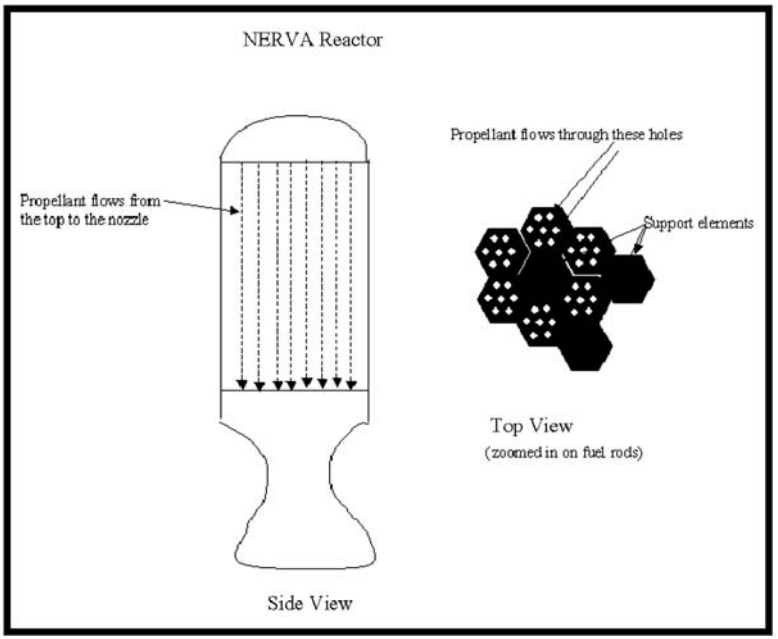


Fig. 7 NERVA fuel element. This figure shows how individual fuel elements are configured and nested together with additional elements for structural support [17].

many studies at NASA Glenn Research Center by S.K. Borowski and his coworkers. Bimodal means that the NTR doubles also as a high-power supply, a key feature for planetary exploration, for instance, of the moon, and for manned Mars missions [28]. In fact, the power of a NTR might be partitioned between the NTR proper and a generator feeding and electric thruster, as in other hybrid concepts, but with

the added benefit of having a choice between large thrust at I_{sp} of order 900 s and much lower thrust with I_{sp} that nowadays might be close to 10,000 s (see Chapter 3 in this book).

B. Particle-Bed Reactor

The particle-bed reactor (PBR) (USA) (see Fig. 8) is a reactor concept originally developed by the U.S. Department of Defense/U.S. Air Force in the 1980s and designed to provide a core with high power density (by increasing the propellant temperature and the fuel surface area). The goal was a nuclear rocket engine with high (that is, higher than NERVA) thrust-to-weight ratio. The core consists of a

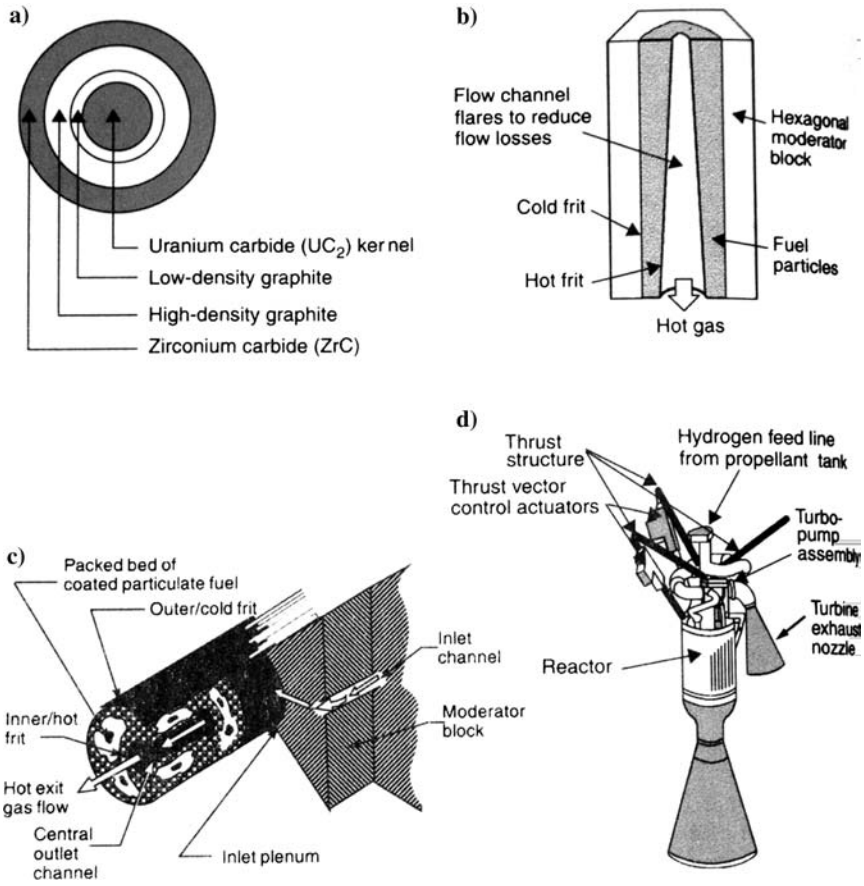


Fig. 8 Configuration of a particle-bed reactor. This illustration shows the details of a) a fuel particle; b) a fuel element; c) flow through the moderator block to the fuel bed; and d) an assembled engine [17] (Maise, G., and Ludwig, H., private communication, Brookhaven National Lab., 1995).

number of fuel particles packed in a bed and surrounded by hexagonal moderator blocks arrayed in a cylindrical assembly (Fig. 8) [29]. Its distinguishing feature is that the hydrogen propellant directly cools small (200–500-mm diam), coated, particulate fuel spheres. The uranium-carbide fuel (coated with graphite buffer layers and an outer layer of zirconium hydride) is packed between two concentric, porous cylinders called frits, which confine the fuel but allow the flow of coolant. These small, annular fuel elements rest in a cylindrical moderator block. Candidate materials for the moderator block are beryllium or lithium hydride. Coolant flow moves radially inward through the cold frit, the packed bed, and the hot frit. At the same time, it moves axially out through the inner annular channel and then expands through the nozzle to produce thrust.

The PBR advantages come from its high specific impulse, thrust, and thrust-to-weight ratio (~40:1). This performance enables missions that the NERVA derivative, with its lower thrust-to-weight (~5:1), cannot do. The PBR has undergone several small proof-of-concept tests but has not had a full-scale engine test. Because the PBR and NERVA have had the most money invested in them, they represent near-term options.

Most of the PBR development was done as part of the U.S. Air Force Space Nuclear Thermal Propulsion program (SNTP). This program lasted until 1993, with a budget of about $40 million per year. Its goal was to design a particle-bed reactor for various U.S. Air Force missions. It ended having achieved the following: fuel tests to temperatures as high as 3000 K (NERVA only reached 2650 K); nuclear tests of single fuel elements; criticality experiments for a prototype 1000-MW core; tests of thermal hydraulics in multiple fuel elements at high power densities (up to 40 MW/liter, as compared to about 2 MW/liter for NERVA); various mission designs (e.g., detailed analysis of a stage for a Mars mission); and validation of computer codes to simulate reactor physics.

The PBR program under SNTP envisaged a NTR of 220-KN thrust and weighing only 800 kg, including turbopumps and auxiliaries (see http: //www.nuclearspace.com/A_HEADNA.htm for an extensive description). This low weight estimate is the result of the flow topology of PBR, watch is multidimensional in comparison with that in more conventional fuel pins. Some of the scientists working on PBR developed further this concept into a compact NTR engine using the PBR as reactor concept. This NTR is called the miniature reactor engine (MITEE). MITEE can be assembled as a cluster of individual modules, each of about 50-cm diameter, with thermal power density at least 10 MW/liter. Figure 9 shows the potential range of MITEE applications for space propulsion.

The MITEE concept has been presented at space propulsion meetings, for instance, see [30–33]. Recently an even smaller and compact concept has been developed for fast, unmanned (robotic) missions that has been called Mini-MITEE, and that could be the prototype of future, larger NTR [34].

C. CERMET

The U.S. Air Force–developed CERMET-core nuclear rocket (see Fig. 10) uses a fast-fissioning neutron spectrum (that is, greater than 1 MeV) compared to thermal reactors that slow down neutrons to fission energies of less than 1eV. Therefore, it does not need a moderator. The CERMET has a lower thrust to weight than the

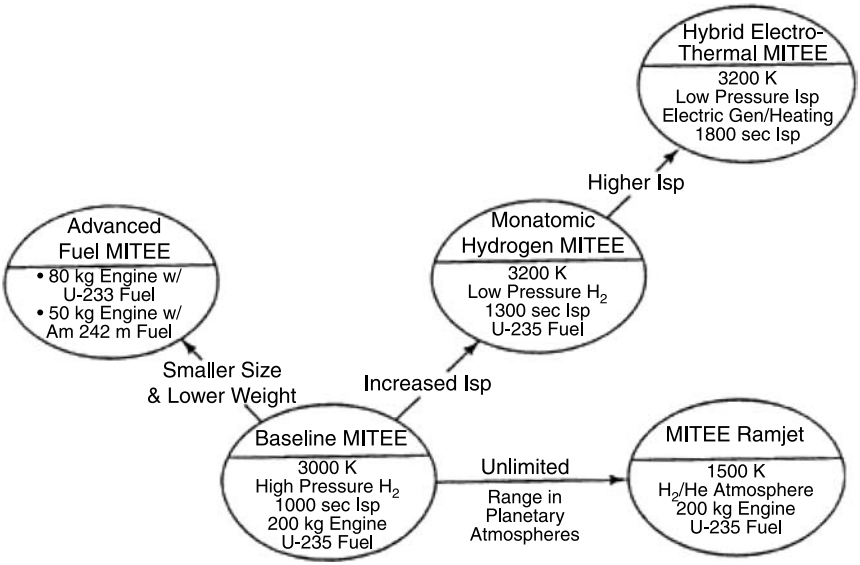


Fig. 9 MITEE family for space propulsion (http://www.nuclearspace.com/A_HEADNA.htm).

particle bed and has not been tested as extensively as the NERVA-type engines. Fuel testing has shown that the CERMET-type fuel is much more robust than that for either NERVA or PBR. This feature makes CERMET attractive for applications such as a reusable orbital-transfer vehicle (OTV), which might need as many as 50 "burns."

The reactor consists of hexagonal fuel elements similar to those in the NERVA design, except that the fuel is made of uranium-dioxide (urania, UO_2) particles embedded in a tungsten or tungsten/rhenium matrix. The advantages of CERMET fuel are its potential for very long operating life (more than 40 h), ability to restart, handling of high temperature cycling, and greater compatibility between the fuel and hydrogen coolant, resulting in high fuel integrity and retention of fission products. However, the metal matrix can increase system mass because of competition for neutron absorption in uranium and tungsten. By using an axial, two-zone fuel element, system mass can be reduced. In this two-zone concept, the fuel loading in the upper (low-temperature) half of the core uses a molybdenum/urania matrix configuration. The lower (high-temperature) part of the core uses a tungsten-rhenium/urania matrix configuration. This concept reduces the total mass of the reactor system and gives it a thrust-to-weight ratio of 5.3:1—slightly better than NERVA. The system, shown in Fig. 10, consists of a CERMET core surrounded by a cooled pressure-containment shell. A neutron reflector and reactivity-control assembly mounts to the outside of the pressure vessel. So far, tests of the CERMET have checked only the fuel—successfully tested up to 1900 K for 10,000 h. The CERMET technology can be applied to any space nuclear reactor and combined with NERVA-derivatives, enabling much longer life reactors than

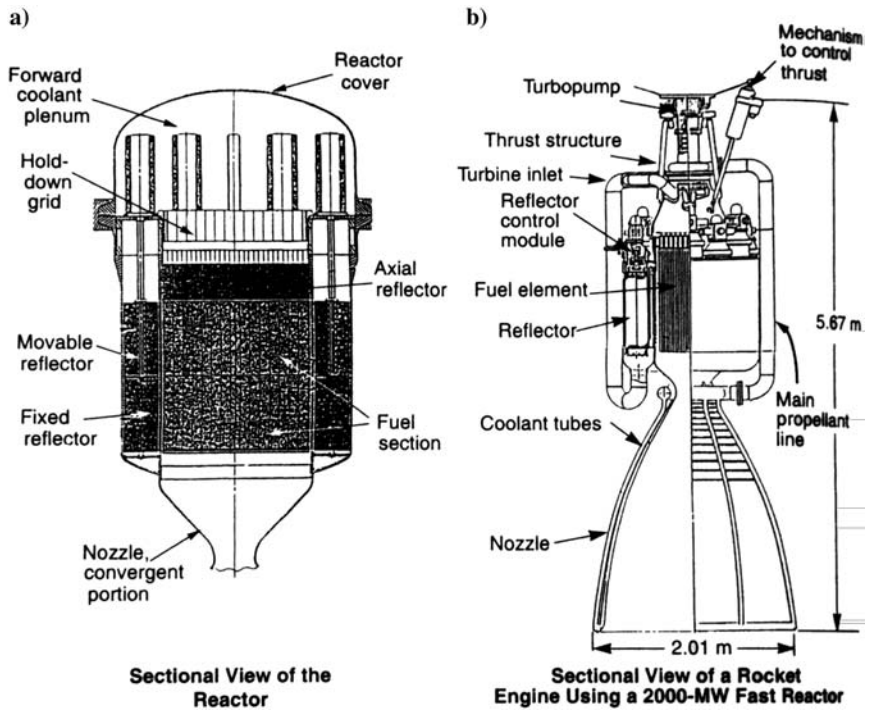


Fig. 10 Configuration of the CERMET Engine a) showing details of the reactor and b) showing a split view of the engine configuration, with interior details on the left side and exterior details on the right side [36].

those envisaged during the ROVER program. In particular, it can be the core of a bimodal, augmented NTR, as recently proposed, for instance, see [35]. This concept would offer the most flexibility and operational convenience of all NTR proposed so far.

Of the reactors discussed so far, NERVA-1 (the flight engine developed in the early 1970s) offers the lowest performance in terms of specific impulse. But it has the most money invested in it and was just ready for a demo flight before the program ended. The PBR offers the highest performance for a solid-core design. The CERMET reactor core might be a good design to pursue if reusability becomes an issue because its fuel lasts longer than other types of cores investigated. Table 3 shows the characteristics of the three engine concepts.

Other advanced concepts were studied and also partly explored using component hardware since NERVA times. Most of them are indeed studies, but should nevertheless be cited. In particular, to overcome structural limitations caused by the melting temperature of solid fuels, liquid- and gas-core fission reactors were investigated (see also Chap. 1, Sec. 1.4.1, and [12]). In the former Soviet Union a gas-core reactor, the IVG-1, was in fact partially tested. Component testing of two gas-core reactor concepts proposed took place also at the Los Alamos Scientific Laboratories (LASL) in the United States; see [23]. LASL is still continuing work in this area,

Table 3 Comparison of possible near-term concepts for reactors

Characteristics	NERVA	Particle bed	CERMET
Power, MW	1,570	1,945	2,000
Thrust, N	334.061	333.617	445.267
Propellant	H_2	H_2	H_2
Fuel element	Solid rod	Porous particle bed	Solid rod
Maximum propellant temperature, K	2361	3,200	2,507
I_{sp}, s	825	971	930
Chamber pressure, MPa	3.102	6.893	4.136
Nozzle expansion ratio	100	125	120
Engine mass, kg	10,138	1,705	9,091
Total shield mass, kg	1,590	1,590	1,590
Engine thrust/weight (no shield)	3.4	20.0	5.0

The engine using a particle-bed reactor has higher performance and is lighter than the NERVA, but NERVA is more developed [37]. CERMET is a possible fast-reactor concept that can also be reused.

albeit at a low funding level. The main issues of gas-core fission are how to ensure efficient heat transfer between fission fragments and the hydrogen propellant and how to limit leakage of the fissioning fuel. Details of these concepts can be found in the proceedings of the STAIF meetings. (These are conferences hold by the American Institute of physics every year in Albuquerque, New Mexico. Proceedings include a variety of nuclear topical areas, ranging from propulsion concepts to fuels and their metallurgy; they can be requested from the American Institute of Physics, c/o Springer at orders@springer-sbm.com, http:// proceedings.aip.org.)

D. Hybrid Nuclear Thermal/Chemical Rockets

After a suggestion by S.K. Borowski [38], joint work with Aerojet has produced a hybrid nuclear-chemical propulsion concept [liquid-oxygen augmented NTR (LANTR)]. To obtain relatively short bursts of thrust, liquid oxygen is injected downstream of the throat of a hydrogen-fed NTR. The resulting supersonic combustion between hydrogen (some of it still atomic) and oxygen boosts the engine thrust, at the expense of oxygen consumption and thus of I_{sp}; see [39–42]. Interesting applications of LANTR include liftoff from planetary bodies using in situ oxygen production, emergency maneuvering, and asteroid intercepting. The LANTR concept has been tested using as NP-ersatz a conventional liquid hydrogen rocket engine run in rich combustion mode and has demonstrated thrust can be augmented by 40–60%. A recent LANTR cycle analysis is in [26]. LANTR is, in the near term, the most promising of hybrid NTR propulsion systems because it is based on supersonic combustion technology already available. Many other hybrid cycles have been proposed, including NTR/nuclear electric. A summary is in [23].

IV. MagOrion and Mini-MagOrion

This is actually a combined NTR-electromagnetic technology that stems from the Orion project of the 1950s and 1960s. The Orion propulsion concept was

based on nuclear explosions for propelling a spacecraft. In essence, small atomic bombs were to be released and detonated sequentially aft of a large spacecraft; the plasma created by the explosion would impinge on a massive thrust plate, ablating its surface and pushing it forward. The plate was to be connected to the spacecraft by means of shock absorbers, to soften and reduce the impact of the acceleration pulses on the crew. This concept was theoretically proven viable. Its physics, in particular that of ablation, is fascinating.

The Orion concept was revisited in the 1990s, with a major change: the pushing effect of a nuclear plasma, which in the original Orion concept was driven by ablation of the thrust plate, was replaced by a Lorentz force in a superconducting (SC) ring. The force is the result of the interaction between the plasma released by a miniature atomic explosion and an applied magnetic field. Calculations indicated that I_{sp} of order 10^4 s could be obtained with a 2-km-diam ring, with a thrust/mass ratio between 0.2 to 10 [43]. This was called the MagOrion concept.

For practical reasons the superconducting material was a high-temperature SC, for example, a YBCO ceramic. However, its brittleness and the size of the ring suggested to scale down MagOrion to a smaller and more feasible concept, Mini-MagOrion, or MMO [44]. Technically, MMO is based on the following elements: an unconventional fissile fuel, that is, ^{245}Cm, with a lower critical mass than ^{239}Pu or ^{235}U; criticality reached by *impulsive* compression by a plasma Z-pinch which also moderates the energy yield per explosion; and the single large ring of MagOrion is replaced by multiple smaller coils girding a MHD nozzle.

Curium was chosen based on its neutronics, conversion fraction α (see Chapter 1), and availability. Operation of the MMO can be schematically described as follows: current is made to flow along a electrically conducting conical mylar sheet, from the periphery toward the apex, where the mylar is vaporized by the increasingly high current density and becomes plasma. This plasma pinches the nuclear fuel near the apex, compressing it impulsively so that it implodes, becomes critical and fissions. Energy yield theoretically predicted is in the 50–500-GJ range per fission event. The fuel itself is in the form of hollow ^{245}Cm spheres encapsulated by a neutron-reflecting Be layer. Upon fissioning, the ionized debris and the current flowing in the superconducting rings bracing the large, diverging B field inside the magnetic nozzle create the Lorentz force pushing the spacecraft.

The I_{sp}, as theoretically calculated at Andrews Space, the U.S. company leading this study, depends on the energy yield almost logarithmically. [43] shows the payload mass fraction achievable as a function of I_{sp}.

The MMO team examined all key aspects of this concept and found it workable, albeit with many engineering problems still waiting to be solved. A baseline concept ship, designed for a 100-ton payload, has an initial mass about 730 tons.

In summary, provided all engineering problems can be solved, MMO is definitely a futuristic but physics-wise feasible concept. The mass of the baseline vehicle mentioned would command a very high price for orbiting and assembling all of its components, but probably no higher than R&D and engineering costs. As with all advanced propulsion technologies for interplanetary travel, the crucial cost item is reaching LEO; however, once in orbit MMO has the potential of reducing drastically both mass consumption and travel time because thrust and I_{sp} are equally large in comparison with other more conventional propulsion concepts.

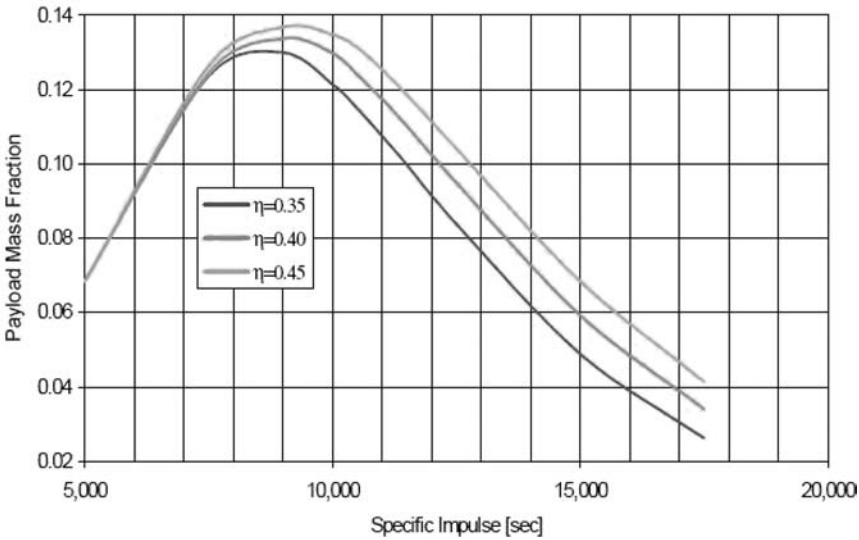


Fig. 11 Specific impulse vs payload mass fraction for the MiniMagOrion concept [43].

V. Safety

Nuclear energy is an unique discovery in that safety concerns were addressed from the very beginning of the discovery. Safety is paramount in any nuclear program developed for space. The U.S. Navy Naval Reactor development program has shown that nuclear energy can be developed with safety as a concern and a zero nuclear accident record. One of the attractive features of a nuclear space program is that the reactor is inert and can be handled like any typical payload (as long as U^{235} is the fuel) until it is turned on in space. It represents a zero radiological hazard until operation, and then the exposure is based upon the amount of time it operates.

There are a few myths on the use of a nuclear rocket in space. There is no United Nations treaty violation for nuclear power or propulsion applications in space, just for nuclear weapons (see Chapter 6 by Lenard in this book). Radioisotope thermo-ionic generators, or RTG, have flown Plutonium-238 safely for many missions. Despite being toxic both chemically and because of its ionizing radiation, plutonium is far from being "the most toxic substance on Earth" or so hazardous that "a speck can kill." There are substances in daily use that, per unit of mass, have equal or greater chemical toxicity (e.g., arsenic, cyanide, caffeine) and radiotoxicity (e.g., smoke detectors, using the alpha particles-emitting ^{241}Am, or Americium-241, isotope). Isotopes of plutonium such as ^{238}Pu characteristically give off short-range alpha particles, that is, helium nuclei that usually travel no farther than about three inches in air and are stopped by aluminum foil, but that would be deadly if ingested. In fact, there are three principal routes by which plutonium can reach human beings: ingestion (hardly common, and thus not a significant hazard), contamination of open wounds, and inhalation.

Table 4 Acute radiation effects from whole-body exposure to gamma radiation[a]

Level, rem	Acute irradiation somatic effect
15–25	Subtle reductions in white-blood-cell counts, not generally apparent from exposure for one person unless a blood sample was taken before the exposure
50	Reduction in white-blood-cell count after exposure; the count returns to normal in a few weeks
75	10% chance of nausea
100	10% chance of temporary hair loss
200	90% chance of radiation sickness; moderate depression of white-blood-cell fractions
400–500	50% chance of death within 30 days without extensive medical treatment
>600	Lethal to most people in 3 to 30 days; even with extensive medical treatment; death is likely within a few months from infection and hemorrhage
>10,000	Lethal within 24 hours from damage to central nervous system

[a]As the radiation dose increases, the biological effect increases correspondingly. These somatic effects appear after exposure to acute doses over short times rather than over longer periods, during which the cells can repair some damage.

Workers at U.S. nuclear weapons facilities have occasionally come in contact with or inhaled plutonium. Intensive health checks of these people have revealed no serious consequences.

A nuclear reactor in space requires a radiation shield to protect the crew, payload, or other spacecraft equipment sensitive to radiation. The unit that describes the damaging effects of radiation is the rem (absorbed radiation dose × quality factor).

The absorbed radiation dose (see Appendix in this book) is traditionally defined in terms of the rad (radiation absorbed dose). One rad equals the amount of radiation required to cause the absorption of 100 ergs (1 joule = 10^7 ergs) per gram of material. Therefore, the rad is the amount of energy imparted to a component or person. Experimental data have shown that different types of radiation (wavelength or particle energy) produce different effects: the quality factor accounts for the effect of a particular type of radiation. Table 4 shows the biological consequences

Table 5 Allowable limits for skin dosage, as agreed by the U.S. National Committee on Radiation Protection and Measurement

Criteria	General public	Occupational workers	Astronauts
30-day limit	0.04 rem	0.4 rem	150 rem
Annual limit	0.50 rem	5 rem	300 rem
Career limit	N/A	5 × (age in years – 18) rem	600 rem
Accident limit	25–100 rem	N/A	
Acute limit	N/A	N/A	10 rem

of acute, short-term radiation effects from whole-body exposure to gamma radiation.

To put these numbers into context, here are some typical exposures:

- Natural radioactive material in the bones: 0.034 rem/year
- Flight in an aircraft: 0.001 rem/h at a 9-km altitude
- Chest x ray (lung dose): 0.01 rem
- Living one year in Houston, Texas: 0.25 rem
- Living one year in Denver, Colorado: 0.35 rem (higher elevation allows more cosmic radiation)
- Working in a nuclear power plant for 1 year: less than 0.5 rem
- Skylab astronauts on 84-day mission: 18 rem
- 90-day space station mission: 16 rem (NASA estimate)
- Van Allen belts: 16 rem/year
- Cosmic radiation outside of the Van Allen belts: 19 rem/year
- A single solar flare with moderate energy protons: 303 rem/year
- A properly shielded nuclear space engine: 10 rem/year

In this context, Table 5 shows allowable skin-radiation dosages, as given by the U.S. National Committee on Radiation Protection and Measurement.

To limit exposure and radiation doses, a reactor shield must surround the reactor. Propellant itself (e.g., liquid hydrogen) can be part of the shield. Many factors influence the geometry, composition, and mass of the radiation shield, including size and nature of the power source, type of radiation, configuration of the spacecraft or platform and its payload (radiation flux level decreases by a factor of $1/\text{distance}^2$ from the radiation source), generic operational procedures and requirements for the mission, length of the mission, and total permitted levels of radiation dosage.

As one can surmise, the key to reducing radiation exposure (from space sources as well as the spacecraft reactor) is in practice to *limit mission time*. As a consequence, the key is to have a high-power propulsion system (e.g., like that of a nuclear thermal rocket) that can get the payload and crew to destination in the fastest possible way.

VI. Conclusions

In 2005 U.S. President Bush signed into law a $16.2 billion budget for NASA, an increase of about $822 million from 2004. This last was a package funding the entire Project Prometheus program at $430 million and providing $10 million for nuclear thermal propulsion to be studied at the Marshall Space Flight Center. In Greek mythology, Prometheus was the wisest of the Titans; he gave the gift of fire to humankind (the name Prometheus means in Greek "forethought"). The goal of Prometheus was to develop plans for an ambitious mission to orbit three planet-sized moons of Jupiter—Callisto, Ganymede, and Europa—which might harbor vast oceans beneath their icy surfaces. The mission, the Jupiter Icy Moons Orbiter (JIMO) would orbit each of these moons for extensive investigations of their makeup, their history and their potential for sustaining life. In fact, the joint NASA–ESA Galileo spacecraft found evidence for these subsurface oceans, a finding that ranks among the major scientific discoveries of the Space Age.

We hope that the ideas considered in this chapter will reinforce the case for nuclear propulsion, in particular nuclear thermal propulsion, and support the revival of this technology.

References

[1] Gunn, S., "Nuclear Propulsion—an Historical Perspective," *Space Policy*, Vol. 17, No. 4, 2001, pp. 291–298.

[2] Gunn, S. V., and Ehresman, C. M., "The Space Propulsion Technology Base Established Four Decades Ago for the Thermal Nuclear Rocket Is Ready for Current Applications," AIAA Paper 2003-4590, July 2003.

[3] Dewar, J. A. *To the End of the Solar System: The Story of the Nuclear Rocket*, The Univ. Press of Kentucky, Lexington, KY, 2004.

[4] Goldin, A. Ya., Koroteev, A. A., Semyonov, V. F., Konopatov, A. D., Pavshuk, V. A., and Ponomarev-Stepnoy, "Development of Nuclear Rocket Engines in the USSR," paper presented at the AIAA/NASA/OAI Conference on Advanced SEI Technologies, Sept. 4–6, 1991.

[5] Rachuk, V. S., Belogurov, A. I., Grigorenko, L. N., and Mamontov, Y. I., "Russian Investigations in the Area of Nuclear Rocket Engines (NRE) (NRE) Research International Programs," 5th International Symposium on Propulsion for Space Transportation, 22–24 May, Paris, 1996.

[6] Ponomarev-Stepnoy, N. N., Talyzin, V. M., Pavshuk, V. A., Putko, V. Ya., Konovalov, V. A., Raskach, F. L., Ulasevich, V. K., Smetannukov, V. P., Kolganov, V. D., Fedik, I. I., D'yakov, Ye. K., Mogil'ny, I. A., Rachuk, V. S., and Mamontov, Yu. I., "Rabotyi po Otiechiestvennogo ARD," *Atomic Energy*, Vol. 86, No. 4, 1999, pp. 296–302 (in Russian).

[7] Demyanko, Yu. G., Koniukov, G. V., Koroteev, A. S., Kuz'min, E. P., and Pavel'ev, A. A. *Nuclear Rocket Engines*, Norma Inform Publisher, Moscow, 2001 (in Russian).

[8] Koniukov, G. V., Petrov, A. I., Popov, S. A., Rachuk, V. S., Belogurov, Y. I., Mamontov, Yu. I., Fedik, I. I., D'yakov, Ye. K., Mogil'ny, I. A., Konovalov, V. A., Raskach, F. L., and Zakarkin, I. I., "Prototype of Atomic Rocket- IRGIT Reactor," *Atomic Energy*, Vol. 97, No. 3, 2004, pp. 173–177 (in Russian).

[9] Bussard, R. W., and DeLauer, R. D., *Nuclear Rocket Propulsion,* McGraw–Hill, New York, 1958.

[10] Hill, P. G., and Peterson, C. R., *Mechanics and Thermodynamics of Propulsion*, Addison–Wesley, Reading, MA, 1970, Chap. 15.

[11] Lawrence, T. J., Witter, J. K., and Humble, R. W., "Nuclear Rocket Propulsion Systems," *Space Propulsion Analysis and Design*, edited by R. W. Humble, G. N. Henry, and W. J. Larson, McGraw–Hill, New York, 1995, Chap. 8.

[12] Koroteev, A. S. (ed.), *Rocket Engines and Powerplants Based on Gas-Core Nuclear Reactor*, Mashinostroenie, Moscow, 2002 (in Russian).

[13] Sublette, C., "Nuclear Weapons Frequently Asked Questions – V. 2.18," 1999, http://www.nuclearweaponarchive.org/Nwfaq/Nfqa6.html.

[14] Drake, M. K., "Data Formats and Procedures for the ENDF Neutron Cross Section Library. BNL-50274 (T-601)," Brookhaven National Lab., Brookhaven, NY, June, 1970.

[15] "Monte Carlo Neutron/Photon Transport Code," Los Alamos National Lab., Los Alamos, NM, 1986.

[16] Angelo, J., and Buden, D., *Space Nuclear Power*, Krieger, Malabar, FL, 1985.
[17] "NASA/DOD/DOE Nuclear Thermal Propulsion Workshop Notebook," NASA Lewis Research Center, Cleveland, OH, April 1993. Also reported in *Space Propulsion Analysis and Design*, edited by R. W. Humble, G. N. Henry and W. J. Larson, McGraw-Hill, New York, 1995, p. 446.
[18] Czysz, P. A., and Bruno, C., *Future Spacecraft Propulsion Systems*, Springer-Praxis, London, Sec. 7.3, 2007.
[19] Benedict, M., and Pigford, T. H. *Nuclear Chemical Engineering*, McGraw–Hill, New York, 1957.
[20] Witter, J. K., "Modeling for the Simulation and Control of Nuclear Reactor Rocket Systems," Ph.D. Dissertation, Department of Mechanical Aerospace and Nuclear Engineering, Massachusetts Inst. of Technology, Boston, MA, April, 1993.
[21] Henry, A. F., *Nuclear Reactor Analysis*, MIT Press, Boston, MA, 1986, Chap 1–3.
[22] Knief, R. A., *Nuclear Engineering: Theory and Technology of Nuclear Power*, Hemisphere, Washington, D.C., 1992, Chap. 1–4.
[23] Czysz, P. A., and Bruno, C., *Future Spacecraft Propulsion Systems*, Springer-Praxis, London, 2006, Chap. 7.
[24] Bulman, M., "Aerojet's NERVA Engine Program: The Real Facts and Lessons," *Proceedings of the STAIF-2006*, edited by M. S. El-Genk, Conference Proceedings Vol. 813, American Inst of Physics, available from orders@springer-ny.com.
[25] "Technical Summary Report of the NERVA Program," Vol. I–VI, Westinghouse Astronuclear Lab., Publication WANL TNR-230, Pittsburgh, PA, July 14, 1972.
[26] Fusselman, S. P., Borowski, S. K., Frye, P. E., Gunn, S. V., and Morrison, C. Q., "NERVA-Derived Concept for a Bimodal Nuclear Thermal Rocket," *Space Technology and Applications International Forum (STAIF) 2005*, edited by M. S. El-Genk, Conference Proceedings Vol. 746, American Inst. of Physics, Melville, NY, 2005, p. 512.
[27] Fittje, J. E., and Buehrle, R. J, "Conceptual Engine System Design for NERVA Derived 66.7kN and 111.2kN Thrust Nuclear Thermal Rockets," *Space Technology and Applications International Forum (STAIF) 2006*, edited by M. S. El-Genk, Conference Proceedings Vol. 813, American Inst. of Physics, Melville, NY, 2006, available from orders@springer-ny.com.
[28] Borowski, S. K., Packard, T. W., and McCurdy, D. R., "Crewed Orbiter/Moon Survey Mission to Mars Using 'Bimodal' NTR Propulsion," *Proceedings of the STAIF-2006*, edited by M. S. El-Genk Conference Proceedings Vol. 813, American Inst. of Physics, available from orders@springer-ny.com.
[29] Ludewig, H., "Summary of Particle Bed Reactor Designs for the Space Nuclear Thermal Propulsion Program," Brookhaven National Lab., Rept. BNL-52408, Brookhaven, NY, 1993.
[30] Powell, J., Maise, G., Ludewig, H., and Todesow, M., "High-Performance Ultra-Light Nuclear Rockets for Near-Earth Objects Interaction Missions," *Annals of New York Academy of Science*, Vol. 822, No. 1, 1997, pp. 447–467.
[31] Powell, J., Paniagua, J., Ludewig, H., Maise, G., and Todosow, M., "MITEE: A New Nuclear Engine Concept for Ultra Fast, Lightweight Solar System Exploration Missions," *Space Technology and Applications International Forum-1998 (STAIF1998)*, edited by Mohamed S. El-Genk, Publication CP-420, American Inst. of Physics, New York, 1998, p. 1131.
[32] Powell, J., Maise, G., Paniagua, J., Ludewig, H., and Todosow, M., "The MITEE Family of Compact, Ultra Lightweight Nuclear Thermal Propulsion Engines for

Planetary Exploration Missions," International Astronautical Federation, Paper IAF-99-S.6.03, Oct. 1999.

[33] Maise, G., Powell, J. R., Paniagua, J., Ludewig, H., and Todosow, M., MITEE and SUSEE: Compact Ultra Lightweight Nuclear Thermal Propulsion Systems for Interplanetary Space Missions," International Astronautical Congress, Paper IAC-04-1AA-R.4/5.7-04, Oct. 2–4, 2004, Vancouver, Canada.

[34] Powell, J., Maise, G., and Paniagua, J., "Mini-MITEE: Ultra Small, Ultra Light NTP for Robotic Science and Manned Exploration Missions," *Space Technology and Applications International Forum (STAIF) 2006*, edited by M. S. El-Genk, Conference Proceedings Vol. 813, American Inst. of Physics, Melville, NY, 2006, available from orders@springer-ny.com, p. 879.

[35] Joyner, R., Rowland, R., and Lentati, A., "Multi-Disciplinary Analysis of CERMET Nuclear Thermal, Bimodal Nuclear Thermal, and Thrust Augmented Nuclear Thermal Propulsion for Human Exploration Missions," *Space Technology and Applications International Forum (STAIF) 2006*, edited M. S. El-Genk, Conference Proceedings Vol. 813, American Inst. of Physics, Melville, NY, 2006, available from orders@springer-ny.com.

[36] Bhattacharyya, S., et al., "CERMET Reactor Orbit Transfer Vehicle Concept," U.S. Air Force, Rept. AFAL-TR-88-033., U.S. Air Force Astronautics Lab., Edwards AFB, CA, 1988.

[37] Clark, J. S. (ed.), *An Historical Collection of Papers on Nuclear Thermal Propulsion*, AIAA Washington, D.C., 1991.

[38] Borowski, S. K., "A Revolutionary Lunar Space Transportation System Architecture Using Extraterrestrial LOX-Augmented NTR Propulsion, AIAA Paper 94-3343, July 1994.

[39] Bulman, M. J., Messitt, D. G., Neill, T. M., and Borowski, S. K., "High Area Ratio LOX-Augmented Nuclear Thermal Rocket (LANTR) Testing," AIAA Paper 2000-3897, July 2000.

[40] Bulman, M. J., Messitt, D. G., Neill, T. M., and Borowski, S. K., "High Area Ratio LOX-Augmented Nuclear Thermal Rocket (LANTR) Testing," AIAA Paper 2001-3369, July 2001.

[41] Bulman, M. J., Messitt, D. G., Neill, T. M., and Borowski, S. K., "Continued LOX-Augmented Nuclear Thermal Rocket (LANTR) Testing," AIAA Paper 2002-3650, July 2002.

[42] Bulman, M. J., Neill, T. M., and Borowski, S. K., "LANTR Engine System Integration," AIAA Paper 2004-3897, July 2004.

[43] Ewig, R., "Mini-MagOrion Program Document Final Report," Andrews Space Co., Rept. AST-MMO-P-DC-02-2594, Seattle, WA, Jan. 2003.

[44] Ewig, R., and Andrews, D., "MiniMagOrion: A Pulsed Nuclear Rocket for Crewed Solar System Exploration," AIAA Paper 2003-4525, July 2003.

Copyrighted Materials
Copyright © 2008 AIAA Retrieved from www.knovel.com

Chapter 3

Application of Ion Thrusters to High-Thrust, High-Specific-Impulse Nuclear Electric Missions

D. G. Fearn*
EP Solutions, Hampshire, England, United Kingdom

I. Introduction

DEEP-SPACE missions are characterized by the velocity increment ΔV required to accomplish them. As this parameter becomes greater, the conventional rockets necessary to achieve the stated objectives become larger and more expensive, with the result that very few missions of this kind can be mounted, even by the countries and agencies with the largest budgets.

An excellent example of this problem is provided by the initial proposal by NASA Jet Propulsion Laboratory (JPL) to send a spacecraft on a fast flyby of Pluto [1]. In this, a Titan 4 launcher aided by a Centaur upper stage was required to deliver into an interplanetary trajectory a spacecraft with total mass of only 160 kg. The payload was just 7 kg, with a power availability of 6 W, and the mission time to Pluto was 7 to 10 years. Despite this time and the high cost, with the launch vehicle priced in the range $250M to $400M in 1992, the data acquisition and scientific return would have been very limited. The flyby time over the last 100,000 km would have been only 1.7 h, and crossing the orbit of Charon, Pluto's satellite, would have taken just 30 minutes. Clearly, a cost-benefit analysis of such a mission would not produce encouraging results.

To reduce costs to affordable levels, the prime objective must be to reduce overall initial spacecraft mass, so that smaller and less expensive launch vehicles can be employed. Bearing in mind the very large values of ΔV required for the missions under consideration, and thus the dominance of the propulsion system in determining total mass, this offers the greatest scope for improvement. Indeed, this system, including the propellant, can account for 50% to 90% of the launch mass. This is the primary role of electric thrusters, which can replace chemical engines in this role with great advantage.

Copyright © 2008 by the American Institute of Aeronautics and Astronautics, Inc. All rights reserved.
*Deceased.

Thus one of the most exciting and challenging applications of electric propulsion (EP) is to the exploration of the far reaches of the solar system and, perhaps eventually, of the nearest stars. This process has begun, with the flight of NASA's Deep Space 1 (DS-1) spacecraft [2], which was propelled by a gridded ion engine (GIE) and completed an extended mission to both an asteroid and a comet. Other exciting projects are currently underway, such as ESA's SMART-1 technology demonstrator mission to the moon [3], in which a Hall-effect thruster (HET) was used to transfer the spacecraft from a geostationary transfer orbit (GTO) to lunar orbit, which was acquired during November 2004. Even more ambitious was Japan's Muses-C mission to return a sample from asteroid 1998 SF36 [4]; although partially successful, the GIE performance was excellent. This spacecraft was launched on 9 May 2003 by an M-5 rocket, and the velocity increment provided by the electric propulsion system (EPS) was about 3.7 km/s. The EPS consists of four small radio-frequency (RF) ionization GIEs, each producing a maximum thrust of 8.1 mN. However, despite these impressive successes, as the energy required increases, the mass of propellant becomes larger if present thrusters are used, resulting in a heavier spacecraft, a longer mission duration, and a higher cost. Thus large increases in specific impulse (SI), and thus in exhaust velocity, v_e are required.

This challenge has been recognized by NASA by commencing a search for completely new ways of accomplishing space travel [5]. This, the Breakthrough Propulsion Physics Programme, has examined many interesting suggestions, some involving extensions to the existing laws of physics. However, no positive results offering a near-term solution to the problem just outlined have so far emerged. It is therefore necessary, at the moment, to assume that such solutions, if any, are probably decades away from implementation. It is therefore prudent to consider these advanced missions employing extensions of existing technologies.

However, a superficial analysis of the missions in question indicates that the energy required is vastly in excess of that available from solar arrays or any other non-nuclear substitute. In addition, a large proportion of the most challenging missions involves travel to vast distances from the sun, where the solar radiation flux is very low indeed. Thus nuclear power is essential; in most recent studies, this is initially assumed to be derived from a fission reactor. It is therefore necessary to consider whether electric thrusters can consume power of the order of 100 kW to several megawatts because this level is necessary to achieve many important scientific objectives.

A cursory examination of the EP devices at present available (e.g., see [141]) reveals that only the gridded ion thruster offers a way of increasing v_e by orders of magnitude, while providing thrust levels of the order of $\mathcal{O}(1)$ N (Newton) at this power level. Such values of these parameters would be necessary for relatively economical missions beyond the regions of the solar system that have already been explored. Lower values of SI, coupled with larger thrusts, would also be available and would be suitable for manned missions to Mars, among other objectives. The HET is a strong competitor in the latter cases because high power consumption and correspondingly large thrusts have been demonstrated at values of SI up to about 3000 s. Power levels reaching 50 to 100 kW have been achieved in both Russia [6] and the United States [7], with NASA's 457M thruster attaining a thrust of almost 4 N at 100 kW.

Many mission analyses have assumed the use of magnetoplasmadynamic (MPD) thrusters because they offer exceptionally high thrust density, coupled with moderately large values of SI. However, the enormous current densities required to achieve good performance lead to various life-limiting erosion processes. Solutions to the resulting problems are being sought, but there is no guarantee that they will be found, bearing in mind the need for thruster lifetimes of the order of 15,000 to 30,000 hours.

Various extremely challenging missions are now deemed to be of increasing importance and include Pluto and its satellite Charon [8], the Kuiper belt [at 30 to 100 astronomical units (AU) distance] [9], the heliopause [10] (at about 100 AU), the gravitational lens focus of the sun [11] (at 550 AU), and ultimately the nearest stars. Preliminary theoretical work [12, 13] has revealed that a combination of a reduced atomic mass propellant, an improved ion extraction grid system, and much increased extraction potentials, could conceivably lead to values of power consumption, SI, and thrust suitable for such advanced missions. At the extreme, values of SI above 150,000 s might be achieved, permitting various missions to be undertaken, which are currently regarded as nearly impossible. Experimental studies with simplified grid systems have verified that values of SI of 30,000 s are entirely feasible [14].

This report reviews the capabilities and limitations of gridded ion-thruster technology in the context of high-energy mission objectives, with emphasis on reaching megawatt power levels at much increased values of SI. This analysis is based on the performances of existing thrusters, coupled with simple theory, and so does not represent a major departure from current practice. The required performance characteristics can be attained by the use of high ion extraction potentials, coupled with a comparatively minor redesign of grid systems. If found necessary, low-atomic-mass propellants can be used to provide any further increase in SI deemed to be needed.

Although relevant analyses have been reported previously [15, 16], they have been entirely theoretical in nature and do not appear to have considered the practical limitations likely to be encountered. The predictions of the present report include some discussion of these limitations, which are caused primarily by the properties of the materials employed in constructing ion thrusters and the internal erosion processes.

II. Background

A. Space Nuclear Programs

It has long been realized that high-energy deep-space missions cannot be accomplished using solar arrays to provide the necessary power, unless very long flights can be accepted, together with only brief flybys of the associated target bodies and extremely large and costly launch vehicles. Such options cannot be regarded as cost effective in any way. As a consequence, various programs have been commenced in several countries to develop suitable reactors for space power generation [17], focusing on radioactive thermo-ionic devices (RTG), but only those of the Soviet Union have reached operational status [17]. The most highly developed version of the latter is the Topaz-2 reactor [18], which was intended to be flown in conjunction with United States and United Kingdom ion thrusters in

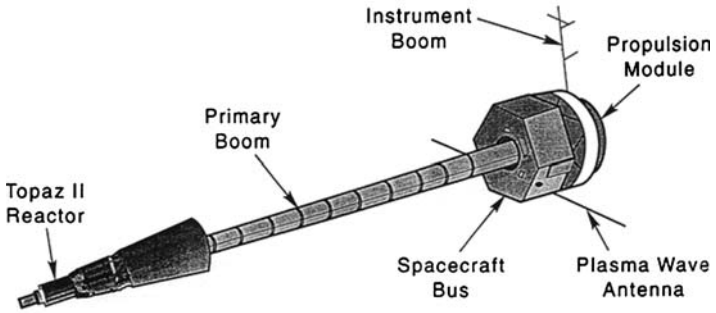


Fig. 1 Schematic diagram of NEPSTP spacecraft.

the NEPSTP (Nuclear Electric Propulsion Space Test Program) orbit-raising technology demonstration mission [19], until funding for this was withdrawn. Similarly, cancellation was the eventual fate of the US SP-100 reactor program [20].

Assuming, however, that nuclear power sources in the 100 kW to multimegawatt range will eventually become available, it is clearly necessary to establish whether appropriate electric thrusters can be provided in a commensurate time frame. It is the purpose of this report to show that this can be accomplished in the case of GIEs, provided that high values of SI are acceptable (5000 s and above); the latter is, in fact, a mandatory requirement of very many challenging missions. In circumstances where high SI is not suitable, HETs provide a fully adequate alternative. Unfortunately, it is not recommended that MPD thrusters be selected under the present circumstances, owing to their development status, which leaves lifetime as an issue that has not been resolved.

Devices utilizing power at high potential provide an additional advantage. This is that power transmission losses are much reduced, a fact that is important in the case of nuclear sources, where the reactor and its associated conversion equipment are located at a considerable distance from the main body of the spacecraft. This latter feature, depicted in Fig. 1 for the proposed NEPSTP spacecraft, is necessary to reduce the radiation flux reaching the payload from the reactor.

This section of the report provides additional clarification of the benefits of utilizing EP for high-energy missions and also discusses the principles underlying the operation of the three technologies mentioned to date: the GIE, HET, and MPD thruster. Although the bulk of the report deals with the GIE, some further brief mention will be made of high-power HETs. Further discussion of MPD devices is provided elsewhere.

B. Advantages of Electric Propulsion

It has long been recognized that the achievement of higher SI results in a reduction of the propellant mass required to accomplish a given mission. This has usually been one of the objectives of research into new and improved propulsion systems, including those in the EP category. It is well established that electric thrusters can provide values of SI an order of magnitude greater than those of chemical engines, so that they are clearly candidates for deep-space missions

requiring large velocity increments. Indeed, if orbit raising [21, 23] is included in the mission plan to achieve greater economy, EP becomes critical to success.

These conclusions follow directly from Newton's Laws of Motion because it can be shown, by equating the instantaneous rate of change of momentum to the force applied to a spacecraft by its propulsion system, that

$$\Delta V = v_{\text{eff}} \log_e \left(\frac{M_o}{M_f} \right) = v_{\text{eff}} \log_e \frac{M_o}{M_o - \Delta M} \tag{1}$$

where $\Delta M = M_o - M_f$ is the mass of propellant consumed.

This, the so-called rocket equation, illustrates the importance of achieving a high value of v_{eff}, assuming that adequate power is available. For a given value of ΔV, a low exhaust velocity must be compensated for by a large increase in ΔM and therefore in the size and cost of the vehicle. It is this dependence of ΔV on the logarithmic term in Eq. (1) for constant v_{eff}, which has provided the incentive for EP development.

An example of the advantages of EP operating at high SI is given in Fig. 2, in which different propulsion technologies are compared for a mission to Pluto. This analysis, by Widman *et al.* [22] assumed the availability of advanced nuclear-thermal-propulsion (NTP) and nuclear-electric-propulsion (NEP) systems. The initial spacecraft mass was taken to be 20 tons, and this was assumed to be launched into a circular low Earth orbit (LEO) at an altitude of only 200 km. The final orbit around Pluto was circular, with an altitude of 100 km. A long coast period was assumed during the journey, which was possibly imposed by doubts concerning propulsion system durability.

The results, in which the NEP and NTP systems are compared against a cryogenic chemical alternative, show very clearly the superiority of the EP option, because of the high SI achieved. This was assumed to be 8000 s, using argon

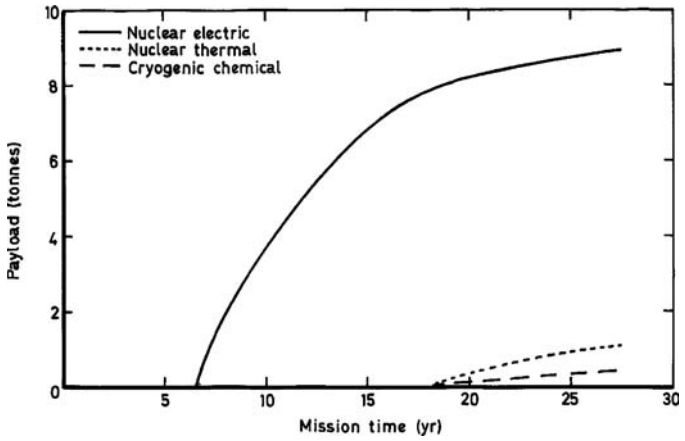


Fig. 2 Payload mass in Pluto orbit, as a function of mission duration for three propulsion systems [22].

propellant, with a thruster total efficiency of 77%. In comparison, the NTP system was assumed to operate at below 1000 s, and the performance of the chemical option was taken to be typical of current technology. These ion-thruster performance values are readily achievable in the laboratory at present, and there are no reasons to suppose that practical, flight-qualified thrusters cannot be developed. It will be shown later that the consumption of the 310 kW assumed in this study is entirely feasible, if high SI operation is required. It was thus concluded that only the NEP system can provide a large payload, and this is also possible in a relatively short time. Indeed, a very reasonable mission can be achieved in under 10 years, whereas the other two options need at least double that time, and then provide an extremely poor performance.

The latter point emphasizes that, in such ventures, the time taken to acquire useful data must be sufficiently short to maintain interest within the associated scientific community and funding agencies. Therefore such missions must normally be productive within a decade at most, implying a very high maximum velocity. This, in turn, demands a relatively high thrust, but the need to minimize propellant consumption also necessitates a large value of SI. These two requirements dictate the need for a very substantial power supply, which can be met at present only by nuclear fission technology.

Bearing in mind the fact that spacecraft in this mission category that employ chemical propulsion gain most, if not all, of their initial velocity from the launch vehicle; the proposal to use EP to reduce total mass must involve a fundamental change in strategy. Rather than boost the spacecraft to an initial very high velocity using the launch-vehicle upper stages, only a modest velocity beyond that needed to escape from the Earth's gravitational field is necessary. The remaining velocity increment can then be provided over a long period of time, usually many thousands of hours, by operating the EP system. Further large reductions in launch-vehicle size are possible through using the EP system for spiral orbit raising from LEO [21] or from GTO, as has been demonstrated by ESA's SMART-1 spacecraft [3]. Of course, disadvantages also accompany such strategies; these include the extended mission duration and the additional radiation damage within the Earth's radiation belts. However, as has been demonstrated by SMART-1 and other recent missions that have encountered the radiation belts, modern electronics and the associated design techniques are fully capable of withstanding successfully extremely high radiation doses.

C. Propulsion System Parameters

In all missions, it is recognized that the SI and thrust attainable are crucial to success and that they together determine the power required. Of course, these two parameters can be traded off against each other in most situations, where the power is defined by other factors. This can be shown by recalling that the thrust T of an EP device is given by

$$T = \dot{m} v_{\text{eff}} \tag{2}$$

where $\dot{m}$ is the rate of flow of propellant. It will be shown later that the power consumed P is approximately that in the exhaust beam in the types of device considered here, so that

$$P = 0.5\,\dot{m}v_{\text{eff}}^2 \tag{3}$$

As the SI, denoted by I_{sp}, is defined as the ratio of thrust to the rate of consumption of propellant in units of sea-level weight, using Eq. (2)

$$I_{\text{sp}} = \frac{T}{\dot{m}g_0} = \frac{v_{\text{eff}}}{g_0} \tag{4}$$

where g_0 is the acceleration caused by gravity at sea level. Combining Eqs. (3) and (4) gives

$$T = \frac{2P}{I_{\text{sp}}g_0} \tag{5}$$

It is clear from Eq. (5) that, for a given power supply, a higher thrust can be achieved only at the expense of a reduced SI. Such a compromise is usually necessary in devising the optimum strategy for a particular mission, hence the important need for thrusters able to operate over wide ranges of these parameters. Thus it might be necessary to reduce the SI in order to achieve a shorter mission duration through the provision of a greater thrust, although the mass of propellant consumed will then be larger. It can be concluded that in all cases a detailed examination of the overall mission is needed, taking into account the major factors of time, likely maximum power, and launch capability, so that an optimum SI can be predicted.

As already described, the achievement of the higher values of SI at constant power must be accompanied by a reduction of thrust, in accordance with Eq. (5). There is, however, another parameter that can assist in achieving high values of ΔV, and this is the thrusting duration. Clearly, with a nuclear power source, this can be very long, reaching many years, although thruster lifetime will then become a severe limitation. As in previous studies [8, 23], this problem can be resolved in principle by incorporating additional thrusters into the spacecraft, which will be used sequentially. This is not a particularly heavy option because they are of relatively low mass. The power conditioning units (PCUs), which are much heavier, can be switched between these thrusters.

As an example of what can be achieved by use of an EP system with high SI, Fig. 3 shows the initial mass M_o, in LEO for a Pluto rendezvous mission as a function of v_e, for a range of masses delivered to the planet, which are denoted by the parameter M_s. The equivalent ion-beam accelerating voltage V_B is also shown for xenon propellant. This graph illustrates clearly the benefits of increased SI and should be compared to Fig. 2.

Despite the inevitable compromise between thrust and SI, the overall mission requirements dictate that the SI must increase rapidly as the objectives become more demanding. This is illustrated in Table 1 for a variety of increasingly challenging objectives, in which minimum acceptable values are shown, together with the associated velocity increments. Although these values are somewhat arbitrary and depend on a number of assumptions, they confirm this important and challenging trend.

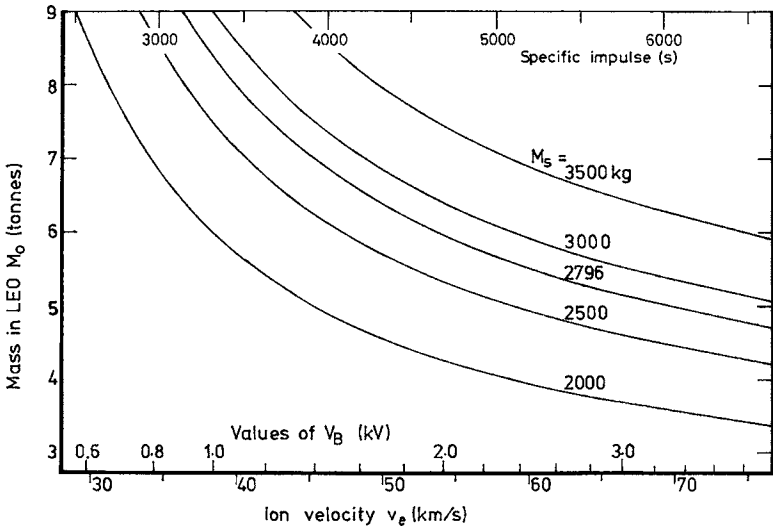


Fig. 3 Mass in LEO required to place a specified payload M_s into Pluto orbit as a function of v_e.

Those values given in Table 1, which are appropriate to the inner and outer planets, can be achieved with current technology, although a considerable increase in SI would be of benefit in both cases. For example, the BepiColombo mission [24] to Mercury is at present based on gridded thrusters operating at about 4500 s. This need for higher values is greater if the launch is to LEO or to GTO, with an electrically propelled orbit-raising maneuver then required to achieve escape velocity. Similarly, the values of ΔV and SI required increase again if it is necessary to rendezvous with and orbit the target body.

D. Propulsion Technology Review

The three propulsion technologies that could, in theory, meet the power, thrust, and SI requirements of challenging NEP missions are summarized next.

Table 1 Values of velocity increment and SI for a variety of missions employing EP

Mission	Typical ΔV, km/s	Minimum SI, s
Nearby planets	5–7	3,000
Outer planets	10–15	3,000–5,000
100–1000 AU	100	10,000
10,000 AU	1000	100,000
Interstellar	30,000	3×10^6

As mentioned earlier, the GIE is the main topic of this chapter with some limited additional information also included next concerning the HET. The MPD thruster is dealt with in more detail in Chapter 5.

1. Gridded Ion Engines

A schematic diagram of a gridded ion engine is shown in Fig. 4. This consists of a cylindrical discharge chamber, which is closed at one end and has a set of perforated and accurately aligned grids at the other. The propellant, in gaseous form, is ionized by an electric discharge in this chamber, forming a moderately dense plasma. The positive ions in the plasma diffuse towards the grids and are extracted and accelerated by the potentials applied to them. The space charge of the emerging ion beam is neutralized by electrons provided by an external cathode, termed the *neutralizer*.

This discharge can be direct current (dc), between an axial hollow cathode located in the center of the closed end of the chamber, and a concentric anode. The ionization efficiency is enhanced by the application of a magnetic field to the discharge chamber. A relatively weak divergent axial field is used in the case of the Kaufman-type thruster [23, 25, 26], whereas much stronger more localized fields are used in the alternative cusp-field geometry device [27], as used on the Boeing/Hughes HS-601 and HS-702 communications satellite platforms [28]. In another variant, a RF plasma is formed within an insulating discharge chamber, using an external coil energized by an oscillator [29, 30]. Alternatively, a microwave source of RF energy can be employed [4, 31], usually in conjunction with an auxiliary magnetic field.

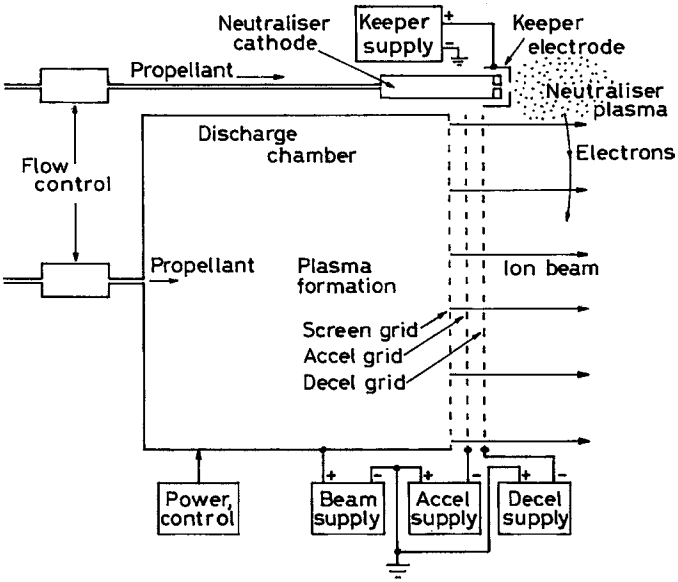


Fig. 4 Schematic diagram of a gridded ion engine.

In all cases, accurately controlled flows of propellant gas are mandatory; in most present ion propulsion systems this gas is xenon, although any other chemically inert gas is also acceptable. These flows are produced by an external control system, which, in turn, is fed at constant pressure by a regulator connected to the storage tank via appropriate valves. Separate flows are needed to the discharge chamber, neutralizer, and, if one is used, to the cathode.

It is normal to use a triple-grid system on thrusters of this type. This operates in an accelerate/decelerate mode to enhance the throughput of ions at the voltages usually employed. In this scheme, the thruster body is at the high potential appropriate to the ion-beam velocity required. For example, if xenon ions are to be accelerated to a velocity of 40 km/s, which is appropriate for a value of SI of about 3500 s, a potential of 1.1 kV is needed. This is thus the potential of the inner or screen grid and of the thruster body. The next grid, the accel, is at a negative potential of perhaps −250 V, to provide focusing of the beamlets and to enable the required current to be extracted. Deceleration to space potential then follows, via a low negative voltage applied to the outer decel grid and the coupling of the beam to the space plasma.

The neutralization process involves the production of a weak external plasma by means of a dc discharge between the neutralizer cathode and an adjacent keeper electrode; this is also closely coupled to the space plasma. Electrons are extracted from this plasma by the ion beam as necessary to neutralize its space charge. This is a natural automatic process involving no active control.

The spacecraft potential is determined ultimately by its interaction with the space plasma, and the difference in potential would normally be very small, assuming that ion-beam neutralization is fully effective. Despite the enormous differences in plasma conditions that can exist between the external environment and the plasma produced by the propulsion system, the very great mobility of the electrons and the rapidity with which energy equalization between different electron populations occurs ensure that potential differences will remain small.

Of course, the characteristics of the space plasma vary enormously over very many orders of magnitude, according to the location of the spacecraft. If it is in low Earth orbit, where the residual gas is ionized by solar radiation, this will constitute a moderately dense plasma, albeit with quite a low electron temperature. Moving to geostationary orbit, the density will be far less, but there will be a considerable contribution from the energetic solar wind, causing all temperatures to be much greater than at low altitude; these are the electron, ion, and neutral gas temperatures, which are not necessarily identical owing to the collision particle processes that occur. Then in interplanetary space the influence of the Earth's atmosphere is absent, and the plasma characteristics are dominated by the solar wind, which decreases in density according to the inverse square law as distance from the sun increases.

As an example of the variability of these plasmas, the solar wind in the vicinity of the Earth has a velocity in the range 300 to 800 km/s [32], which can exceed 1000 km/s when solar flares occur. Overall, these natural plasmas have densities that vary from less than 0.01 to 1000 particles per cm^3, temperatures from less than 1 eV to more than 1000 eV, and particle energies from less than 1 eV to many MeV [33]. To add to the complexity of analyzing any particular spacecraft utilizing ion thrusters in interplanetary space, the plasma produced by the thrusters close to the

spacecraft is likely to be at least three orders of magnitude more dense than the natural plasma. However, as just implied, interactions are generally benign.

To return to the description of the thruster, a more important function of the outer grid is to minimize the erosion damage caused to the accel grid as a result of bombardment by low-energy charge-exchange ions [34]. These ions are generated by interactions between beam ions and the neutral gas atoms that escape from the discharge chamber and that also originate from the neutralizer. The low-energy ions are attracted to the accel grid by its negative potential, and so shielding by the decel grid diverts many of them, reducing the resulting damage. Of course, if this erosion problem is not of concern for a particular mission, or is circumvented by other means, the decel grid can be omitted, reducing complexity and also cost.

Several different thrusters in this category have flown on a variety of spacecraft [2, 4, 28, 35–37], and they and others are appropriately qualified for operational use. Including experimental devices, grid diameters vary from 5 cm up to 65 cm, with thrusts from less than 1 mN up to nearly 1 N. Power consumption ranges from a few tens of watts up to more than 10 kW. Typical electrical efficiencies are 70 to 90%, and the SI is usually in the range 2500 to 5000 s, although both higher and lower values are possible.

A major advantage of the GIE is that the plasma production mechanism, the ion extraction and acceleration, and the ion-beam neutralization are separate processes. They can be treated as such when designing a new thruster, greatly simplifying what might otherwise be a complex procedure. This separation of these functions also applies to thruster operation. For example, it is normal to change the ion accelerating potential, and thus the SI, without altering the discharge characteristics in any way; this is not possible with most other EP devices. As will be shown later, a further separation of functions is possible if a four-grid configuration is adopted for ultrahigh SI operation. In that case, the ion extraction and acceleration processes can be dealt with independently [12, 13].

2. *Hall-Effect Thruster*

The Hall-effect thruster (HET) [38], also known as the stationary plasma thruster (SPT), is an ingenious device, originating in Russia in the 1950s and 1960s, in which the ions are accelerated entirely within the discharge plasma. This type of engine has flown on numerous Russian and Soviet spacecraft with considerable success [39, 40] and has now been adopted by many European and American organizations [41, 42], primarily for application to communications satellites [43]. This technology's first Western success has been to transfer the SMART-1 spacecraft from its initial GTO to lunar orbit [3], utilizing Snecma's PPS-1350G thruster [44].

An HET is shown schematically in Fig. 5a, with the high-power 457M thruster in Fig. 5b. The typical HET consists of an annular discharge chamber made from ceramic material, with a ring-shaped hollow anode situated at its closed end. The propellant gas, again usually xenon, is injected through this anode, and the correct application of a magnetic field is critical to success. The magnetic circuit provides an almost radial field across the annular discharge chamber, but with very careful shaping along the axial direction to give high efficiency. The field is produced by four to eight external solenoids bolted between a front circular

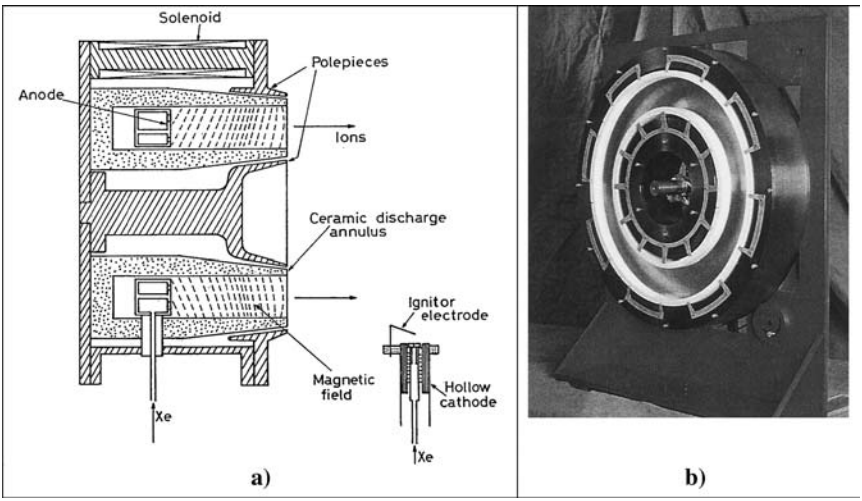


Fig. 5 Hall-effect thrusters: a) schematic diagram and b) NASA 457M high-power thruster. (From NASA photo [7].)

polepiece and a ferromagnetic backplate. An axial polepiece is also bolted to the backplate; in some thrusters this is surrounded by another coil.

The discharge current is provided by an external hollow cathode, which is often duplicated for redundancy. The electrons emitted by the cathode are attracted into the annular discharge chamber by the anode, which is at a potential of typically 200 to 350 V, although values of up to 1 kV have been tried experimentally [45]. However, they cannot penetrate far into the annulus because of the radial magnetic field and spiral around the field lines, colliding with propellant gas atoms and causing ionization to occur. The resulting axial current interacts with the magnetic field, generating an azimuthal Hall current, hence the name of the device.

The anode potential appears mainly across the relatively thin plasma layer in which ionization occurs and the Hall current flows azimuthally. The ions are accelerated by the electric field in this region, attaining velocities of the order of 16 to 18 km/s, with an anode potential of 300 V. As they have mean free paths and cyclotron radii much larger than the channel dimensions, this acceleration is mainly in the axial direction, but the beam divergence is relatively large, at 40 to 50 deg. Nonaxial ions impact the edges of the downstream end of the discharge chamber, causing erosion and limiting life. Neutralization of the ion beam is accomplished automatically, electrons being provided by the external cathode as required.

Although very effective, the HET operates in a relatively noisy mode, with violent oscillations of the discharge current often observed [46]. This feature generates a need for careful isolation from the spacecraft power system. Lifetime is limited to about 6000 to 8000 hours by the erosion mechanism just mentioned, but this is adequate for many missions of interest. Throttling over a modest range is possible, but the large ion-beam divergence can cause problems with thruster-spacecraft integration.

HETs with nominal diameters of 5, 7, and 10 cm and thrusts of up to more than 80 mN have been flown on more than 60 occasions in Soviet and Russian missions [40, 45]. No failures have been reported, but operational times have generally been of the order of hundreds of hours. Much larger devices are under development in both Russia [6, 40] and the United States [7], with thrusts that reach above 1 N. For example, the experimental NASA 457M shown in Fig. 5b has operated at up to 72-kW input power.

As with most propulsion devices, efficiency and SI increase with size and power. However, the SI available from thrusters with qualified status, or near to this, is limited to about 1600 to 1800 s. Numerous mission analyses suggest that this is inadequate for the majority of deep-space missions. So, although this technology has been used successfully by ESA on the SMART-1 demonstrator mission [2, 47], it would not appear at present to be a serious contender for most future projects requiring a large ΔV, unless success is achieved in developing the larger thrust devices with high SI to qualified status.

Another approach to achieving high SI is the dual-stage device [48, 49], in which the plasma production and acceleration processes are separated within the same thruster. This work has preliminary experimental status at present, and it is not possible to predict whether it will be successful. In any case, it would seem to be very unlikely that values of SI much above about 3500 to 4000 s will be achieved by this means.

Another development, which has already achieved success, is to move the acceleration region within the thruster along the axis towards the exit plane, so that the high-energy ions are less likely to impact on the ceramic wall [50, 51]. This increases lifetime, but the associated drawback is a greater ion-beam divergence. In this form, the thruster has the generic name of thruster with anode layer (TAL).

As regards the suitability of HET/TAL technology for high thrust, high-SI NEP missions, many recent studies have confirmed that values of SI well above 5000 s are necessary. Indeed, as will be shown later, the more challenging missions are likely to require values in the range 10,000 to 14,000 s. There is no prospect of HET/TAL devices reaching this regime using xenon propellant because the most advanced experimental thrusters currently operate at the 3000 to 4000 s level. As an example, the Keldysh Research Center's X-85M thruster [45] is designed to operate at up to 1 kV. At 750 V its SI is reported to be 3200 s, which is itself a considerable achievement. The best that can be expected at 1 kV is about 3800 s, and lifetime remains a serious issue at such high anode potentials.

These and other results have been obtained using the standard propellant, xenon. As with most types of EP technology, the substitution of a propellant with a lower atomic mass will automatically increase the recorded SI at a given accelerating potential, via a square-root relationship discussed later. It is thus no surprise that an SI of 4700 s has been obtained at NASA John H. Glenn Research Center using krypton in the new 400M thruster at 1.05-kV anode potential [42]; the power input was 43 kW, and the total efficiency was 54%. Earlier, the 457M operated at an SI of 4500 s, with 1 kV applied and a discharge (not total) efficiency of 64%. However, the 8000 s reported earlier by TsNIIMASH, with a dual-stage device and using bismuth, is much harder to understand and requires verification [7]; 800 s would be more likely with this high atomic mass propellant.

High thrust, coupled with high power consumption, is a different issue and presents no problems, provided that adequate lifetime can be ensured. For example, several years ago the Fakel SPT-290 [6] was operating successfully at 1.5 N, with a power consumption of 30 kW and an SI of 3000 s. The NASA 457M thruster (Fig. 5b) later reached 50 kW, then 72 kW [7], with an SI of up to 3250 s. A thrust of up to 2.9 N was measured. More recently, NASA's high-thrust HET program has achieved a power consumption of 64 kW with the 400M thruster, using krypton propellant and an accelerating potential of 1.1 kV [42]. However, durability testing is still being discussed in terms of 200 hours of operation, which is a factor of at least 30 away from times of interest for real missions.

A further problem with high power operation concerns thruster temperatures. Unlike the GIE, in which the bulk of the power is deposited directly into the ion beam, in the HET it is all fed into the discharge chamber, which naturally becomes very hot indeed. With power levels of the order of 50 kW, the 457M thruster takes more than four hours to reach thermal equilibrium, at which time many of the temperatures are well above 300°C, with the actual discharge chamber ceramics in the region of 600°C to 800°C [42]. This adds to the problem of ensuring adequate durability.

It can be concluded from the preceding discussion that the HET offers little promise of being able to provide the values of SI required for the most challenging interplanetary missions using nuclear power. Although efforts to increase the SI are yielding some success, the values achieved do not approach those of interest. However, the power levels and thrusts currently being attained are relevant to certain missions in which SI and propellant mass have to be sacrificed in order to accomplish maneuvers within specified periods of time. Thus large thrusters, as exemplified by the 457M, could be utilized in such circumstances where a reactor might be producing a few hundred kilowatts. However, they would still probably not be suitable in the multimegawatt regime because too many would have to be mounted on the spacecraft to utilize this power. As will be shown later, this restriction does not apply to the advanced GIE operating at high SI.

3. Magnetoplasmadynamic Thrusters

In the longer term, much higher thrusts and thrust densities will be achieved by using MPD thrusters. These are currently pulsed devices, in which the discharge current rises to kilo-ampere levels and well beyond, perhaps to many hundreds of kilo-amperes, so that the electromagnetic forces expelling the plasma from the discharge vessel dominate all other effects [52]. Within the same power category are high-power arcjets, in which the exhaust is further heated by an RF discharge; the ATTILA device is a good example of this technology [53, Chapter 4 in this book]. However, these concepts have at present an experimental or developmental status, and practical devices with long life are unlikely to appear for at least a decade [54]. A further problem to be overcome if viable MPD applications are to materialize is that of the power supply. Present versions utilize capacitors, which are massive and bulky, and a great deal of effort will be needed to reduce their mass and volume to acceptable levels, unless it is found practicable to operate continuously.

A typical MPD thruster, shown schematically in Fig. 6, consists of a tungsten cathode at one end of a cylindrical or conical discharge chamber made of a

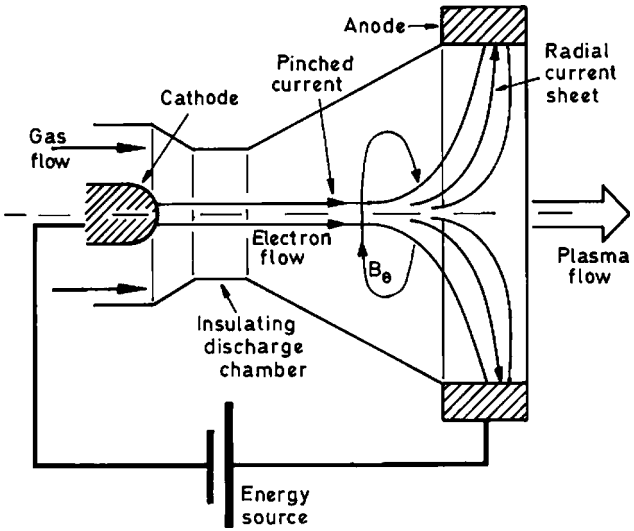


Fig. 6 Schematic diagram of a conical MPD thruster.

refractory insulating material, usually a ceramic. A ring-shaped anode is situated at the other end of this vessel. A very low inductance source of high voltage, such as a capacitor, is applied to these electrodes as a pulsed valve admits a puff of propellant gas into the cathode end of the chamber. With low inductance, the discharge current rises very rapidly, and the instantaneous power dissipation is often in the hundreds of kilowatts to multimegawatt regime. To match more precisely the current and gas flow profiles, the current source is frequently a series of capacitors and inductances, forming a transmission line with a time constant of the order of a few milliseconds.

Although Paschen breakdown can initiate the discharge, an auxiliary process can be used, such as a separate high-voltage spark or a laser pulse. Once the current flows, it pinches onto the axis of the anode. The interaction between the azimuthal magnetic field B_θ around the pinched axial current and the radial current j_r to the anode produces a very large expulsive force $j_r \wedge B_\theta$, which can provide instantaneous thrusts of the order 1 to 100 N. This is attractive, as is the associated high thrust density, but many difficult problems must be overcome before such devices can be considered for practical applications. In the meantime, the most promising option for low-cost interplanetary exploration is the gridded ion thruster.

4. Variable-Specific-Impulse Magnetoplasma Rocket (VASIMR)

This device, devised and pioneered by astronaut Franklin Chang-Diaz [55], has been under development since 1994 with NASA funding, but is very complex, and so it is still at the laboratory investigation stage. However, it promises to provide eventually a very high thrust density and SI, with an electrical efficiency of 50%. The SI has been predicted to reach 30,000 s [56] with propellant gases having low atomic masses, and will be readily variable over a wide range.

Table 2 Summary of high-power thruster capabilities

Thruster	Prop	Beam diam, cm	Beam current, A	Typical SI, s	Thrust, mN	Thrust density, mN/cm^2	Power, kW	Power density, W/cm^2	Specific power, W/mN	S[a]	Ref
T5 (high SI)	Xe	10	1.05	4334	71	0.90	2.22	28.3	31.3	E	128
RIT-10 Evo	Xe	8.7	0.85	3700	35	0.59	0.98	16.5	28.0	Q	90
RIT-15LP	Xe	14.2	0.90	3400	50	0.32	1.3	8.2	26.0	E	87
SERT II	Hg	15	0.25	4770	29	0.16	0.91	5.1	31.4	F	36
RIT-XT	Xe	21	2.41	6419	218	0.63	8.06	23.3	37.0	Q	30
T6	Xe	22	3.38	4650	230	0.61	7.05	18.6	30.7	Q	93
ESA-XX	Xe	25	3.25	3500	240	0.49	8.45	17.2	35.2	E	92
XIPS-25	Xe	25	4.0	4338	245	0.50	6.8	13.9	27.8	F	98
UK-25	Xe	25	4.45	4500	316	0.64	9.5	19.4	30.1	E	76
NSTAR	Xe	30	1.76	3100	90	0.13	2.33	3.3	25.9	F	72
NSTAR derivative	Xe	30	2.7	5000	172	0.24	4.6	6.5	26.7	Q	103
NASA J-Series	Xe	30	4.0	3310	201	0.28	5.1	7.2	25.4	E	101
NASA 900-Series	Hg	30	2.0	3000	128	0.18	2.6	3.7	20.3	E	104
Hughes MESC	Xe	30	5.6	5160	364	0.51	11.1	15.7	30.5	E	124
RIT-35	Xe	33.5	1.95	3195	104	0.12	2.97	3.4	28.6	L	106
RIT-35	Hg	33.5	2.45	4343	250	0.28	7.5	8.5	30.0	L	106
BBM-2	Xe	35	2.88	3518	150	0.16	3.3	3.4	22.0	E	108
Tokyo MESC	Xe	30	2.5	3710	153	0.22	3.5	5.0	22.9	L	110
NEXT (design)	Xe	40	5.8	4400	380	0.30	10.0	8.0	26.3	E	111
NEXT (test)	Xe	40	3.52	4110	237	0.19	6.9	5.5	29.1	E	113
NEXIS	Xe	57	4.0	7500	415	0.16	20	7.8	48.2	L	115
HiPEP (dc)	Xe	91 × 41	5.5	9620	670	0.18	39.3	10.5	58.7	L	118
NASA interstellar (predicted)	Kr	3 × 30 dia	2.3	14,000	345	0.16	30.0	14.1	87.0	L	122

[a]S = status, E = engineering model, F = flight model, L = laboratory model, Q = qualification model.
[b]Wallace, N.C., private communication, Space Dept., Qinetiq, Farnborough, England, U.K., June 2003.

The basic concept is similar to the magnetic "bottle" plasma confinement concepts that were widely investigated over several decades in the context of controlled thermonuclear fusion programs [57]. In the VASIMR device, three magnetic confinement regions are created. In the first, a so-called "helicon" discharge (*helicon* being the name for the radiofrequency ionization) is used to generate the source plasma, the ions then drift into a volume in which they are more tightly confined by a much larger magnetic field. There, they are heated by the ion-cyclotron resonance mechanism, configured as a downstream propagating wave, until they emerge into a diverging magnetic nozzle. The variable SI feature is achieved, at constant input power, by changing both the propellant flow rate and the division of power between the helicon discharge and the subsequent ion heating. A high flow rate, with most of the power supplied to the helicon discharge, results in a relatively low SI. As flow is progressively reduced and more power is diverted to ion heating, the SI increases.

A recent laboratory version [58], designated VX-10, is based on a 9-cm-diam helicon discharge tube, with an axial magnetic field of about 0.05 T and an input power of up to 3.5 kW. The plasma, of density of about $10^{11}\,\mathrm{cm}^3$, is then heated by the ion-cyclotron wave in a carefully shaped magnetic containment field of up to about 0.3 T. The heating power in this version is up to 3 kW, and the complete device is about 1.5 m long. The SI achieved, using deuterium propellant and 1.5-kW heating power, was between 5000 and 12,000 s. With helium, a target-type thrust balance indicated a thrust of 1.4 mN using a heating power of 3 kW. The overall efficiency has not been given, but a simple calculation indicates a value of 1.8% if the SI reached 12,000 s with helium. Recent VASIMR developments may be found in [140].

Although it has been predicted that this device can in the future be operated at the megawatt level, and an upgrade to 50 kW is underway [58], a comparison with Table 2 of this report suggests that it is not currently a viable competitor for relatively near-term missions. The high value of SI achieved is a consequence of the use of a propellant with a low atomic mass, and it is also easy to change the SI of a gridded thruster over a very wide range, merely by altering the potentials applied to the grids.

III. Gridded Ion Engines—Current Devices

A short summary of the operating principles of GIEs is provided in Sec. II.D.1 of this chapter. However, as these devices are the most likely to be employed for high-energy deep-space missions powered by nuclear reactors, and least in the near to medium term, further information concerning them is given next. As the different categories of thruster can be identified by the various ionization mechanisms utilized, these are covered qualitatively in more detail. In addition, brief descriptions are given of the higher-power devices currently available; these are either space qualified or have shown promise in development or in laboratory tests.

A. Ionization Mechanisms

As mentioned earlier, the major feature that differentiates between the several varieties of GIE now available is the ionization mechanism employed.

Four main mechanisms are to be found; these are RF ionization at a frequency of about 1 MHz, electron-cyclotron-resonance (ECR) RF ionization, with frequencies in the range 0.1 to 5 GHz, and dc discharge ionization in a weak or a strong magnetic field. In all cases, the resulting ions are extracted and accelerated by a system of carefully aligned multi-aperture grids, and the space-charge of the resulting ion beam is neutralized by electrons from a hollow cathode discharge plasma.

Because there is nothing to differentiate in a generic way between the ion beams generated by these thrusters, as far as mission analysis and thruster-spacecraft interactions are concerned, there is little to choose between them. Nevertheless, other issues, including lifetime, reliability, efficiency, and cost, can dictate that one type be preferred to another. For this reason, more detailed explanations of their modes of operation are given next.

1. Radiofrequency Discharge Thrusters

The RF thruster has been developed in Germany over many decades [59–61] and has reached an advanced status in its 10-cm beam diameter form, which is designated RIT-10 [62]. In this context, the acronym RIT is the radiofrequency ionization thruster. It was flown successfully on ESA's Eureca spacecraft [63], although the test was terminated prematurely by a wiring fault. More recently, it has been employed very successfully for emergency orbit raising of ESA's Artemis communications satellite [35], following the partial failure of the Ariane 5 launch vehicle, although its primary task on this spacecraft is north-south stationkeeping (NSSK). Further developments of this device [64], using different grid materials and designs, show significant performance improvements, but they are not yet qualified. This ionization principle has also been used in several other thrusters of larger size [29, 30, 60], extending to 35-cm beam diameter, and all could become available for applications within the medium term, provided that adequate funding was provided.

In this type of thruster, shown schematically in Fig. 7, ionization of the propellant gas, which is usually xenon, is accomplished by winding an RF coil on the outside of the discharge chamber, which is made from quartz or alumina. The coil, when fed from an RF generator operating at about 1MHz, produces a rapidly varying magnetic field within the discharge chamber. This, in turn, induces an electric field that is adequate to cause ionization to occur, resulting in the formation of a dense plasma. The initial electrons required to start this process diffuse in through the grid system from the neutralizer plasma, which is initiated as the first stage of the startup process. Thrust levels are readily adjusted by altering the plasma density in the discharge by changing the RF power level and the propellant flow rate. The SI is typically about 3300 s, but higher values are immediately available by increasing the beam acceleration potential.

It is notable that the power supplies required are very similar to those utilized by the dc discharge thrusters, as will be confirmed later. The supplies used to extract and accelerate the ion beam are identical in function and configuration in the two cases, as are those employed to provide the neutralizing electrons. The only difference, as implied by the names of the thrusters, is in the production of

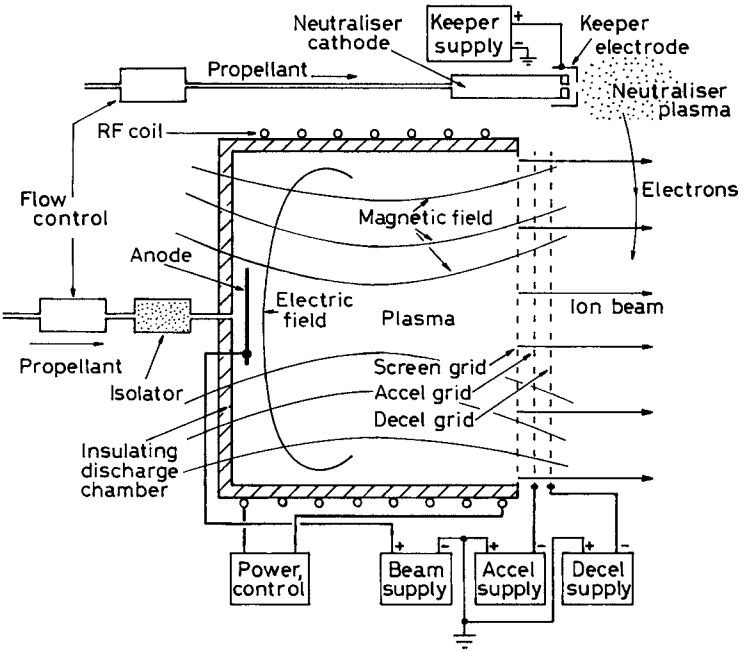


Fig. 7 Schematic diagram of an RF gridded ion engine.

the plasma in the discharge chamber. In the RF thruster the energy source consists of an RF current with a frequency of about 1 MHz, whereas in the dc device a current regulated dc discharge is used.

A component not mentioned earlier is also indicated in Fig. 7. This is the electrical isolator situated between the propellant flow control unit (FCU) and the discharge chamber. This is necessary because the feed system is at spacecraft potential, whereas the discharge chamber is connected to the positive terminal of the beam supply, which is typically at 1 to 1.5kV. These isolators are very simple yet effective devices, requiring no power and no active control. They operate by requiring the propellant gas to pass through a porous medium with a very high surface area. This causes any ion-electron pairs formed in the high applied electric field to recombine immediately, thereby inhibiting breakdown.

Of course, there is no absolute guarantee that RF thrusters, or any other type of device, will operate without failure. Indeed, two failures have been recorded to date, both owing to problems not associated in any way with the fundamental principles of this technology.

The first occurred in the Eureca mission [63], in which a RIT-10 thruster was flown on the European Retrievable Carrier, deployed into orbit from the space shuttle. After more than 200 hours of operation, the thruster ceased working,

apparently because of a failure in the RF circuit. After retrieval of the spacecraft by the shuttle, laboratory examination showed that a soldered joint had failed; this was clearly a problem associated with design, manufacture, or quality assurance, not with the thruster itself. Indeed, the thruster was found to be in perfect condition.

The second failure occurred on the Artemis mission [35], when the neutralizer of one of the two RIT-10 thrusters failed to operate, although the thruster itself was subsequently operated successfully using the neutralizer on one of the T5/UK-10 thrusters mounted on the same spacecraft. The probable reason for the failure was found to be damage caused to the neutralizer cathode by vibration during launch. Again, this was attributable to detailed design, manufacture, or quality assurance, and the thruster itself was not at fault.

2. *Radiofrequency Discharge Thrusters Operating at High Frequencies*

An alternative to the RF ionization process used in the RIT series of thrusters is to raise the frequency considerably and also apply a steady magnetic field to the discharge chamber. This concept relies upon the gyration of the electrons within the discharge chamber around the magnetic field lines, thus improving their chances of suffering an ionizing collision with a neutral gas atom. If the cyclotron and RF frequencies are equal, a resonance condition that aids in the effective absorption of the input energy, further enhancing overall efficiency, was created. The latter is the ECR discharge, as used by the Japanese team responsible for the thrusters employed on the Muses-C asteroid sample return spacecraft [4, 65, 66].

This thruster also employs the ECR principle within the neutralizer cathode. However, although this eliminates the need for a source of low work function material [34], it does not remove the major life-limiting factor of sputtering by relatively high-energy ions.

A small Italian thruster, under development by Laben/Proel [67], utilizes this magnetic enhancement principle. Termed the radiofrequency with magnetic field thruster (RMT), it is similar in concept to the RIT series, except that the plasma-production process employs RF power in the very-high-frequency (VHF) range, together with an axially symmetric magnetic field of about 100G. This device, shown schematically in Fig. 8, relies upon the increased ionization rate caused by the cyclotron motion of the electrons, but without resonance. Using a variable magnetic field component provided by a solenoid to optimize the discharge, it enables low thrusts to be achieved while maintaining good efficiency.

In Fig. 8, both permanent magnets and the solenoid are shown; I_c is the current supplied to the latter, for which a power supply is needed. The ion-beam current is denoted by I_b and the currents to the accel and decel grids by I_a and I_d, respectively. The beam accelerating potential, which is applied to the screen grid, is V_s and the accel grid potential V_a. The current I_s, provided by the screen power supply, is almost identical to I_b. The RF input power is denoted by W_{RF} and the propellant flow rate to the discharge chamber by $\dot{m}$. The neutralizer cathode is not shown in this figure; it is very similar to those depicted in Figs. 4 and 7 and requires the same power supplies.

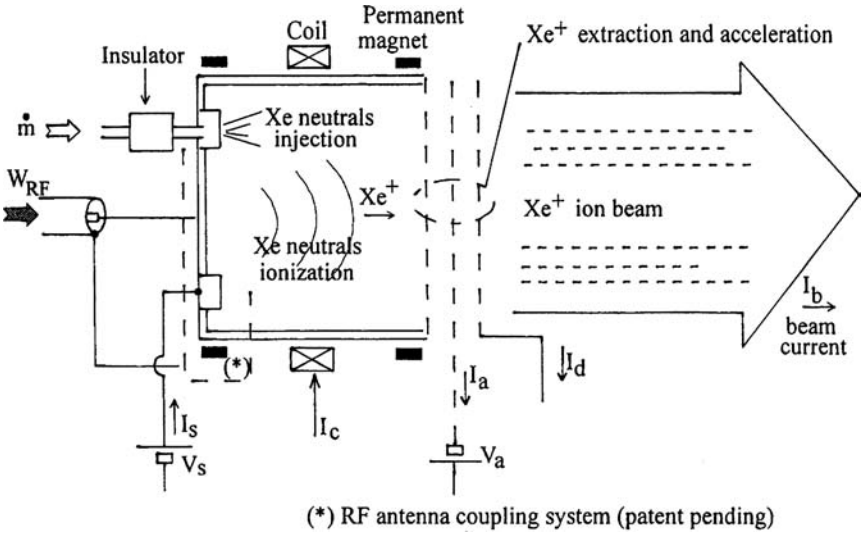


Fig. 8 Schematic diagram of the high-frequency RF gridded ion engine (Laben diagram).

3. Kaufman-Type Direct-Current Discharge Thrusters

Thrusters of this general type are under development in the United Kingdom and Russia, and discontinued work in this field was undertaken in Germany. All devices now use xenon propellant, although any other gas that does not interact chemically with thruster components can also be employed. The United Kingdom and Russian types are similar, in that they employ the Kaufman ionization principle [68]. In this (Fig. 9), the propellant gas is ionized in a dc discharge between an axial hollow cathode [34] and a downstream cylindrical anode. A divergent magnetic field, generated by solenoids external to the discharge chamber, is provided to prevent the primary electrons from reaching the anode directly. They are obliged to spiral around the field lines, thereby enhancing their chances of suffering ionizing collisions with neutral gas atoms. Because the hollow cathode requires a propellant flow for its operation [34], two feeds are usually employed to the discharge chamber. However, small thrusters can often be operated successfully with only a single flow, which is passed through the cathode.

High propellant utilization efficiency is ensured by causing the primary electrons from the cathode to acquire the correct energy to maximize the probability of ionization within the discharge chamber. These electrons emerge from the cathode orifice [34], into the coupling plasma, where they have a relatively low energy/temperature of 1 to 2 eV. Because they are attracted by the potential of the anode, which is typically at 30 to 40 V above cathode potential, they travel through the annular gap between the inner magnetic polepiece and the circular baffle disc to enter the main discharge chamber. However, the fringing magnetic field across this gap causes an impedance to their flow, resulting in an azimuthal Hall current and a well-defined energy increase, which can be adjusted at will by altering the

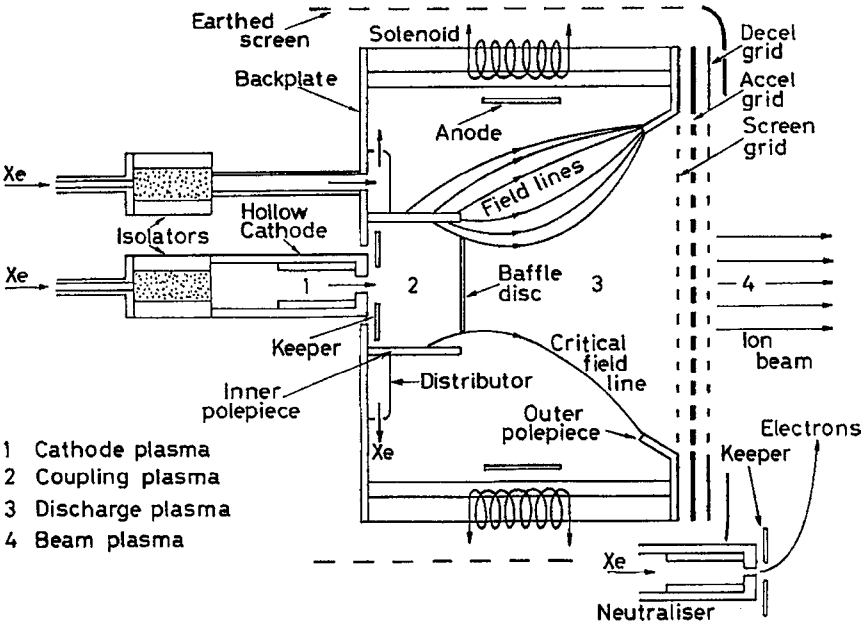


Fig. 9 Schematic diagram of Kaufman-type gridded ion engine.

magnetic field. Thus the operating parameters of the thruster can be set as required to optimize performance at any required thrust.

There is no thruster parameter that intrinsically provides a measure of propellant flow rate, although indications can be derived from the voltages at constant current of both the main discharge and neutralizer cathode keepers, and by the anode potential for constant cathode conditions, discharge current, and magnetic field. However, so many parameters interact in determining the performance of a thruster that it is far from easy to deduce unambiguously what any of the three flow rates might be under a given set of conditions. Thus, in diagnosing faults and in assessing absolute performance, the use of flowmeters [69] is highly recommended. As they are small, of low mass, and consume little power, their insertion into a propellant-fed system carries few significant overheads. In addition, should a flowmeter fail, it will not jeopardize the mission, because all thrusters up to the present have been flown without them.

The power conditioning system required by a Kaufman-type thruster is as indicated in Fig. 4, with the addition of the current regulated discharge supply and the heater and keeper supplies needed for the hollow cathode used to provide the ionizing electrons. Although the positive terminal of the beam supply is often connected to the anode, an alternative arrangement is sometimes employed, by making this connection to the thruster body. In that case the beam current passes through the anode supply, but the ion accelerating potential is increased by the plasma potential in the discharge chamber.

All current gridded thrusters of this type have roughly comparable performances, when measured in terms of SI and the various thruster efficiencies. The typical SI has, until recently, been in the region of 3000 to 4500 s, but greater values are now being considered for very high-energy interplanetary missions [12]. The available thrust covers the very wide range of a few milliNewtons to more than 300 mN. In addition to the thruster design variations implied by this range, some differences caused by individual performance features can be significant. For example, flexibility in operation is enhanced by employing a separately controllable propellant feed to the hollow cathode, but this might not be necessary if no throttling were required.

4. Magneto-Electrostatic Containment (MESC) dc Thrusters

The MESC, or cusp-field thruster [70, 71], is very similar in most respects to the Kaufman device, apart from using a very high value of magnetic field for plasma containment, and relying upon the difference between the discharge plasma and cathode potentials to accelerate the primary electrons emitted by the cathode. The diagram shown in Fig. 10 is based on the very successful NSTAR thruster [72] flown on the DS-1 interplanetary spacecraft [2, 73]. It indicates the positions of the

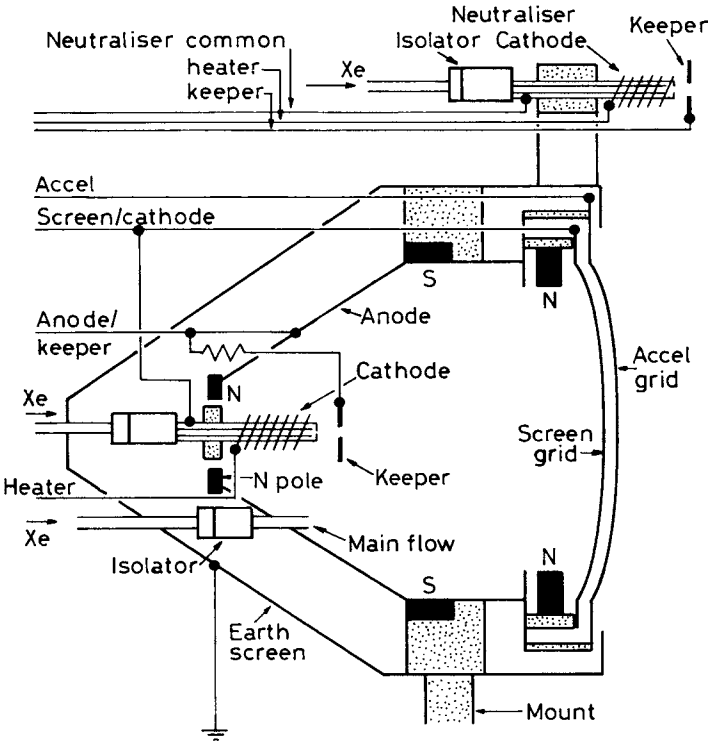


Fig. 10 Schematic diagram of the MESC concept, based on the NSTAR thruster.

permanent ring magnets, often made of samarium-cobalt, which provide the magnetic field. This field is located closer to the discharge chamber walls than in the Kaufman-type thruster and is of the order of kiloGauss near the magnets. A separate anode is not normally used because the complete discharge chamber wall usually performs this function. The hollow cathode is of the same type as used in most Kaufman-type thrusters.

In operation, the primary electrons emitted by the cathode are accelerated from the vicinity of the keeper electrode into the main plasma, gaining energy in the process; this energy is determined approximately by the difference between the keeper and anode potentials. These electrons are constrained to orbit around the magnetic field lines, as in the Kaufman thruster, only diffusing to the anode via collisions with other particles. As the field is much stronger close to the magnets in this device, the reflection of the electrons there is very effective, and this allows the discharge power to be lower for a given thrust; typical values of the discharge power to beam current ratio are 150 and 250 W/A, respectively, in the two types of device. As indicated in Fig. 10, the close proximity of the most important region of the magnetic field to the discharge chamber wall can allow the thruster to be designed with a conical shape, although in some cases a hemispherical alternative has been selected. Also, outward (convex) dishing of the grids was chosen in the case illustrated, and an electrical isolator was fitted in the propellant flowpath to the neutralizer.

Although the electrical efficiency can be very high, the thruster cannot be controlled as readily as the Kaufman type using a variable magnetic field, so that the active throttling range at sustained high efficiency is somewhat lower. Nevertheless, extensive operational experience with this type of thruster has been gained owing to its use in the Boeing/Hughes HS-601 and HS-702 communications satellites for north-south stationkeeping [74] and, in the latter case, for the final phase of orbit raising [28] and for east-west stationkeeping.

Although these commercial applications have been very successful, with more than 100 thrusters in orbit and over 125,000 hours of operation achieved [75], it is understood that failures have been encountered in the case of the XIPS-13 thrusters. Unfortunately, no information concerning the severity of these rumoured failures or of their cause has been published, and representatives of the company (now L3 Communications) have not been at liberty to provide any information. Of course, it is possible to surmise what might have occurred, based on published knowledge of the various subsystems involved, but this would not be productive here, bearing in mind that no evidence whatsoever is available.

B. Current Gridded Thrusters

The thrusters listed and described next are in the high-power category, where "high" in this context means the use of an input of 1 kW or greater. This, of course, is very much below the values required for NEP applications, by orders of magnitude, but these devices provide the starting point for future developments to much higher power levels.

The one exception to this rule is the T5 thruster [54], which is the first to be described. This is included because its design involved the formulation of scaling

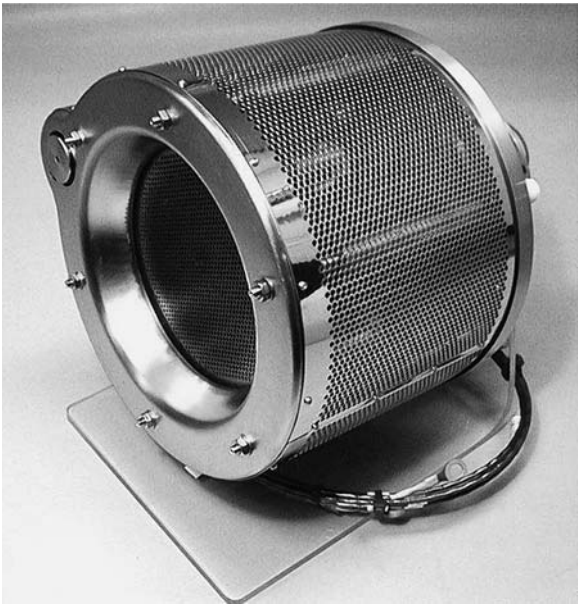


Fig. 11 Photograph of T5 Kaufman-type thruster (QinetiQ photo).

relationships that have been successfully employed subsequently in the development of the much larger UK-25 [7, 76] and T6 [77] devices. These scaling relationships provide the basis on which much of the analysis in this report is founded.

1. T5 Thruster

This United Kingdom thruster [23, 78], which was flown on the Artemis communications spacecraft [35, 79], is shown in Fig. 11. It was developed jointly [34, 80] by RAE/DRA/DERA/QinetiQ, the Culham Laboratory, and Matra Marconi Space (MMS) UK Ltd., now Astrium UK/EADS. As with the RIT-10, this version has operated in the orbit-raising and NSSK roles on Artemis, as part of the UK-10 ion propulsion system (IPS). In addition, the same basic thruster was selected for the now cancelled Nuclear Electric Propulsion Space Test Program (NEPSTP) mission [19, 81] by Johns Hopkins University, and a specially developed version has also been chosen for the drag compensation propulsion task on ESA's GOCE spacecraft [82].

The T5 GIE has several special features that permit very precise throttling [83] over an extremely wide range, 0.3 to 30 mN, and give a low ion-beam divergence of less than 15 deg under most conditions. These features are the use of solenoids (see Fig. 9) to generate the magnetic field applied to the discharge chamber, independently controlled propellant flows to the cathode, the neutralizer and the discharge chamber, and inward (concave) dishing of the grid system.

When operated at high SI, with values of V_B reaching beyond 2kV, the T5 thruster provides much enhanced performance [84], with the thrust extending to 71mN and the SI approaching 4500 s. The input power under these conditions reaches nearly 2kW, but temperatures do not become excessive because the bulk of this power is then fed into the ion beam. No mechanical changes to the thruster are needed to permit this operating regime to be explored. This represents a considerable achievement for a 10-cm beam diameter device. It is this latter accomplishment, as well as the verified scaling relationships, that render the design features of this device of interest for high-power missions.

2. *RIT-15*

Recent development of the RIT-15 commenced in the late 1980s [85] when it became clear that the increasing mass and lifetime of communications satellites necessitated a higher thrust level for NSSK than could be provided by the RIT-10. Scaled from the RIT-10 and an early version initially investigated at the University of Giessen in the 1970s [85], initial concepts [86] utilized a variety of flat grid configurations, but all providing a beam diameter of between 13 and 14.2 cm; an engineering model is shown in Fig. 12. The main design objective was a thrust level in the region of 50 mN and an SI exceeding 4000 s.

Later versions [87] utilized carbon-carbon grid technology for greater lifetime, and the shape of the discharge chamber was modified from cylindrical to hemispherical to reduce the internal energy losses caused by recombination on the walls. The latter idea reduced the discharge chamber power losses by up to 23%. Two variants were investigated. The RIT-15LP was aimed at relatively low-power

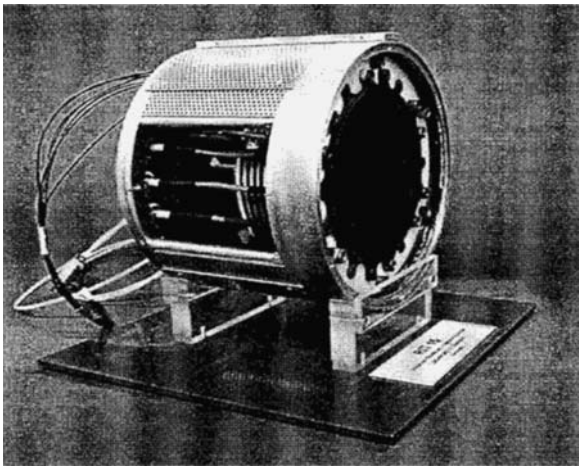


Fig. 12 Photograph of early version of the RIT-15 thruster. (Courtesy of University of Giessen.) [85].



Fig. 13 Two Kaufman-type thrusters mounted on the SERT II spacecraft. (From NASA.)

missions, for which a moderate specific power was required; 25.5 to 26.5 W/mN was achieved at an SI of 2900 to 3600 and a thrust of up to 50 mN. The other, the RIT-15S, was intended for high SI applications, with beam accelerating potentials in excess of 2 kV. However, as the RIT-15LP has been more extensively documented, this version is included later in Table 2.

3. SERT II

Ion propulsion was thought to be ready for actual scientific and commercial applications in the mid-1960s, with the final confirmation of this status expected from NASA's SERT II mission, which was launched in February 1970. As anticipated, this mission was the first to demonstrate conclusively in space that GIEs will work as designed for very long periods of time, producing the calculated thrust, without causing thruster-spacecraft interaction problems.

This mission included two 15-cm beam diameter Kaufman-type thrusters [36] developed by the NASA Lewis Research Center in the 1960s. Using mercury propellant, these thrusters each provided a nominal thrust of 29 mN with an SI of 4770 s. The latter has still to be exceeded in space. The mission was not without difficulties, which were largely predicted before launch, but managed to continue until all propellant was exhausted. This took 11.5 years from the launch in Feb 1970 [88]. A photograph of the spacecraft showing the two thrusters is reproduced in Fig. 13.

It was known before launch that there was severe charge-exchange erosion of the grid system of this type of thruster, and the solutions to this difficulty had been determined. However, there was no time in which to implement them

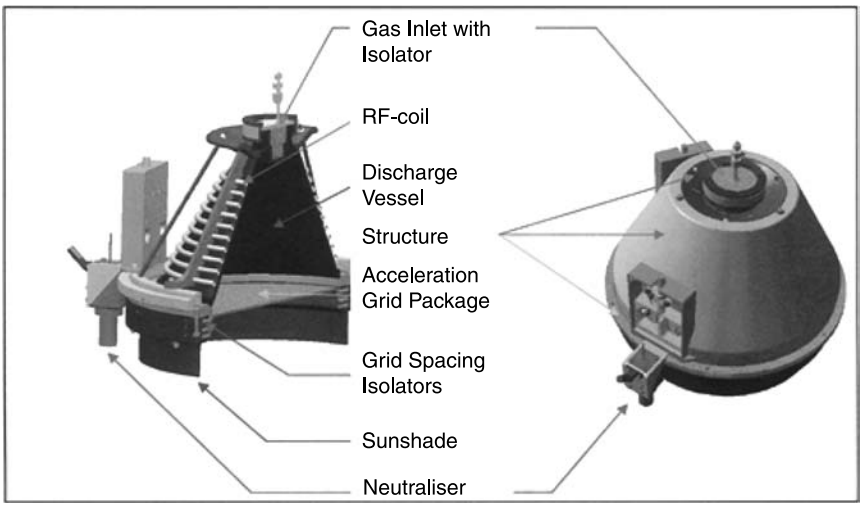


Fig. 14 Diagrammatic representation of the RIT-XT thruster. (From Astrium GmbH.) [30].

before launch, and so a relatively short operational lifetime was envisaged from the outset. One thruster did, indeed, fail from this problem early in the flight, but the operation of its discharge chamber continued to be demonstrated, thereby showing excellent durability of all components apart from the grid system. The other engine continued to operate reasonably satisfactorily until all of the mercury propellant was used, giving an aggregate thruster running time of nearly 4000 h.

4. RIT-XT/RIT-22

This 20.8-cm beam diameter RF gridded device [30, 89] has a long heritage, including the RIT-10 [62], and RIT-10 Evo [90] and the RIT-15 [87] thrusters. It is shown in diagrammatic form in Fig. 14, and a photograph is presented in Fig. 15. It has now been extensively characterized at thrust levels of interest for the BepiColombo mission [24], including an investigation of its throttling capabilities. It was originally designed as a 100-mN-class device, with a published design thrust extending to around 150 mN, but this has now exceeded 200 mN [91]. Values of SI of up to 6420 s have been reported, with a beam accelerating potential of 3 kV and an input power of 8 kW.

Figure 14 shows that the hemispherical discharge chamber of the RIT-15 has evolved to a conical design to further reduce energy losses as a result of electron-ion recombination. The carbon-carbon grid design has benefited considerably from the experience gained from the RIT-10 Evo, RIT-15, and ESA-XX [92] thrusters and now provides a very high perveance, with a potentially long lifetime. As it nears qualified status, it has been renamed the RIT-22, having been previously known as the RIT-XT.

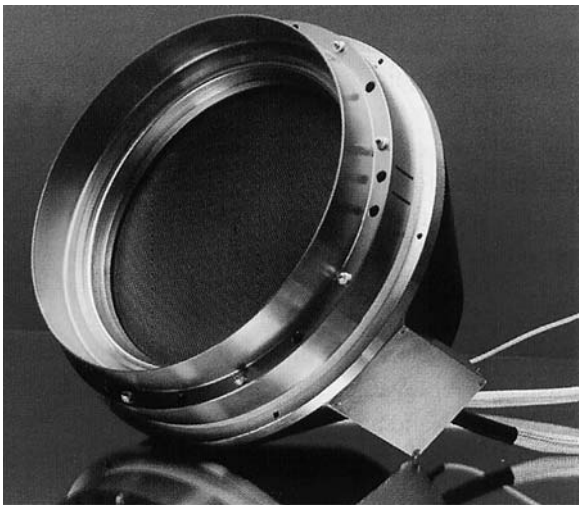


Fig. 15 Photograph of the RIT-XT thruster. (From Astrium GmbH.) [30].

5. T6 Kaufman-Type Thruster

This is a 22-cm beam diameter dc gridded thruster [77, 93] originally developed for NSSK on large geostationary communications satellites, but with the inherent capability to provide high thrust and SI for interplanetary missions. An engineering model is shown in Fig. 16. It was designed using basic scaling data derived

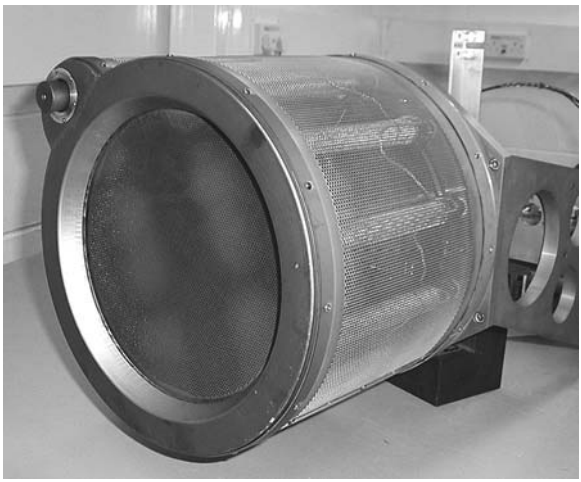


Fig. 16 T6 engineering model ion thruster. (From QinetiQ.)

from the T5 [80, 94] and UK-25 [76] programs, with a nominal thrust of 150 mN for NSSK and 200 mN for deep-space missions, and an SI of between 3000 and 5000 s. A smooth, wide throttling range is an intrinsic capability of this concept [83, 95], which also provides the low beam divergence and very stable thrust vector direction found with the T5 design [83, 95, 96].

The program has proceeded well beyond the characterization of the thruster's performance, vibration resistance, and beam parameters, and has entered the long-duration test phase; this is at 200 mN to meet the requirements of the BepiColombo mission to Mercury [24]. The thruster uses either molybdenum or carbon grids, the latter being employed when a need for considerably enhanced total impulse has to be met, as in the case of the BepiColombo application. A further potential application is to the stationkeeping of the new European communications satellite platform, AlphaBus [97], for which a high SI is a significant advantage.

6. ESA-XX RF Thruster

This 25-cm beam diameter RF ionization gridded thruster [92] was developed in Germany (DASA/MBB and Giessen University), the United Kingdom (AEA Technology), and Italy (Proel/Laben), under ESA sponsorship. The respective responsibilities were the discharge chamber, the grids, and the neutralizer. The aim was to combine the best features available at the time in European gridded thrusters, with basic development data being taken from the RIT-35 discharge chamber [60], the UK-25 grid system [76], and the RIT-10 neutralizer [62]. A sectional diagram is shown in Fig. 17, from which the heritage is clear, with the discharge chamber resembling that of the RIT-35, and the

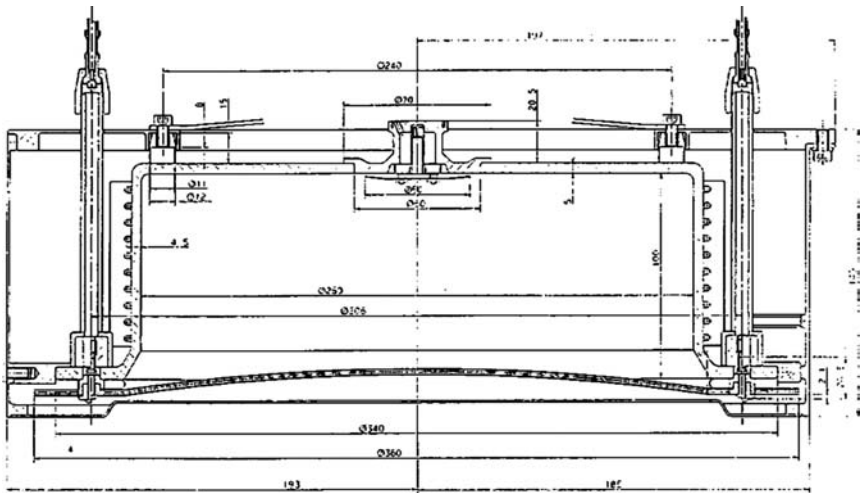


Fig. 17 Diagrammatic representation of the ESA-XX RF thruster (Astrium GmbH diagram).

inwardly dished grids those of the UK-25, T5 (Fig. 11), and T6 (Fig. 16) thrusters. The neutralizer (not shown in Fig. 17) is an enlarged version of that of the RIT-10 thruster.

Using Xenon propellant, the nominal thrust is 200 mN, the demonstrated thrust range is 10 to 200 mN, and the SI at a maximum power of 8.5 kW is 5400 s, so that this device clearly meets the basic requirements of many possible deep-space missions.

7. XIPS-25 MESC Thruster

The XIPS-25 thruster, initially designed by Hughes prior to the development of the smaller XIPS-13 [70], is a high-power and -thrust device [98] intended for the NSSK role [74] on the HS-702 series of communications satellites. It is also employed for the later stages of orbit emplacement [28], thereby saving large quantities of chemical propellant. It was further developed, with a larger diameter, as the NSTAR thruster [72] so successfully used on the DS-1 mission [2, 23].

This 25-cm beam diameter design recorded values of discharge chamber efficiency of about 110 W/A at an uncorrected propellant utilization efficiency of 80%, rising to 140 W/A at nearly 95%. This outstanding performance was partly a result of the large volume of the device, which kept losses low. By comparison, the smaller XIPS-13 thruster operates typically at about 220 to 240 W/A at 80% utilization efficiency, which is very similar to Kaufman thruster values. However, the anode voltage is much less than in a Kaufman thruster, being typically at 28 to 30 V. This increases discharge chamber and screen grid lifetime, and values as high as 25,000 h have been predicted for this grid.

The 25-cm thruster was successfully operated for 4350 h, including 3850 on-off cycles, using a flight-type propellant feed system and a breadboard model power conditioners [98]. This experience, in which significant performance degradation occurred, led to the doubling of the accel grid thickness to increase lifetime. Perhaps surprisingly, the opportunity to bias the decel grid to enhance further overall lifetime was not taken; this is now standard practice on the T5 thruster. With the thicker accel grid, a lifetime in excess of 12,000 h is predicted. As just mentioned, many flight-qualified thrusters have been deployed with great effect on several Boeing/Hughes HS-702 communications satellites; a photograph of a flight thruster is shown in Fig. 18.

8. UK-25 Kaufman-Type Thruster

This 25-cm beam diameter dc gridded thruster [76], shown in Fig. 19, was originally designed for interplanetary missions at more than 200-mN thrust, with the cancelled Comet Nucleus Sample Return Mission [99] being the initial objective. It was based on scaling relationships [94, 100] derived during work on the earlier T4A and T5 thrusters, and initial laboratory tests confirmed the validity of this approach. It was established that the performance envelope is very wide, extending to at least 320 mN, with values of SI approaching 5000 s and an input power of nearly 10 kW. The program reached engineering model status, but no long-duration testing was undertaken.



Fig. 18 Photograph of XIPS-25 MESC ion thruster [98]. (From Boeing/Hughes.)



Fig. 19 UK-25 engineering model ion thruster with earth screen removed [76]. (From Culham Laboratory.)

For the purposes of this report, data for the UK-25 taken at a thrust of 250 mN were assumed to be typical, noting that the device can be throttled over a very wide range, certainly up to 320 mN, and that a gridded thruster has no "best" operating point. In passing, it should be recalled that the lifetime of a gridded thruster falls as the thrust is increased, owing mainly to greater grid erosion. Consequently, the choice of 250 mN will ensure a longer life than would be achieved at the highest values of thrust. Clearly, this is somewhat arbitrary, but it allows a reasonably accurate impression to be gained of the overall characteristics of this thruster. At a higher thrust, the overall performance would be better, but the lifetime would be somewhat reduced.

9. NSTAR MESC Thruster

The 30-cm-diam NSTAR thruster [72] flown on the Deep Space 1 interplanetary spacecraft [2, 73] has been remarkably successful and has exceeded its original objectives. It is shown mounted in the rear of the spacecraft in Fig. 20. Developed jointly by NASA Lewis/Glenn Research Centers and Hughes, it is considerably derated from the earlier 30-cm thrusters [101], with a maximum thrust of 92.6 mN at an input power of 2.3 kW and a wide throttling range. A successful flyby of the asteroid 1992 KD was completed on 29 July 1999, and the spacecraft then went on to observe from a relatively close distance the nucleus of the comet Borelly [73]. The thruster operating time in space amounted to more than 16,000 h, and a ground test subsequently exceeded 30,000 h [102].

Following this success, a derivative thruster has been designed [103, 104] with an enhanced performance. The aim is to extend the performance envelope to 5 kW, with the capability to "process" 400 kg of xenon. This is not a particularly difficult objective because thruster operation has been demonstrated at beyond 10 kW, with values of SI at up to 4500 s. To accomplish the necessary total impulse, a

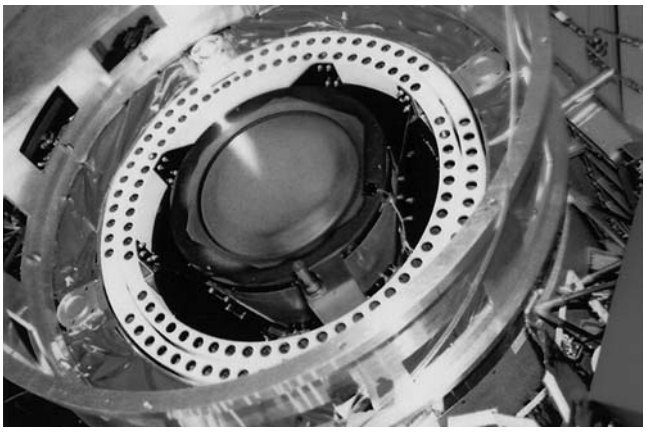


Fig. 20 NSTAR thruster mounted in rear of Deep Space 1 spacecraft [72]. (From NASA.)

change to titanium or carbon grids is being studied; the former have been tested to 4.6 kW and 172-mN thrust. Even under the new operating conditions, the thruster is very considerably derated, so that there should be no difficulty in meeting the revised requirements

10. NASA 30-cm Beam Diameter Thrusters

In the context of large ion thrusters, mention should be made of the very extensive experience gained in the United States over nearly four decades of research and development effort on a wide variety of 30-cm beam diameter devices. These have used both the Kaufman-type and cusp-field discharge chamber configurations, and the work has included the accumulation of a great deal of life-test data with mercury and xenon propellant. Many lifetests of the 30-cm beam diameter Kaufman-type thruster developed jointly by NASA Lewis and Hughes have been reported, including close to 10,000 hours with the J-Series device [101]. In other work, this thruster exceeded input power levels of 10kW [105].

Despite these successes, the U.S. program was eventually diverted to become concentrated exclusively on the cusp-field geometry device [70], with a variety of thrusters being developed to flight status. Nevertheless, the performances achieved with the earlier devices remain of interest, and so the J-series and 900-series are represented later in Table 2, using xenon and mercury propellant, respectively.

As mentioned earlier, the Hughes 30-cm MESC thruster is also capable of a much greater performance than indicated by the NSTAR thruster [72] or its derivative [103, 104]. It has, in fact exceeded 10 kW by a considerable margin, reaching a thrust of 364 mN at an SI of 5160 s.

11. RIT-35 RF Thruster

This is an older 35-cm beam diameter RF gridded thruster, which has been the subject of many years of work at Giessen University; a schematic diagram is shown in Fig. 21. It showed very good potential in tests in the 1970s using mercury propellant [106], and should not be disregarded because excellent results were obtained later using xenon and redesigned extraction grids [60, 107]. Although estimated thrusts extended to 500 mN with an input power of 18 kW and an SI of about 5000 s using mercury, experimental data reached only 250 mN. There the power input was about 7 kW. With xenon, testing attained only 104 mN, but this is not a true reflection of the thruster's capabilities.

The diagram of the thruster in Fig. 21 represents the version using mercury propellant and flat grids. Later developments employed outwardly dished grids to enhance thermal stability because carbon-carbon technology was not available at the time to provide a superior capability. As this grid technology is inferior to that of the latest RIT thrusters, high perveance could be obtained only by operating the accel grid at −1700 V, with a major impact on potential life.

12. NAL/NASDA/Toshiba BBM-2 MESC Thruster

This Japanese consortium has developed a very promising dc gridded thruster of 35-cm beam diameter [108, 109] and has also investigated experimentally larger

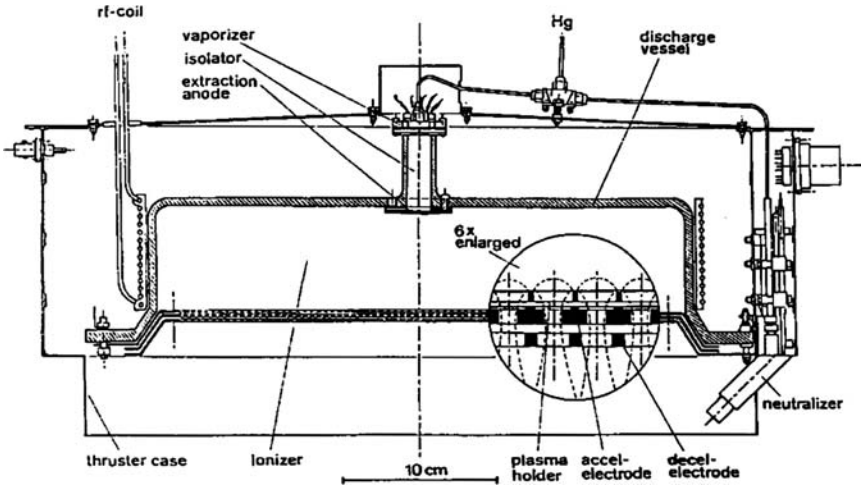


Fig. 21 Diagrammatic representation of the RIT-35 thruster (University of Giessen diagram).

devices. The target for this work was a thrust of 150 to 180 mN at an SI of 3500 s. The input power was specified to be in the region of 4 kW, and ring cusp MESC geometry was selected for the discharge chamber. A very ambitious objective was set for the lifetime, 30,000 hours. A recently reported long-duration test reached 2659 h at 150 mN, with an SI of 3518 s, the latter being partly caused by the excellent utilization efficiency achieved, which was 90%.

13. Tokyo Metropolitan Institute of Technology 30-cm MESC Thruster

This development [110] is supported by Melco and again exploits the ring cusp discharge chamber principle. The thruster has demonstrated a very high standard of performance, reaching 153 mN at an SI of 3710 s and with an input power of 3.5 kW. As with the BBM-2, the utilization efficiency is very impressive, as indicated by the modest beam accelerating potential of 1 kV, with values of around 93 to 94% being reported. The total thruster efficiency is very close to 80%, which is among the best available. However, this is a laboratory device, with no indication of lifetime and with no attempt reported of qualification activities.

14. NEXT MESC Thruster

This is an advanced, larger diameter version of the NSTAR thruster, with the title "NASA's evolutionary xenon thruster" (NEXT) [111, 112]. It has a beam diameter of 40 cm and an initial design input power of up to 10 kW, with a throttling range of 8:1. However, these values were later modified to 6.9 kW and 11:1 [113]. The maximum SI was originally specified as 4040 s, with a total efficiency of greater than 68%, but later values are greater than 4100 s and 70%. Following

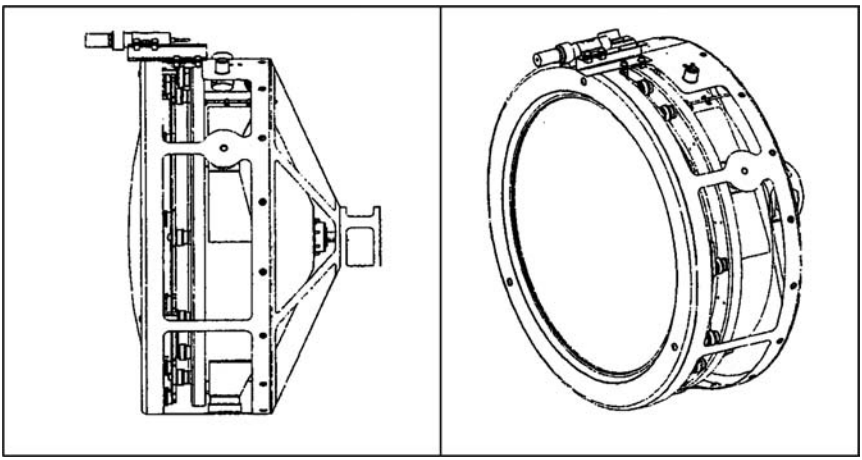


Fig. 22 Two views of the NEXT thruster [111]. (From NASA.)

extensive development effort, the mass is now to be less than 1.8 kg/kW and the total impulse very large, with a throughput of xenon of more than 270 kg [113]. Drawings of two views of the thruster are shown in Fig. 22.

Work has reached the engineering model and preliminary endurance testing stage, with additional research concentrating on the grid design [112]. Three engineering model thrusters were constructed, and one of these was tested to 2038 h, at an average SI of 4110 s and total efficiency of 69.4% [114]. The mean thrust at the maximum power point of 6.9 kW was 237 mN. Although the objectives are ambitious, particularly concerning the grid design, the limitations of the cusp-field concept are clearly illustrated by the severe fall in SI as the thrust is reduced. In one set of tests, the thruster operated at 4060 s at 6.9 kW, but only 2300 s at 1.1 kW. The efficiency fell from 69 to 51%.

15. NEXIS MESC Thruster

For the more challenging interplanetary missions, probably using nuclear-power sources, NASA has decided to invest in the development of ion thrusters much larger than NEXT. The more conventional of these is the NEXIS (nuclear electric xenon ion system) device [115], this is a 65-cm discharge chamber diameter thruster, again employing the MESC principle, and with a configuration similar to those of NSTAR [72] and NEXT [111, 114] GIEs. However, the exit from the discharge chamber is masked down to a diameter of 57 cm, so that grid-erosion problems caused by low plasma densities at the periphery are avoided. The initial mission for which it was intended is the Jupiter Icy Moons Orbiter (JIMO) [116, 117].

Development is being led by JPL, and the objectives include a power consumption of 20 kW, an SI of 7500 s using xenon propellant, with a beam accelerating potential of 7 to 8 kV, and a total efficiency of more than 78%. It is hoped to achieve a total xenon throughput of no less than 2000 kg by combining a new

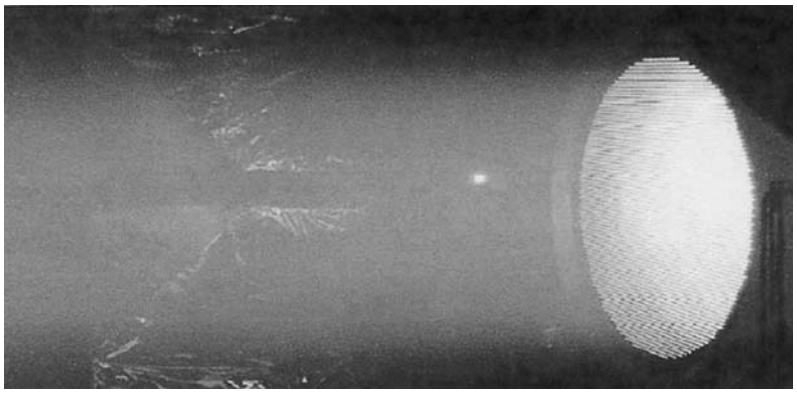


Fig. 23 NEXIS thruster operating at 27 kW [115]. (From NASA.)

reservoir hollow cathode, a new carbon-carbon grid configuration, and the flat plasma density profile permitted by masking the outer region of the grids.

The operating thruster is shown in Fig. 23. This photograph was taken when the power consumption was 27 kW, the total ion extraction potential 7 kV, and the thrust 517 mN. The SI was 8700 s, the propellant utilization efficiency 94% and the total efficiency 81%. Thus all of the goals have been surpassed, although durability has yet to be demonstrated; an operating time of 5 to 10 years has been specified by NASA.

Clearly, it is impossible in a meaningful program to demonstrate a thruster lifetime of 5 to 10 years. Bearing in mind that it is usually necessary to include a margin of 50% in a life-test program, the thruster would have to be tested for between 7.5 and 15 years. The cost of this would be prohibitive, the program would be extremely protracted, and a failure well into the test, for any reason, would greatly extend the total time required even further. With a program of this sort, a conventional life test is not in any way viable.

It is now assumed, with programs of this sort, that qualification must be carried out by calculation, assuming a good understanding of the fundamental life-limiting factors. The latter must be determined by means of a detailed research program, which must include experimental validation of the main mechanisms that limit lifetime. However, full reliance cannot be placed on such a process, at least for early missions, and so additional redundant thrusters should be carried. The latter requirement is not too difficult to implement because the masses of such thrusters are relatively small in comparison with the masses of other parts of the system. As an example, the mass of each T5/UK-10 thruster carried on the Artemis spacecraft was about 1.8 kg, whereas each power conditioner weighed 11.7 kg [35].

16. HiPEP MESC Thruster

One of the most innovative ideas is the configuration of the high-power electric propulsion (HiPEP) thruster, which has a rectangular discharge chamber and grids. The initial application for this technology is likely to be the JIMO mission

[114, 115], for which a total power consumption of 100 to 250 kW is envisaged [115], with an SI of 6000 to 9000 s and a total thruster efficiency of greater than 65%. The operating time is specified as 14 years, which is equivalent to a propellant throughput of 100 kg/kW. The aim for an individual thruster is a power consumption of 20 to 50 kW.

The 91 × 41 cm rectangular shape [118] was selected to simplify the scaling process, both of the grids and of the discharge chamber. Two approaches to the discharge chamber ionization are being studied; one is the conventional dc discharge in an MESC magnetic field configuration using a hollow cathode electron source. The other is the ECR mechanism, with an applied frequency of either 2.45 or 5.85 GHz. Both are illustrated in Fig. 24, in which the dc thruster is operating with an input power of 34 kW and the ECR variant at 13 kW. Clearly, the dc variant offers the best prospects at present, but ignores the influence of the discharge mode on potential lifetime.

To date [116], the dc variant has operated at up to 40 kW, providing a thrust of 670 mN at an SI of 9620 s. Under these conditions, the beam accelerating potential was 7 kV, the propellant utilization efficiency about 92.5%, and the discharge power slightly over 1 kW. The total thruster efficiency was 80%, and throttling down to 9.7 kW and 240 mN was demonstrated. These results were obtained with curved titanium grids, but flat pyrolytic carbon grids [119] represent the next stage in the development process; these have now been tested.

17. Very Large Diameter Thrusters

Over several decades, NASA has shown interest in very large diameter thrusters for a variety of missions involving large and heavy spacecraft, usually requiring extremely high values of ΔV.

As examples, at the beginning of their EP program, NASA Lewis investigated the possibility of building a 1.5-m-diam GIE [120]. Although this was constructed, the performance achieved did not meet expectations, and the project was discontinued. The difficulties associated with such large grids were found later to still be present at 50 cm diam [121], leading to the conclusion that the 40 cm of the

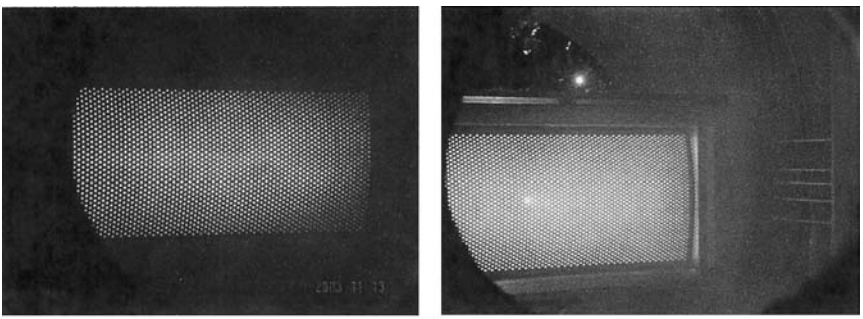


Fig. 24 HiPEP thrusters operating at a) 13 kW (ECR discharge) and b) 34 kW (dc discharge). (From NASA.) [116].

NEXT engine might be the maximum possible with present technology. However, as just reported, successful results have been reported from the larger NEXIS and HiPEP devices.

In this context, it should also be mentioned that NASA Glenn has commenced a program to develop a very high-power, high-SI thruster for precursor interstellar missions [122]. Owing to the difficulties inherent in manufacturing and operating very large diameter grid systems, this employs a 76-cm-diam discharge chamber fitted with three separate 30-cm-diam grid sets, as shown in Fig. 25. The SI is expected to reach 14,000 s using krypton propellant. The specification includes a maximum beam accelerating potential of 13 kV, a thrust of 112 mN at an input power of 10.3 kW, and a total efficiency of 76%. Initial results confirm that, using xenon, the efficiency is lower than in the NSTAR thruster; this was expected because the ion extraction area is much less than the total discharge chamber cross-sectional area (Fig. 25). The SI has covered the range 1800 to 3550 s, with a maximum input power of 4.4 kW and a thrust of 154 mN.

C. Summary of Capabilities of Existing Gridded Thrusters

Selected performance data from the thrusters just described are summarized in Table 2. This includes all known thrusters with a power consumption above 1kW, excluding some devices that are at an extremely early stage in their development. That status is denoted by the heading "S," and the references quoted are examples only.

Before commenting on the thruster characteristics presented in Table 2, it should be mentioned that three propellants are included: mercury, Xenon, and Krypton. These represent three phases of the decades-long gridded ion-thruster development period. Before explaining the broad features of this, it should be pointed out that any material which can be a vapor or pure gas at a convenient discharge chamber temperature can be used as a propellant, provided that it does not chemically attack any part of the thruster. It is also desirable, but not

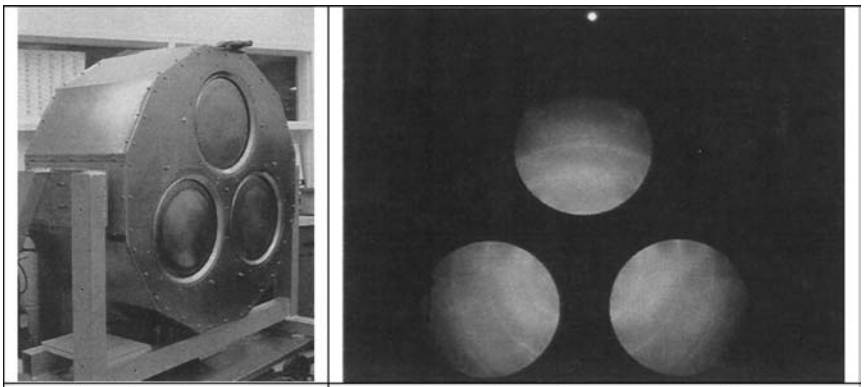


Fig. 25 Photographs of NASA's high SI thruster [122]. (From NASA.)

essential, that it will not attack chemically any part of the spacecraft. This broad range of possible propellants is discussed later in Sec. V.C.3, including Fig. 32.

In the early days of research into gridded thrusters, it was initially decided that the highest possible thrust should be achieved for a given beam current and power. Thus the atomic mass (AM) of the propellant should be as large as possible, and mercury was selected, because its AM is 200. This was very satisfactory, and the flight of two thrusters for 11.5 years on the SERT-2 spacecraft [36] did not indicate that this propellant was other than totally acceptable. However, personnel and spacecraft safety considerations later led all agencies in this field to change to an inert gas, xenon, with an AM of 131. Although not so good as mercury, from the point of view of thrust for a given beam current, it performs satisfactorily, and nearly all present programs rely on it.

However, with the possible need for much higher values of SI, programs with that requirement are now moving towards gasses with lighter AM, such as argon and krypton. Although much more difficult to store onboard a spacecraft for a long period of time, they offer the required performance enhancement, as is specified for the NASA interstellar effort [122].

It is clear from Table 2 that all thruster technologies are capable of scaling to higher power levels and that the general requirements of many NEP missions can be satisfied. A power input of 10 kW has been reached or exceeded by all types, with the HiPEP concept attaining 40 kW. The basic conclusion is that it is possible to design large thrusters which consume power levels of interest; how far this process can continue is largely dictated by the ability to design grid systems with adequate durability and resistance to the launch environment.

Similarly, twin- and triple-grid ion extraction systems have been shown to be entirely viable at much higher potentials than usually applied, with voltages of up to 7 kV routinely used. Indeed, laboratory experiments have been conducted successfully at up to 30 kV [14]. As a result, values of SI of close to 10,000 s have been reported for the HiPEP thruster, using xenon propellant, and it is predicted that 14,000 s will be achieved with the NASA interstellar precursor thruster with Krypton. However, under these circumstances the power fed into the beam is much higher than with low SI, so that the power-to-thrust ratio becomes much greater; it reaches 87 W/mN in the case of the interstellar precursor thruster. This trend cannot be avoided and must be accepted, so that this ratio is no longer of use as a performance indicator.

Thrust levels are also seen to rise with the dimensions of the thruster and with power consumption, as expected, reaching 670 mN in the case of the HiPEP device. However, this is not impressive when compared to some of the smaller devices; for example, the 25-cm beam diameter UK-25 attained 316 mN under test with only a modest value of SI [76], and the smaller T6 [93] and RIT-XT [30, 91] routinely operate at above 200 mN. In this context, the parameter of importance is the thrust density, because this determines how much thruster mounting area will be required on a spacecraft to produce a specified thrust. This area is sometimes very restricted and can thus become a primary design parameter [135, 126].

Table 2 shows that all of the advanced large thrusters operate at very modest values of thrust density, typically below 0.2 mN/cm^2. This follows the trend set

very early in the GIE development process by the SERT II thrusters [36], which achieved 0.16 mN/cm^2, a trend continued by the NSTAR GIE [72] with 0.13 mN/cm^2. Even the NSTAR Derivative [103, 104] only extends this value to 0.24 mN/cm^2. Whereas the reason for these low values is the need to ensure long grid life, what can be accomplished by a qualified device is indicated by the XIPS-25 [101], which is in commercial service on many communications satellites [127]. This reaches 0.5 mN/cm^2. This value is surpassed by two thrusters in the qualification phase of their development for missions of very long duration, which include the challenging BepiColombo mission to Mercury [24]; these are the T6 [93] and RIT-XT [30, 91], with typical thrust densities of 0.61 and 0.63 mN/cm^2, respectively.

What can be accomplished, at moderate SI, is indicated by the high-power version of the T5 GIE [34, 128], with a maximum thrust density of 0.90 mN/cm^2, at an SI of 4334 s. If the SI were increased at constant beam current density, this thrust density would be much larger.

Thus it is thus clear that the beam current density is of prime importance in achieving a high thrust density. The values for the thrusters listed in Table 2 vary by more than an order of magnitude, with the lowest being recorded for the larger devices; this is surprising because they are operated at higher values of SI, and therefore larger extraction potentials. It will be shown later that such conditions are conducive to attaining higher values of beam current density, but this has certainly not been achieved. The values derived from Table 2 vary from 1.1 mA/cm^2 for the interstellar precursor thruster and 1.6mA/cm^2 for NEXIS, through 2.5mA/cm^2 for NSTAR, reaching 14.3 mA/cm^2 for the RIT-10 Evo and 13.4 mA/cm^2 for the T5. The value for T6 is 8.9 mA/cm^2. It is therefore certain that the performances of the larger thrusters in Table 2 can be increased very considerably, with close to an order of magnitude being feasible.

This conclusion is amplified by an examination of power density, which should increase dramatically with SI, if the physical principles utilized in designing these devices remain the same and independent of dimensions. This is certainly not the case, with the power densities for all of the newly developed large GIEs being well under the values achieved by the older, smaller thrusters. The highest recorded power density is that of the T5 GIE, with 28.3 W/cm^2, with the RIT-XT reaching 23.3 W/cm^2. Many other relatively low SI thrusters exceed 15 W/cm^2, whereas the best of the more modern high-SI devices, the HiPEP, achieves experimentally only 10.5 W/cm^2, and that is at an SI of nearly 10,000 s. There is, very clearly, considerable room for improvement here. That this can be realized is shown later in this report.

IV. Scaling Process

The scaling relationships that primarily determine the performance of a gridded thruster concern the ion extraction and acceleration grid system. In evaluating the capabilities of any grid system, it is assumed that the required flux of ions to the screen grid (Fig. 4) can be supplied from the discharge chamber plasma under all circumstances. The scaling of this plasma is reasonably well understood for both RF and dc thrusters. It should be emphasized that the separation of the process for producing the ions from that for extracting and accelerating them is a major advantage, which is not found in most other EP devices. A further advantage of

this concept is that the important performance parameters can be dealt with separately to first order. Thus, although there is, for example, an impact on thrust if the SI is modified by altering either the extraction potential or atomic mass of the propellant, this can be compensated for precisely by a change of beam current.

A much more complex problem is to design an extraction system to meet specified lifetime requirements, although the ion-optics models now available permit reasonably accurate estimates to be made of total erosion rates and of the locations of the dominant erosion sites. However, an important limitation of this modeling activity concerns the lack of accurate primary data regarding sputtering yields as functions of energy and angle and also charge-exchange cross sections as functions of particle energy. In most thrusters, there is also inadequate information concerning the way in which the plasma density and electron temperature profiles in the discharge chamber vary with operating conditions; such information is costly to obtain in a comprehensive way.

A. Grid Design Options

In all present thrusters the ion extraction system is of either twin- or triple-grid configuration, as depicted in Fig. 26. Such grids operate in an accelerate/decelerate mode to enhance the throughput of ions. In this scheme, the thruster body and screen grid are at the high potential V_B necessary to achieve the ion-beam velocity required. For example, if xenon ions are to be emitted at 40 km/s (SI ~ 3500 s), a potential of 1.1 kV is needed. The accel grid is at a negative potential V_{ac} of perhaps –250 V, to provide focusing of the beamlets, to enable the required current to be

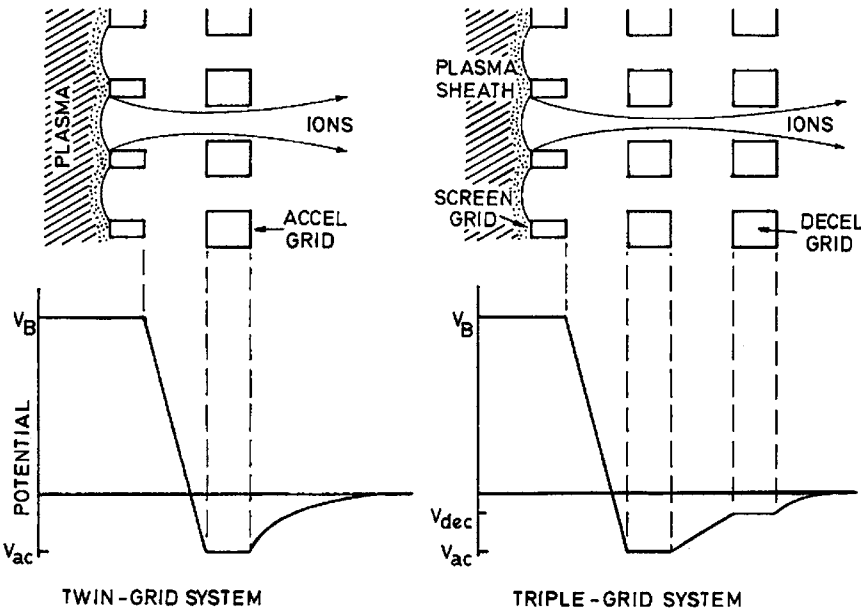


Fig. 26 Schematic diagrams of twin- and triple-grid ion extraction systems.

extracted, and to prevent electron backstreaming into the discharge chamber from the external plasma. Deceleration to space potential then follows; with the triple-grid variant this is via a less negative voltage V_{dec} applied to the decel grid.

To raise the ion velocity v_e and thus the SI, it is merely necessary to increase V_B as appropriate. However, this causes a greater penetration of the intergrid electric field into the discharge chamber plasma. Some penetration, as depicted in Fig. 26, is desirable, because this results in a curved plasma sheath that both increases the ion emission area and aids focusing. Unfortunately, the curvature becomes severe at high voltages, influencing the ion trajectories adversely and causing direct impingement on the outer grids.

This situation is depicted in Fig. 27, in which the sheath positions for a moderate and a high electric field E are shown. Direct ion impingement on the accel grid is evident in the latter case. Moreover, the plasma number density n in the discharge chamber must also be taken into account, because the penetration of the sheath increases as n falls. This effect is illustrated in Fig. 28 for the grid configuration of the T5 thruster [129]. This problem is relevant to the use of a wide throttling range, or if the radial plasma density distribution is strongly peaked. However, in the latter case the dimensions of the screen grid apertures can be matched to this distribution to alleviate adverse effects [129].

Thus it is clear that high values of E and/or low values of n allow the sheath to penetrate deeply into the plasma. The resulting curvature of the surface from which the ions are extracted causes many of the trajectories to diverge from the desired paraxial direction and to impact upon the accel or decel grids. The erosion that this causes severely limits lifetime and cannot be tolerated for any but short missions.

This problem is avoided by the use of four grids because the extraction field is defined by the first two of these (Fig. 29). Most of the ion acceleration then takes place between the second and third grids, where the greater part of the applied

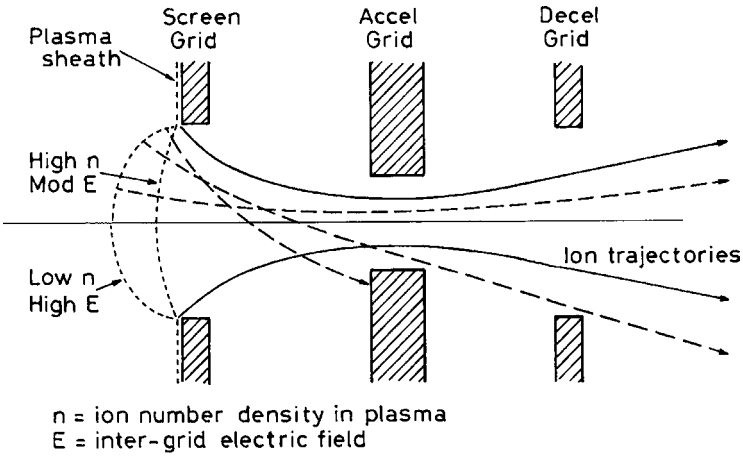


Fig. 27 Triple-grid configuration, indicating the effects of the sheath shape on ion trajectories.

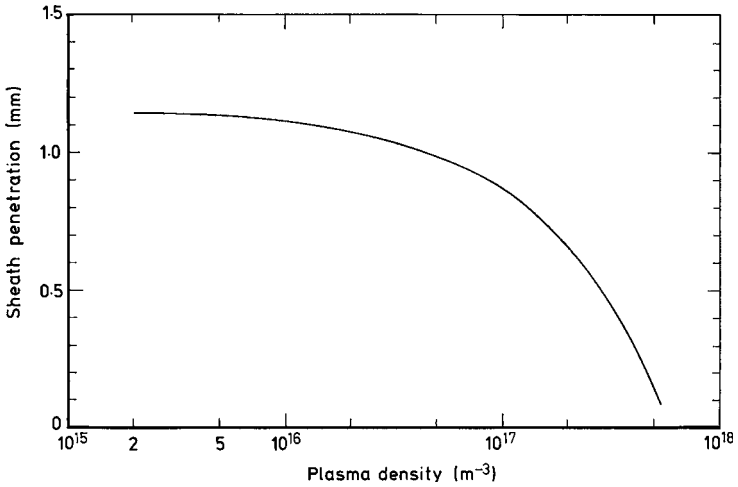


Fig. 28 Plasma sheath penetration as a function of number density for the T5 thruster.

voltage appears. Thus the ion extraction process can remain constant no matter what final velocity and SI are required. This configuration originated in the controlled-thermonuclear-reactor (CTR) research community in order to produce very high-energy particles for injection into fusion machines [130, 131]. Plasma sources fitted with such grid systems are used to accelerate ions, usually hydrogen, to energies that can exceed 100 keV. They are then passed through a charge-exchange gas cell to produce the required high-energy beams of neutral atoms. These are necessary to penetrate the large magnetic fields within fusion devices.

Thus in the four-grid system the ion extraction process is separated from any subsequent acceleration. The ions are extracted from the plasma by the first two grids, which can operate at a potential difference providing an acceptable field penetration into the discharge chamber plasma, and direct impingement onto the

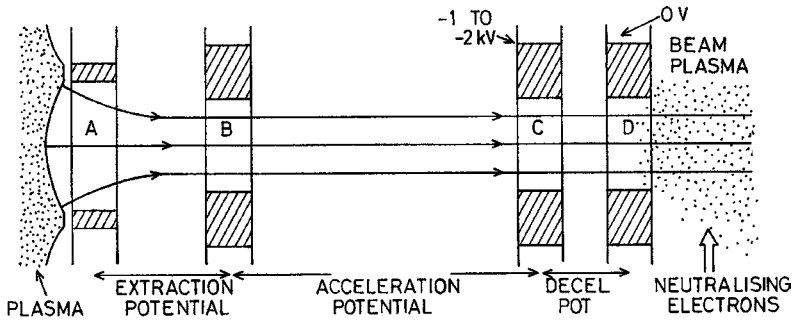


Fig. 29 Schematic diagram of four-grid system.

downstream grids is avoided. The bulk of the acceleration then occurs between the second and third grids, which can be widely separated to accommodate the potential applied, which can be very large. The negative third grid acts in the same way as the accel grid in the conventional two- or three-electrode system, as does the fourth grid. The potential of the third grid in Fig. 29, −1 to −2 kV, applies to the large grid apertures often found in CTR devices. A more realistic value for a typical ion thruster would be −250 V.

B. Exhaust Velocity and SI

From the point of view of many missions, the most important parameter is v_e, which determines the value of SI achieved. This is given by

$$v_e = \sqrt{\frac{2eV_B}{m_i}} \tag{6}$$

where e is the charge on an electron, m_i is the ion mass, and the ions are assumed to be singly charged. Thus v_e is determined by V_B and by m_i. In practice, V_B is the potential of the body of the thruster and of the screen grid, which is typically 1 to 2.5 kV in present designs. The total accelerating potential is larger than this because $V_{\text{mt}} \sim -200$ to -500 V. With triple grids, the decel grid is at $V_{\text{dec}} \sim -50$ V and decelerates the ions. Further deceleration occurs within the space plasma.

Although v_e is given by Eq. (6), in reality it is reduced to an effective value v_{eff} determined by the total propellant utilization efficiency η_{mt}, where this is the fraction of the total propellant flow rate $\dot{m}_t$ accelerated into the ion beam. Thus, $v_{\text{eff}} = \eta_{\text{mt}} v_e$. If I_B is the ion-beam current,

$$\eta_{\text{mt}} = \frac{I_B m_i}{e} \frac{1}{\dot{m}_t} \tag{7}$$

As shown before in Eq. (4), the SI, denoted also by I_{sp}, can be defined as the ratio of thrust T to total rate of use of propellant, in units of sea-level weight. Thus,

$$I_{\text{sp}} = \frac{T}{\dot{m}_t g_0} \tag{8}$$

where $\dot{m}_t$ is now used rather than $\dot{m}$ to differentiate between it and the other propellant flows into a thruster. Using $v_{\text{eff}} = \eta_{\text{mt}} v_e$ and Eq. (6) and (7),

$$I_{\text{sp}} = \frac{v_{\text{eff}}}{g_0} = \frac{I_B}{\dot{m}_t g_0} \sqrt{\frac{2V_B m_i}{e}} \tag{9}$$

Thus it is possible to calculate the SI with good accuracy without using a thrust balance.

With screen to accel grid separations of the order of 0.5 to 1 mm, operation at the few kilovolt level is satisfactory, providing values of v_e for xenon of up to about 65 km/s and giving an SI of between 2800 and 5500 s [76]. With greater

separations and suitable insulator designs, higher values of V_B can be used, so that, from Eq. (9), enhanced values of SI are feasible until the plasma sheath curvature demands a change to a four-grid system.

A further benefit arising from an increased extraction potential is a gain in the perveance or extraction efficiency. This causes more of the ions drifting towards the grids within the discharge chamber to emerge into the beam, increasing I_B and T, and also power consumption. Moreover, an associated improvement in η_{mt} reduces the rate of grid erosion. As an example of what can be achieved, the values of v_e and I_{sp} attained using a relatively low atomic mass propellant, argon, are plotted in Fig. 30 for potentials of up to 40 kV. The latter voltage (which would necessitate the use of a four-grid system) gives a velocity of over 400 km/s and an SI of about 40,000 s, assuming $\eta_{mt} = 0.88$.

Equation (6) shows that v_e is dependent upon the propellant employed, as demonstrated by the high values for argon plotted in Fig. 30. Xenon was originally chosen, as was mercury in earlier times, for its high atomic mass; this is beneficial because it provides an excellent momentum transfer and thrust for a given beam current. However, for ultrahigh SI missions, a lower m_i might be required. The best that can be achieved is to use hydrogen, but this presents storage difficulties because very high pressures or extreme cryogenic temperatures are required. Nevertheless, suitable compounds of hydrogen exist with average atomic masses when completely dissociated of 4 to 5 atomic mass units (amu) [12, 132]. Although dissociation must occur within the discharge chamber, the power required is not excessive, and the SI can be increased by a factor of about five compared to xenon.

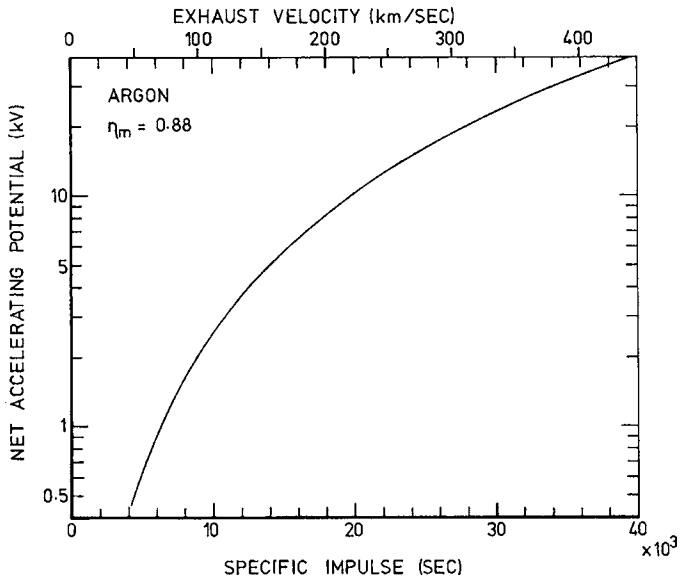


Fig. 30 Exhaust velocity and SI for argon as functions of accelerating potential.

C. Thrust and Perveance

As mentioned earlier, the thrust and thrust density achievable are also important, especially for missions where a time constraint exists. In such cases, if power is limited, it might be necessary to forego the advantages of a very high SI in order to achieve a particular level of thrust determined by mission requirements. In addition, low thrust densities might not be permissible because adequate volume and surface area might not then be available for the propulsion system [126].

Thrust is related to the other parameters by

$$T = I_B\sqrt{\frac{2V_B m_i}{e}} = \frac{I_B m_i v_e}{e} \tag{10}$$

Thus, T will increase with V_B, but decrease if m_i is reduced. Compensation for this can be obtained by extracting a larger I_B, which requires a higher plasma density in the discharge chamber and thus a greater discharge power. The limit is the ability of the grids to pass this increased current. This is determined by their *perveance*, which can be defined [94] as

$$\text{Perveance} = \frac{I_B}{V_T^{3/2}} = \frac{4\varepsilon_o}{9}\left(\frac{2e}{m_i}\right)^{1/2}\frac{AT_g}{d^2} \tag{11}$$

where $V_T = (V_B + |V_{ac}|)$, ε_0 is the dielectric constant of free space, d is the ion acceleration distance, A is the area of the grids, and T_g is the effective transparency of the screen grid. This leads to the definition of a perveance parameter P_g, which is

$$P_g = \frac{I_B m_i^{1/2} d^2}{AT_g} = \frac{4\varepsilon_o\sqrt{2e}}{9}V_T^{3/2} \tag{12}$$

As can be seen in Fig. 31, a logarithmic plot of P_g against V_T is linear; here I_B is in amperes, m_i is in amu, d is in millimeters, and A is in square meter. Experimental points from the T5 [15, 34, 128] and UK-25 [76] Kaufman-type thrusters were used to provide the indicated trends and are consistent with the expected ⅔ power law.

From Eq. (12), I_B will fall if grids of a given design have to be separated by a greater distance to accommodate higher potentials. However, increased ion currents are readily accessible at the enhanced values of V_T discussed here.

The data in Fig. 31 fall on two lines, labeled "peak performance" and "Artemis conditions." The former represents the maximum perveance case, where lifetime is likely to be limited. The Artemis line applies to the conditions required for long life, as specified for the T5 thruster for operational use on the Artemis communications satellite [78], for which a lifetime of close to 15,000 h was required.

D. Current, Power, and Thrust Densities

The maximum current density J_B emitted by the grids is, from Eq. (11),

$$J_B = \frac{4\varepsilon_o}{9}\left(\frac{2e}{m_i}\right)^{1/2}\frac{T_g}{d^2}V_T^{3/2} \tag{13}$$

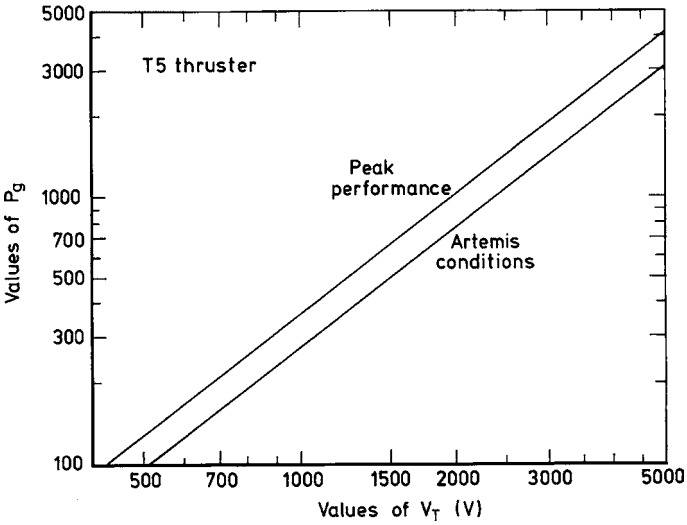


Fig. 31 Values of P_g as a function of V_T.

Assuming that the bulk of the power supplied to the thruster is used to accelerate the beam, and thus operation is at high SI, the power density P_d is found by multiplying J_B by V_B, so that

$$P_d = \frac{4\varepsilon_o}{9}\left(\frac{2e}{m_i}\right)^{1/2}\frac{T_g}{d^2}V_T^{3/2}V_B \tag{14}$$

From Eq. (10), the maximum thrust density T_d is

$$T_d = J_B\left(\frac{2m_iV_B}{e}\right)^{1/2} \tag{15}$$

where J_B is given by Eq. (13).

E. Discharge Chamber

The grid relationships just discussed are applicable to all gridded thrusters. The only difference between the detailed design for one thruster and another concerns the plasma density distribution at the screen grid. This determines the radial ion-beam density distribution and influences the maximum and mean values of all parameters. Thus the only part of the scaling process that is dependent upon the type of thruster is that applicable to the discharge chamber.

Of course, a main parameter for scaling the thrust is the effective area of the grid system. This can in principle be increased as necessary, keeping the maximum current density (usually on the axis) constant. This is accomplished by raising $\dot{m}_t$

and the discharge power in the same ratio as the specified increase in I_B. Second-order effects include the improvement in ionization efficiency as the size increases, owing to the internal surface area being dependent upon the square of the radius, whereas the volume has a cubic relationship.

With the RIT-XT/RIT-22 type of RF thruster [133], the skin effect will cause the ionization rate to depend on radius, so that, for the larger devices, it can peak somewhere between the center line and the wall. The plasma density distribution, and thus the beam current density, might therefore be "hollow." This can be avoided by careful design, although it does not adversely effect performance in most cases. The scaling of ECR devices is similar, although more account must be taken of the skin effect because of the use of frequencies that can reach above 5 GHz. Thus the geometries of both the waveguide/antenna combination and of the discharge chamber are more significant than at 1 MHz.

Owing to the more complex geometry, scaling Kaufman-type dc thrusters to different diameters is more complicated than for RF devices. However, reasonably accurate scaling relationships exist [94, 134], which were successfully employed in designing the UK-25 [76] and T6 thrusters [93]. Indeed, these designs worked well "off the drawing board," thereby validating the scaling process that starts by considering the need to ensure that the mean flux density of ions to the screen grid remains constant and that there is no change in the radial plasma density distribution. This leads to quantification of the ionization rate, then to the current of primary electrons required, assuming that their energy remains constant to first order. The next step is to consider the conditions in the annular gap between the baffle disc and the inner polepiece (Fig. 9), in which the primary electrons gain their energy. This determines the dimensions of this region, the cathode operating conditions, and the magnetic field. However, the latter is changed during optimization and throttling, and so only a broad specification is required at this stage.

The scaling of an MESC thruster follows similar principles, although the magnetic field value is much greater than in the Kaufman device, and its geometry is different (Fig. 10). However, the ionization process and the magnetic containment principles are the same, so that the physical situation in the two devices is similar, and the ultimate requirements are essentially identical. However, there is no direct control of the energy of the primary electrons, which is determined by the difference between the cathode and discharge chamber plasma potentials, which are not easy to regulate.

V. High-SI, High-Power Operation

A. Parametric Variations

To illustrate the influence of AM and V_B on performance at high SI, the maximum thrust density is plotted against AM in Fig. 32 for values of V_B of between 1.5 and 70 kV and for constant I_B. The use of a four-grid system is assumed, with a constant ion extraction potential, except in the 1.5-kV case. These results are based on the use of Eq. (10) and on data from the T5 thruster operating with xenon at maximum perveance, at a thrust of 64 mN [15]. Under these conditions, $V_T = 2$ kV, $V_B = 1500$ V, $I_B = 1.0$ A, $V_{ac} = -500$ V, $I_{sp} = 4071$ s, and the total input power P_T is 1930 W. This is clearly an exceptional performance for a 10-cm beam

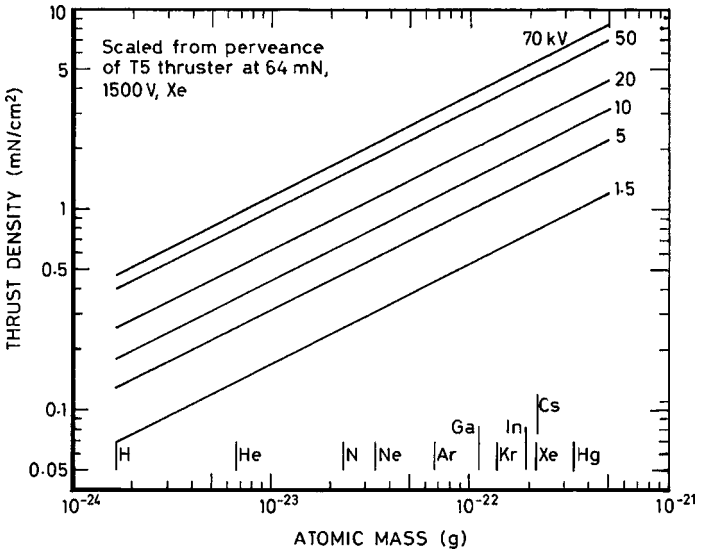


Fig. 32 Thrust density as a function of atomic (ion) mass and net ion accelerating potential.

diameter thruster, although the performance envelope for this device extends beyond this point to more than 70 mN.

As anticipated from Eq. (10), at any value of V_B and constant I_B the thrust density falls with decreasing ion mass, with a square-root relationship. Although this trend can be counteracted by increasing I_B, a higher perveance might then be necessary. At constant V_B, this can be achieved only by making the accel grid more negative, with adverse lifetime implications, or by closing the intergrid gap [see Eq. (11)].

Also as indicated by Eq. (10) and Fig. 32, at any value of AM the thrust density increases with V_B, again with a square-root relationship. As a consequence, the rate at which gains are made in thrust density diminishes as V_B is increased, and so the greatest values are to be achieved by combining high values of V_B and m_i with maximum perveance. The latter implies a small intergrid gap and a large value of V_{ac}, neither of which are conducive to long life. Thus a compromise will always be required.

The values of T_d given in Fig. 32 extend to well beyond those quoted for existing thrusters in Table 2. Indeed, they reach about 7 mN/cm^2 for mercury propellant, which is more than an order of magnitude greater than found in most present devices. This confirms, as stated earlier, that thrust densities of interest for many future high-power missions can be generated by increasing the ion energy. It also confirms that the objectives in developing the NEXIS [115], HiPEP [118], and interstellar precursor [122] thrusters are far from ambitious; much more can be achieved with devices of this generation, bearing in mind their dimensions and intended values of SI.

B. Operation at Hundreds of Kilowatt Level

As a more specific example of the parametric variations that are predicted by the scaling relationships just discussed, the case was considered of a 30-cm beam diameter thruster operating under the conditions appropriate to the T5 engine at 71-mN thrust [15], where the SI was 4334 s. For the purpose of this illustration, it was assumed that this thruster would be run at a higher SI to ensure that the grids would not be at their perveance limit. Thus a nominal value of 5000 s was deemed to be more appropriate. The beam current density is then 13.4 mA/cm^2, giving a beam current with 30-cm-diam grids of 9.47 A. Assuming the use of xenon, the thrust density is then 0.9 mN/cm^2 and the power density 28.3 W/cm^2, giving a thrust of 636 mN and a power consumption of exactly 20 kW. Such a device would be appropriate for a 100-kW application, assuming that a cluster of five or more mounted on the spacecraft would be acceptable.

1. Increase of Thruster Diameter

To cater for different applications in this power regime, Fig. 33 illustrates how the thrust varies with diameter, when operating under these high perveance conditions. Also plotted are derated values, derived from T5 data at 64 mN; lifetime would be enhanced in this case. For completeness, these plots extend to 50 cm diam, although the development of satisfactory grid systems of this size will be difficult, owing to problems associated with maintaining the very small gaps required in an environment that includes severe vibration at launch and high but variable temperatures during operation. Indeed, the largest diameter thruster that has successfully overcome these problems inherent to space qualification to date is the 30-cm NSTAR device [72] of the DS-1 spacecraft [2, 73].

The useful thrust for relevant missions is within the range 0.5 to 1.7 N, which is certainly appropriate to many applications. However, as will be shown next, it can be increased very considerably by operating at higher values of SI than the

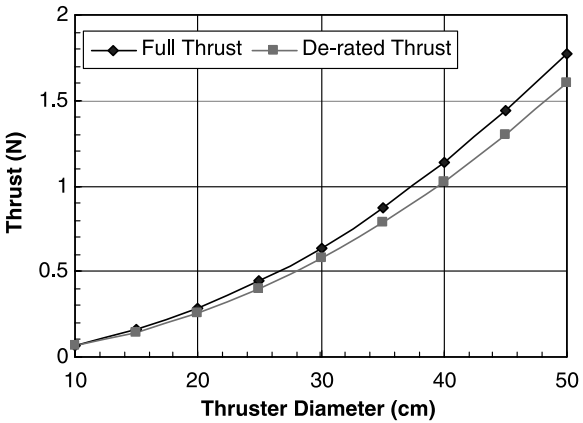


Fig. 33 Thrust as a function of thruster diameter.

5000 s assumed here. The equivalent power consumption is shown as a function of diameter in Fig. 34. This is also consistent with clustered operation at the 100-kW level; indeed, just two 50-cm thrusters would be needed at 100 kW.

2. *Increase of SI*

Thrust density values scaled directly from the T5 thruster when operating at 64 mN were presented in Fig. 32, as functions of net accelerating potential and propellant atomic mass, assuming that the ion extraction potential remains constant at 2 kV. This operating point was selected to provide some derating from the maximum performance achieved, 71 mN. As a consequence of the assumption concerning the extraction potential, all lines in Fig. 32, apart from that for 1.5 kV, are appropriate to a four-grid system.

As an example of what might be achieved at a higher value of SI than just considered, a net accelerating potential of 5 kV was assumed, while keeping the extraction potential at 2 kV. As stated earlier, this requires the use of the four-grid concept. For xenon, this yields about 1.5 mN/cm^2 for a 40-cm-diam thruster, which will provide a thrust of about 1.87 N at an SI of 7500 s, assuming that η_{mt} is 85% and $V_B = 5$ kV. The power consumption will be around 86 kW, assuming that there is no increase in ionization efficiency in the discharge chamber.

With a perhaps more realistic diameter of 30 cm, these figures become 1.05 N and 48.6 kW. Such a performance is certainly relevant to a 50- to 300-kW requirement and suggests that appropriate improvements to existing technologies will permit such objectives to be attained with very few thrusters, if necessary. Indeed, it would seem to be feasible to consume 300 kW using just six thrusters of 30 cm diam, operating with just a modest increase in SI above current maximum values.

As just stated, this conclusion was reached assuming an ion extraction potential limited to 2 kV. While larger values have been investigated only rarely up to the

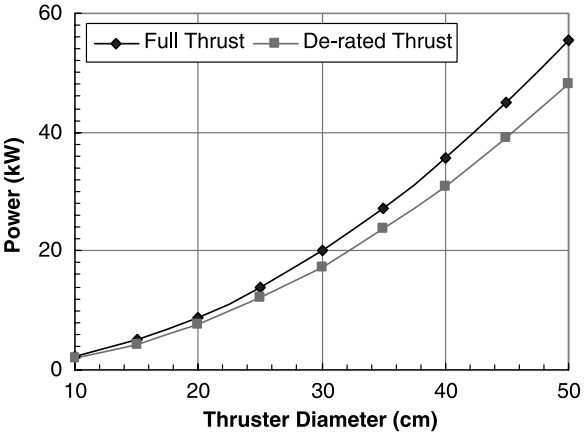


Fig. 34 Power consumption as a function of thruster diameter.

present, considerably higher values have already been achieved using a triple- or twin-grid systems [115, 118, 122], and Wilbur has reported using up to 30 kV successfully [14]. However, the design of fully practical devices operating at such high potentials and thus perveance values must assume that the discharge chamber plasma is dense and that the radial density distribution is not excessively peaked. From Eq. (11), such a change will increase the available beam current, power consumption, and thrust dramatically, via the $(V_T^{3/2})$ relationship in this equation. However, as mentioned earlier, existing advanced thrusters (Table 2) do not appear to have been designed to take advantage of this.

Taking again the operating parameters of the T5 thruster at 64-mN thrust and extending them to higher values of SI by means of Eqs. (13–15), the results obtained are plotted in Fig. 35. They show clearly the major impact of the improved perveance achieved by increasing the potential between the screen and accel grids. With the triple- or twin-grid system this increase is caused automatically if the SI is raised because V_B, and thus V_T, must then be higher. The beam current can increase to as much as 41 A for a 30-cm-diam thruster at 5 kV, assuming that the discharge chamber can provide the necessary flux of ions to the screen grid. The corresponding thrust will be 4.8 N and the power consumption 264 kW. Although these figures might appear to lack realism in view of the need to achieve also an appropriate lifetime, they do confirm that performance parameters consistent with a requirement to consume hundreds of kilowatts are achievable with an extension of existing technology.

As an example, if there is a need to achieve 300 kW with perhaps six thrusters, these results show that this will be possible with any value of SI above about 5200 s, remembering that it is not necessary to operate at maximum beam current. Thus, as an example, if 7000 s is needed for a particular application that will use six thrusters, the value of V_B required is around 4.5 kV, but the thruster can then

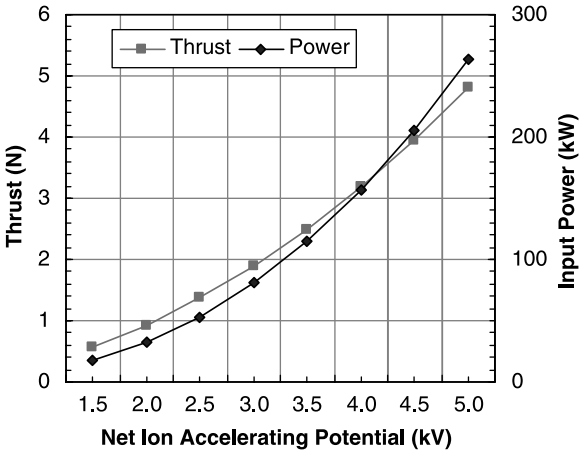


Fig. 35 Thrust and power consumption as a function of V_B for a 30-cm beam diameter thruster.

be derated from its maximum performance by a factor of four, to reduce the power consumption from 200 to 50 kW. This will normally be extremely beneficial as regards lifetime. However, note should be taken of the resulting reduction of the plasma density in the discharge chamber and of the consequential further penetration of the plasma sheath at the screen grid in the upstream direction. This must not be permitted to extend so far that lifetime is compromised as a result of direct ion impingement on the accel or decel grids (Fig. 27).

3. *Increase of Perveance*

The analysis just presented has illustrated the major effects that can be obtained by increasing the perveance through the process of employing a higher value of SI. Basically, to increase the value of SI achieved, the ion accelerating voltage, V_B, applied to the grids must be larger, which also improves the ion extraction capabilities of the grid system, or its perveance [see Eq. (12)].

Unfortunately, owing to mission constraints, it might not be permissible in practice to operate at a larger SI, and so this avenue of improvement (i.e., the use of a higher acceleration voltage) might not be available. However, the perveance of twin- and triple-grid systems is also dependent upon the accel grid potential V_{ac}, so that this can also be changed to achieve the desired results. Of course, more negative values of V_{ac} will accelerate the damage caused by charge-exchange ions, thereby reducing lifetime. This is because the charge-exchange ions created between and outside the grids gain an energy close to V_{ac} in being accelerated back to the grid system. The higher the negative value of this voltage, the more damage they cause.

This was originally a difficulty that could not be overcome easily, but the advent of carbon grid technology has allowed much more negative potentials to be used. As the earlier RIT RF thrusters [59, 63] operated successfully with potentials as negative as about −1.5 kV, without the benefit of carbon grids, it is likely that the −2 kV will be acceptable now.

To illustrate the results of examining a range of values of V_{ac}, calculations were performed for the intermediate SI case of 5260 s, for which $V_B = 2.5$ kV, assuming the use of a 30-cm beam diameter thruster. In this assessment, the value of V_{ac} was varied from −250 to −2000 V. The results are presented in Fig. 36, from which it can be seen that the thrust covers the wide range from 1.2 to 2.5 N and the power consumption from 47 to 98 kW. To take one specific operating point, the thrust is 1.4 N and the power consumption 53 kW if $V_{ac} = -500$ V. These are, of course, maximum values for the conditions under consideration, and the thruster can be operated at any reasonable lesser ones.

This assessment illustrates the strong influence of grid system perveance, or ion extracting capability, on the maximum performance of a gridded thruster, for given ion-beam diameter and SI. These and the earlier results show that there are several ways in which high performance can be achieved and suggest that present devices, modified in appropriate ways, can probably meet a multi-hundreds-of-kilowatt-power-consumption requirement, even if a mission demands that very few thrusters be flown and that long lifetime must therefore be achieved. It is also clear that, in this case, there is no need to utilize very high values of SI, unless they are advantageous for saving propellant mass.

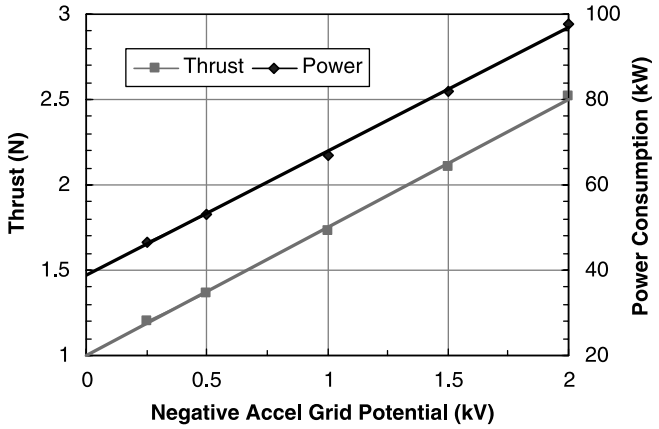


Fig. 36 Thrust and power consumption as a function of V_{ac} for a 30-cm beam diameter thruster operating with $V_B = 2.5$ kV.

4. Technology Readiness

The analysis presented in Table 2 suggests that present thrusters cannot meet the high-power end of a 50 to 100 s of kilowatt-range requirement. However, an array of certain existing devices could probably consume up to 100 kW or so, although none of these thrusters are space qualified, and they all require life testing. Thus they are not yet ready for this application, and considerable funding would be needed to reach qualified status; in this, the life testing of large, high-power thrusters requires the use of major facilities with substantial pumping speeds, which are costly to build and to operate.

The higher end of this power range can be met by the further development of existing thrusters, utilizing modified grid systems and by operating at higher SI and/or perveance than normal. The latter can be achieved solely by making the accel grid more negative, although the increase of SI has the same effect if twin or triple grids are used. The more complex alternative is to employ a four-grid system with both a greater perveance and providing an increased SI. In all cases, additional research and development are needed because this regime has not been properly explored to date. The lifetime implications are of particular interest and might dictate the way forward.

C. Operation at the Megawatt Level

From the preceding assessment, it is necessary to employ the four-grid system to bring a large thruster into the hundreds of kilowatt to megawatt class. To establish what might be possible, the maximum performance of a 30-cm beam diameter thruster was again evaluated, using xenon propellant and the scaling relationships in Section IV. This diameter is the largest for which full confidence exists regarding tolerance to launch vibration and lifetime. In these calculations, the screen and accel grids were separated by 1 mm, and a 5-kV ion extraction potential was applied. However, only 50% of maximum grid perveance [Eq. (12)] was assumed

to avoid any direct ion-beam impingement on the downstream grids (Figs. 26 and 27), and V_B was taken to be 7 to 70 kV and η_{mt} to be 90%.

The results, presented in Table 3, also include the case when full perveance is assumed. It can be seen that values of P_T in the specified range can be readily achieved, provided that the SI is allowed to rise to well beyond current values. As these high values of P_T result from depositing most of the energy supplied directly into the beam, the discharge power required remains relatively modest in all cases. Thus a high thruster temperature should not be a major problem.

It is pertinent at this point to refer to earlier information from the CTR field to confirm that the calculations presented in Table 3 have some foundation in fact. Of course, these CTR devices, listed in Table 4, do not use xenon propellant because only hydrogen is of interest in this field. However the ion optics principles remain the same. A further difference lies in the operating times because CTR injection machines are required to produce high-energy ions for only a few seconds on each activation; 10 s appears to be one of the longest times mentioned in the literature [131]. Thus lifetime is not addressed, although it is of critical importance in the space field. Finally, high-efficiency plasma production processes are of no significance in CTR machines because waste heat is readily removed. This is not possible in space, and so much more attention must be paid to the minimization of losses and to thermal design.

The individual power consumptions given in Table 4 are very high, rising to nearly 5 MW for the 40 × 18cm device [130] developed by the Culham Laboratory. With a beam energy of 80kV, the SI is exceptionally large at 400,000 s, but this confirms that MW operation is entirely feasible. The thrust is 2.4N and the power density 6670 W/cm^2, which is well above all of the values quoted in Table 2. The equivalent value for the 12-cm-diam device is even larger, at 9947 W/cm^2. Similarly, the thrust densities, derived using Eq. (10), are 8.1 and 5.2 mN/cm^2, which are the highest experimental values yet recorded, as far as is known. For comparison, the largest published value for a gridded ion engine is for high SI operation of the T5 thruster [15], at 0.9 mN/cm^2. The predictions in Table 3 are generally greater at 8.8 to 28 mN/cm^2, owing to the use of xenon propellant, rather than hydrogen.

Because the open area ratio usually achieved in ion thrusters is well in excess of the 30 to 50% of these CTR devices, a much improved extraction efficiency should be expected. This will lead to enhanced current, thrust, and power densities compared to those indicated by Table 4. However, the calculations that gave the data in Table 3 assumed an open area ratio typical of present thrusters.

The beam-divergence values in Table 4 are more than an order of magnitude below those typical of existing thrusters [34, 128] and suggest that grid impingement by primary ions might not be a problem. In addition, the variation of 0.4 to 2 deg indicates that further benefits can accrue from modeling work aimed at determining the best design solution. There has been considerable progress in the ion-optics modeling field since the devices listed in Table 4 were designed in the late 1970s and early 1980s.

Recent work by Wilbur [14] has confirmed the viability of high-voltage operation in a thruster environment, using a twin-grid configuration. With a screen grid aperture diameter of 29 mm, the results with argon suggest that a beamlet energy of 2.3 kW with a 30 kV acceleration potential should be achieved. The thrust from

Table 3 Predicted performance of a 30-cm beam diameter thruster utilizing xenon propellant, a four-grid extraction system, and beam potentials of up to 70 kV

Net beam accelerating potential, kV	Maximum thrust, N	Thrust density, mN/cm^2	Max beam current, A	Input power at 50% perveance, MW	SI, s	Power density, W/cm^2	Input power at full perveance, MW
7	5.3	8.8	43.9	0.32	9,300	451	0.64
10	7.5	10.6	43.9	0.46	11,100	644	0.92
15	9.2	13	43.9	0.69	13,600	966	1.37
20	10.6	15	43.9	0.91	15,700	1,288	1.82
30	13.1	18.5	43.9	1.37	19,300	1,933	2.74
50	16.8	23.8	43.9	2.28	24,900	3,221	4.56
70	19.9	28.1	43.9	3.19	29,400	4,509	6.38

Table 4 Characteristics of CTR machine ion-beam accelerators

Reference	Grid Size, cm	Grid form	Open area ratio, %	Beam energy, keV	Beam current, A	Beam power, kW	Beam diverg. deg	Current density, mA/cm^2
Okumura [131]	10 dia	Flat	31	70	4–7	280–490	1.4	170–190
Ohara[a] [135]	12 dia	Flat	40	75	15	1125	0.6	133
Menon [136]	18 dia	Dished	51	35–65	7–20	245–1300	2	27–79
Martin[b] [130]	40 × 18	Flat	40	80	60	4800	0.4	200

[a]Design study. [b]Production devices from the UKAEA Culham Laboratory.

a single beamlet is then 12 mN, the SI is 27,000 s, and the grid lifetime was estimated to be 30,000 h. The power and thrust densities were 350 W/cm^2 and 1.8 mN/cm^2, respectively. These are remarkable results, bearing in mind the limitations of the twin-grid extraction system.

It can thus be concluded that MW operation of a single ion thruster is possible, provided that the SI can be permitted to exceed 10,000 s using xenon propellant. Of course, if a heavier atom is utilized, such as mercury, the requirements can be met at lower values of SI. The operation of two different EP technologies with different values of SI can enable any intermediate performance to be attained. This concept has recently been studied for a combination of gridded thrusters and Hall-effect thrusters [137].

1. Specific Designs at the Megawatt Level

To be of some use in actual mission analyses, three design studies were undertaken at the 0.5-, 1-, and 1.5-MW power levels, assuming the thruster beam diameter to be 40 cm in each case. Arbitrary beam accelerating potentials of 6, 18, and 12 kV, respectively, were assumed, as examples of what can be achieved. The analysis was identical to that providing the data presented in Table 3, but proceeded further into the details of the three thrusters and their operating parameters. The results are given in Table 5, in which the mass has been estimated from current large devices. It is clear from this example that the aim of consuming 1 MW or more at high SI can be achieved.

2. Peak Thruster Performance

In the context of this study, an attempt was made to establish the maximum performance that might be extracted from a given thruster, using a propellant with a low average atomic mass of about 4.5 AMU. A 22-cm beam diameter Kaufman-type design was selected, so that a comparison could be made with existing devices of this size, such as the T6 and RIT-XT (see Table 6). The aim was to extend the SI as far as possible by utilizing the very high values V_B noted in Table 4, bearing

Table 5 High-power thruster design parameters

Parameter	Power input/thruster, kW		
	500	1500	1500
Propellant	Xe	Xe	Xe
Grid diameter, cm	40	40	40
No. of grids (carbon)	4	4	4
Total propellant utilization efficiency, %[a]	90	90	90
Total SI, s[a]	8617	14,925	12,187
Thrust, N	10.3	18.2	22.2
Ion-beam current, A	80.3[b]	82.3[b]	122.7[c]
Beam acceleration (screen grid) potential, V	6000	18,000	12,000
Extraction grid potential, V	1000	13,000	7000
Accel grid potential, V	−500	−500	−500
Decel grid potential, V	−50	−50	−50
Total propellant flow rate, mg/s[a]	121.4	124.4	185.4
Total efficiency, %[a]	86.7	88.9	88.3
Power/thrust, W/mN	48.7	82.4	67.7
Thruster mass, kg	32	35	35

[a]Includes allowances for neutralizer power and propellant flow rate.
[b]Assumes grid system operating at 50% of maximum perveance.
[c]Assumes grid system operating at 75% of maximum perveance.

Table 6 Peak performance of 10- and 22-cm beam diameter thrusters

Parameter	10-cm beam	22-cm beam
Thruster beam diameter, cm	10	22
Discharge chamber temperature, °C	790	500
Ion extraction potential, kV	5	5
Net beam accelerating potential, kV	70	70
Beam current density, mA/cm^2	150	34
Anode current, A	77	85
Beam current, A	11.8	13
Perveance factor P_g	4550	580
Thrust, N	0.95	1.05
Input power, kW	828	913
Total propellant flow rate, mg/s	0.65	0.714
Discharge power, kW	2.7	3.0
Beam divergence, deg	<2.0	<2.0
Exhaust velocity, m/s	1.7×10^6	1.7×10^6
Propellant utilization efficiency, %	85	85
Electrical efficiency, %	99.7	99.7
Specific impulse, s	150,000	150,000
Total impulse in 10,000 hours, N/s	3.4×10^7	3.8×10^7

in mind that these are, in general, measured parameters from actual laboratory devices. An arbitrary value of 70 kV was adopted. The main limitation was assumed to be the temperature of the thruster because the insulation of the windings of the solenoids is currently unable to exceed about 600°C; thus, 500°C was selected as the maximum temperature.

In parallel, a similar exercise was conducted for the 10-cm diameter, equivalent to the T5 and RIT-10 Evo thrusters (see Table 2). No upper temperature was assumed in this case; it was calculated from the discharge power and an estimate of the mean emissivity of the discharge chamber and other external materials. The results for both cases are presented in Table 6.

It can be seen that both devices approach the MW level, despite their small size. However, it is not suggested that thrusters as small as this should be developed to meet the requirements of this study or that accelerating potentials as large as 70 kV would normally be employed. This exercise merely puts the previous estimates into context and shows that they are probably reasonable and will eventually be fully viable.

The high discharge chamber temperatures are not of any great concern for Kaufman-type dc thrusters, the RIT-type RF thrusters, or the ECR devices, which do not utilize permanent magnets. In each case, the limit is generally set by the insulation on electrical wiring, either that required for solenoids or for RF field generation. However, the MESC thruster employs permanent magnets (see Fig. 20) that produce fields of the order of several kiloGauss. These cannot withstand temperatures much higher than about 300°C, and so the ability of this technology to perform at these very high power levels is extremely doubtful. In this context, it will be observed that the high-energy CTR devices avoid permanent magnets for this reason.

3. Propellant Selection

Although xenon is the preferred propellant for most of the present applications of interest, others are of relevance, especially as the supply of xenon is limited and its price will increase as demand rises. In general, a propellant should be selected according to the SI required and the available power level. As a general rule, and according to Eq. (9), a high SI requires a low atomic mass, and a large thrust at a given power level benefits from a much increased atomic mass.

Any material that can be vaporized and that does not react chemically with the thruster or spacecraft construction materials can be used. If chemical reactions occur with the cathode(s), a separate inert propellant can be employed to feed these components, although this dual-propellant supply represents an additional complexity that would best be avoided. Cryogenic or high-pressure storage of gases is also to be avoided because both incur a large mass penalties.

The ideal propellant is stored as a liquid at spacecraft temperature to achieve a good storage density under a low pressure. Compounds and mixtures are acceptable in principle. Such a liquid would be fed to the thrusters via vaporizers, which would operate ideally at about 300°C. Dissociation of compounds would occur in the discharge and possibly in the vaporizer. Using this principle, the average atomic mass can be reduced to about 4.5 AMU, as indicated in Table 7, if very high values of SI are required.

Table 7 Possible low-average atomic mass propellants

Compound	Formula	Melting point, °C	Boiling point, °C	Mean atomic mass, AMU
Cyclohexane	C_6H_{12}	6.5	80.7	4.7
Diethylamine	$C_4H_{11}N$	−50	55.5	4.6
Heptane	C_7H_{16}	−90.6	98.4	4.3
Hexane	C_6H_{14}	−95.3	68.7	4.3
Octane	C_8H_{18}	−56.8	125.7	4.4

4. Parameter Ranges

It was thought to be a useful exercise to attempt to suggest likely ranges for parameters of interest to this study. These are listed in Table 8. They are derived from participation in a number of other studies relevant to the present one, but must be regarded as tentative only.

The major parameters that determine the characteristics of most missions are as follows: the power available from the reactor (or solar array) and possibly its change with time; the velocity increment and the total impulse required; the total time allowed for the mission; the thrusting time allowed; the thrust required to ensure that the mission can be accomplished in the noted time; and the maximum

Table 8 Possible parameter limits

Parameter	Lower limit	Upper limit	Comments
Beam diameter, cm	~3	~40	Upper limit due to grid distortion
Beam accelerating potential, V	10	70,000	Values > 5 kV need 4 grids
Beam current density, mA/cm^2	——	150	Determined by perveance
Grid perveance factor P_g	——	4,500	Limit determined by T5 thruster data
Thrust density, mN/cm^2	——	30	Determined by perveance
Power density, W/cm^2	——	4,500	——
Specific impulse, s	2000	150,000	Determined by max voltage, assumed to be 70 kV, and ion mass
Mean ion mass, AMU	~4.5	~200	Minimum value is hydrogen compound, maximum is mercury
Thruster temperature for Kaufman-type, RIT-type, and ECR thrusters, °C	——	~800	Determined by solenoid and RF coils, also wiring
Thruster temperature for MESC thrusters, °C	——	~300	Determined by permanent magnets

propellant load, which is usually determined by a tradeoff between numerous other parameters, and will often result in the selection of an optimum SI.

Consideration of these parameters will lead to a need to set values for many others, some of which are tabulated in Table 8. If those requirements are then outside the ranges indicated, a review of the complete design process will be necessary because a conservative approach is preferable. For example, if it is found that the thruster required will have a diameter of, say, 50 cm, this should be regarded as impractical, and the analysis should be repeated to determine whether a smaller dimension might be acceptable. Similarly, a very high perveance should be discounted because it could lead to an impractically small spacing between the screen and accel grids, which would not be maintained in the high-temperature operating environment.

D. Systems Considerations

In the context of this study, a number of systems considerations require attention, particularly owing to the very high power levels envisaged. The first of these is the in-rush current on applying the ion accelerating potentials to the grids of the thruster and, indeed, on first turning on the discharge. In the latter case it is simple to ramp up the discharge current in a completely controlled manner, selecting the speed at which this is done to match the capabilities of the power generation system. This applies no matter what form of ionization mechanism is selected. In the case of the grids, this process also determines the rate at which ions are able to be extracted and therefore totally controls the way in which the beam current increases. Again, this can be matched exactly to the power system, and transient effects can be avoided without difficulty.

In many missions a significant throttling capability will be required, in order to match the power consumption of the thrusters to the output of the power system, or to meet specific trajectory requirements. In the case of an array of thrusters, this capability also provides a thrust vectoring opportunity that can be of considerable value. This throttling capability is readily available with all types of gridded thrusters, unless they have been designed to exclude it, as is the case with the XIPS-13 [27], for example. The best performance is available from the Kaufman-type device using solenoids to produce the discharge chamber magnetic field and from the RIT-type of RF thruster. A throttling ratio of 200:1 has been recorded with the former technology [83, 95], but with certain lifetime implications; 10:1 is easily achievable with both concepts.

Lifetime is clearly of concern for missions requiring a very large total impulse. To illustrate overall capability, several thrusters have achieved very long operating durations in test facilities and in space. The most encouraging example is that of DS-1, which reached in excess of 30,000 h in the laboratory and 16,000 h in space [102]. The Muses-C thrusters were tested to 18,000 h [138], and the operation of the Artemis version of the RIT-10 at ESTEC passed the 20,000-h mark [139]. These examples show that the technology has an inherently long-life capability, but it is extremely costly to demonstrate this. Lifetime is mainly limited by sputtering damage to the discharge chamber and grids, and this will be more severe at high power, high plasma density, and high thrust density. However, this process can be controlled by design, the selection of materials, and the careful choice

of the operating point. Unfortunately, modeling is not, in general, sufficiently accurate to be used as a substitute for life testing, and so the cost of this activity cannot at present be avoided.

A recommendation is therefore that modeling capabilities be improved so that they can be used to predict lifetime with greater confidence than at present. In association with this advance, more effort needs to be deployed to measure the fundamental physical data that are needed to make realistic modeling predictions; these include sputtering yields and charge-exchange cross sections. However, no matter what progress is made in this field, lifetesting will remain necessary. To circumvent the cost of this, mission designers should also consider the possibility of accepting a shorter guaranteed life and flying more thrusters as a compensation, in order to achieve the required total impulse. A study of this option might well suggest that it provides significant financial benefits when dealing with very large, high-power systems.

Because megawatt-level thrusters will require several kilowatts of discharge power (see Table 6), and this must be radiated to space, the correct thermal design of the installation will be an important consideration. In general, the thrusters must be mounted externally and be thermally isolated from the spacecraft. Provided that this is accomplished, the only additional thermal effects will concern the removal of the waste heat from any power conditioning and control electronics. It is assumed that this will be a relatively minor problem because the bulk of the energy consumed will be supplied directly from the source to the ion accelerating grids, without any additional power conditioning circuitry; this option should be selected where possible in future design studies.

In the context of EP systems, the issue of spacecraft charging is often raised. It must therefore be emphasized that the evidence from every flight that has taken place, using all types of electric thruster, is that the existence of the exhaust plasma couples the spacecraft very effectively to space potential. Thus there is no spacecraft charging effect whatsoever. Indeed, a neutralized ion beam couples the spacecraft to space plasma potential usually to within 10 V. The residual concern is that charging effects can occur if the neutralizer of the propulsion system fails. Although this might possibly be the case, a suitable sensing circuit will enable the EP system to be turned off sufficiently rapidly to ensure that no damage occurs.

VI. Conclusions

This chapter has reviewed the ways in which gridded ion-thruster systems might cover the power range from tens of kilowatts to several megawatts, with the aim of performing a very wide variety of challenging interplanetary missions utilizing nuclear-power sources. It has been shown that reasonable extensions of current technologies should permit this to be accomplished.

By consideration of the relevant scaling relationships, which have been validated up to about 40 kW, it has been concluded that the same basic concepts will suffice for the entire range of power levels and applications specified. This conclusion is certainly valid for the Kaufman-type of direct-current discharge thruster, for the RIT type of radiofrequency ionization device, and for ECR ionization thrusters, which do not use permanent magnets. Unfortunately, the severe temperature constraints on high field permanent magnets suggest that the cusp-field,

MESC type of thruster cannot operate at the very high power levels considered here, unless derated to very low thrust density.

The design process is aided considerably by the separation of the ion production and extraction/acceleration regions in gridded thrusters. Thus the ion-beam parameters can be deduced without reference to the ionization mechanism employed to produce the plasma from which the ions are extracted. Consequently, the two regions of the thruster can be designed separately, which is a simplifying benefit only available to gridded devices. Similarly, the ion-beam neutralization process can be treated independently.

It has been concluded that the required power density can be achieved and exceeded using gridded ion thrusters, by operating their grid systems at very high perveance and by raising the specific impulse to values that are significantly above those commonly employed at present. The latter ensures that most of the energy supplied is used in accelerating the beam ions, thereby allowing extremely high values of electrical efficiency to be achieved; in the limit, this parameter exceeds 99%. With propellant utilization efficiencies of above 85%, the overall thruster efficiency becomes in excess of 84%.

For the applications at the lower end of the preceding power range, normal twin- or triple-grid configurations might suffice, especially if higher perveance operation is adopted and if the specific impulse can be increased above current values. However, the limit here is caused by the penetration of the plasma sheath at the screen grid into the discharge chamber plasma, which increases as the electric field becomes larger or the plasma density lower. This greater curvature of the sheath, which effectively emits the beam ions, then causes direct impingement onto the accel and decel grids, severely limiting lifetime. With this configuration, the maximum extraction potential is likely to be about 5 kV. If the accel potential is −500 V and if xenon is used, this gives an SI of approximately 7000 s, depending upon the propellant utilization efficiency achieved. About 100-kW power consumption can then be realized with a small array of thrusters.

The power range can be extended to several hundred kilowatts by the further development of existing thrusters, utilizing modified grid systems and by operating at higher SI and/or perveance than normal. Whereas the latter can be achieved solely by making the accel grid more negative, a more complex but satisfactory alternative is to employ a four-grid system with both a greater perveance and providing an increased SI. In all cases, additional research and development are needed because this regime has not been properly explored to date. The lifetime implications are of particular interest and might dictate the way forward.

Thus the operational envelope can be massively extended by use of the four-grid configuration. There is considerable documentation concerning such systems in the CTR community, where ion accelerators of the size required, or smaller, have been constructed, which produce megawatt beams at 70 or 80 keV. This is possible because the four-grid arrangement permits the ion extraction process to be separated from the main acceleration region, and the limitation of the sheath penetration no longer applies. Thus the extraction part of the system can be designed to operate at near-maximum perveance, and the subsequent further acceleration of the ions can be dealt with independently in the design process. An additional advantage of this configuration is the very low beam divergence typically found. This can be less than 1 deg at an acceleration potential of 70 kV.

It is thus concluded that well-understood thruster technology, when combined with the four-grid configuration based on that utilized in CTR ion-injection machines, will permit megawatt power levels to be achieved. Thus a relatively small array of thrusters, with beam diameters not exceeding 40 cm, will be able to consume many megawatts, although the SI, using xenon propellant, is likely to be somewhat above 10,000 s. With this arrangement, the power density can reach 4.5 kW/cm^2 and the thrust density 30 mN/cm^2, and, if required, the specific impulse can attain 30,000 s with xenon. If higher values of SI are required, the utilization of lower atomic mass propellants will permit this to be achieved, with an ultimate limit using hydrogen compounds of about 150,000 s.

As a specific example, an array of nine 40-cm beam diameter thrusters using xenon propellant and operating at 10 kV, but with an ion extraction potential of 5 kV, will consume 7.4 MW if the perveance is limited to 50% of its maximum value. The total beam current will be 702 A, the thrust 120 N, the SI 11,100 s, and the power density 644 W/cm^2. If full perveance operation can be achieved while maintaining long life, the power consumption is 14.7 MW.

To summarize, the design for a 20- to 50-kW thruster can be extrapolated directly from current capabilities, taking advantage of the higher perveance values made possible by introducing improved grid technologies. However, at the higher power level it would be advantageous to utilize a four-grid configuration. Thus an array of certain existing devices could probably consume up to 100 kW or so, although none of these thrusters are space qualified and they all require life testing. Thus they are not yet ready for this application, and considerable funding would be needed to reach qualified status. The work required to meet a higher power level, utilizing the four-grid configuration, would be much more extensive, and so would require more time and greater funding.

A multimegawatt system can be implemented using extended scaling relationships, but there is no precedent for such an exercise. Thus this complete process, encompassing design, development, performance testing, environmental testing, and life testing, would need to be organized and funded. Bearing in mind the need to coordinate such a development with that of the power source, work on both systems should be conducted in parallel, with very close collaboration at all times. This cooperation is desirable because it is envisaged that the bulk of the power consumed by the thrusters would be supplied directly from the source, with no further power conditioning.

For very high SI operation, the most significant challenge is to prove that the four-grid ion extraction and acceleration mechanism can be made to function successfully and to provide long life. Although not simple, this objective is tenable because of the prior experience of the CTR community.

The scale of the endeavour is indicated by looking at the values of the most important parameters included in Table 2, accepting the T6 values as representative of a thruster approaching qualified status, and comparing them with the ultimate objectives in Table 3. The numbers are somewhat daunting, but should be achievable, mainly because the additional power is to be fed directly into the ion beam and will not appear within the thruster. With xenon propellant, the aim is to improve the SI by a factor of between 2 and 6.3. The corresponding increase in power density is by a factor of between 24 and 240, and the thrust density will, as a consequence, increase by a factor of between 14 and 46.

Although it might seem to be overly optimistic to predict that such extrapolations are feasible, it should be recalled that this process is aided very considerably by three factors. The first is that the separate processes occurring within a gridded thruster can be dealt with independently, to first order. Thus the discharge chamber, the grid system, and the neutralizer can be designed and tested independently, at least initially. The second factor is that the mathematical design processes applicable to the grid system are well understood and the ion optics and erosion modeling capabilities are excellent; these are critical to success. The third factor, already mentioned, is that the huge increase in power contemplated in this study is fed directly into the ion beam.

Finally, the performance and life testing of large, high-power thrusters requires the use of major facilities with substantial pumping speeds, which are costly to build and to operate. The provision of such facilities must precede the development of the thrusters.

References

[1] Staehle, R. L., Carraway, J. B., Salvo, C. G., Terrile, R. J., Weinstein, S. S., and Hansen, E., "Exploration of Pluto: Search for Applicable Small Satellite Technology," *Proceedings of the 6th Annual AIAA/Utah State University Conference on Small Satellites*, AIAA, Washington, D.C., 1992.

[2] Rayman, M. D., Varghese, P., Lehman, D. H., and Livesay, L. L., "Results from the Deep Space 1 Technology Validation Mission," *Acta Astronautica*, Vol. 47, 2000, pp. 475–488.

[3] de Cara, D. M., and Estublier, D., "SMART-1; an Analysis of Flight Data," International Astronautical Federation, Paper IAC-04-S.4.02, Oct. 2004.

[4] Kawaguchi, J., Fujiwara, A., and Uesugi, T., "The Ion Engines Cruise Operation and the Earth Swingby of 'Hayabusa' (Muses-C)," International Astronautical Federation, Paper IAC-04-Q.5.02, Oct. 2004.

[5] Millis, M. G., "NASA Breakthrough Propulsion Physics Program," *Acta Astronautica*, Vol. 44, No. 2–4, 1999, pp. 175–182.

[6] Archipov, B., Vinogradov, V., Kozubsky, K., Kudriavtsev, S., and Murashko, "Development and Application Of Electric Thrusters at EDB 'Fakel'," International Astronautical Federation, Paper IAF-99-S.4.02, Oct. 1999.

[7] Manzella, D. H., Jankovsky, R. S., and Hofer, R. R., "Laboratory Model 50 kW Hall Thruster," AIAA Paper 2002-3676, July 2002.

[8] Rodgers, D. and Brophy, J., "Ion Propulsion Technology for Fast Missions to Pluto," International Electric Propulsion Conference, Paper 01-176, Oct. 2001.

[9] Henry, P. K., Terrile, R. J., Maddock, R. W., and Sobel, H. R., "Exploring the Kuiper Belt: an Extended Pluto Mission," *Acta Astronautica*, Vol. 44, No. 2–4, 1999, pp. 85–90.

[10] Kluever, C. A., "Heliospheric Boundary Exploration Using Ion Propulsion Spacecraft," *Journal of Spacecraft and Rockets*, Vol. 34, No. 3, 1997, pp. 365–371.

[11] West, J. L., "Design Issues for a Mission to Exploit the Gravitational Lensing Effect at 550 AU," *Acta Astronautica*, Vol. 44, No. 2–4, 1999, pp. 99–107.

[12] Fearn, D. G., "The Ultimate Performance of Gridded Ion Thrusters for Interstellar Missions," *Proceedings of the STAIF-2000 Forum*, American Inst. of Physics, CP-504, Springer-Verlag, New York, 2000.

[13] Fearn, D. G., "The Application of Gridded Ion Thrusters to High Thrust, High Specific Impulse Nuclear-Electric Missions," International Astronautical Federation, Paper IAC-04-R.4/S.7.09, Oct. 2004.

[14] Wilbur, P., "Limits on High Specific Impulse Ion Thruster Operation," AIAA Paper 2004-4106, July 2004.
[15] Martin, A. R., Bond, A., and Bond, R. A., "Ultimate Performance Limits and Mission Capabilities of Advanced Ion Thrusters," International Electric Propulsion Conference, Paper 88-084, Oct. 1988.
[16] Hanley, G. M., "Satellite Power Systems (SPS) Concept Definition Study. Vol. IV. Transportation Analysis," NASA CR-3321, Sept. 1980.
[17] Reese, R. T., and Vick, C. P., "Soviet Nuclear Powered Satellites," *Journal of the British Interplanetary Society*, Vol. 36, 1983, pp. 457–462.
[18] Polansky, G. F., Schmidt, G. L., Reynolds, E. L., Schaefer, E. D., Ogloblin, B., and Bocharov, A., "A Plan to Flight Qualify a Russian Space Nuclear Reactor for Launch by the United States," AIAA Paper 93-1788, 1993.
[19] Cameron, G. E., and Herbert, G. A., "System Engineering of a Nuclear Electric Propulsion Testbed Spacecraft," AIAA Paper 93-1789, 1993.
[20] Truscello, V. C., and Rutger, L. L.,"The SP-100 Power System," *Proceedings of the 9th Symposium on Space Nuclear Power Systems*, American Inst. of Physics, Melville, NY, CP-246, 1992, 1–23.
[21] Fearn, D. G., "The Use of Ion Thrusters for Orbit Raising," *Journal of the British Interplanetary Society*, Vol. 33, 1980, pp. 129–137.
[22] Widman, F. W., North, D. M., Cross, E. H., and Burr, A. D., "Evaluation of Nuclear Propulsion for Solar System Exploration Missions," AIAA Paper 93-1952, 1993.
[23] Fearn, D. G., and Smith, P., "A Review of UK Ion Propulsion in a Maturing Technology," International Astronautical Federation, Paper IAF-98-S.4.01, Sept./Oct. 1998.
[24] Novara, M., "The BepiColombo ESA Cornerstone Mission to Mercury," International Astronautical Federation, Paper IAF-01-Q.2.02, Oct. 2001.
[25] Wallace, N. C., Mundy, D. H., and Fearn, D. G., "A Review of the Development of the T6 Ion Thruster System," International Astronautical Federation, Paper IAF-99-S.4.08, Oct. 1999.
[26] Ozaki, T., Nishida, E., Gotoh, Y., Tsujihata, A., and Kajiwara, K., "Development Status of 20 mN Xenon Ion Thruster," AIAA Paper 2000-3277, July 2000.
[27] Beattie, J. R., Williams, J. D., and Robson, R. R., "Flight Qualification of an 18-mN Xenon Ion Thruster," International Electric Propulsion Conference, Paper 93-106, 1993.
[28] Ocampo, C., "Geostationary Orbit Transfer Using Electric Propulsion for the Hughes HS-702 Satellite," International Astronautical Federation, Paper IAF-98-A.1.08, Sept./Oct. 1998.
[29] Groh, K. H., Leiter, H. J., and Loeb, H. W., "Design and Performance of the New RF-Ion Thruster RIT 15," AIAA Paper 98-3344, 1998.
[30] Leiter, H., Bassner, H., Frölich, T., Kukies, R., Müller, H., and Killinger, R., "Development and Performance of the Advanced Radio Frequency Ion Thruster RIT_XT," International Electric Propulsion Conference, Paper 2003-115, March 2003.
[31] Pessana, M., Noci, G., Matucci, A., and Ricciardi, A., "Low Thrust Ion Propulsion for Orbit Maintenance and Drag-Free Control of the Gravity Explorer Satellite," *Proceedings of the Second European Spacecraft Propulsion Conference*, Noordwijk, May 27–29, edited by M. Perry, ESA, Paris, ESA SP-398, 1997, p. 295.
[32] Baker, D. N., "Critical Issues in Space Plasma Physics," *Physics of Plasmas*, Vol. 6, No. 5, 1999, pp. 1700–1707.
[33] Barne, S. J., McComas, D. J., Young, D. T., and Belian, R. D., "Diagnostics of Space Plasmas," *Review of Scientific Instruments*, Vol. 57, No. 8, 1986, pp. 1711–1716.

[34] Fearn, D. G., "Ion Thruster Lifetime Limitations Imposed by Sputtering Processes," 23rd International Electric Propulsion Conference, Paper 93-177, Sept. 13–16, Seattle, WA, 1993.

[35] Notarantonio, A., Killinger, R., and Amorosi, L., "Ion Propulsion System Saves Artemis Satellite," International Astronautical Federation, Paper IAC-03-S.4.01, Sept./Oct. 2003.

[36] Kerslake, W. R., Goldman, R. G., and Nieberding, W. C., "SERT II: Mission, Thruster Performance, and in-Flight Thrust Measurements," *Journal of Spacecraft and Rockets*, Vol. 8, No. 3, 1971, pp. 213–224.

[37] Shimada, S., et al., "Ion Engine System Development of ETS-VI," International Electric Propulsion Conference, Paper 91-145, Oct. 1991.

[38] Kim, V., "Main Physical Features and Processes Determining the Performance of Stationary Plasma Thrusters," *Journal of Propulsion and Power*, Vol. 14, No. 5, 1998, pp. 736–743.

[39] Gorshkov, O. A., Koroteev, A. S., Maslennikov, N. A., Murashko, V. M., Lukyashenko, V. I., Utkin, V. V., Kim, V., and Popov, G. A., AIAA Paper 1998-3176, 34th AIAA/ASME/SAE/ASEE Joint Propulsion Conference and Exhibit, Cleveland, OH, July 13–15, 1998.

[40] Bober, A., et al., "Development and Application of Electric Propulsion Thrusters in Russia," International Electric Propulsion Conference, Paper 93-001, 1993.

[41] Cadiou, A., "An Overview of the CNES Electric Propulsion Programme," International Electric Propulsion Conference, Paper 2003-169, March 2003.

[42] Jacobson, D. T., Manzella, D. H., Hofer, R. R., and Peterson, P. Y., "NASA's 2004 Hall Thruster Program," AIAA Paper 2004-3600, July 2004.

[43] Garnero, P., "Astra 1K and Stentor Plasma Propulsion Subsystem Experience," AIAA Paper 2003-4547, July 2003.

[44] Dumazert, P., Marchandise, F., Prioul, M., Darnon, F., and Jolivet, L., "PPS 1350-G Qualification Status," International Electric Propulsion Conference, Paper 03-270, March 2003.

[45] Gorshkov, O. A., and Koroteev, A. S., "New Trends in Hall-Effect Thruster Development," *Proceedings of the 6th International AAAF Symposium on Propulsion for Space Transportation of the XXIst Century*, Versailles, France, May 2002.

[46] Randolph, T., Fischer, G., Kahn, J., Kaufman, H., Zhurin, V., Kozubsky, K., and Kim, V., "The Mitigation of Discharge Oscillations in the Stationary Plasma Thruster," AIAA Paper 94-2857, June 1994.

[47] Racca, G. D., Foing, B. H., and Rathsman, P., "An Overview of the Status of the SMART-1 Mission," International Astronautical Federation, Paper IAA-99-IAA.11.2.0, Oct. 1999.

[48] Jolivet, L., Secheresse, O., Kharchevnikov, V. K., Bugrova, A., and Morozov, A. I., "Development and Testing of a Two-Stage Hall Effect Thruster," International Electric Propulsion Conference, Paper 2003-290, March 2003.

[49] M., Dumazert, P., Bugrova, A. I., Morozov, A. I., Harchevnikov, V. K., Desyatskov, A. V., Kozintceva, M. V., Saveleiev, V. V., Jolivet, L., Gengembre, E., Chesta, E., Boeuf, J. P., Boniface, C., Rigollet, R., Saverdi, M., Castro, F., Simpson, H., "Double Stage Hall Effect Thruster Development Activities at SNECMA Moteurs" Prioul, *Proceedings of 4th International Spacecraft Propulsion Conference*, Chia Laguna (Cagliari), Sardinia, Italy, Oct. 2004, edited by A. Wilson, ESA SP-555, ESTEC, Noordwijk, The Netherlands, 2004.

[50] Sankovic, J. M., Haag, T. W., and Manzella, D. H., "Operating Characteristics of the Russian D-55 Thruster with Anode Layer," AIAA Paper 94-3011, June 1994.
[51] Semenkin, A., et al., "Development Program and Preliminary Test Results of the TAL-110 Thruster," AIAA Paper 99-2279, June 1999.
[52] Andrenucci, M., Paganucci, F., Frazzetta, M., La Motta, G., and Schianchi, G., "Scale Effects on the Performance of MPD Thrusters," International Electric Propulsion Conference, Paper 01-123, Oct. 2001.
[53] Böhrk, H., Laure, S. and Auweter-Kurtz, M., "Feasibility Study of Application of ATTILA to In-Space Propulsion for Piloted Missions," International Astronautical Federation, Paper IAC-04-S.4.03, Oct. 2004.
[54] Fearn, D. G., and Cohen, R. B., "The Future Development of Non-Chemical Propulsion," International Astronautical Federation, Paper IAA-98-IAA.3.3.05, Sept. 28–Oct. 2, 1998.
[55] Chang Diaz, F. R., "Research Status of the Variable Specific Impulse Magnetoplasma Rocket," *Bulletin of APS*, Vol. 42, No. 10, 1997, p. 2057–2063.
[56] Batishchev, O., and Molvig, K., "VASIMR Thruster Operation with Hydrogen and Helium Gas Propellants," International Electric Propulsion Conference, Paper 2003-191, March 2003.
[57] Glasstone, S., and Lovberg, R. H., *Controlled Thermonuclear Reactions*, Van Nostrand, New York, 1960.
[58] Glover, T., Chang-Diaz, F., Jacobson, V., Tarditi A., Squire, J., and Chavers, G., AIAA Paper 2004-3639, 40th AIAA/ASME/SAE/ASEE Joint Propulsion Conference and Exhibit, Fort Lauderdale, FL, July 11–14, 2004.
[59] Loeb, H. W., "Recent Works on Radio Frequency Ion Thrusters," AIAA Paper 70-1102, Aug. 31–Sept. 2, 1970.
[60] Groh, K. H., and Loeb, H. W., "State-of-the-Art of Radio-Frequency Ion Thrusters," AIAA Paper 89-2381, July 1989.
[61] Leiter, H. J., Loeb, H. W., and Schartner, K-H., "The RIT-15 Ion Engines—a Survey of the Present State of Radio Frequency Ion Thruster Technology and Its Future Potentiality," *Proceedings of the Third International ESA/CNES Conference on Spacecraft Propulsion*, ESA SP-465, ESA-ESTEC, Noordwijk, The Netherlands, 2000, pp. 423–432.
[62] Bassner, H., Berg, H.-P., and Kukies, R., "RITA Development and Fabrication for the Artemis Satellite," International Electric Propulsion Conference, Paper 91-057, Oct. 1991.
[63] Bassner, H., et al., "Flight Test and Ground Investigation Results of the RITA Experiment on Eureca," AIAA Paper 94-2848, June 1994.
[64] Leiter, H., Killinger, R., Bassner, H., Muller, J., Kukies, R., and Frohlich, T., "Evaluation of the Performance of the Advanced 200mN Radio-Frequency Ion Thruster RIT-XT," AIAA Paper 2002-3836, 38th AIAA/ASME/SAE/ASEA Joint Propulsion Conference, July 7–10, 2002.
[65] Toki, K., "Flight Readiness of the Microwave Ion Engine System for Muses-C Mission," International Electric Propulsion Conference, Paper 03-098, March 2003.
[66] Kawaguchi, J., and Uesugi, T., "Technology Development Status of the Muses-C Sample and Return Project," International Astronautical Federation, Paper IAF-99-IAA.11.2.02, Oct. 1999.
[67] Capacci, M., Matticari, G., Noci, G. E., Severi, A., Ricciardi, A., and Svelto, F., "Radiofrequency with Magnetic Field Ion Thruster (RMT): Review of the

Engineering Phase Accomplished Under ASI Contract," International Electric Propulsion Conference, Paper 03-289, March 2003.
[68] Kaufman, H. R., "An Ion Rocket with an Electron Bombardment Ion Source," NASA TN-585, Jan. 1961.
[69] Edwards, C. H., Mundy, D. H., and Clark, S. D., "The Development of Gas Flow Control Equipment at DERA," International Astronautical Federation, Paper IAF-99-S.4.09, Oct. 1999.
[70] Beattie, J. R., and Robson, R. R., "18-mN Xenon Ion Propulsion Subsystem," International Electric Propulsion Conference, Paper 91-010, Oct. 1991.
[71] Beattie, J. R., and Wilbur, P. J., "Cusped Magnetic Field Mercury Ion Thruster," AIAA Paper 76-1011, Nov. 1976.
[72] Christensen, J. A., Benson, G., Bond, T. A., Gallagher, J. T., and Matranga, M., "The NSTAR Ion Propulsion Subsystem for DS1," AIAA Paper 99-2972, June 1999.
[73] Brophy, J. R., Brinza, D. E., Polk, J. E., Henry, M. D., and Sengupta, A., "The DS1 Hyper-Extended Mission," AIAA Paper 2002-3673, July 2002.
[74] Anzel, B., "Stationkeeping the Hughes HS 702 Satellite with a Xenon Ion Propulsion System," International Astronautical Federation, Paper IAF-98-A.1.09, Sept. Oct. 1998.
[75] Chein, K-R., et al., "L-3 Communications ETI Electric Propulsion Overview," International Electric Propulsion Conference, Paper 2005-315, Oct./Nov. 2005.
[76] Latham, P. M., Martin, A. R., and Bond, A., "Design, Manufacture and Performance of the UK-25 Engineering Model Thruster," AIAA Paper 90-2541, 1990.
[77] Wallace, N. C., Mundy, D. H., and Fearn, D. G., "A Review of the Development of the T6 Ion Thruster System," International Astronautical Federation, Paper IAF-99-S.4.08, Oct. 1999.
[78] Gray, H. L., "Development of Ion Propulsion Systems," *GEC Review*, Vol. 12, No. 3, 1997, pp. 154–168.
[79] Oppenhaeuser, G., van Holtz, L., and Bird, A., "The Artemis Mission – ESA's Latest Communication Satellite," International Astronautical Federation, Paper IAF-01-M.1.08, Oct. 2001.
[80] Fearn, D. G., "The UK-10 Ion Propulsion System: a Technology for Improving the Cost Effectiveness of Communications Spacecraft," International Electric Propulsion Conference, Paper 91-009, Oct. 1991.
[81] Bythrow, P. F., Mauk, B. H., and Gatsonis, N. A., "Operational Experiments and Thruster Performance Plan for the Nuclear Electric Propulsion Space Test Program (NEPSTP)," AIAA Paper 93-1896, June 1993.
[82] Bassner, H., Killinger, R., Marx, M., Kukies, R., Aguirre, M., Edwards, C., and Harman, H-P., "Ion Propulsion for Drag Compensation of GOCE," AIAA Paper 2000-3417, July 2000.
[83] Mundy, D. H., and Fearn, D. G., "Throttling the T5 Ion Engine over a Wide Thrust Range," AIAA Paper 97-3196, 1997.
[84] Martin, A. R., and Latham, P. M., "High Thrust Operation of the UK-10 Rare Gas Ion Thruster (T4A)," International Electric Propulsion Conference, Paper 88-062, Oct. 1988.
[85] Freisinger, J., Reinek, S., Rumpf, E., and Loeb, H. W., "RIT 15 – Laboratory Prototype of a 20 mN NSSK Engine," AIAA Paper 76-1038, 1976.
[86] Groh, K. H., Leiter, H. J., and Loeb, H. W., "Design and Performance of the New RF-Ion Thruster RIT 15," AIAA Paper 98-3344, 1998.

[87] Leiter, H. J., Loeb, H. W., and Schartner, K-H., "RIT15S and RIT15LP – the Development of High Performance Mission Optimised Ion Thrusters," AIAA Paper 99-2444, June 1999.
[88] Kerslake, W. R., "SERT -II Thrusters -Still Ticking After Eleven Years," AIAA Paper 81-1539, July 1981.
[89] Leiter, H. J., Killinger, R., Bassner, H., Müller, J., Kukies, R., and Fröhlich, T., "Evaluation of the Performance of the Advanced 200 mN Radio Frequency Ion Thruster RIT-XT," AIAA Paper 2002-3836, July 2002.
[90] Killinger, R., Bassner, H., and Müller, J., "Development of an High Performance RF-Ion Thruster," AIAA Paper 2000-2445, July 2000.
[91] Leiter, H. J., Killinger, R., Müller, J., Kukies, R., and Frölich, T., "Extended Performance Evaluation of EADS ST's 200 mN Radio Frequency Ion Thruster," AIAA Paper 2003-5010, July 2003.
[92] Bassner, H., Bond, R., Thompson, V., Harmann, H-P., and Groh, K., "Development and Performance Testing of the ESA-XX Ion Thruster," AIAA Paper 99-2441, June 1999.
[93] Huddlestone, J., et al., "An Overview of the T6 Gridded Ion Propulsion System Pre-Development Activities for Alpha-Bus," *Proceedings 4th International Spacecraft Propulsion Conference*, Chia, Sardinia, edited by A. Wilson, ESA-ESTEC, Noordwijk, The Netherlands, June 1–6, 2004.
[94] Harbour, P. J., Wells, A. A., Harrison, M. F. A., and White, B. M., Paper AIAA-1973-1112, presented at the 10th Electric Propulsion Conference, Lake Tahoe, NV, Oct. 31–Nov. 2, 1973.
[95] Mundy, D. H., "Factors Affecting the Beam Divergence of a T5 Ion Engine," International Electric Propulsion Conference, Paper 97-095, Aug. 1997.
[96] Pollard, J. E., and Welle, R. P., "Thrust Vector Measurements with the T5 Ion Engine," AIAA Paper 95-2829, 1995.
[97] Lsyzyk, M., "Propulsion on α Bus Platform," International Electric Propulsion Conference, Paper 03-170, March 2003.
[98] Beattie, J. R., Matossian, J. N., Poeschel, R. L., Rogers, W. P., and Martinelli, R., "Xenon Ion Propulsion Subsystem," AIAA Paper 85-2012, Sept. 30–Oct. 2, 1985.
[99] Melita, O. (ed.), "The Comet Nucleus Sample Return Mission," ESA SP-249, Dec. 1986.
[100] Wells, A. A., Harrison, M. F. A., White, B. M., and Harbour, P. J., "Laws for Scaling Electron Bombardment, Thrusters," *Proceedings of Conference on Electric Propulsion of Space Vehicles*, Inst. of Electrical Engineers, Publication 100, London, 1973, pp. 250–257.
[101] Beattie, J. R., and Matossian, J. N., "High-Power Xenon Ion Thrusters," AIAA Paper 90-2540, July 1990.
[102] Sengupta, A., Brophy, J., Anderson, J., Garner, C., Banks, B., and Sovey, J., "An Overview of the Results from the 30,000 hr Life Test of Deep Space 1 Flight Spare Ion Engine," AIAA Paper 2004-3608, July 2004.
[103] Soulas, G. C., "Improving the Total Impulse of the NSTAR Ion Thruster with Thick-Accelerator-Grid Ion Optics," International Electric Propulsion Conference, Paper 01-081, Oct. 2001.
[104] Soulas, G. C., "Design and Performance of 40 cm Ion Optics," International Electric Propulsion Conference, Paper 01-090, Oct. 2001.
[105] Patterson, M. J., and Rawlin, V. K., "Performance of 10-kW Class Xenon Ion Thrusters," AIAA Paper 88-2914, July 1988.

[106] Groh, K. H., Abel, P., Rumpf, E., and Loeb, H. W., AIAA Paper 1979-2053, 14th International Electric Propulsion Conference, Princeton, NJ, Oct. 30–Nov. 1, 1979.
[107] Groh, K. H., Loeb, H. W., Mueller, J., Schmidt, W. and Schuetz, B., "RIT 35 RF-Ion Thruster – Design and Performance, *Journal of British Interplanetary Society*, Vol. 41, 1988, pp. 209–214.
[108] Hayakawa, Y., Miyazaki, K., Kitamura, S., Yoshida, H., Yamamoto, Y., and Akai, K., "Endurance Test of a 35-cm Xenon Ion Thruster," AIAA Paper 3530, July 2000.
[109] Tahara, H., and Nishida, M., "Overview of Electric Propulsion Activity in Japan," AIAA Paper 99-2159, June 1999.
[110] Komurasaki, K., Arakawa, Y., and Takegahara, H., "An Overview of Electric and Advanced Propulsion Activities in Japan," *Proceedings of Third International ESA/CNES Conference on Spacecraft Propulsion*, 2000, SP-465, ESA-ESTEC, Noordwijk, The Netherlands, Oct. 2004, pp. 27–39.
[111] Patterson, M. J., Foster, J. E., Haag, T. W., Rawlin, V. K., Soulas, G. C., and Roman, R. F., "NEXT: NASA's Evolutionary Xenon Thruster," AIAA Paper 2002-3832, July 2002.
[112] Soulas, G. C., Haag, T. W., and Patterson, M. J. "Performance Evaluation of 40 cm Ion Optics for the NEXT Ion Engine," AIAA Paper 2002-3834, July 2002.
[113] Hoskins, W. A., et al., "Development of a Prototype Model Ion Thruster for the NEXT System," AIAA Paper 2004-4111, July 2004.
[114] Soulas, G., Kamhawi, H., Patterson, M., and Gardner, M., "NEXT Ion Engine 2000 h Wear Test Results," AIAA Paper 2004-3791, July 2004.
[115] Randolph, T. M., and Polk, J. E., "An Overview of the Nuclear Electric Xenon Ion System (NEXIS) Activity," AIAA Paper 2004-3450, July 2004.
[116] Prockter, L., et al., "The Jupiter Icy Moons Orbiter: an Opportunity for Unprecedented Exploration of the Galilean Satellites," International Astronautical Federation Congress, Vancouver, Canada, Paper IAC-04-IAA.3.6.4.02, Oct. 2004.
[117] Oleson, S. R., "Electric Propulsion Technology Development for the Jupiter Icy Moons Orbiter Project," AIAA Paper 2004-3449, July 2004.
[118] Elliott, F. W., Foster, J. E., and Patterson, M. J., "An Overview of the High Power Electric Propulsion (HiPEP) Project," AIAA Paper 2004-3453, July 2004.
[119] Williams, G. W., et al., "Performance Characterisation of HiPEP Ion Optics," AIAA Paper 2004-3627, July 2004.
[120] Nakanishi, S., and Pawlik, E. V., "Experimental Investigation of a 1.5-Meter Diameter Kaufman Thrustor," AIAA Paper 67-725, Sept. 1967.
[121] Patterson, M. J., "50 cm Ion Thruster Research," AIAA Paper 87-1034, May 1987.
[122] Patterson, M. J., Roman, R. F., and Foster, J. E., "Ion Engine Development for Interstellar Precursor Missions," AIAA Paper 2000-3811, July 2000.
[123] Aston, G., Brophy, J. R., Garner, C. E., Pless, L. C., Owens, A. G., and Toomath, R. L., "Operating Characteristics of a 10 kW Xenon Ion Propulsion Module," AIAA Paper 87-1006, May 1987.
[124] Masek, T. D., Poeschel, R. L., Collett, C. R., and Schnelker, D. E., "Evolution and Status of the 30-cm Engineering Model Ion Thruster," AIAA Paper 76-1006, Nov. 1976.
[125] Kitamura, S., Hayakawa, Y., Miyazaki, K., Yoshida, H., Kajiwara, K., and Akai, K., "Research and Development of a 150-mN Xenon Ion Thruster," International Electric Propulsion Conference, Paper 2003-165, March 2003.

[126] Fearn, D. G., "The Manned Exploration of Mars Using Nuclear Electric Propulsion: a Gradual, Minimum Cost Strategy," *Proceedings 4th International Spacecraft Propulsion Conference*, Chia, Sardinia, June 1–6, 2004, edited by A. Wilson, ESA-ESTEC, SP-555, Noordwijk, The Netherlands, 2004.

[127] Christensen, J., "Boeing EDD Electric Propulsion Programs Overview," AIAA Paper 2004-3967, July 2004.

[128] Fearn, D. G., Martin, A. R., and Smith, P., "Ion Propulsion Development in the UK," International Astronautical Federation, Paper IAF-93-S.5.490, Oct. 1993.

[129] Bond, R. A., Fearn, D. G., Wallace, N. C., and Mundy, D. H., "The Optimisation of the UK-10 Ion Thruster Extraction Grid System," International Electric Propulsion Conference, Paper 97-138, Aug. 1997.

[130] Martin, A. R., "High Power Beams for Neutral Injection Heating," *Vacuum*, Vol. 34, No. 1–2, 1984, pp. 17–24.

[131] Okumura, Y., et al., "Quasi-dc Extraction of 70 keV, 5 A Ion Beam," *Review of Scientific Instrumentation*, Vol. 51, 1980, pp. 728–734.

[132] Fearn, D. G., "The Possible Application of Ion Propulsion to Precursor Interstellar Missions," AIAA Paper 2000-3415, July 2000.

[133] Leiter, H., et al., "RIT-22 – the Ion Thruster of the RITA Propulsion System for Commercial and Scientific Applications," *Proceedings of 4th International Spacecraft Propulsion Conference*, Chia, Sardinia, June 1–6, 2004, edited by A. Wilson, ESA-ESTEC, SP-555, Noordwijk, The Netherlands, 2004.

[134] Fearn, D. G., "The Design of a Versatile Ion Thruster for Large Communications Spacecraft," International Astronautical Federation Congress, Turin, Italy, Paper IAF-97-S.3.01, Oct. 6–10, 1997.

[135] Ohara, Y., "Numerical Simulation for Design of a Two-Stage Acceleration System in a Megawatt Power Ion Source," *Journal of Applied Physics*, Vol. 49, 1978, pp. 4711–4717.

[136] Menon, M. M., et al., "Power Transmission Characteristics of a Two-Stage Multiaperture Neutral Beam Source," *Review of Scientific Instruments*, Vol. 51, 1980, pp. 1163–1167.

[137] Chesta, E., et al., "Flexible Variable-Specific-Impulse Electric Propulsion Systems for Planetary Missions," *Proceedings of 5th International Conference on Low-Cost Planetary Missions*, ESA SP-542, 2003; also *Acta Astronautica*, Vol. 59, Nos. 8–11, Oct.–Dec. 2006, pp. 931–945.

[138] Kuninaka, H., Funaki, I., Nishiyama, K., Shimizu, Y., and Toki, K., "Result of 18,000-Hour Endurance Test on Microwave Discharge Ion Thruster," AIAA Paper 2000-3276, July 2000.

[139] Tartz, M., Hartmann, E., and Neumann, H., "Study of Extraction Grid Erosion in a Long-Time Ion Thruster Operational Test," International Electric Propulsion Conference, Paper 03-176, March 2003.

[140] Negrotti, A., "Vasimr Prefeasibility Analysis," *Advanced Propulsion Systems and Technologies, Today to 2020*, edited by C. Bruno and A. Accettura, AIAA Progress in Astronautics and Aeronautics, Vol. 223, AIAA, Reston, VA, 2008, pp. 333–356.

[141] Rossetti, P., Saverdi, M., and Biagioni, L., "Electronic Propulsion Systems," *Advanced Propulsion Systems and Technologies, Today to 2020*, edited by C. Bruno and A. Accettura, AIAA Progress in Astronautics and Aeronautics, Vol. 223, AIAA, Reston, VA, 2008, pp. 223–289.

Copyrighted Materials
Copyright © 2008 AIAA Retrieved from www.knovel.com

Chapter 4

High-Power and High-Thrust-Density Electric Propulsion for In-Space Transportation

Monika Auweter-Kurtz* and Helmut Kurtz†
University of Stuttgart, Stuttgart, Germany

I. Introduction

MISSION scenarios such as building a scientific outpost on the moon or human exploration of Mars require new propulsion systems for in-space transportation of heavy payloads [1]. A thrust level of at least 100 N and a specific impulse level of 30 km/s are of central importance to increase the payload capacity and shorten the trip time as much as possible. The propulsion system mass should be as lightweight as possible.

Therefore, both thrust density and efficiency of the propulsion device should be high. Nuclear and solar *thermal* propulsion offer very high thrust densities but are still weak in their specific enthalpy level and thus specific impulse (see Chapter 1), which is clearly below 10 km/s (see Table 1). Ion and Hall-ion thrusters offer both the required exit velocity level but their thrust density is still relatively low.

Promising in-space propulsion candidates for heavy payloads are currently thermal arcjet thrusters with which an exit velocity of 20 km/s at 100 kW and a thrust density of more than 2100 N/m^2 can already be achieved. This technology is in an advanced developmental stage; low power devices have been implemented in commercial applications with hydrazine as propellant and are exceptionally reliable. The highest thrusts and thrust densities reached to date have been achieved with MPD self-field thrusters. However, the effective exit velocity is still limited to 15 km/s. Although the achievable thrust density is an order of magnitude lower, applied-field MPD thrusters should still be considered for this

The material presented in this chapter is updated from the paper published in *Space Technology*, "High Power Plasma Propulsion for In-Space Transportation," Vol. 27, No. 1, 2007, pp. 51–75, and is reproduced with permission. Copyright © 2008 by the authors. Published by the American Institute of Aeronautics and Astronautics, Inc., with permission.

*Professor, University of Hamburg.
†Engineer, Institute of Space Systems.

Table 1 Performance data of a solar thermal rocket [2], a nuclear thermal rocket NERVA [3], a high-power thermal arcjet HIPARC [4], a self-field MPD thruster DT2 [5], applied-field MPD thrusters [6], ion propulsion system DS1 [7], a Hall ion thruster SPT 100 [8] with the Saturn V data as reference

	Thrust F, N	Exhaust velocity c_e, km/s	Nozzle-exit area A, m^2	Thrust density, N/m^2
Saturn V (1st stage S-IC, Rocketdyne F-1)	6,680,000	<5	10.752	621,280
Solar thermal rocket	25	<8	0.002	12,732
Nuclear thermal rocket (NERVA)	340,000	<8	11.282	30,138
Thermal arcjet (HIPARC) IRS	6	20	0.003	2,122
MPD self-field (DT2) IRS	28	<15	0.008	3,565
MPD applied field (T)	4.50	42	0.020	225
Ion propulsion (DS1)	0.092	<60	0.071	1.302
Hall-ion thruster (SPT100)	0.10	<30	0.008	12.732

type of application because it is possible to achieve very high exit velocities. Hybrid thrusters are also an interesting development, but they have not been investigated extensively as much yet. The hybrid concept ATTILA, in which a thermal arcjet thruster is combined with a second inductive stage, is remarkable for its high thrust densities. A significant increase in the effective exit velocities of these devices compared to the thermal arcjet thrusters can be expected.

All of these high-power, high-thrust-density thrusters are still at a relatively rudimentary development stage and are far from being able to be used in space. Up to now, mostly basic investigations have been performed, and some tools for the construction have been developed. A systematic investigation and optimization of these technologies is still outstanding. Appropriate developmental test facilities are necessary in some cases. Following is a detailed description of the developmental stage of these stationary operated thrusters and of future development needs.

II. Thermal Arcjets

In the last two decades, electrothermal arcjets have been investigated in a wide power range (0.1 to 100 kW) for a wide range of uses [9, 10]. Low-power arcjet thrusters from General Dynamics (Primex), United States, have been used since 1993 as north-south-stationkeeping (NSSK) thrusters with hydrazine as propellant [11], and were foreseen as primary propulsion for the AMSAT P3 satellite with ammonia as propellant [12]. The medium-power ammonia arcjet thruster on the U.S. Air Force Argos satellite, the ESEX experiment [13], also of Primex origin, proved the feasibility of such a thruster for orbit transfer. In the area of high electric power up to approximately 100 kW, an operable laboratory model

for hydrogen as propellant has been developed [4], and the potential for this kind of technology has been investigated.

A. Operational Principle

In an arcjet thruster, electric power from an external power source is used to heat a propellant gas by means of an electric arc. The heated gas expands through a converging–diverging nozzle to produce thrust as shown in Fig. 1. The thruster is axisymmetric, with a central cathode normally made of a tungsten alloy (1–2% ThO2) and with the nozzle, also made of refractory materials, switched as anode. The gas flows through this inner-electrode region, and the arc is heated by Ohmic heat and is at least partially dissociated and ionized.

The arc originates at the cathode tip (typically about one to several square millimeters, depending on the arc power) and is stabilized by the nozzle throat, which is built in the form of a "constrictor." (Its length-to-diameter ratio is typically 1 to 2.) The arc is forced by the gas flow through the constrictor to attach downstream at the beginning of the diverging part of the nozzle. Arc attachment in the converging part is unfavorable and has to be avoided ("low-voltage mode"). A diffuse arc attachment at the anode minimizes anode erosion and maximizes the heat transfer to the propellant. The attachment zone moves downstream in the nozzle with rising mass flow and/or rising discharge current. Heating of the gas takes place mainly in the core zone of the arc; the surrounding cold gas cools and therefore protects the nozzle throat preventing the arc from attaching there.

Using a simplified one-dimensional model, the exhaust speed c_e and hence the specific impulse I_{sp} of an ideal thermal expansion through a de Laval nozzle are proportional to

$$I_{sp} \sim \sqrt{\frac{T}{M}}$$

with T the plenum temperature of the gas and M the average molecular mass [14]. (This is strictly true only for ideal gases. The effect of increasing temperature on chemistry, electronic excitation, or ionization for nonideal gases will change the energy available for propulsion.) This means that higher specific impulses are obtained by increasing the temperature and decreasing the molecular mass of the gas. The upper limits on the temperature are determined by the heat transfer from the gas to the thruster body and the body's materials. The practical lower limit on

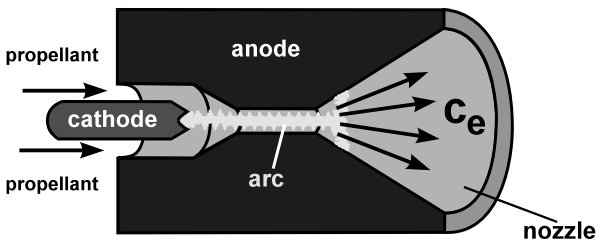


Fig. 1 Operational principle of an arcjet.

the molecular mass M is dissociated (atomic) hydrogen, with 1 amu (atomic mass unit). This is the main reason that hydrogen and gases containing a high fraction of hydrogen (like ammonia or hydrazine) are the most common propellants.

During expansion, a large fraction of the thermal energy of the propellant gas is converted to kinetic energy. With the exception of high-power arcjets (>50 kW), electromagnetic forces do not play any role in generating the thrust. But also at a level of some hundred kilowatts, this portion is very low. The energy that is deposited in the arc plasma by Ohmic heating is converted to internal, kinetic, and chemical energy. It is distributed to the surrounding cold propellant gas through heat transfer and diffusion, and mainly in the constrictor.

The average gas velocity c_e of arcjets is high with respect to chemical rockets (up to 20,000 m/s at 100 kW), but because of the high gas temperatures and the low mass flow rates, the Reynolds numbers are low (100–1000). This means there is an appreciable amount of viscous losses, especially with small thrusters. The plume of an arcjet shows a pronounced velocity profile with high core velocities and low border velocities. Other losses are thermal losses (heat deposition into the thruster body, especially cathode and anode, that has to be removed by radiation).

1. Efficiency

The main losses in arcjet propulsion are frozen flow losses: because the residence time of the propellant in the nozzle is in the order of 1 μs, the energy comprised in dissociation, ionization, and excitation cannot be completely recovered in the nozzle as kinetic energy of the exhaust jet. Therefore, the efficiency η of arcjets with molecular gases is restricted to $\eta < 50\%$.

The parameter that determines the I_{sp} is the specific power of the gas, defined as the electric power divided by the mass flow, or $P/\dot{m}$. The higher this specific power is, the higher the specific impulse also; see Chapter 1. The amount of specific power that can be sustained by a thruster body is a function of the size and material: small thrusters are limited to about 150 MJ/kg and large thrusters to >700 MJ/kg (for H2). This $P/\dot{m}$ parameter correlates with the performance parameter I_{sp}; this correlation is only relatively weakly affected by geometry changes in the thruster. Also the quantity thrust/power (T/P) is correlated by this performance parameter. They are connected by the efficiency, defined as thrust power over input power:

$$\eta = \frac{T^2}{2\,\dot{m}\,P} = \frac{c_e^2}{2\left(\dfrac{P}{\dot{m}}\right)} = \frac{c_e}{2}\left(\frac{T}{P}\right)$$

At fixed $P/\dot{m}$ an increase in I_{sp} will increase the efficiency, enabling an increased propellant mass saving. Operation at fixed I_{sp} and higher $\dot{m}$ will lower $P/\dot{m}$ and hence increase the lifetime of the thruster.

As can be seen from the preceding equation, by increasing the specific power $P/\dot{m}$ of an arcjet to increase its I_{sp} the gas temperature and hence the frozen flow losses are also increased. This leads to the unfavorable effect that with increasing I_{sp} the efficiency will inherently decrease, as shown for example in Fig. 2.

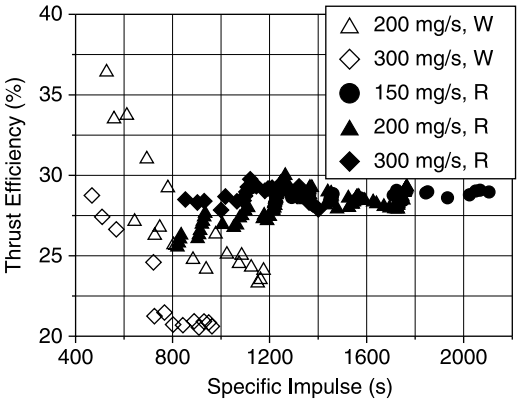


Fig. 2 Exemplarly efficiency/I_{sp} curve for HIPARC, water-cooled W and radiation-cooled R version, with hydrogen as propellant [14].

There are only few means to increase the efficiency:

1) ***Regenerative cooling***—With regenerative cooling, the cold propellant is made to pass through the hottest parts of the thruster. Part of the thermal losses can be recovered as increased propellant enthalpy, and the efficiency is raised. The gain in η naturally depends on the heat capacity of the propellant, that is, on its specific heat c.p. and mass flow and on the ΔT. From the propellant prospective, H_2 is the best suited. Its c.p. is more than five times higher than that of NH_3 at the same temperature $T = 1000$ K. An extra advantage of regenerative cooling consists of reducing the extreme heat stresses near the arc attachment area and nozzle throat and hence prolonging the lifetime of the thruster.

2) ***Bi-exit or dual-cone nozzle***—Primex first suggested the bi-exit anode [15] (Fig. 3) to recover some of the frozen flow losses. The idea is to provide an area of relatively high gas density and sufficient time to achieve some recombination.

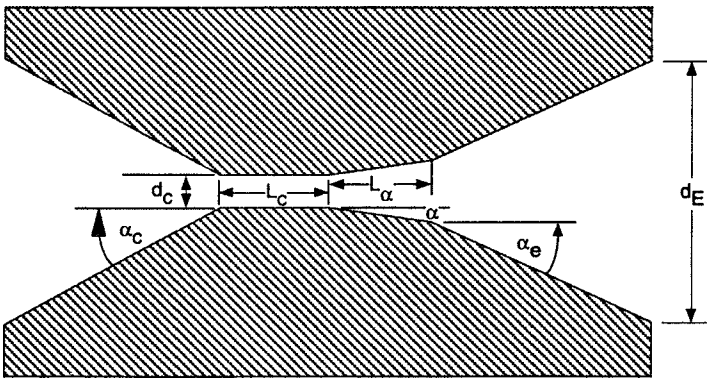


Fig. 3 Bi-exit nozzle principle [16].

This could be accomplished by a dual-cone anode; that is, the diverging part of the nozzle is divided into two regions: the first (of length *Lc* in Fig. 3) with a slowly varying area allowing some recombination and the second a conventional diverging nozzle for rapid expansion. Because this first section bears higher heat loads, it is preferably combined with regenerative cooling. A similar approach was presented by Aston [16].

2. Discharge Voltage

For introducing power (current × voltage) into the arc, the current should be as low as possible to alleviate the heat load to the electrodes, meaning the discharge voltage should be high. An arcjet thruster system is normally "current controlled." The discharge voltage results from, and is determined by, several factors:

1) ***Propellant***—Monoatomic gases with low dissociation potential such as argon show the lowest voltage at constant current and H_2 the highest.

2) ***Mass flow***—The discharge voltage rises with rising mass flow.

3) ***Constrictor length***—The length of the constrictor, that is, the length of the arc, determines the voltage drop caused by the Ohmic losses.

4) ***Cooling system***—Regenerative cooling allows significantly higher voltage at constant $P/\dot{m}$. (The preheated gases increase the plenum pressure and hence the discharge voltage.)

5) ***Constrictor diameter***—At constant mass flow and current the voltage is lower with larger constrictor diameter (lower plenum pressure).

B. Theory and Numerics

Although the design of an arcjet thruster as illustrated in Fig. 1 seems simple, the flow and heating processes involved are very complex. Sophisticated numerical analysis and design tools are needed for proper physical modeling and performance assessment. The theoretical treatment of arcjets and the numerical prediction of their behavior is an ongoing task, mainly in the academic environment of many countries such as the United States, Japan, Germany, and Italy.

The standards required for accurate predictions are high. Recent simulations refinements are concentrating on nonequilibrium chemistry, transport coefficients, and electrode models. The goal is to calculate all of the arcjet system characteristics and its performance using only global input parameters, such as propellant type, mass flow, and discharge current, with geometry imposing a second set of conditions. The most efficient computational models have been developed for *hydrogen*. Examples of these are Miller [17], Gölz [4], Butler [18], and Fujita [19].

Nitrogen as propellant, both experimental and numerical, is considered for basic investigations mainly in Japan by Kyushu University [20]. In *nitrogen/hydrogen mixtures* simulating hydrazine for low-power arcjets, the standard reached is almost as high as with hydrogen alone; the results are very encouraging [21].

C. System Description

Figure 4 shows a simplified electrical scheme of an arcjet system. It consists of the thruster, the power supply system, and the propellant feed system.

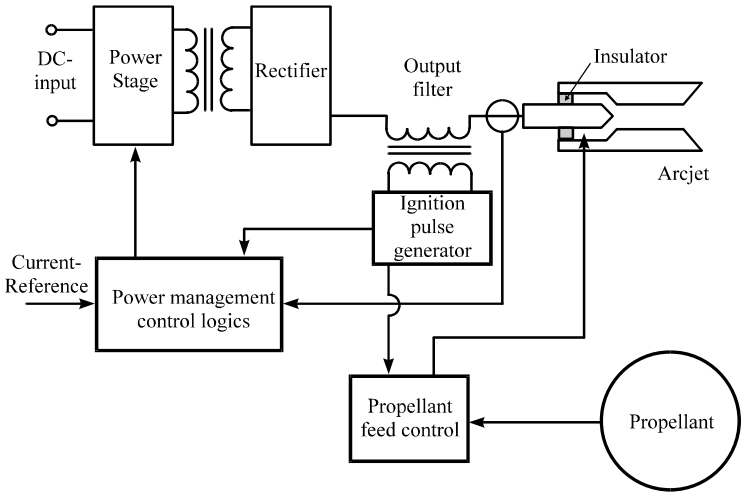


Fig. 4 Simplified arcjet thruster system with current and propellant circuits.

The power supply system is a key component in operational arcjet systems. It has to ensure reliable arc initiation and a stable steady-state operation. The arc is ignited by a series of high-voltage (>2 kV) pulses across the arcjet electrodes. This generates sparks (via a so-called Paschen breakthrough) in the propellant gas, leading the way to the main discharge. The power control unit (PCU) must take over the incipient discharge by means of a fast control unit, maintain the discharge stable, and withstand or correct its possible instabilities, mainly caused by erratic arc attachments. Because the voltage/current characteristic of an arcjet has the typically negative slope of arc discharge, (see Fig. 5 for the water-cooled case), this leads to demands on the PCU. Normally the power supply is current controlled.

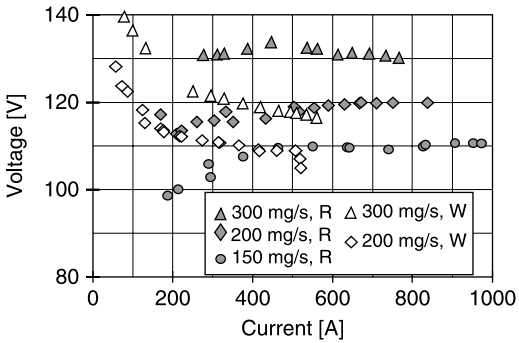


Fig. 5 Typical voltage/current characteristics of a 100-kW hydrogen arcjet thruster; radiation-cooled R water-cooled W [4].

As shown in Fig. 4, the high-power ignition circuit is normally integrated in the power supply and uses inductive coupling. In solar-powered satellites, the power conversion from the nominal satellite bus dc is done by a pulse-width-modulated PCU, resulting in a current controlled output.

In the last few years, mainly by the application of modern digital electronics, immense progress has been made in reducing the mass of power supplies for low-power arcjets [22] leading to PCU efficiencies between 90 and 95%.

D. Influence of Propellants

Arcjets can operate on a variety of propellants. As just discussed, the molecular mass of the propellant should be as low as possible. On the other hand, the propellant and/or the dissociated products might not react chemically with the thruster body and electrode materials. This excludes all compounds containing either oxygen or carbon. For use on the International Space Station (ISS), H_2O-containing propellant mixtures show some development potential. A laboratory model has already been developed [23]. Compounds containing elements that could be deposited on the spacecraft should also be ruled out. This restricts the preferred choice to H_2 and hydrogen/nitrogen compounds. Another advantage of H_2 is its higher discharge voltage, which helps to relay power to the propellant at low discharge currents.

Hydrazine (in laboratories normally replaced by simulated hydrazine, that is, $N_2 + 2H_2$) is already in use for low-power arcjet applications. Hydrazine has to be gasified and decomposed in a reactor yielding a mixture of hydrogen, nitrogen, and a small amount of ammonia. The I_{sp} is limited from 500 s for small arcjets (<1 kW) to more than 650 s for medium-size arcjets (around 2 kW) [22]. Efficiencies lie between 30% at high I_{sp} and 40% at $I_{sp} \approx 500$ s. No experimental data for high-power thrusters have been measured, but one can extrapolate to an I_{sp} in the order of 900 s at power levels >30 kW, corresponding to specific power values $P/\dot{m}$ in the 150-kJ/g range. One additional advantage of hydrazine as propellant for arcjets is that in case of arcjet malfunctions (i.e., no arc ignition) the thruster can still act as a monopropellant thruster, although at lower I_{sp}.

Ammonia represents space-qualified technology already used on ESEX and ATOS satellites and on resistojets in Russia at the NIIEM Institute [25]. The I_{sp} is limited from 500 s for small arcjets (<1 kW) to about 900 s extrapolated for medium-size arcjets (<30 kW). Efficiencies lie in the 30–40% range. The preceding data are for nonregeneratively cooled thrusters. With an appropriate design embodying regenerative cooling, some improvements could be expected.

For both hydrazine and ammonia propellants, the I_{sp} range for high-power arcjets must still be established, which is very important for assessing the limits of arcjet propulsion.

Hydrogen is the best choice for arcjets in terms of I_{sp} because of its low atomic mass and good thermophysics properties. Because of frozen flow losses, efficiencies are low, about 25 to 40%, when using hydrogen, but they can be improved by proper design and especially by including regenerative cooling. The maximum I_{sp} depends on the size of the thruster, ranging from about 1000 s with1 kW and 1500 s with 10 kW to over 2000 s with 100 kW (see Fig. 6). The data for the ESEX thruster ($I_{sp} = 786$ s, $\eta = 27\%$, $P/\dot{m} = 105$ kJ/g) fit well into the I_{sp} curve of

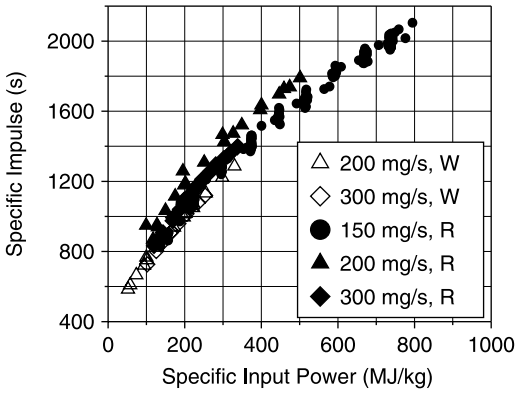


Fig. 6 Specific impulse vs specific power for a radiation-cooled R and a water-cooled W high-power arcjet thruster [4].

Fig. 6. A disadvantage of hydrogen is its problematic storage for long missions because it is a cryogenic liquid. However, for high-power missions this issue seems to be now of lesser concern.

By using hydrogen propellant and solar-powered *electric* thrusters on orbit-transfer vehicles (EOTV), a tank fraction of 0.15 has been estimated [10], which would yield mass savings of 43% for a 2000-kg payload on a LEO to GEO transfer mission. This result applies to an I_{sp} of 1200 s, a 30-kW engine, and 200-d transfer time. The system conceived in [10] does away with long-term cryogenic storage requirements by utilizing hydrogen boil-off cooling.

Mono-atomic gases are in principle preferable in terms of efficiency, as there are no dissociation losses. However, only helium seems of interest because of its low atomic weight. But results achieved to date by The Aerospace Corporation and Stanford University [26, 27] have been disappointing, both in terms of low I_{sp} and unstable operation. In addition, the storage of liquid helium is difficult and expensive. Only seeding helium with hydrogen (or vice versa) could offer advantages [27, 28] and could possibly result in stable arcjet behavior, but other issues related to helium as propellant, such as unstable discharge, still remain unsolved.

E. Lifetime Limiting Factors

At high power, the operational lifetime of an arcjet thruster is limited mainly by the degradation of the cathode. Cathode-tip erosion is a major problem because it can lead to severe ignition problems. The arc attaches on the tip of the cathode rod and (ideally) is sustained in a stable discharge by thermionically emitted electrons. That requires a cathode-tip temperature >2000°C. During ignition, when the cathode is still cold, arc attachment can cause local melting on the tip, leading to high erosion by dislodging cathode material, a "spitting" process observed in the laboratory. Cathode erosion increases the discharge voltage by increasing the inner electrode gap and can drive discharge instabilities caused by the loss of cathode-tip symmetry and therefore erratic arc attachment. Erosion increases with tip

temperature, so that the cathode geometry (i.e., diameter) has to be designed carefully and must not be thermally overloaded by excessive specific power $P/\dot{m}$.

Cathode erosion is especially sensitive to oxidizing gases: the propellant must be very clean and cannot contain any oxygen or humidity. The maximum arcjet specific input power $P/\dot{m}$ is primarily limited by the maximum heat load the nozzle throat (the constrictor) can withstand. Therefore, adequate cooling (i.e., regenerative cooling) and good refractory materials should be used.

F. Qualification Advantages

In comparison with other electric propulsion systems, such as ion, Hall-ion, and applied-field MPD thrusters, the qualification requirements of arcjets are much less demanding. The PCU is simpler. Beside the ignition pulse generator, only one power circuit is needed, and that at relatively low (80–200 V) voltage. The physics of arcjets allow representative operation at tank pressure in the range of 1–10 Pa, allowing the use of roots-pump vacuum systems, and a factor ~10^3 less demanding than with ion thrusters or solid propellant thrusters (SPT). Because of the high thrust levels achievable with arcjets, the accumulated test time is also about a factor 10 smaller than with the just-mentioned thruster types.

G. Existing Arcjet Thruster Technologies

This section describes recent or ongoing activities concerning high-power arcjet thruster technologies and available arcjet systems worldwide.

High-(to medium-) power arcjet (10 to 100 kW) research has been restricted to only a few places—JPL and Primex in the United States and the Institut für Raumfahrt Systeme (IRS) at the University of Stuttgart in Germany—because of the lack of funding and testing facilities (sufficient large pump systems) elsewhere.

1. United States

Work on arcjet propulsion started here in the late 1950s and 1960s and resulted in quite remarkable laboratory thrusters [29]. After a pause of roughly 20 years as a result of a lack of sufficient lab power and missions, work was resumed by government agencies, such as NASA, JPL, U.S. Air Force (USAF), Strategic Defense Initiative Organization (SDIO), and others. Part of the task was soon handed over to industry, mainly RRC, Rocket Research Company (later renamed PRIMEX and now part of General Dynamics and TRW). It should be emphasized, however, that the years of industrial development were accompanied by either direct scientific support from the government agencies just mentioned or through sponsorship of universities.

2. Germany

High-power arcjet development is currently performed only in Germany at IRS. The high-power arcjet HIPARC has been designed and investigated to establish operation in the 100-kW range and to produce first performance maps. With its large

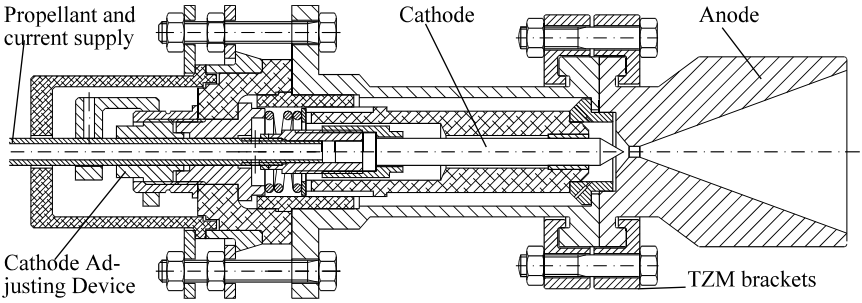


Fig. 7 Schematic drawing of the 100-kW HIPARC-R thruster; constrictor diameter 4 mm [4].

roots-pump system capable of volumetric flowrates >250,000 m³/h at 10 Pa, IRS is well equipped for high-power, high-mass flow-rate testing. Of the two HIPARC versions built, one was water cooled one for testing diagnostics and geometry changes, whereas the other was radiation cooled (see Fig. 7) Although in no way optimized, it yielded I_{sp} over 2000 s at an efficiency of 28% (see Fig. 2) [4].

In Fig. 5 the current/voltage characteristics for the radiation-cooled and the water-cooled HIPARC thrusters are shown. In the case of the radiation-cooled HIPARC, the voltage is independent of the current over a wide range. It does not decrease, as is the case with low-and medium-power arcjets and with water cooling. This is a clear sign that hydrogen is almost completely dissociated and ionized, as also predicted by calculations [22], and that the magnetic acceleration caused by the self-induced magnetic field does not play a significant role. In addition, the efficiency of the radiation-cooled HIPARC is independent of the specific impulse over a wide range.

It is to be expected that a thruster optimization using regenerative cooling and a biconical nozzle design will allow for a significant increase of the effective exit

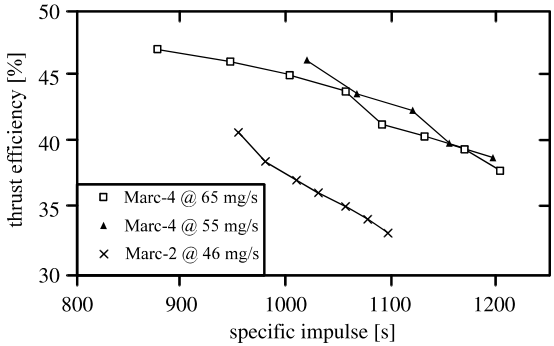


Fig. 8 Efficiency gain with regenerative cooling; hydrogen, 5-kW class; MARC 2 radiation cooled [31].

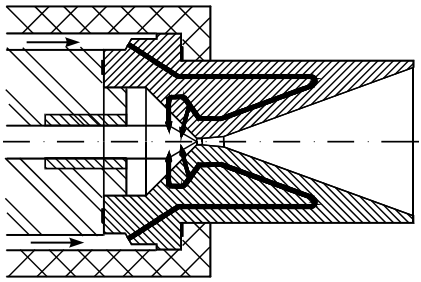


Fig. 9 Cross section of the MARC 4 thruster head [31].

velocity. Intensive investigations of the potential of regenerative cooling were carried out at IRS with the medium-power arcjet MARC in the 5–12 kW region [30]. In particular, numeric design tools were developed and tested for optimizing the design of arcjets. Figure 8 shows that specific impulse and, especially, efficiency increase during the transition from the purely radiation-cooled MARC2 to the regenerative device (Fig. 9).

III. Magnetoplasmadynamic Thruster

The main operating principle of MPD thrusters is to use also electromagnetic forces (the Lorentz force) to accelerate the propellant. Ohmic heating and the resulting thermal thrust portion play a subordinate role, but often one that should not be ignored.

Generally, two main types of MPD systems can be defined: self-field MPD thrusters and applied-field MPD thrusters.

MPD applied-field thrusters are always operated in a stationary mode. Self-field thrusters have three operating modes: continuous, quasi-stationary, and nonstationary. Because from today's perspective of space transportation high average thrust can only be achieved with stationary MPD self-field accelerators, only this type of thruster will be considered.

When designing MPD thrusters, one must be aware that only charged particles can be accelerated by electromagnetic force. Therefore the propellant should be almost completely ionized to achieve high efficiency. Recombination is undesirable, anywhere in the entire thruster. To this purpose, the gas temperatures in MPD devices are higher, and the pressure is lower than in thermal arcjet devices. Pressure in the energy deposition (ionization) chamber is typically between $5 \cdot 10^{-4}$ bar and 0.5 bar depending on geometry, power level, and mass flow.

A. Self-Field Thrusters

The self-field (SF)-MPD thrusters (Fig. 10) have been much more extensively investigated experimentally than the other thrusters discussed here, both in continuous and in pulsed quasi-steady operation, and with many propellants. The principle of operation should be clear from Fig. 10, showing how the self-induced circumferential (azimuthal) magnetic field B_θ, interacting with the applied meridian

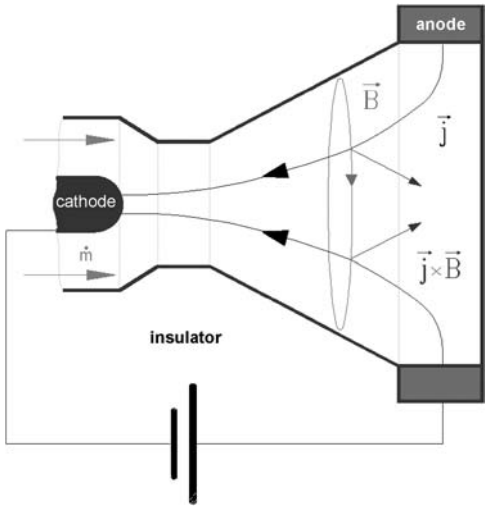


Fig. 10 Operating principle of the self-field MPD thruster.

currents, produces meridian forces on the plasma that are normal to the current and directed mostly axially and radially inward. These forces, called "blowing" and "pumping" by Maecker [32] result in direct (*electrodynamic*) acceleration and in a pressure ("pinch" pressure) and temperature rise, driving also a *thermodynamic* expansion and acceleration, respectively [33]. The pinch pressure may also enhance nozzle recombination through the increase of collision rate, scaling with the cube of pressure.

Of the thruster types discussed here, the SF-MPD thrusters have the lowest arc voltages for a given power level because the self-induced magnetic fields are relatively weak unless very high currents (that is, tens of kiloamps) are applied. Typical values (for nozzle-type thrusters with argon propellant) are ≈50–70 V for a ≈200-kW continuous thruster. Because the electrode loss voltages change much less rapidly with the current or power level, the thermal efficiencies of these thrusters improve with increasing power. Because of the high currents required, the SF-MPD thrusters also have the most severe electrode erosion and cooling problems.

For in-space transportation missions considered here, only continuous-mode thrusters make sense: pulsed and quasi-steady pulsed thrusters are disregarded in the following, despite having been investigated in many laboratories over decades. By directly comparing geometrically identical thrusters in continuous operating mode to quasi-steady (q-s) pulsed mode [34], it was shown that results of q-s thrusters could not be extrapolated to the steady operation case, and therefore that most q-s results are irrelevant to designing real high-power and high-thrust missions.

The phenomenon of self-magnetic plasma acceleration was first investigated by Maecker [32], Wienecke [35], and others in Germany (circa 1955), who studied

velocity distributions in the cathode jets of carbon arc lamps. A simple integral formula by Maecker [32] gives the electromagnetic thrust fairly precisely for any thruster geometry and current distribution (assumed or measured) on the cathode and anode. In this way the contribution of the electromagnetic forces to the average axial exhaust velocity was found in the form

$$c_{\mathrm{EM}} = \frac{\mu_0 I^2}{4\pi \dot{m}} f(\mathrm{geom}) = (1.85 \div 3.05)\cdot 10^{-7} \frac{I^2}{\dot{m}}$$

where c_{EM} is the electromagnetically produced exhaust velocity, I is the total electric current, $\dot{m}$ the propellant mass flow rate, and f(geom) is a function of the electrode geometry and of the radial current distribution on the electrodes [33]. The numerical values given in this equation are typical for thruster models tested so far. It is important that the purely theoretical Maecker integral formula for the thrust and the resulting electromagnetic contribution to the average axial component of the exit velocity—which is well verified experimentally—are independent of any assumed model, or rotational (circumferential) uniformity, of the discharge. Any arc spokes and/or anode spot attachments have no influence on the result. These details of the arc form and spatial distribution, however, affect the exit velocity distribution, the resulting thrust direction, and the efficiency of electromagnetic thrust production. Of course, models generally used to evaluate the factor f(geom) are simple, and herein lie some uncertainties.

Especially if the thruster is nozzle shaped, a nonnegligible electro*thermal* thrust adds to the purely MPD thrust. The thrust vs current curves for various argon mass flow rates for the IRS DT-2 thruster (Fig. 11) are shown in Fig. 12. Also plotted in this graph is the pure electro*magnetic* thrust T_M, calculated in [32, 33]

$$T_M = \frac{\mu_0}{4\pi} I^2 \left(\lambda\nu \frac{r_a}{r_c} + \frac{3}{4} \right)$$

$T_{\mathrm{m,max}}$ and $T_{\mathrm{m,min}}$ are calculated with cathode radius r_c and for the maximum and minimum possible anode radius r_a. It can be seen that at lower current levels the electrothermal part of the thrust is prevalent, and only with rising current levels the total thrust does approach the gradient angle of the magnetic thrust.

Empirically, it has been known for some time that the current-to-gas-mass flow ratio $I^2/\dot{m}$ has a limit for each thruster and propellant, beyond which stable operation of the arc becomes impracticable. Beyond that so-called "onset" value, pronounced arc voltage fluctuations, severe anode spots, and anode erosion, increased anode losses and thruster efficiency drop are observed. Attempts to exceed the onset limit $(I^2/\dot{m})_{\mathrm{crit}}$ are foiled by erosion of the anode, exposed insulators, and perhaps cathodes. This erosion apparently supplies the additional mass flow in front of the anode that limits $I^2/\dot{m}$, as demonstrated, for instance, by Suzuki et al. [36].

The great importance of the onset or critical $I^2/\dot{m}$, values is clear because practically useful thruster efficiencies (say above ≈30%) can (if at all with a given thruster) be achieved only with each propellant at the highest specific impulse (or $I^2/\dot{m}$) values at present attainabl e with that propellant, as will be seen.

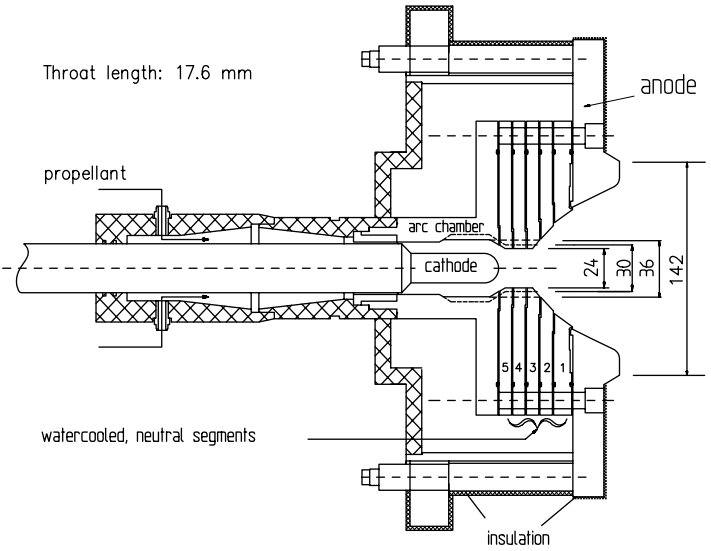


Fig. 11 Nozzle-type MPD thruster DT (DT2 with 24-mm throat, DT6 with 36 mm).

For SF-MPD thrusters, Hügel [37] has correlated the onset ($I^2/\dot{m}$) ratios from different sources and thrusters with different propellants against their atomic weights. The rough correlation found is

$$\left(\frac{I^2 M_a^{1/2}}{\dot{m}}\right)_{\text{crit}} \approx (15-33)\cdot 10^{10}\left[\frac{A^2 s}{kg}\right]$$

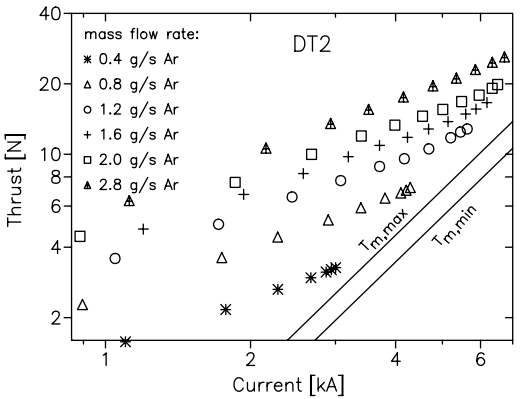


Fig. 12 Thrust vs current curves for the DT2 thruster at various mass flow rates.

or

$$(c_{\mathrm{EM}})_{\mathrm{crit}} \approx (3-10)\cdot 10^4 \; Ma^{-1/2} \left[\frac{m}{s}\right]$$

where M_a is the dimensionless atomic weight of the propellant and the empirical constants in these equations depend on the thruster geometry and the power level. These results agree with those of Malliaris [38]. Both researchers confirmed these data using noble gases as propellant. With molecular gases, however, this dependence could not be verified at IRS [39].

Pulsed SF thruster data from Princeton University and the University of Tokyo report electromagnetic velocities by a factor of two times larger than the upper value of the preceding equation for argon, that is, ≈33 km/s, but they could not be verified with steady-state thrusters.

Hügel [37] calculated the current and gas density distributions for some of these thrusters using several simplified flow models and empirical electron temperatures. He showed that near the onset, the ion density at the anode approaches zero because of the pinch (or radial inward) component of the electromagnetic force distribution. Assuming singly ionized plasma, he concluded that the onset episodes occur when the ion densities at the anode become too low to neutralize the anodic electron current. This explanation is immediately plausible from the fact that the ratio of the magnetic pinch pressure rise Δp_M to the mean gas pressure in the jet p_j is proportional to the current/mass flow ratio parameter:

$$\frac{\Delta p_M}{\overline{p_j}} \sim \frac{I^2}{\dot{m}}$$

as can be verified by simple approximations.

However, there appear to also be other theoretical approaches for arriving at critical values of $I^2/\dot{m}$. Cann [40] arrives at this from his minimum arc voltage principle. Schrade [41] shows from his arc stability criterion that instability must occur above certain $I^2/\dot{m}$ values.

King [42] has approximated the MPD accelerator flow with a one-dimensional channel theory and from this has estimated values of the Hall parameter in MPD accelerators. He ascribes the onset limit of $I^2/\dot{m}$ and the observed current distributions to excessively large Hall parameter values (that is, approaching ≈10) as also previously suggested by Rudolph et al. [43]. Incidentally, the Hügel model would also indicate increasing Hall parameter near the anode surface as a result of the decreased plasma density there. The induced or "back-emf" ($\delta E_R = -c_e B_\theta$), which was neglected in the Hügel model, would add to this effect, as pointed out by Lawless [44] and others. Wagner [45, 46] showed in a detailed analysis that these macro-instabilities could be caused by drift- and gradient-driven instabilities. The cause of the instabilities found was the space charge or diode instability, which in its nonlinear development could lead to so-called "current chopping" instabilities.

All of these different simplified analysis models are not in contradiction with each other and predict some of the experimentally observed trends, but they cannot yield absolute limits of the performance of thrusters. The discharge behavior near

the onset, for example, the arc attachment on the face of the anode, does not lend itself to analyses with either the Hügel or the King model. However, these models suggest ways in which the limiting values of $I^2/\dot{m}$, hence the achievable specific impulse with each propellant and, generally, also the efficiencies, could be improved. They are 1) injecting neutral gas near the anode to increase the gas and ion density there; 2) extending the cathode to achieve (if possible) radial current flow to eliminate the radial ("pinch") pressure gradient; and 3) lengthening the thruster anodes to reduce current densities and Ohmic heating and thereby improve the thruster efficiencies.

Cold (neutral) gas injection near the anode surface has been used in pulsed self-field thrusters by the Princeton University group [47] and by the University of Tokyo group [48], in each case apparently with success in improving the specific impulse or onset velocity limit. With the IRS steady-state DT thrusters no significant influence of anode propellant injection could be found. An improvement in the onset behavior could be achieved by a very precisely symmetrically adjusted thruster: The onset of oscillations did not shift, but when it occurred it did without the formation of anode spots.

To counteract the just mentioned anode starvation caused by pinch forces (that would not occur with a purely radial current flow), extended cathodes and long cylindrical anodes have been designed and operated in steady-state mode at IRS (e.g., the ZT thruster series) and in quasi-steady pulsed mode by the Princeton University group [42]. With these MPD devices, which should have a mainly radial current distribution and therefore low discharge voltage, an attempt was made to achieve a maximum of the ratio between magnetoplasmadynamic thrust and thermal thrust and a low pinch effect at high power.

The cylindrical ZT3, shown in Fig. 13, consists of three anode segments, two neutral segments, and a backplate, all out of water-cooled copper, and a thoriated

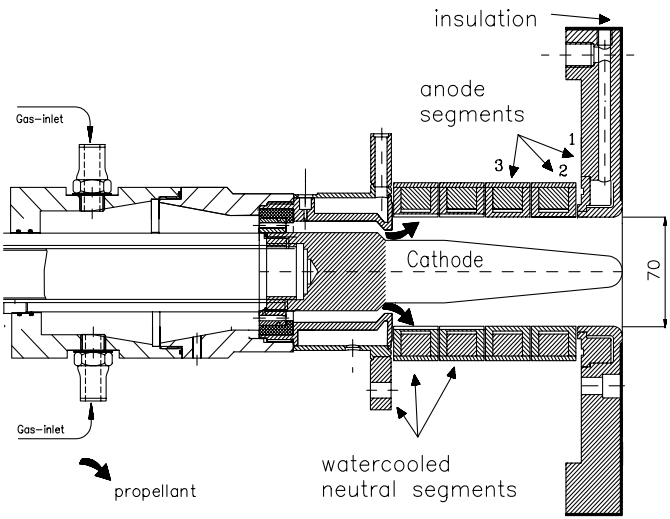


Fig. 13 Scheme of the ZT3 thruster developed at IRS.

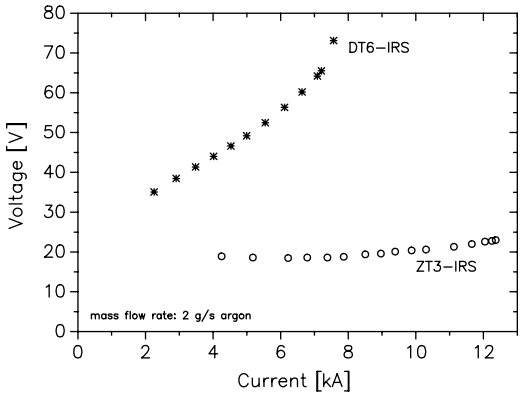


Fig. 14 Voltage-current characteristics of the ZT3 and DT6 thrusters.

tungsten cathode. The discharge chamber diameter is 70 mm and its length 150 mm. The current through each anode segment can be measured separately. The cathode was designed to counterbalance thermal damage effects encountered at high current levels (see the figure). In the back the anode diameter is 40 mm and is subsequently reduced to a 10-mm radius at the tip.

In Figs. 14 and 15 experimental results of the ZT3 thruster with a mass flow rate of 2-g/s argon are presented. The voltage dependence is compared to the results of the nozzle-shaped thruster DT6 with 36-mm throat diameter, both running at the same mass flow rate. This comparison shows that the voltage of the cylindrical thruster is low and increases only slowly with the current, whereas for the nozzle-shaped thruster it is a factor two to four times higher and rises steeply. At about 7450-A plasma instabilities occur for the DT6, recognizable also by the additional

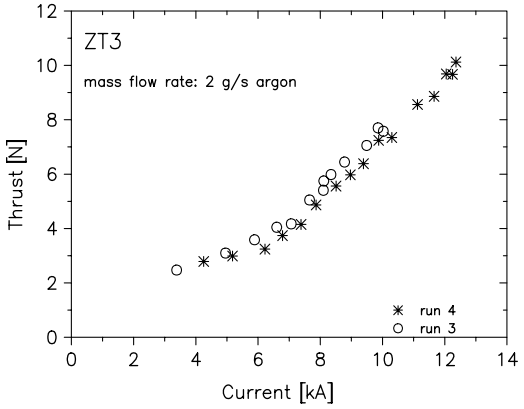


Fig. 15 Thrust vs current curve for the ZT3 thruster.

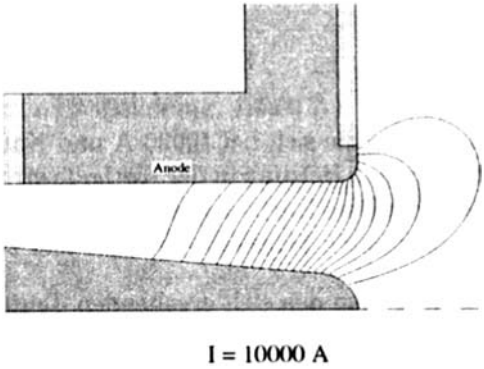


Fig. 16 Calculated current distribution: 10,000 A.

voltage rise. For the ZT3 thruster, no indication of an occurrence of instabilities could be detected up to 12,700 A where an $I^2/\dot{m}$ value of more than 8×10^{10} A^{2}s/kg was reached, whereas for the nozzle-type MPD thruster a critical $I^2/\dot{m}$ value of around 2.7×10^{10} A^{2}s/kg was found, with argon as propellant with all thrusters of the DT series.

With the ZT3 the thrust increases with current and reaches about 10 N at 12.7 kA (see Fig. 15). No higher values could be reached, because with even higher current severe anode cooling problems were experienced that prevented the thruster from being run to its $I^2/\dot{m}$ limits. This is caused by a current concentration at the "anode edge," verified also by numerical calculations [49] (see Fig. 16).

Through such geometric variations, found mostly empirically, but partly also by model calculations [50], considerable performance improvements have been achieved. It has been shown that the onset limits and thereby also the achievable specific impulse and efficiency values depend very strongly on the thruster geometry, the propellant used, and on the absolute thruster size, power level, and operating regime relative to the thruster size.

The dependence of the performance on the propellant has not been as thoroughly explored as that of the geometry. Very roughly, the maximum exhaust velocities still appear to vary like the Alfven velocities, or like $\mathrm{Ma}^{-0.5}$ at least with noble gases as propellants, and maximum efficiencies at the maximum velocities are expected to be relatively insensitive to the propellant atomic weight.

In summary, steady water-cooled self-field thrusters have, under reliable test conditions (adequate vacuum), reached efficiencies with argon of up to ≈25% at I_{sp} values of about 1400 s and power levels up to ≈500 kW. The low overall efficiencies are caused by low arc voltages, compared to those of thermal arcjet thrusters and to low thermal efficiencies (55 to 80%). Radiation-cooled SF thrusters should have higher thermal efficiencies, but are mostly low-power devices.

To investigate the influence of hot anodes on the operation behavior of steady-state SF-MPD, such as anode voltage drop and critical $I^2/\dot{m}$ values, the MPD thruster HAT (hot anode thruster) was built at IRS. HAT is geometrically similar to the DT2 of Fig. 17. Its anode is made of thoriated tungsten and partly coated with TaC to increase the emissivity. Figure 18 shows that the arc voltage is clearly

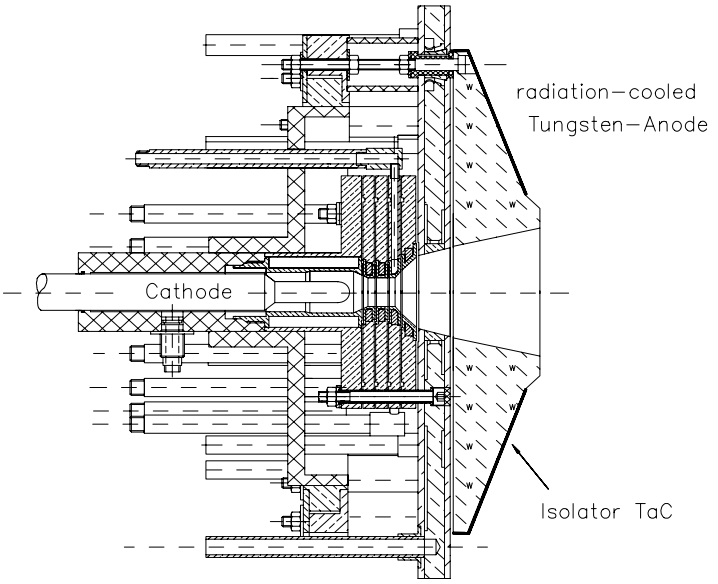


Fig. 17 Configuration of the HAT of IRS.

below those of the DT2 thruster with water-cooled anode. Also the critical $I^2/\dot{m}$ seems to be higher, but this could also be an effect of the yet slightly different geometry that will be checked in the future. (The critical $I^2/\dot{m}$ with HAT was not explored, in order to avoid he potential destruction of its expensive anode).

For *pulsed* SF-MPD thrusters at power levels of 3 to 6 MW, efficiencies into the mid-1930s at I_{sp} levels of 2000–3000 s and correspondingly much higher voltages

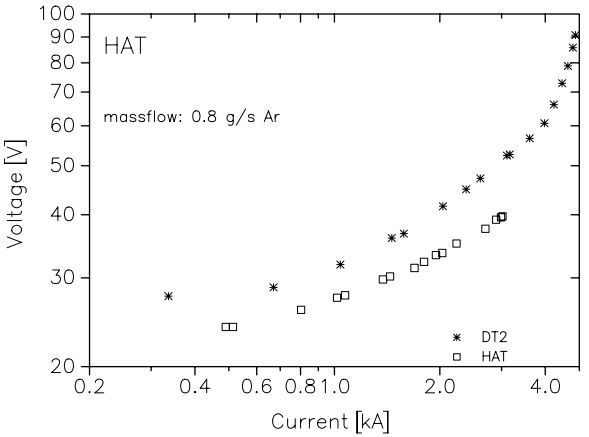


Fig. 18 Voltage vs current curve of the HAT compared to the DT2 thruster.

and thermal efficiencies have been reported for argon, but it is very doubtful if these values could be reached by continuously running SF-MPD thrusters.

1. Importance of Electrode Design

An understanding of the electrode arc attachment regions is essential for successful thruster design and operation in view of the following problems: electrode erosion, which is critical both for thruster life and for spacecraft surface contamination; transition from uniform to spot attachment on the anodes ("onset" effect), which limits the performance (I_{sp} and η) and causes both excessive erosion and electromagnetic noise (EMI); and electrode losses, which critically affect thruster efficiency and cooling requirements (i.e., thruster weight).

Erosion of cathodes is not an issue from the viewpoint of thruster life if the propellant is purified from oxidizing components (see the following) because the limits imposed by spacecraft contamination cannot be stated generally. Anode erosion might be manageable, as long as uniform (i.e., spot-free) attachment is achieved.

The formation of macrospots on the electrodes, that is, the shift from diffuse and more or less even arc distribution (which at the cathode might include an even distribution of microspots) to locally concentrated arc attachments is, of course, akin to arc filament formation in the midstream region but is also influenced by the specific boundary conditions at each of the electrodes. It must therefore be discussed separately for each electrode type. In MPD thrusters, macrospots can cause excessive (destructive) erosion of both electrodes.

Electrode losses (notably on the anode) dominate the efficiency limits of small MPD thrusters, where electrode losses can take up to 50–60% of the overall voltage drop. For larger thrusters (in the megawatt regime) this loss is probably less dominant (at least as extrapolated from pulsed SF-MPD data), but it does limit severely the current densities on anodes if simple radiation cooling is required.

2. Electrode Voltage Drops and Losses

In MPD thruster designs, as in many other arc devices (such as short-arc noble gas and carbon arc lamps, welding arcs, . . .), a major portion of the ionization takes place at or near the cathode. In these cases there is therefore a relatively large potential drop in the arc near the cathode, much of which must, however, be attributed to ionization (frozen flow loss) rather than to a cathode loss. The plasma thus formed is blown as a cathode jet toward the anode, where there is usually no mechanism or need for additional ion generation if the ion density there is sufficient to neutralize the imposed electron current. As long as that is satisfied, the anode potential drop can be quite small (even negative). In spite of this, the overall losses at the anode can be very large, as will be shown. Another energy loss that must be assigned to the cathode is the electron work function Φ ($\approx$4 to 5 V for most metals), which appears as an additional heat load at the anode and is frequently accounted for as an anode loss, although actually it should be considered as a usually unrecoverable "cost" of running an arc.

MPD thruster cathode phenomenology. Cathodes made of refractory metals (W, Ta) are at present the only ones known to be potentially suitable for larger MPD thrusters, where the so-called high current regime [from a few hundred

amperes (A) into the high kiloamperes, with gas pressure at the cathode from a few hundred millibars on down] is applicable.

In their design range of conditions, cathodes of continuous thrusters can operate with an apparently spot-free diffuse arc attachment covering a fairly large area. To reach this optimal (from the viewpoint of erosion) condition, the cathode must be of the right material (e.g., thoriated tungsten), capable of reaching the required temperature (2600–3300 K) over a sufficient area (implying adequate but not excessive cooling), and be surrounded with sufficient gas density for the imposed current. Under all other conditions, such as warm-up of continuous thrusters, cathodes with inadequate gas pressure or design or with "aged" material (e.g., thoria depletion), as well as cold cathodes and therefore pulsed thrusters, operate in some form of spot mode. This mode results in local melting and substantial vaporization of cathode material, as will be discussed.

The conditions for diffuse cathode attachments ("thermionic cathodes") in MPD thrusters are most comprehensively treated by Hügel and Krülle [51] together with Cann and Harder [52] and Goodfellow [53]. Hügel and Krülle [51] also examines the possible effects of the B_θ self-field on macrospots of cylindrical cathodes.

With diffuse cathode attachments Hügel and Krülle [51] obtained current densities up to 2000 A/cm^2 with argon and 5000 A/cm^2 with hydrogen at 100 mm Hg and 1000 A, at $Ts \approx 2800$ to 2900 K and 3200 to 3300 K, respectively. The net heat fluxes into the cathode ranged from 0.6 to 2.5 kW/cm^2 for argon and 1.7 to 4.0 kW/cm^2 for hydrogen, the largest values occurring at the highest pressure (100 mm Hg). Note that the limit for reradiation at the melting point is 1 kW/cm^2, so that generally a larger area than the arc attachment area must radiate to cool the cathode.

Thoriated tungsten cathodes can operate in the spot-free thermionic mode, with current densities up to at least 2 kA/cm^2 with minimal losses at 2800 K, the highest still acceptable surface temperature from the viewpoint of vapor pressure.

Much higher current densities (to at least 5 kA/cm^2) are possible, but at excessive temperatures for long life (i.e., above 3000 K) because of high sublimation rates. Aging of the material (presumably thoria depletion) was found to be a serious problem in some cases [54].

Thruster anode phenomenology. In a long arc without axial flow there is a small ion drift (i.e., a positive ion current) away from the anode. These ions must be replaced at the anode to provide plasma (space charge) neutralization and thus allow the main electron current to reach the anode. To produce these ions, either from ambient neutral atoms or from anode material, an anode arc contraction and fall zone sets itself up. This fall zone, at the lower densities, has a voltage close to the ionization potential of the substance to be ionized. Normally an anode spot develops, from where anode material is evaporated and ionized, because in practically all arcs (except alkali vapor arc) anode metals are more easily ionized than other arc gases. These anode contractions, although less concentrated than those at cathode spots, produce self-field anode jets (similar to those from cathodes) that raise the ion flow (ion current contribution) away from the anode above the normal ion drift of an arc column. If they occur in SF-MPD thrusters, the anode will be destroyed.

Spot-free anode functioning is, however, possible in SF-MPD thrusters. There the plasma is generated mostly near the cathode and in some cases also in the midstream discharge and is blown toward the anode surface. Under these conditions there is normally no need for ion generation near the anode, and the anode potential drop

becomes zero or even negative, as predicted by the classical anode theory for this case [55].

For such MPD thrusters (with rear cathode), Hügel [56] has described three regimes of spot-free anode operation. The first regime is characterized by a sufficient supply of ions for neutralization and replacement of those drifting (or blowing) away and by a sufficiently large natural diffusion of electrons toward the anode to provide the current drawn. If normal electron diffusion flux exceeds the electron current drawn by the external circuit, the anode surface, if "cold," becomes slightly negative relative to the plasma, similarly to a cold floating probe in a hot plasma. (If "hot," it will reemit some electrons). Depending on the electron temperature, this anode could be 3 to 5 V negative, though the cooler gas near the wall boundary layer will somewhat impede this electron flow.

As the current is increased at constant mass flow rate (or $I^2/\dot{m}$ is increased by any path), a second regime is reached through the increased magnetic pinch effect and increased relative current density, that is, closer to "the onset of instabilities" conditions. This second regime described by Hügel is one in which the natural electron diffusion no longer supplies the demanded current density to the anode, although the ion supply to the anode is still sufficient. This anode regime occurs for the thruster type and operating regime treated here, where with increasing $I^2/\dot{m}$ the ion supply carried by the jet to the anode exceeds the anode current demand for longer than the natural electron diffusion satisfies the required electron current. In this second regime, a positive voltage drop develops near the anode; using argon, it increases linearly with increasing I from 0 to ≈6 to 8.5 V.

This results in primarily an electron drift current increasing mainly caused by the potential gradient, plus small contributions caused by increased ion generation δn_e and temperature δT_e. Because in this regime the anode voltage rise is proportional to the increase in current density δj_e imposed, this voltage (loss) rise should in principle be reduced by enlarging the anode area exposed to the plasma flow.

With further increase in the current/mass flow parameter ($I^2/\dot{m}$), a third regime of theoretically possible spot-free attachments is reached where also the ion flow rate toward the anode becomes insufficient. In this regime, called by Hügel that of the genuine or classical anode fall, the anode potential must instantly increase to the potential drop required for ion generation.

Using classical anode theories [56, 57] and the "field" ionization process appropriate for the low density regime, Hügel calculated an anode fall voltage of 12.4 V for singly ionized argon and slightly lower values (10.7 and 8.8 V) for xenon and krypton. Double ionization requires roughly twice these values.

Because all practical electrode materials have lower ionization potentials (below 8 V), a diffuse anode attachment of this last type is unstable and will break down to anode spots with anode vaporization, the normal operating mode of all anodes already described, resulting in a lower anode potential. Furthermore, the third regime just described, where the plasma density near the anode approaches zero, is in fact close to or at the critical $I^2/\dot{m}$ value, where probably various other arc instabilities appear in addition to anode spot formation. The beginning of this third (i.e., the classical) anode operating regime is therefore (also in Hügel's nomenclature) the onset point, at least for these thrusters where "anode starvation" as a result of the pinch pressure gradient is dominant. This regime has to be avoided in SF-MPD thruster operation by all means.

3. Electrode Erosion

The limits of allowable electrode erosion are first of all set by thruster life requirements. Much lower erosion limits could be imposed by spacecraft surface contamination standards, if the eroded material vapor can end up in the form of slow ions (e.g., formed by charge exchange) in the spacecraft vicinity and deposit itself on charged insulator surfaces of the spacecraft. This latter erosion limit is difficult to estimate in a general way, but all condensable vapors near a spacecraft constitute a surface contamination hazard.

From the viewpoint of thruster life, the allowable erosion depends on the life requirements—typically 1000 to 10,000 h for near-Earth missions—and the thruster design, type, and size. Some typical numbers for a 10-N continuous self-field thruster (4 kA, 1-g/s argon) for a 3000-h life (and consuming 4.3×10^{10} C, or 11,000-kg propellant) would be as shown in Table 2.

This corresponds to a loss of material roughly a few millimeters per year (or of the order of 10^{-7} mm/s) from the faces of the electrodes exposed to the arc for that size and type of thruster. Note that this is about or less than the normal vaporization rate of tungsten at 3000 K, and 1/2000th of that rate at the melting point.

The possible erosion mechanisms for both cathodes and anodes are macro particle ejection (spitting) and massive vaporization (boiling) from molten pools at the macrospots; localized vaporization (boiling) at microspots; vaporization from larger molten surface areas (without boiling or spots); sputtering caused by ion impact (normally negligible); and continuous surface vapor loss without melting, as a result of excessive average surface temperature.

With brittle metals (e.g., tungsten) there is, in addition, the possibility of cracking as a result of thermal fatigue.

To prevent substantial overall vaporization at excessive average surface temperatures, the average electrode temperatures must be controlled by adequate cooling. Typical average temperature limits for three electrode metals, as dictated by their vapor pressures, are 2800 K for tungsten, 2600 K for tantalum, and 2200 K for molybdenum. Generally, the average electrode temperatures should be held below those given for, say 1-mm surface loss per year, to allow for local overheating. This should be readily achievable at anodes, but with cathodes these temperatures are at the lower limit for effective thermionic emission, in the sense that the arc can reach sufficient current density and drive higher surface temperatures in spite of radiation cooling.

This leaves the various kinds of spots as the major sources of erosion beside the sublimation of material caused by the high temperature. But with duly constructed cathodes, spots should only occur during ignition.

Table 2 Typical numbers for 10-N continuous self-field thruster

Allowable erosion mass loss m_{er}, g	Cathode, *W*	Anode, *Mo*
	50	250
m_{er}/Coulomb, g/C	1.2×10^{-3}	5.8×10^{-3}
m_{er}/propellant mass	4.6×10^{-6}	2.3×10^{-5}

Cathode erosion. In a steady-state MPD device one has to discern between two operation regimes: 1) the ignition phase, lasting typically about one second (depending on the ignition current and cathode mass and design), and 2) the steady operating phase, which lasts (at least in the laboratory) between several minutes and several hours.

The ignition phase is characterized by a cold cathode and a highly instable, spotty arc attachment. These arc spots jump irregularly over the cathode surface, causing melting with relatively high erosion and leaving "craters" of sizes ranging from some microns to a tenth of a millimeter. This starting phase ends when the cathode is hot enough for the thermionic emission to support the current demand. The measured averaged erosion during this phase is about 13 μg/s [58] and is insensitive to the propellant gas.

Contrary to the erosion during the ignition phase, the erosion in the thermionic phase [58] depends on the propellant: nitrogen yields the lowest (about 0.5 ng/C) and hydrogen the highest (about 2.2 ng/C) with argon in between (about 1.5 ng/C). That shows that steady-state erosion is very sensitive to the grade of the propellant: the values cited were reached with high-grade gases, further cleaned from oxygen and humidity. With standard grade-welding argon, the erosion rates were about a factor 20 higher.

During a pure thermionic emission, erosion is dominated by the sublimation rate s, which can be calculated with the Dushman equation:

$$s(T) = \frac{\dot{m}_{\text{subl}}}{I} = \sqrt{\frac{M}{2\pi \Re T}} \frac{p_v(T)}{j} \left[\frac{\text{kg}}{\text{C}}\right]$$

with p_v the vapor pressure.

With a cathode temperature of 3000 K and a current density of $j = 5 \times 10^6$ A/m^2, this sublimation rate yields 2 ng/C, which agrees well with the experiment.

A serious life-limiting process in cathodes could be the depletion of thoria or other additives. This is difficult to detect in cathode sections after, say, 50 h of life and might require long life tests for accurate determination and special provisions to counteract, if at all possible.

Anode erosion. Anode erosion in SF-MPD thrusters can vary over wide ranges, but there are only few accurate data available. To avoid rapid destruction, continuous self-field thrusters must be operated at currents below the onset of instabilities, or anode voltage rise regime, by some safe margin. At the first sign of any onset phenomena like spots, foot points, and/or fluctuations, the current must be instantly turned off or reduced. With diffuse anode attachment the anode erosion rates, if any, are so small as to be difficult to detect. On the contrary, on cooled copper anodes the same grey deposits (presumably of tungsten cathode vapor) are observed, which tend to build up rather than erode the anodes. With hot anodes, no erosion investigations are known.

In summary, the erosion of tungsten cathodes appears acceptable in the thermionic regime, as long as the additive (thoria, etc.) remains present at the surface. For cooler cathodes (typical of present pulsed thrusters) and for frequent cold starts, cathode erosion remains still excessive.

Anode erosion appears manageable with diffuse attachment (i.e., far from onset conditions) and possibly also with spots in pulsed and/or axial applied-field thrusters, using refractory metals.

4. Electrode Losses and Cooling

Electrode losses are hard to separate out precisely because of the complicated and interlacing energy-transfer mechanisms that occur at the electrodes. However, without attempting to resolve all of these still open questions, we will attempt to put down a few orders of magnitude on the net heat loads and draw conclusions on limiting permissible current densities and cooling capabilities.

Cathodes. For typical thermionic cathodes of continuous operation thrusters, the net heat loads have been estimated in [51] as 1 to 5 W/A and 0.7 to 2 W/A for argon and hydrogen, respectively, with the lower values applying to the higher current densities. Many other propellants fall somewhere in between. The net heat-flux values ranged from 0.6 to 2.5 kW/cm^2 for argon and 1.7 to 4.0 kW/cm^2 for hydrogen, depending on pressure and current density.

Radiation cooling at the allowable temperature for long life (2800 K, with emissivity 0.35 for tungsten) removes only about 120 W/cm^2. Therefore, purely radiation-cooled cathodes in continuous operation can be loaded only to about 50 to 100 A/cm^2, a factor of 10 to 100 lower than the possible current densities, according to [51]. In a radiation-cooled thruster, the cathode will receive same additional radiative heat load from the anode and other hot parts of the thruster. If higher current densities than those just given are required (or unavoidable), additional cooling must be provided. With a few propellants (e.g., H_2, NH_3, Li) this can be done regeneratively (see the following). Otherwise, heat removal by simple conduction or (for larger thrusters) by a liquid metal heat pipe must be provided.

In any case, cathode cooling does not appear to present insurmountable problems if macrospots can be avoided.

At high current densities *within* the cathode, ohmic heating gives rise to severe problems. Cracks release molten material from the interior near to the rear end of the cathode, behind the arc attachment zone. Figure 19 depicts a cathode of the IRS-built DT2 thruster with a diameter of 16 mm, which failed at a current of 6500 A.

Investigations [58] lead to the conclusion that at the high temperatures inside the cathode the thoria lumps together, forming spheres of ThO_2, which reduce the conducting cross section of the cathode and hence favor further rising the temperature as a result of ohmic heating. This process continues until the thoria

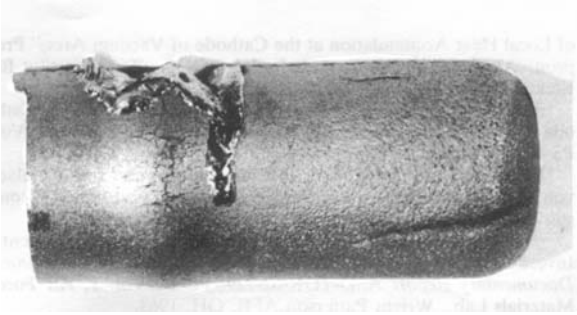


Fig. 19 Damaged cathode of DT2 (16 mm, 6500 A).

evaporates and the cathode is destroyed. This was the motivation for the tapered cathode of the ZT3 thruster in Fig. 13. In summary, the cathode has to be designed very carefully to avoid overheating inside its shaft and to minimize erosion.

Anodes. The anode net energy input equation in simplified form as given by Hügel (assuming the total current being carried by the electrons) is:

$$QA = I(V\hat{A} + 5/2\ k\ Te + (\Phi_0 + V_{\text{conv}})$$

which must be removed by cooling. The first three terms on the right are energies brought in by the electrons, while V_{conv} is the normal (heavy particle) convective heat transfer; radiation from gas and cathode is neglected.

For liquid-cooled copper anodes of continuous thrusters, the anode fall voltage V_A is 0 to 10 V, the upper value being applicable near the onset of instabilities. With $(5/2)kTe \approx 3.5$ V, $\Phi_0 = 4.4$ V, and $V_{\text{conv}} \approx 2$ V, the net anode heat loads run from about 9 to 20 V times the current, where the higher value applies to the interesting performance points. With optimized high-performance thrusters, these values can run considerably higher.

If the anode is to be radiation cooled, then the average heat-flux values and thus the average current densities are quite limited. At the maximum allowable temperature for long life, tungsten can radiate only about 120 W/cm^2 and molybdenum less than half of that. The effective emissivity of the anode can be increased by coatings or by fins on the metal, the latter being more and more effective for decreasing thruster size. Still, except for very small thrusters, the current densities in radiation-cooled anodes will be limited to $\approx$30 A/cm^2 on the inside surface, assuming a 20-V anode loss.

Regenerative cooling of anodes (at specific impulse values typical in the MPD regime) is possible only with hydrogen or with alkali metal propellants, notably lithium. In the latter case, the ideal anode operating mode would be evaporation and ionization of the propellant on the porous or wetted anode surface, resulting in increased ion current fraction, reduced anode fall, and utilization of part of the anode lost energy. Otherwise, where higher current densities are required or desirable, additional anode cooling on larger thrusters can be achieved with built-in heat pipes or with a liquid metal convective cooling loop.

Propellant choice. The propellant choice affects the thruster, the system, the spacecraft, the atmosphere environment, and the operating logistics. Historically, if the thermal thrust portion is not taken into account, the thrust-to-power ratio seemed to favor heavy propellants like argon, but also lighter mixtures like N_2H_4 and NH_3 have been considered, which also are storable and can be logistically (e.g., N_2H_4) the most desirable with still fair thrust-to-power ratios. Further thruster tests and system/mission studies are needed before any final choice of propellant.

Liquid metals such as lithium, potassium, indium, and others, have great advantages concerning storage, cooling capacities, and ionization potential, but will probably be ruled out because of contamination of the spacecraft by condensing and depositing of propellant on cool parts of the spacecraft.

The regenerative cooling capability is minimal for most propellants in the MPD regime, except possibly for lithium and hydrogen. Lithium could remove $\Delta h_{\text{RC}} \approx 2.5 \cdot 10^7$ J/kg during vaporization and heating, and hydrogen about

2.9×10^7 J/kg during heating (by $\Delta T \approx 2000$ K) alone. Assuming, for example, $\eta = 0.30$ and the jet exhaust speed $c_e = 30$ km/s, the ratio

$$\frac{\text{regen. cooling power}}{\text{input power}} = \frac{2\,\eta\,\Delta h_{RC}}{c_e^2}$$

would approach ≈2 to 3% for these two propellants. For continuous MPD thrusters of the 250-kW class, this regenerative cooling capability would be too small to be significant. For an MPD in the c_e=10 km/s regime with >40% efficiency, the preceding ratio becomes >23%, which with proper design can be adequate for an almost fully regenerative cooling. Most other propellants have small to negligible regenerative cooling capability for the MPD regime.

For storage weight and volume, the highly cryogenic, low-density hydrogen propellant is of course the worst. Hydrogen might be acceptable for missions requiring more or less continuous propellant use from the very beginning, when the boil-off keeps the rest cold enough and enabling it to be used as propellant. In the far future, hydrogen might be produced in space from water (where oxygen is also needed for crewed missions) or from some other compound, using nuclear energy. That can also power cryocoolers maintaining hydrogen liquid during interplanetary or other long-lasting missions.

The acceptability of cryogenic propellants will be generally very dependent on specifics of missions and on future space storage facilities.

For possible propellant sharing with high thrust systems, and of course for emergency thrust with insufficient or no electric power available, hydrazine stands out. Hydrogen also can give emergency thrust with still reasonable specific impulse.

B. Magnetoplasmadynamic Thruster with Coaxial Applied Field

In this type of applied-field thruster, the electrodes are arranged coaxially like in an MPD self-field thrusters. By means of a coil or with permanent magnets, an

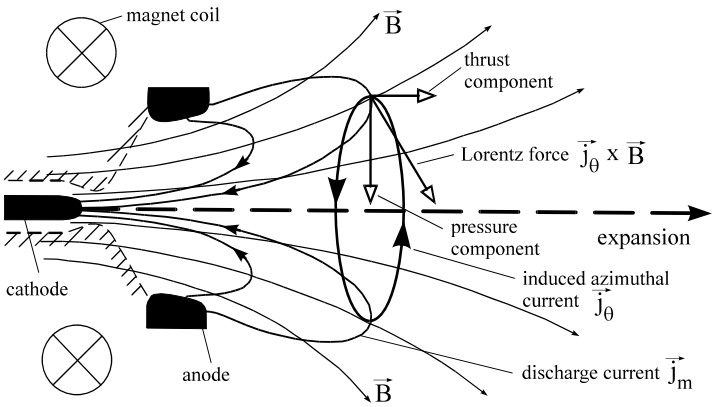


Fig. 20 Principle of an applied-field thruster with a coaxial field.

axial, diverging magnetic field B_f is produced as shown in Fig. 20. Here the magnetic field interacts with the induced, azimuthal flow that can be explained by the Hall effect.

1. *Acceleration Mechanism*

The starting point for a discussion of the acceleration mechanism in applied-field devices with a coaxial field is Ohm's Law for plasmas. Neglecting the grad(p_e) term results in

$$j = \sigma\left[E + v \times B\right] - \frac{\omega_e \tau_e}{B}\left[j \times B\right] \tag{1}$$

The z component B_{fz} of the applied magnetic field causes a ring current j_θ in the direction of θ as a result of the radial current density component j_r according to the Hall term in Ohm's Law. This ring current, also called the Hall current interacts in turn with the magnetic field: it produces with the component B_{fr} an accelerating force in the direction of the flow, and together with the component B_{fz} causes the pressure to rise on the thruster axis (pinch effect).

The formation of these Hall currents is therefore a prerequisite for propellant acceleration in these devices. The ring current can only form if the individual particles seldom collide. A characteristic parameter for these thrusters is therefore the so-called Hall parameter $\omega_e\tau_e$; here ω_e is the gyration frequency and τ_e the mean free flight time of the electrons. The Hall parameter is therefore the ratio of the gyration frequency of the electrons to their collision frequency. The higher the gyration frequency and the lower the collision frequency, the better an azimuthal current can form. That is why the Hall parameter must be as large as possible, in any case much larger than one.

2. *Hall Parameter*

The dependence of the Hall parameter on the strength of the magnetic field, the pressure, and the temperature is easy to estimate. The gyration frequency of the electrons is connected to the magnetic field by

$$\omega_e = \frac{e\,B}{m_e} \tag{2}$$

the collision frequency can be calculated as [14]

$$\nu_e = \frac{n_e\,e^2}{\sigma\,m_e} \tag{3}$$

Taking the equation of state for electrons $p_e = n_e k T_e$ into consideration, the following results:

$$\nu_e = \frac{p_e\,e^2}{k\,T_e\,\sigma\,m_e} \tag{4}$$

Because the electrical conductivity is proportional $T_e^{3/2}$ [14], the result for the Hall parameter is

$$\omega_e \tau_e = \frac{\sigma B}{e n_e} \propto \frac{B T_e^{5/2}}{p_e} \tag{5}$$

This means that large magnetic fields, the lowest possible pressures, and high temperatures are necessary for forming azimuthal flows.

Estimates using this equation confirm that Hall parameters of several 10^3 can be anticipated; however, actual measurements showed results between 3 and 5 [59, 60]. This discrepancy can be explained by the plasma instabilities that hinder the formation of the azimuthal flows.

The anomalous diffusion of electrons across the magnetic field [61] must be seriously taken into account in an assessment of applied-field-(AF)-MPD capabilities (this is, after all, also true for SPT). There are then a number of consequences. For example, the magnetic nozzle is not ideally effective (compare [62]), so that the plume mass is not fully contained within boundaries given by the "anode magnetic lines," that is, the applied-field lines passing through the anode at its widest diameter.

3. Current Distribution

The magnetic field in coaxial applied-field thrusters is so large that, because of the Hall effect, the electrical conductivity is clearly reduced in the direction perpendicular to the magnetic field, and that results in the transport of the current being hindered. The conductivity normal to the magnetic field is

$$\sigma_\perp = \frac{\sigma_o}{1 + \left(\omega_e \tau_e\right)^2} \cong \frac{\sigma_o}{\left(\omega_e \tau_e\right)^2} \tag{6}$$

Therefore the current streamlines are extended far outside the thruster, as, for example, measured by Schock [63] and shown in Fig. 21. The influence of the applied magnetic field is therefore also called "magnetic nozzle."

The discharge current, whose distribution is a function of $\omega_e\tau_e$ (= $\sigma B/en_e$), bulges out far downstream as B/n_e increases. This fact has been experimentally [64–67] and computationally verified [68–70]. Figure 21 shows measured current distributions at different magnetic field strengths. According to the preceding dependence, the same occurs when density decreases. This suggests the important influence of ambient pressure as demonstrated in Fig. 22, where specific thrust (that is, F/I) is shown to decrease with the tank pressure and therefore with decreasing gas density [65]. At higher values of the critical parameter, saturation can occur. Still, environmental influence on the overall process (participation of ambient gas) is present, leading to uncertainty of thrust and particularly of I_{sp}. Even with condensable propellants, this effect cannot be systematically avoided because of the wide extension of the plume and the normally moderate dimensions of the vacuum tank facility.

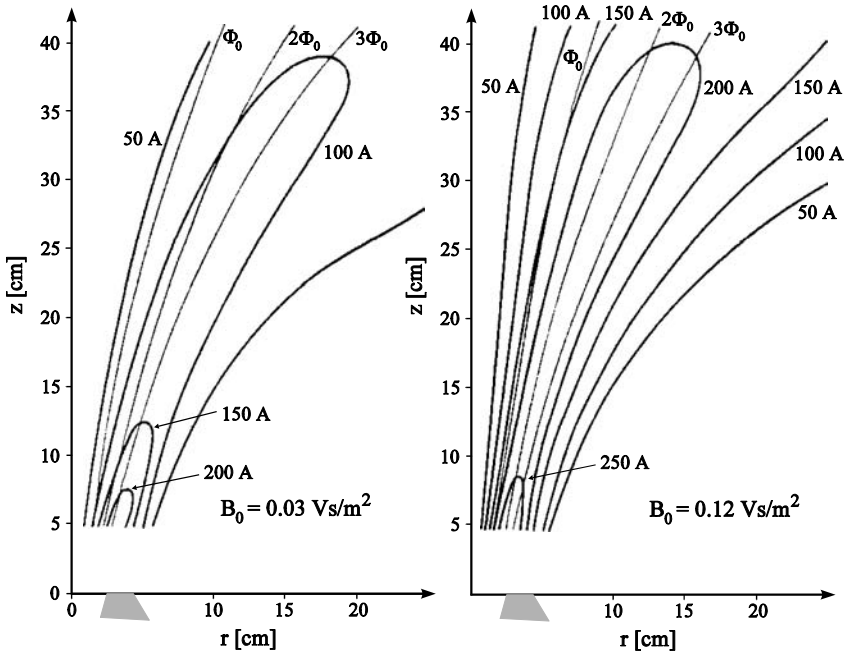


Fig. 21 Axial current distribution in a concentric applied-field thruster X9 from DLR Stuttgart [63], where $n\Phi$o: lines of constant magnetic flow.

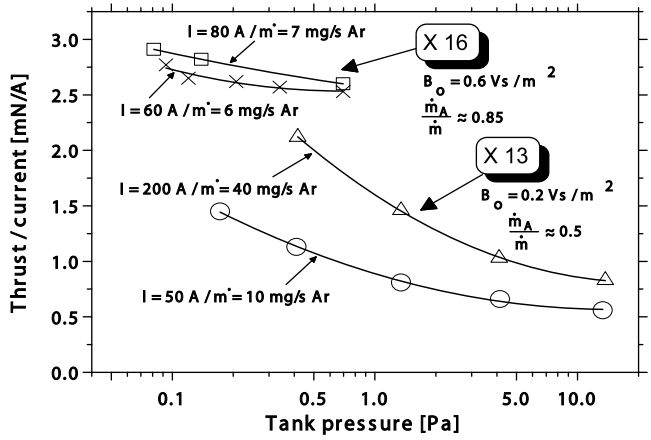


Fig. 22 Thrust per current as function of the tank pressure [68] for experimental thruster X13 and preflight model X16 at DLR-Stuttgart [71].

4. Movements of Charged Particles in E and B Fields

To understand the behavior of an applied-field thruster, and especially of plasma rotation, one must first consider the movement of charge carriers in the presence of E and B fields.

The equation of motion for charged particles is

$$\frac{\mathrm{d}}{\mathrm{d}t}\,\boldsymbol{v} = \frac{q}{m}\left(\boldsymbol{E} + \boldsymbol{v} \times \boldsymbol{B}\right) \tag{7}$$

To find a solution for this equation for the case of $\boldsymbol{E}$ perpendicular to $\boldsymbol{B}$, the following ansatz can be formed:

$$\boldsymbol{v} = \boldsymbol{v}_1 + \frac{\boldsymbol{E} \times \boldsymbol{B}}{B^2} \tag{8}$$

Because $\boldsymbol{E}$ and $\boldsymbol{B}$ are constant in time, with Eq. (8) the following is true:

$$\frac{\mathrm{d}\boldsymbol{v}_1}{\mathrm{d}t} = \frac{q}{m}\left[\boldsymbol{E} + \left(\boldsymbol{v}_1 \times \boldsymbol{B}\right) + \frac{\left(\boldsymbol{E} \times \boldsymbol{B}\right) \times \boldsymbol{B}}{B^2}\right] \tag{9}$$

Upon solving the double cross product, the result is

$$\frac{\mathrm{d}\boldsymbol{v}_1}{\mathrm{d}t} = \frac{q}{m}\left[\boldsymbol{E} + \left(\boldsymbol{v}_1 \times \boldsymbol{B}\right) - \boldsymbol{E}\frac{\boldsymbol{B}\cdot\boldsymbol{B}}{B^2} + \frac{\boldsymbol{B}\left(\boldsymbol{E}\cdot\boldsymbol{B}\right)}{B^2}\right]$$

and after considering the scalar products that appear, the equation reduces to

$$\frac{\mathrm{d}\boldsymbol{v}_1}{\mathrm{d}t} = \frac{q}{m}\left[\boldsymbol{v}_1 \times \boldsymbol{B}\right] \tag{10}$$

The result here is a gyration movement with the gyration velocity ∇.

According to Eqs. (8) and (10), the movement of the particles consists of a constant drift with velocity $\boldsymbol{v}_d$ and a circular movement. The drift is independent of the polarity sign of the charge carriers; thus, electrons and ions drift in the same direction, and therefore the drift is a plasma flow with

$$\boldsymbol{v}_d = \frac{\boldsymbol{E} \times \boldsymbol{B}}{B^2}$$

and in the special case of (11)

$$\boldsymbol{E} \perp \boldsymbol{B} \qquad \boldsymbol{v}_d = \frac{\boldsymbol{E}}{\boldsymbol{B}}$$

If $\boldsymbol{E}$ is not perpendicular to $\boldsymbol{B}$, $\boldsymbol{E}$ has to be divided into a component $\boldsymbol{E}_s$ perpendicular and a component $\boldsymbol{E}_p$ parallel to $\boldsymbol{B}$. The same as just shown then applies to the part $\boldsymbol{E}_s$: $\boldsymbol{E}_p$ on the other hand leads to a particle acceleration parallel to the magnetic field.

5. Plasma Rotational Frequency

The components of the electrical field that are perpendicular to the magnetic field cause a plasma flow in the direction $\boldsymbol{E}_s \times \boldsymbol{B}$. For the applied-field thruster with a coaxial magnetic field, this means that the plasma begins to rotate. The size of the moment of momentum D can be calculated as a closed integral without knowing the current density distribution [72]. If the radial component of the magnetic field at the exit cross section of the thruster can be neglected, the following result for a cathode is assumed to be true at each point:

$$D = \frac{1}{2} B I r_A^2 \tag{12}$$

with r_A as the anode radius.

If one considers the plasma as a rigid body, the moment of momentum can, on the other hand, be estimated with

$$D = \int_0^{r_A} \omega r^2 \, \mathrm{d}\dot{m} = \frac{1}{2} \dot{m} \omega \, r_A^2 \tag{13}$$

By equating the right sides of these two equations, one gets the following result for the rotational frequency of the plasma:

$$\omega = \frac{I B}{\dot{m}} \tag{14}$$

In several experiments, circulating current spokes were observed, and their frequency was measured. It was determined that Eq. (14) reproduces well the dependence of the rotational frequency of the plasma on the current, on the strength of the magnetic field, and on the propellant capacity [72, 73].

DLR Stuttgart compared these results with the own measurements (see Fig. 23) [74].

From Fig. 23 it follows that the rotational frequency is proportional to the empirical expression $I^n B^k/\dot{m}$ whereby the exponents n and k lie between 0.5 and 1.

In addition, it was determined that an explicit dependence on the molecular weight of the propellant exists. Malliaris [73] showed that the rotational frequency is with good approximation inversely proportional to the root of the molecular weight. In this way one gets the empirical equation

$$\omega \propto \frac{I^n \, B^k}{\dot{m} \sqrt{M}} \qquad \text{with } 0{,}5 < n, k < 1 \tag{15}$$

6. Thrust

The thrust of an applied-field MPD device increases significantly with the magnetic field (Figs 24 and 28). It is not possible to derive a simple equation for

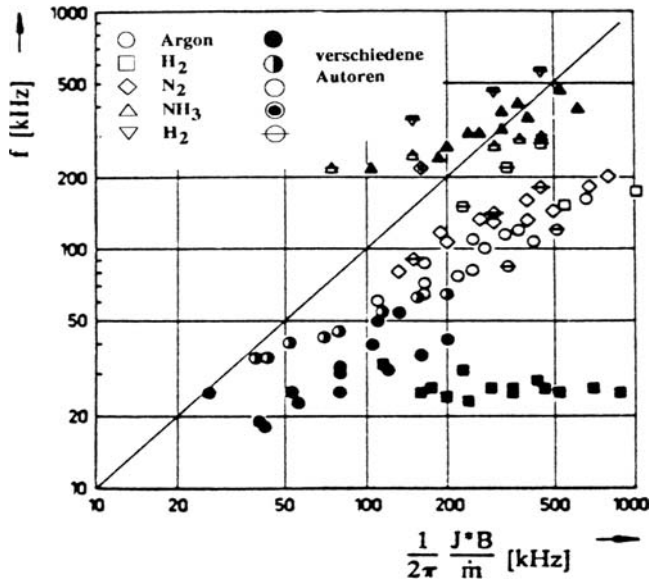


Fig. 23 Rotational frequency of the plasma as a function of $IB/(2\pi\dot{m})$ [74].

this dependence as with self-field thrusters. The thrust in an MPD thruster with a coaxial applied field essentially has four sources, or mechanisms:

1) The first source is the heating of the gas and expansion through a nozzle (thermodynamic effect using the material walls, like in an arcjet). $\rightarrow F_{\text{therm}}$

2) The discharge current crossing the magnetic field results in an azimuthal force component that sets the plasma into rotation, an important source of energy addition. This energy can be partly converted into thrust energy. $\rightarrow F_{\text{swirl}}$

3) As the discharge current crosses the applied magnetic field, azimuthal currents are induced that yield axial and radial Lorentz ($j \times B$) forces, of which the axial component accelerates the plasma directly, while the radial component confines the plasma and thus builds up a pressure gradient. This energy again can be partly converted into thrust energy. $\rightarrow F_{\text{Hall}}$

4) The interaction between the radial component of the primary current and the induced azimuthal magnetic field produces a self-magnetic acceleration. This plays only a subordinate role in applied-field thrusters. $\rightarrow F_{\text{self}}$

The total thrust can be calculated as the sum of these thrust components, that is, $F_{\text{tot}} = F_{\text{Hall}} + F_{\text{swirl}} + F_{\text{therm}} + F_{\text{self}}$.

Whether this simple algorithm is applicable depends, however, on the definition of thrust portions. By quantifying the fraction of each mechanism actually generated by converting the attributed energy added [e.g., $F_{swirl} = \int_V (j_r B_z u_0) 0V$] into useful (axial) velocity, the following dependence is obtained under simplifying assumptions [75, 76]:

$$F = \left[(F_{\text{hall}} + F_{\text{self}})/2\right] + \left\{\left[(F_{\text{hall}} + F_{\text{self}})/2\right]^2 + F^2{}_{\text{swirl}} + F^2{}_{\text{therm}}\right\}^{1/2} \tag{16}$$

Using this formula, one can estimate the order of magnitude of the maximum effect produced by each mechanism. Which mechanism prevails in thrust production depends on the selection of operating parameters [76, 77] and thruster geometry. In Table 3 a comparison is made between the electromagnetic thrust portions for different cases of B, I, and $\dot{m}$ that proves this statement. There is evidence that Joule heating and swirl production are energetically most relevant in the AF-MPD, with a substantial portion of the conversion taking place in the magnetic nozzle.

The discharge current-equivalent mass flow $\dot{m}_{\text{equ}} = (m_i/e)I$ (single ionization), where m_i is the ion mass, is far from being reached in known experiments [68, 76, 79, 80] except in rare cases of light propellants. In the SPT, in contrast, currents are low and voltages comparatively high, so that the $\dot{m}_{\text{equ}}$ requirement is met even with heavy propellants, whereas I_{sp} is still reasonably high but at the expense of low thrust density.

In the ideal case of energy gain and conversion, and especially considering rotational energy, the U voltage (and consequently the thrust F) should depend quadratically on the magnetic field strength B as a result of back electromotive force (EMF) produced by azimuthal velocities. This dependence is not found in the experimental results [81]; see also Eq. (17), which is proof that those energy processes are indeed associated with inherent losses. There are different hypotheses to explain nonideal performance. One is that plasma viscosity plays an important role, hindering deve-lopment of ideal azimuthal velocities by friction on outer (anode) walls, with velocity conversion being additionally limited by anomalous conductivity effects [62]. Plasma turbulence and anomalous diffusion certainly have a substantial influence, which leads to very moderate effective $\omega_e \tau_e$ [68, 69] as explained in Sec. 4.1.2.

7. *Experimental Evidence*

Thrust and discharge voltage generally tend to rise with the strength of the magnetic field and the discharge current [69]

$$F \quad \text{and} \quad U_{\text{tot}} \sim I^{0.8-1} B_0{}^{0.5-1} \tag{17}$$

for example, see Fig. 24. The propellant mass flow rate has a more complex influence: thrust is hardly affected, that is, only its gasdynamic part; voltage tends to go down as mass is increased, the effect depending on whether the mass is fed in

Table 3 Operational conditions and calculated thrust components of some AF-MPD thrusters [78]

Thruster	B, T	$\dot{m}$, kg/s	I, A	F_{hall}, N	F_{swirl}, N	F_{self}, N
Univ. Tokyo	0.10	9×10^{-7}	200	4.4×10^{-2}	1.4×10^{-2}	1×10^{-4}
Los Alamos	0.19	2.5×10^{-5}	350	1.8×10^{-1}	6.9×10^{-1}	9×10^{-3}
Univ. Osaka	0.075	2.75×10^{-3}	15,000	4.0	22.0	22.0

the vicinity of the cathode (subscript K) or the anode (see the effect of $\dot{m}_K$, $\dot{m}_A$ in Fig. 25). Thrust seems more dependent on $\dot{m}_K$, whereas voltage is more influenced by $\dot{m}_A$ as shown in the same Fig. 25. The role of $\dot{m}_A$ is not, or at least not primarily, to carry part of the current as an ion current, but to ensure a certain charge carrier density in the vicinity of the anode, thus reducing anode losses and eventual strong deviations from the discharge axial symmetry [74]. Figure 26 gives anode losses as a function of mass distribution [83].

As a consequence, for AF-MPD acceleration to be effective, at least a strong magnetic B field of adequate shape, an optimal degree of ionization to ensure good coupling of mass to electromagnetic effects, and moderate particle density in the discharge region are required.

8. Applicable Propellants

The magnetic thrust of an applied-field thruster depends essentially on the formation of Hall currents, and for this a Hall parameter as large as possible is necessary. However, as already shown, the Hall parameter is independent of the propellant. Therefore, it imposes no additional criteria on the propellant choice.

In view of the need for a high degree of ionization at moderate losses, certain propellants suitable for AF-MPD engines can be considered. These are preferably easy to ionize monatomic elements. (Here preferred materials are underscored). Among them are noble gases (He, Ne, Ar, Xe) and alkali metals (Li [64, 79, 84], Na, K), but H_2, N_2, and N-H combinations have also been used, for example, [76, 80, 81, 86], suggesting the possible operation of MPD thrusters in parallel to chemical rockets (hybrid systems; see Chapter 1 in this book). The application of alkali metals is combined with considerable feed system problems and the danger

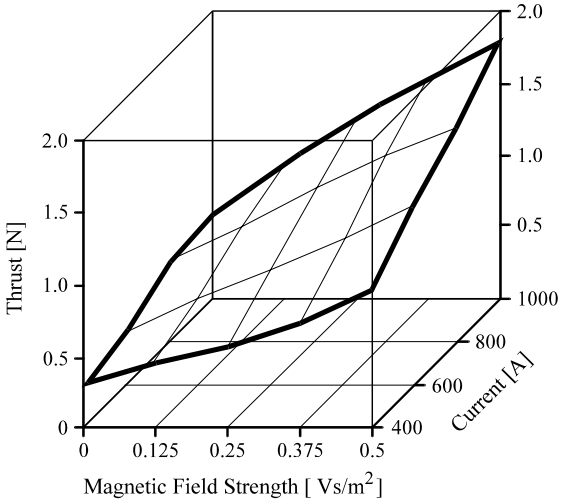


Fig. 24 Thrust as a function of discharge current and magnetic field strength (elevated power of DLR laboratory type X-9, 100-mg/s argon, $p_a = 3.0$ P_a).

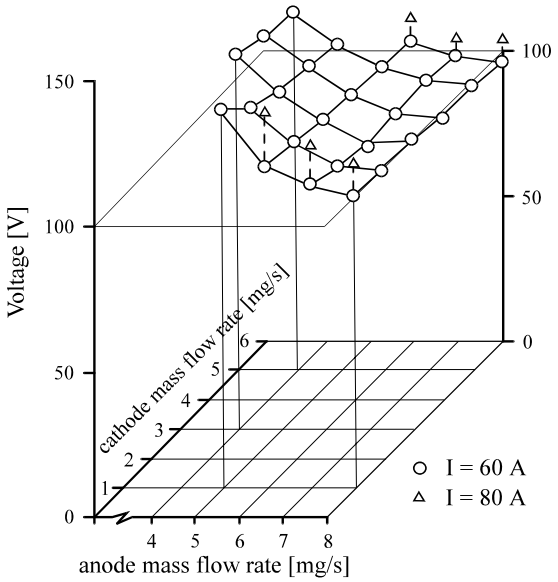


Fig. 25 Voltage as a function of anode and cathode mass fractions (DLR X-1 thruster6, argon [71]).

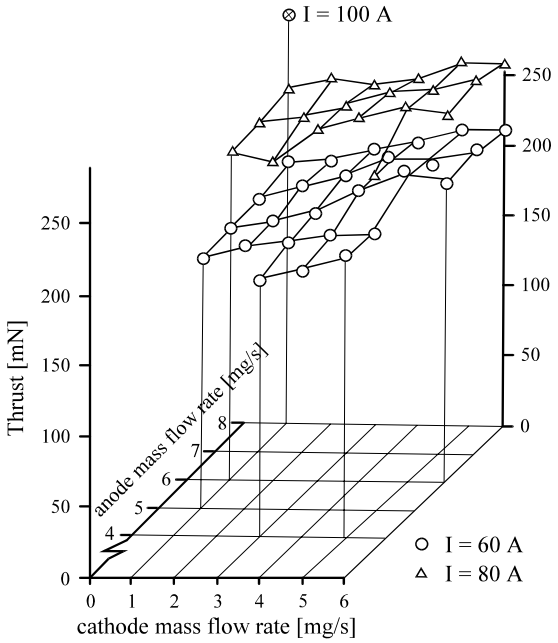


Fig. 26 Relative anode loss as a function of distribution of supplied mass [81], DLR thruster X13 [71].

of spacecraft contamination; note also that the tank pressure attainable in laboratory tests using condensable propellants that have a self-pumping effect is however low [79]. Which propellant is optimal depends on system considerations; this question can therefore still regarded as open.

Although metallic propellants can offer high efficiency, they are not favored today for fear of contamination. Moreover, they produce only a small thermal thrust because of their high atomic mass. Considering the acceleration mechanism, a lightweight propellant appears preferable for I_{sp} gain. In addition, optimization studies have shown that with lithium the exit velocity is too high for many missions [87].

9. Numerical Simulation

The development of efficient simulations is of great importance for the optimization of AF-MPD thrusters and should therefore be started. The AF-MPD thrust depends on plasma parameters and their distributions, which are a priori unknown, in contrast to the electromagnetic thrust of the self-magnetic MPD thruster, which is a function of independent parameters. Consequently, computations are difficult, because a number of far-reaching assumptions have to be made [12, 68, 70, 71, 78, 88, 89].

10. Historical Thruster Developments

Applied-field thrusters with coaxial fields were developed in the United States, Germany, and the Soviet Union in the 1960s and 1970s for power levels between 1–30kW. The strength of the magnetic field was between 0.1T and several Teslas. Averaged exit velocities of approximately 40km/s at efficiencies of up to 40% were achieved. (The power to produce the magnetic field is not included in these data.) Most of the development projects were terminated in the middle of the 1970s, with the exception of the Soviet Union where limited work has been continued.

The typical average data for laboratory devices run at different locations are listed next (data for $I = 1500$ A are in parentheses):

Discharge current I = 100–200 (–1500) A; applied field (maximum) $B_0 = 0.05 - 1.0\,\mathrm{Vs/m^2}$; propellant mass flow $\dot{m} = 5$–50 mg/s of Ar, Li (He, Kr, Xe, H_2, N_2, NH_3); ambient pressure $p_a = 10$–0.05 (-10^{-4}) Pa; discharge voltage $U = (50$—$)$ 100–150 V; thrust $F = 200$–2000 mN; specific impulse $I_{sp} = F/\dot{m} = 15$–35 km/s; and thrust efficiency $\eta_T = F/(2\dot{m}\,U \cdot I) = 20$–$40\%$. Efficiencies reported tend to be low for gaseous propellants, in particular argon (which has been used for the majority of tests), in contrast to alkali propellants, especially lithium [66, 81]. Reference [90], however, reports excellent results using hydrogen and helium. The propellant atomic mass seems to play an important role, and so does the magnetic field strength, which must exceed a certain limit in order to effectively support performance [68, 93] (see Fig. 30). As stated earlier, the overall operating conditions determine performance and, consequently, efficiency.

Data imply that a power range of 10–100 kW is possible, with operational voltage at an unproblematic level. All of these devices work in a stationary mode. There are, however, voltage oscillations (on the order of ±5–10%) as a result of

destabilizing effects typical for plasma accelerators. This noise has to be considered with respect to its potential system impact.

The radiation-cooled applied-field accelerator DFVLR-X16 developed at DLR in the early 1970s, in which the magnetic field is produced by means of a coil, is from today's point of view one of the best devices. At the same time, NASA was examining a thruster with a superconductive magnet. Both of these devices and the results achieved are discussed here as examples of this technology. A more detailed description of the experiments with AF-MPD thrusters is given by Krülle [82].

Today applied-field thrusters are once again being investigated in Japan, the United States, and Germany. A short review follows.

Thruster X-16 from DLR Stuttgart The thruster, which reached the most advanced stage of development, was X-16 (Fig. 27) from DLR Stuttgart. Then in the mid-1970s the development of plasma thrusters was discontinued because of a combination of lack of missions and insufficient qualification facilities. X-16 is equipped with a radiation-cooled anode and a hollow cathode. This device was able to achieve a thrust of 251 mN with a magnetic field of 0.6 T at a current of 80 A and a voltage of 145 V with 7-mg/s argon mass flow rate [91]. This corresponds to an effective exit velocity of approximately 36 km/s at an efficiency of 38.8%.

A similar device from DLR-Stuttgart, X-13, was used to investigate the dependence of the thrust on the magnetic induction [92]. In Fig. 28 the distinct influence of the magnetic field on the thrust is apparent.

NASA thruster with superconductive magnet Among others, a radiation-cooled thruster with a superconductive magnet was tested at the NASA Lewis Research Center (Fig. 29).

One can see from Fig. 30 that, compared to self-field thrusters, the efficiency can only be significantly improved when the strength of the magnetic fields is distinctly larger than 0.1 T. This means that the effort of producing the magnetic field, which is not taken into account in calculating the efficiency, seems to be only justifiable with stronger magnetic fields. Currently JPL (NASA Jet Propulsion

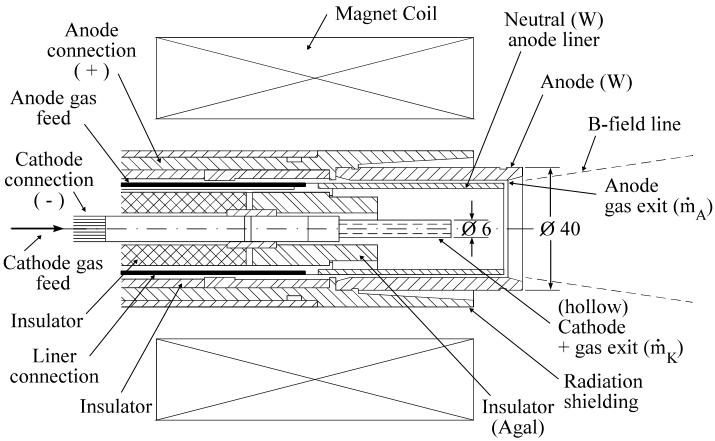


Fig. 27 Applied-field thruster X-16 from DLR Stuttgart [91].

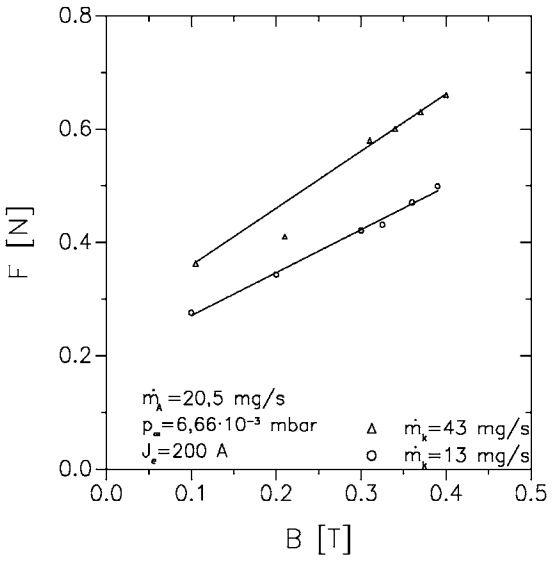


Fig. 28 Thrust dependent on magnetic induction with the DLR X-13 thruster [92].

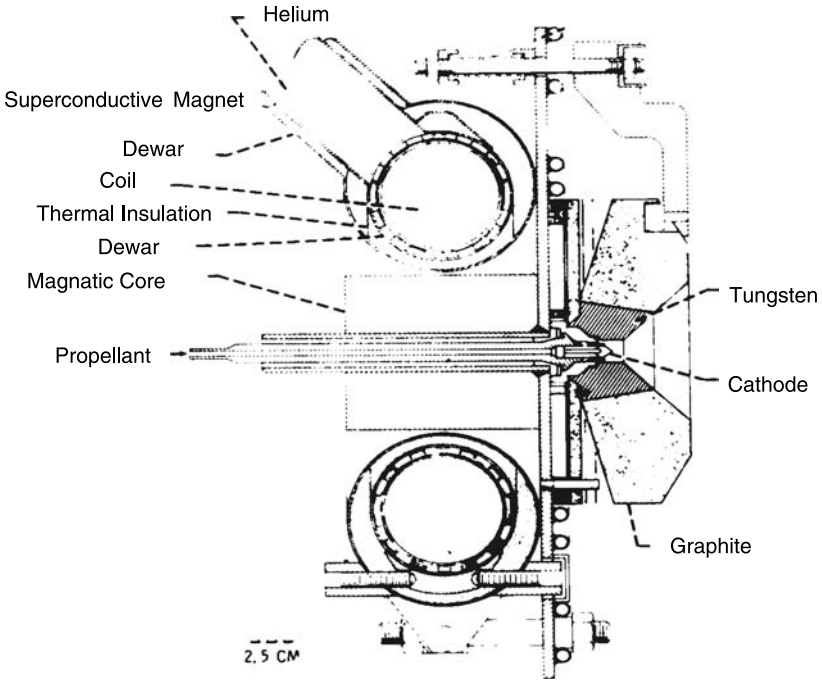


Fig. 29 Thruster with a superconductive magnet [93].

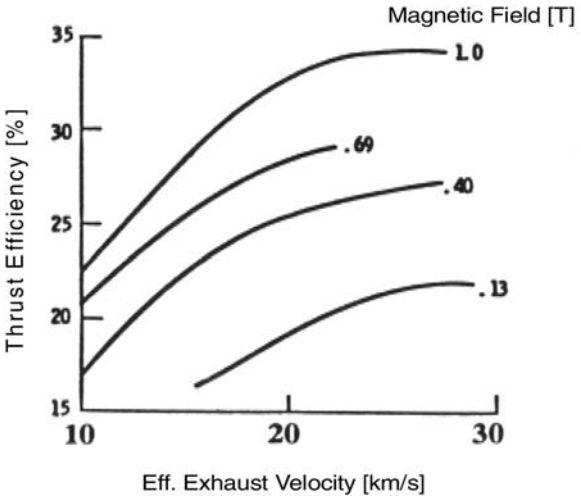


Fig. 30 Dependence of the efficiency on the effective exit velocity with different magnetic fields [93].

Laboratory) is building a test stand for Russian applied-field thrusters (see the following) with lithium as propellant. This test stand will enable predevelopment for thrusters up to several 100 kW to be carried out.

Thruster developments in Russia For several decades the Moscow Aviation Institute (MAI) has been investigating applied-field thrusters with lithium as propellant up to approximately 150 kW. A sketch of this device is shown in

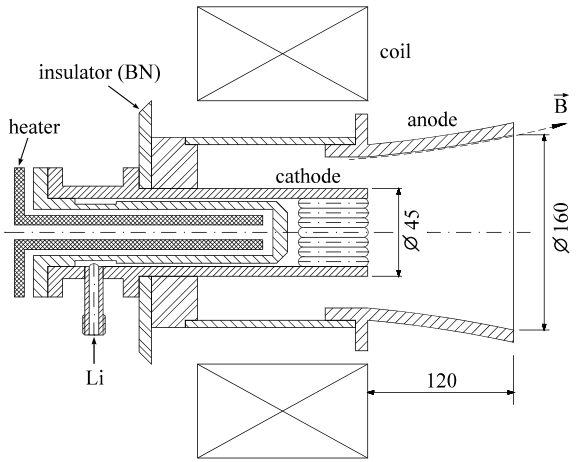


Fig. 31 MAI applied-field thruster with lithium as propellant operated up to about 150 kW.

Fig. 31. The cathode consists of a bundle of hollow cathodes. The tungsten anode is radiation cooled. At relatively low magnetic field strength ($0.075 < B_f < 0.09$ T), a thrust of 4.5 N was achieved at a current of about 2.9 kA and a mass flow rate of 107 mg/s. This is equivalent to an effective exhaust velocity near 42 km/s. The efficiency was about 48% [84].

11. Test Facilities

When testing applied-field thrusters in a laboratory, one must keep in mind that compared to self-field thrusters the current distribution extends quite far outside of the device (Fig. 32). However, interaction with the wall of the test container must be precluded. This means that the tank must be made of nonmagnetic steel. Because of the interaction of the discharge with the residual gas, surrounding gas can be sucked in near the anode if the tank pressure is too high. Therefore, pressures lower than 10^{-3} mbar are required (see Fig. 37). Currently there are no facilities available for testing thrusters at high electric power (higher than 100 kW). At JPL a test stand for lithium thrusters is being built. However, it cannot be used for noble gas propellants because of insufficient pump capacity. At IRS a new test stand that is suitable for thrusters up to 20 kW has been built.

IV. High-Power Hybrid ATTILA Thruster

Among the hybrid thrusters currently being investigated, only the ATTILA concept promises a thrust density high enough so that high thrust can be expected. This hybrid thruster (see Fig. 33) consists of two stages: a thermal arcjet section followed by an induction stage. The plasma jet generated by the thermal arcjet section, which is operated in the power range between 50 and 100kW, is injected

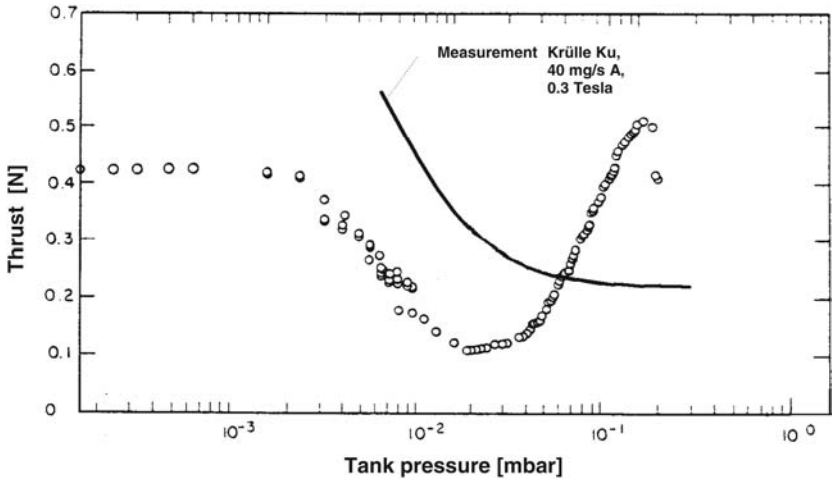


Fig. 32 Thrust dependence on tank pressure in applied-field devices [77, 91].

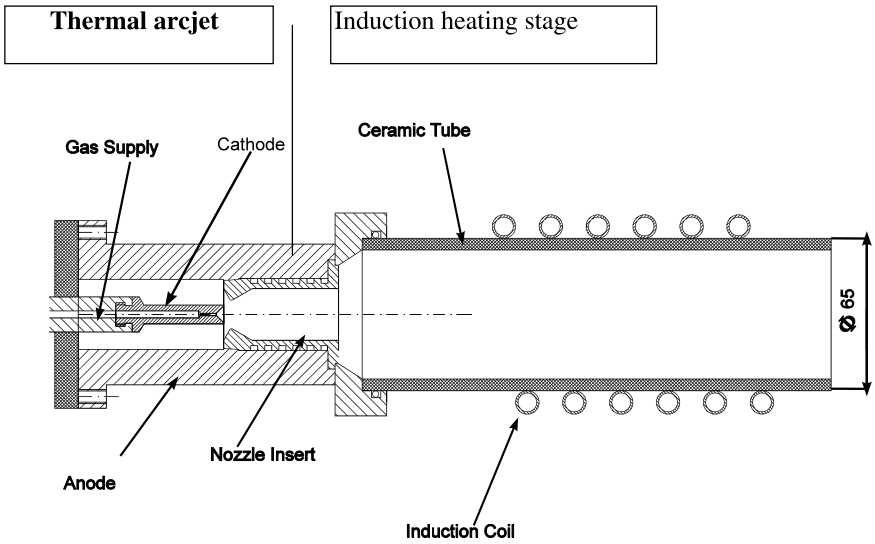


Fig. 33 Hybrid plasma generator.

into a ceramic tube surrounded by a magnetic coil. In this tube (the second stage) additional energy is added by inductive heating prior to the expansion in the nozzle (see Fig. 34) [94]. In the inductive second stage the energy is coupled near the surface owing to the skin effect. In this way the temperature of the thermal arcjet cold-gas casing can be increased considerably, and ultimately a significantly higher exit velocity can be achieved. In preliminary tests this effect has already been proven by means of a baffle plate for force measurements. The initial experiments with the hybrid plasma generator were very promising. They proved that in

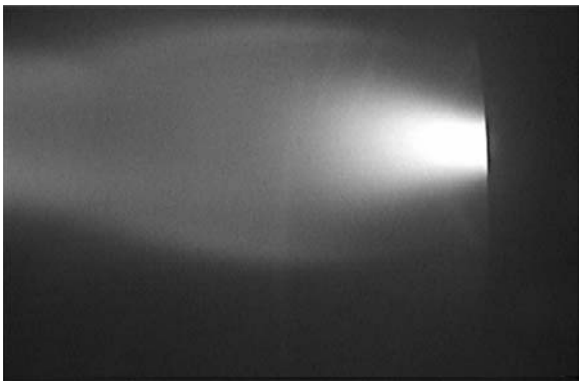


Fig. 34 ATTILA operating in arcjet mode only.

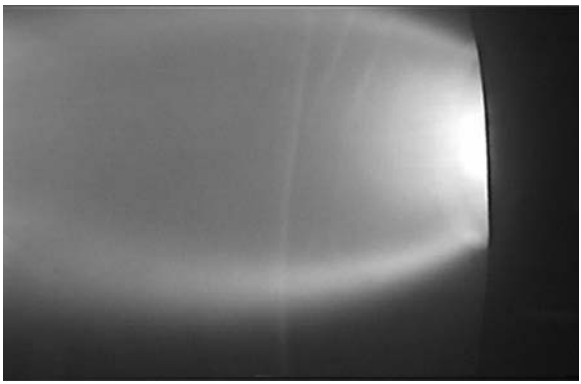


Fig. 35 ATTILA operating in arcjet mode with superposed induction heating.

the second stage a significant increase of the specific power can be achieved (see Fig. 35). Two experiments were carried out, each with 17-kW total power. In the first test, the thermal arcjet was operated with 17kW without the second stage and 0.9N were measured at the baffle plate. By splitting the power in 10kW in the arcjet section and 7kW in the inductive stage, the force increased by more than 20% to 1.1N using the same mass flow rate. Currently a baffle-plate device for measuring the thrust is being developed further and calibrated at IRS with the help of existing thrust balances. Tests with the current ATTILA configuration are planned up to 200-kW total power. The optimal power splitting, maximal thrust, and specific impulse for different propellants will be investigated in the near future. The test stand has already been built. At present a laboratory model is being developed.

V. Conclusions

Promising candidates for heavy payloads in space propulsion are several plasma propulsion systems. Electrothermal arcjets cover a wide range of input power, from several hundred watts to several hundred kilowatts [22]. Low-power devices have been implemented in commercial applications with hydrazine as propellant as an evolutionary step in specific impulse compared to the well-established chemical thrusters, and its simplicity, reliability, and low mass compared to other electric propulsion systems. This technology has been investigated so far up to 100kW in the laboratory, and the results are very promising. With hydrogen propellant the exit velocities achieved were above 20km/s; there is hope to further raise this value by increasing the power level and optimizing the design [4]. High thrust up to 25N has already been achieved in the laboratory with stationary self-field MPD thrusters using argon as propellant [87], but so far plasma instabilities limit the exit velocity to 15km/s for the propellants investigated, including hydrogen. These instabilities have been intensively investigated and there is hope to increase specific impulse by changing the thruster geometry [50, 95]. High exit velocities of 40km/s and 4.5-N thrust have been achieved with an applied field

MPD device using lithium propellant [84]. This said, there are still some disadvantages inherent to MPD systems: thrust density is lower by a factor 10 compared to the other two plasma sources, the performance is not demonstrated so far with non contaminating propellants in stationary operation at high power levels, and much lower tank pressure is required for the investigation of applied-field devices. In addition electrode erosion remains a serious concern for long missions.

A hybrid thruster, consisting of an electrothermal arcjet as a first stage combined with an inductive RF stage, offers the possibility to not only increase the exit velocity but also the thrust density. Preliminary laboratory tests look promising.

References

[1] Schmidt, T., Seboldt, W., and Auweter-Kurtz, M. "Propulsion Options for Manned Mars Missions," 16_333_P, 6th International Symposium, Propulsion for Space Transportation of the XXIst Century, May 2002.

[2] Shoji, J. M., "Solar Rocket Component Study," AFRPL-TR-84-057, Rockwell International Canoga Park, CA, Rocketdyne Div., Feb. 1985.

[3] Farbman, G., "Upgraded Nerva Systems: Enabler Nuclear System," NASA CP 10079, *Nuclear Thermal Propulsion*, 1991.

[4] Auweter-Kurtz, M., Gölz, T., Habiger, H., Hammer, F., Kurtz, H., Riehle, M., and Sleziona, C., "High Power Hydrogen Arcjet Thrusters," *Journal of Propulsion and Power*, Vol. 14, No. 5, 1998, pp. 764–773.

[5] Wegmann, T. "Experimentelle Untersuchung Kontinuierlich Betriebener Magneto-plasma-Dynamischer Eigenfeldtriebwerke," Ph.D. Dissertation, Inst. für Raumfahrt-systeme (IRS), Univ Stuttgart, Germany, Nov. 1994.

[6] Tikhonov, V., Semenikhin, S., Brophy, J. R., and Polk, J. E., "The Experimental Performances of the 100 kW Li MPD Thruster with an External Magnetic Field," *Proceedings of the 24th IEPC*, Moscow, Russia, edited by V. Kim. Moscow Aviation Institute, Moscow, 1995, pp. 718–724.

[7] Christensen, J. A., Freick, K. J., Hamel, D. J., Hart, S. L., Norenberg, K. T., Haag, T. W., Patterson, M. J., Rawlin, V. K., Sovey, J. S., Anderson, J. R., Becker, R. A., and Polk, J. R., "Design and Fabrication of a Flight Model 2.3 kW Ion Thruster for the Deep Space 1 Mission," AIAA Joint Propulsion Conference, AIAA Paper 98-3327, Cleveland, OH, July 1998.

[8] Arkhipov, B. A., Bober, A. S., Gnizdor, R. Y., Kozubsky, K. N., Korakin, A. I., Maslennikov, N. A., and Pridannikov, S. Y., "The Results of 7000-Hour SPT 100 Life Testing," *Proceedings of the 24th IEPC*, Moscow, Russia, edited by V. Kim. Moscow Aviation Institute, Moscow, 1995, pp. 315–321.

[9] Kurtz, H., "Arcjet Thrusters," Inst für Raumfahrtsysteme (IRS), Univ. Stuttgart, Final Report – Propulsion 2000, IB-00-06a, Germany, Sept. 2000.

[10] Curran, F., and Caveny, L., "Hydrogen Arcjet Technology Status," International Electric Propulsion Conference, IEPC-93-215, Seattle, WA, Sept. 1993.

[11] PRIMEX Aerospace Co., Space Systems Capabilities and Technologies, 99-H-2512A, *Proceedings of the Nuclear Thermal Propulsion Workshop*, NASA Lewis Research Center, Redmond, WA, 1999, pp. 105–126.

[12] Riehle, M., Kurtz, H. L., and Auweter-Kurtz, M., "Performance Evaluation of Regeneratively Cooled 1, 10 & 100 kW Arcjets," International Electric Propulsion Conference, IEPC-99-027, Sept. 1999.

[13] Bromaghin, D., et al., "An Overview of the On-Orbit Results from the Electric Propulsion Space Experiment (ESEX)," International Electric Propulsion Conference, IEPC-99-182, Sept. 1999.

[14] Auweter-Kurtz, M., *Lichtbogenabtriebe für Weltraumaufgaben*, B. G. Teubner, Stuttgart, Germany, 1992, pp. 62–83.

[15] Butler, G., Cassady, R., Hoskins, W., King, D., and Kull, A., "Performance of Advanced Concept Hydrogen Arcjet Anodes," International Electric Propulsion Conference, IEPC-93-215, Seattle, WA, Sept. 1993.

[16] Aston, G., and Aston, M. B., "Integrated Design Arcjets for High Performance," International Electric Propulsion Conference, IEPC-97-090, Cleveland, OH, Aug. 1997.

[17] Miller, S., and Martinez-Sanchez, M., "Nonequilibrium Numerical Simulation of Radiation-Cooled Arcjet Thrusters," International Electric Propulsion Conference, IEPC-93-215, Seattle, WA, Sept. 1993.

[18] Butler, G., Kull, A., and King, D., "Numerical Simulation of Hydrogen Arcjet Performance," International Electric Propulsion Conference, IEPC-93-215, Seattle, WA, Sept. 1993.

[19] Fujita, K., "Performance Computation of a Low Power Hydrogen Arcjet," AIAA Joint Propulsion Conference, AIAA Paper 96-3183, Lake Buena Vista, FL, July 1996.

[20] Kuchi-ishi, S., and Nishida, M., "Thermo-Chemical Nonequilibrium Modeling for a Nitrogen Arcjet Thruster," International Electric Propulsion Conference, IEPC-99-029, Sept. 1999.

[21] Megli, T., Krier, H., and Burton, R., "Plasmadynamics Model for Nonequilibrium Processes in N_2/H_2 Arcjets," *Journal of Thermophysics and Heat Transfer*, Vol. 10, No. 4, 1996, pp. 554–562.

[22] Auweter-Kurtz, M., Kurtz, H., and Schöttle, U., "Future Directions for Electrothermal Arcjet Propulsion," 8th International Workshop on Combustion and Propulsion, Rocket Propulsion: Present and Future, June 2002.

[23] Nentwig, G., et al., "Experimental and Theoretical Investigation on an Arc Heated Water Steam Plasma," *Proceedings of the 14th International Symposium on Plasma Chemistry*, Prague, Czech Republic, Aug. 1999, pp. 2393–2398.

[24] Lichon, P., and Sankovic, J., "Development and Demonstration of a 600s Mission Average Arcjet," International Electric Propulsion Conference, IEPC-93-087, Sept. 1993.

[25] Trifonov, Yu., Khodenko, V., Salikhov, R., Avatinyan, G., and Rylov, Yu., "VNIIEM Activity in the Field of EPE," International Electric Propulsion Conference, IEPC-95-010, Sept. 1995.

[26] Walker, Q., Hargus, W., and Cappelli, M., "Characterization of a Low Power Helium Arcjet," 34th International Joint Propulsion Conference, AIAA-98-3636, June 1998.

[27] Welle, R., "Space Propulsion Applications of Helium Arcjets," 35th Aerospace Science Meeting, AIAA Paper 97-0794, Jan. 1997.

[28] Rybakov, A., Auweter-Kurtz, M., and Kurtz, H., "Investigations of a 1 kW Class Arcjet Thruster with Helium as Propellant," 38th Joint Propulsion Conference, AIAA Paper 2002-3659, Indianapolis, IN, July 2002.

[29] Cann, G. L., "State of the Art of Electromagnetic and Electrothermal Propulsion," Technion, Inc., Rept. 07-040, Hada, Israel, July 1977.

[30] Riehle, M., Kurtz, H. L., and Auweter-Kurtz, M., "Performance Evaluation of Regeneratively Cooled 1, 10 & 100 kW Arcjets," International Electric Propulsion Conference, IEPC-99-027, Oct. 1999.

[31] Hammer, F., Riehle, M., Auweter-Kurtz, M., Kurtz, H., and Schöttle, U., "Arcjet Development Capabilities at the IRS: Experiment and Analysis," *Proceedings of the Second European Spacecraft Propulsion Conference*, ESA-ESTEC, Noordwijk, The Netherlands, 1997, pp. 693–700.

[32] Maecker, H., "Plasmaströmungen in Lichtbögen Infolge Eigenmagnetischer Kompression," *Zeitschrift für Physik*, Vol. 141, No. 2, 1955, pp. 198–216.

[33] Jahn, R. G., *Physics of Electric Propulsion*, McGraw–Hill, New York, 1968, pp. 227–232.

[34] Auweter-Kurtz, M., Boie, C., Kaeppeler, H. J., Kurtz, H. L., Schrade, H. O., Sleziona, P. C., Wagner, H. P., and Wegmann, T., "Magnetoplasmadynamic Thrusters: Design Criteria and Numerical Simulation," *International Journal of Applied Electromagnetics in Materials*, No. 4, 1994, pp. 383–401.

[35] Wienecke, R., *Zeitschrift für Physik*, Vol. 143, pp. 118–140, 1955.

[36] Suzuki, H., and Kuriki, K., "Effect of Insulating Anode Hood on MPD Arcjet Performance," AIAA Paper 78-652, April 1978.

[37] Hügel, H., "Zur Funktionsweise der Anode im Eigenfeldbeschleuniger," DFVLR, DFVLR-FB 80-30, Cologne, Germany, 1980.

[38] Malliaris, A. C., John, R. R., Garrison, R. L., and Libby, D. R., "Quasi-Steady MPO Propulsion at High Power," NASA CR-111872, Feb. 1971.

[39] Auweter-Kurtz, M., Kurtz, H. L., Merke, W. D., Schrade, H. O., and Sleziona, P. C., "Self Field MPD Thruster Investigations," Final Rept., Grant No. N 00014-87-G-0119 Plasma Thruster Development, for ONR, Washington DC, Oct. 1988 (IRS-88-P-10).

[40] Moore, R. A., Cann, G. L., and Galagher, L. R., "High Specifie Impulse Thermal Are Jet Thruster Technology," Electro-Optical Systems, Rept. SO90-Phase Final, Pasadena, CA, June 1965; also AFAPL-TR-6S-48.

[41] Schrade, H. O., Rösgen, T., and Wegmann, T., "The Onset Phenomena Explained by Run-Away Joule Heating," International Electric Propulsion Conference, IEPC-91-022, Oct. 1991.

[42] King, D. Q., "Magnetoplasmadynamic Channel Flow for Design of Coaxial MPD Thrusters," Ph.D. Dissertation, Dept. of Mechanical and Aerospace Engineering, Princeton Univ., Princeton, NJ, Nov. 1981; also MAE Rept. 1552.

[43] Rudolph, L. K., "The MPD Thruster Onset Current Performance Limitation," Ph.D. Dissertation, Dept. of Mechanical and Aerospace Engineering, Princeton Univ., Princeton, NJ, Nov. 1980.

[44] Lawless, J. L., and Subramanian, V. V., "A Theory of Onset in MPD Thrusters," Air Force Office of Scientific Research, 18th International Electric Propulsion Conference, AIAA Paper 85-2039, Alexandria, VA, Oct. 1983.

[45] Wagner, H. P., Kaeppeler, H. J., and Auweter-Kurtz, M., "Instabilities in MPD Thruster Flows: 1. Space Charge Instabilities in Unbounded and Inhomogeneous Plasmas," *Journal of Physics D: Applied Physics*, Vol. 31, No. 5, 1998, pp. 519–528.

[46] Wagner, H. P., Kaeppeler, H. J., Auweter-Kurtz, M., "Instabilities in MPD Thruster Flows: 2. Investigation of Drift and Gradient Driven Instabilities Using Multi-Fluid Plasma Flow Models," *Journal of Physics D: Applied Physics*, Vol. 31, No. 5, 1998, pp. 529–541.

[47] Boyle, M. J., Clark, K. E., and John, R. G., "Flowfield Characteristics and Performance Limitations of Quasi-Steady Magnetoplasmadynamic Accelerators," *AIAA Journal*, Vol. 14, No. 7, 1976, pp. 955–962.

[48] Kuriki, K., and Suzuki, H., "Quasi-Steady MPD Arcjet with Anode Gas Injection," *Electric Propulsion and its Applications to Space Missions*, edited by R. C. Finke,

Progress in Astronautics and Aeronautics, Vol. 79, AIAA, New York, 1981, pp. 554–563.

[49] Boie, C., "Numerische Simulation Magnetoplasmadynamischer Eigenfeldtriebwerke mit Hochauflösenden Adaptiven Verfahren," Shaker Verlag, Ph.D. Dissertation, Inst. für Raumfahrtsysteme (IRS), Univ. Stuttgart, Germany, May 2000.

[50] Heiermann, J., "Ein Finite-Volumen-Verfahren zur Lösung Magnetoplasmadynamischer Erhaltungsgleichungen," Ph.D. Dissertation, Inst. für Raumfahrtsysteme (IRS), Univ. Stuttgart, Germany, Oct. 2002.

[51] Hügel, H., and Krülle, G., "Phänomenologie und Energiebilanz von Lichtbogenkathoden bei niedrigen Drucken und Hohen Stromstärken," *Beiträge aus der Plasmaphysik*, Vol. 9, No. 1, 1969, pp. 87–116.

[52] Cann, G., and Harder, R. L., "Study of Electrode Attachment Regions in High Current Gaseous Discharges," Arnold Engineering Development Center, Rept. AEDC-TDR-64-107, Tullahoma, TN, Aug. 1964.

[53] Goodfellow, K. D., "A Theoretical and Experimental Investigation of Cathodes Processes in Electric Thrusters," Ph.D. Dissertation, Faculty of the Graduate School, Univ. of Southern California, Los Angeles, CA, May 1966; also Jet Propulsion Lab, Internal Doc. JPL D-13969, Pasadena, CA, 1996.

[54] Malliaris, A. C., "Phenomena in the Cathode Region of an MPD Accelerator," 5th Aerospace Science Meeting, AIAA Paper 67–47, Jan. 1967.

[55] Hall, L. S., "Thermoelectric Effects in a Joule-Heated Plasma," *Physics of Fluids*, Vol. 7, 1964, pp. 425–427.

[56] Bez, W., Höcker, K. H., and Mayser, B., "Der Anodenfall in Niederdruckentladungen," *Annalen der Physik*, Vol. 18, 1956, pp. 335–344.

[57] V. Engel, A., "A Theory of the Anode Fall in Flow Discharges," *Philosophical Magazine*, Vol. 32, 1941, pp. 417–427.

[58] Auweter-Kurtz, M., Glocker, B., Kurtz, H. L., Loesener, O., Schrade, H. O., Tubanos, N., Wegmann, T., Willer, D., and Polk, J. E., "Cathode Phenomena in Plasma Thrusters," *Journal of Propulsion and Power*, Vol. 9, No. 6, 1993, pp. 882–888.

[59] Auweter-Kurtz, M., "Elektrische Raumfahrtantriebe," Lecture manuscript, Inst. für Raumfahrtsysteme (IRS), Univ Stuttgart, SS 1985.

[60] Patrick, R. M., and Janes, G. S., Preprint, Air Force Office of Scientific Research, Orbit-Raising Propulsion Planning Session, Orlando, FL, 1982.

[61] Janes, G. S., and Lowder, A. S., "Anomalous Electron Diffusion and Ion Acceleration in a Low Density Plasma," *Physics of Fluids*, Vol. 9, No. 6, 1966, p. 1115.

[62] Mikellides, P. G., Turchi, P. J., and Roderick, N. F., "Theoretical Model for Applied Field MPD Thrusters," 31st Joint Propulsion Conference, AIAA Paper 95-2676, July 1995.

[63] Schock, W., "Zur Verteilung der Elektrischen Stromdichte in Magneto-Plasma-Dynamischen (MPD)-Beschleunigern," Ph.D. Dissertation, Aerospace Faculty, Univ. Stuttgart, Germany, July 1974.

[64] Fradkin, D. B., and Roehling, D. J., "Experiments in the New LASL Test Facility," Technical Report LA-5199-Ms, Los Alamos Scientific Laboratory, Univ. California, Los Alamos, NM, Sept. 1973.

[65] Connolly, D. J., and Sovie, R. J., "Effect on Background Pressure on Magnetoplasmadynamic Thruster Operation," *Journal of Spacecraft and Rockets*, Vol. 7, No. 3, 1970, p. 255.

[66] Sovey, J. S., and Mantenieks, M. A., "Performance and Lifetime Assessment of Magnetoplasmadynamic Arc Thruster Technology," *Journal of Propulsion and Power*, Vol. 7, No. 1, 1991, pp. 71–83.

[67] Schock, W., "Diagnostics and Interpretation of the Electric Current Distribution in an MPD Thruster," AIAA 9th Electric Propulsion Conference, AIAA Paper 72-498, April 1972.

[68] Kruelle, G., "Theoretical Treatment of Current, Mass Flow, and Related Distributions in MPD Plumes," AIAA Paper 72-501, 1972.

[69] Krülle, G., "Zur Dynamik des Axialsymmetrischen Magnetoplasmadynamischen Beschleunigers (MPD-Triebwerk) mit Überlagertem Magnetfeld," Ph.D. Dissertation, Faculty of Mechanical and Electrical Engineering, Technische Univ. Munich, Germany, May 1974.

[70] Tanaka, M., and Kimura, I., "Current Distribution and Plasma Acceleration in MPD Arcjets with Applied Magnetic Fields," *Journal of Propulsion and Power*, Vol. 4, No. 5, 1988, p. 428.

[71] Kruelle, G., and Zeyfang, E., "Preliminary Conclusions of Continuous Applied Field Electromagnetic Thruster Research at DFVLR," 11th Electric Propulsion Conference, AIAA Paper 75-417, March 1975.

[72] Cann, G. L., Harder, R. L., Moore, R. A., and Lenn, P. D., "Hall Current Accelerator," NASA CR-54705, Feb. 1966.

[73] Malliaris, A. C., "Oscillations in an MPD Accelerator," *AIAA Journal*, Vol. 6, No. 8, 1948, pp. S 1575–1577.

[74] Maisenhälder, F., Ungerer, E., and Kruelle, G., "Some Experiments on the 'Spoke' Phenomenon in MPD Operation," *AIAA Journal*, Vol. 7, No. 2, 1969, pp. 348–350.

[75] Sasoh, A., "Simple Formulation of Magnetoplasmadynamic Acceleration," *Physics of Plasma*, Vol. 1, No. 3, 1994, pp. 464–469.

[76] Arakawa, Y., and Sasoh, A., "Electromagnetic Effects in an Applied Field Magnetoplasmadynamic Thruster," *Journal of Propulsion and Power*, Vol. 8, No. 1, 1992, p. 98.

[77] Bishop, A. R., Connolly, D. J., and Seikel, G. R., "Test of Permanent Magnet and Superconducting Magnet MPD Thrusters," AIAA Paper 71-696, Jan. 1971.

[78] Sasoh, A., and Arakawa, Y., "Thrust Formula for an Applied-Field MPD Thruster Derived from Energy Conservation Equation," International Electric Propulsion Conference, IEPC 91-062, Oct. 1991.

[79] Fradkin, D. B., Blackstock, A. W., Roehling, D. J., Stratton, T. F., Williams, M., and Liewer, K. W. "Experiments Using a 25-kW Hollow Cathode Lithium Vapor MPD Arcjet," *AIAA Journal*, Vol. 8, No. 5, 1970, p. 886.

[80] Kruelle, G., "Characteristics and Local Analysis of MPD Thruster Operation," AIAA Electric Propulsion and Plasmadynamics Conference, AIAA Paper 67-672, Sept. 1967.

[81] Myers, R. M., "Applied Field MPD Thruster Performance with Hydrogen and Argon Propellants," *Journal of Propulsion and Power*, Vol. 9, No. 5, 1993, p. 781.

[82] Krülle, G., Auweter-Kurtz, M., and Sasoh, A., "Technology and Application Aspects of Applied Field Magnetoplasmadynamic Propulsion," *Journal of Propulsion and Power*, Vol. 14, No. 5, 1998, pp. 754–763.

[83] Schall, W., "Influence of Magnetic Fields on Anode Losses in MPD Arcs," AIAA 9th Electric Propulsion Conference, AIAA Paper 72-502, April 1972.

[84] Tikhonov, V., Semenikhin, S., Brophy, J. R., and Polk, J. E., "The Experimental Performances of the 100kW Li MPD Thruster with an External Magnetic Field,"

Proceedings of the 24th International Electric Propulsion Conference, Moscow, Russia, edited by V. Kim. Moscow Aviation Institute, Moscow, 1995, pp. 718–724.

[85] Polk, J. E., and Goodfellow, K. D., "Ammonia Arcjet Behavior in a Cyclic Endurance Test at 10 kW," International Astronautical Federation, Paper 92-0612, Oct. 1992.

[86] Sasoh, A., Solem, A., and Arakawa, Y., "10kW Steady-State MPD Thruster," *Journal of the Faculty of Engineering*, Univ of Tokyo (B), Vol. 39, No. 3, 1988, pp. 275–296.

[87] Auweter-Kurtz, M., and Kurtz, H., "Optimization of Electric Thrusters for Primary Propulsion Based on the Rocket Equation," *Journal of Propulsion and Power*, Vol. 19, No. 3, 2003, pp. 406–423.

[88] Turchi, P. J., "The Effect of Magnetic Nozzle Configurations on Plasma Thrusters," NASA CR 202341, May 1997.

[89] Thomas, H., "A Numerical Simulation of Axisymmetric, Steady Plasma Flow with Self-Induced and Applied Magnetic Fields," Ph.D. Dissertation, Space Institute, Univ. of Tennessee, Knoxville, TN, Sept. 1991.

[90] Arakawa, Y., and Sasoh, A., "Steady State Permanent Magnet Magnetoplasmadynamic Thruster," *Journal of Propulsion and Power*, Vol. 5, No. 3, 1989, pp. 301–304.

[91] Krülle, G., "Continuous MPDA Development Status," *Proceedings of the 3rd European Electric Propulsion Conference*, edited by J. Freisinger and H. W. Loeb. DGLR Fachbuchreihe, Band 5, Deutsche Gesellschaft fuer Luft- and Raumfahrt, Cologne, Germany, 1974.

[92] Kurtz, H. L., "Integrale Messungen an Einem Axialsymmetrischen Elektromagnetischen Plasmabeschleuniger," Diplomarbeit, Inst. für Raumfahrtsysteme (IRS), Univ. Stuttgart, Germany, Oct. 1971.

[93] Seikel, G. R., York, T. M., and Condit, W. C., "Roles for Magnetic Thrusters in Orbit-Raising Missions," SeiTec, SeiTec-Rept. 8203, Cleveland, OH, 1982.

[94] Laure, S., Heiermann, J., Auweter-Kurtz, M., and Kurtz, H., "ATTILA – Adjustable Throttle Inductively Afterburning Arc Jet," International Electric Propulsion Conference, IEPC-01-142, Oct. 2001.

[95] Wagner, H., "Theoretische Untersuchung drift- und Gradientengetriebener Instabilitäten in MPD-Triebwerksströmungen," Ph.D. Dissertation, Inst. für Raumfahrtsysteme (IRS), Univ. Stuttgart, Germany, March 1994.

Copyrighted Materials
Copyright © 2008 AIAA Retrieved from www.knovel.com

Chapter 5

Review of Reactor Configurations for Space Nuclear Electric Propulsion and Surface Power Considerations

Roger X. Lenard*
GPS Solutions, Inc., Carson City, Nevada

I. Introduction

THE development and safe and effective implementation of the fission reactor module is a key goal of any space nuclear-power project. In addition to providing a significant level of power reliably for over a number of years, perhaps 10 years, the reactor module must satisfy numerous requirements regarding nuclear safety and integration with the rest of the spacecraft while minimizing both programmatic risk and system mass.

It has been recognized from the earliest days of the fission era that the application of nuclear-fission energy to space power and propulsion needs to provide a number of advantages. The very high energy density achievable with fissile fuel leads to compact, high-power, long-lived systems that have great advantages in space use. In recognition of these advantages, a number of programs have been undertaken in the United States and in the former Soviet Union to capitalize on these technologies for space use. These programs have produced a wide array of technologies, many of them space-qualified, that provide an excellent base on which to build a future space nuclear program. *In fact, approximately 35 space reactors have been designed and operated in space—all have been liquid-metal-cooled reactor concepts.*

The SNAP program in the United States resulted in the launch and space demonstration of the SNAP-10A reactor in 1965. This was the United States' first and only launch of a nuclear reactor into space. SNAP-10A produced 43 kW of thermal power ("kWt"), was cooled with a potassium-sodium (NaK) eutectic, and had a peak coolant temperature of about 820 K. It operated for 40 days before an

Copyright © 2008 by the author. Published by the American Institute of Aeronautics and Astronautics, Inc., with permission.

*Currently Chief Technical Manager, Little Prairie Services, Edgewood, New Mexico.

electrical fault on the Agena upper stage triggered an automatic shutdown. The Russian program resulted in 33 reactors launched in space and provided clear demonstration of the feasibility of using nuclear-fission systems in space. The highest power level achieved was ~6 kW of electrical power (kWe) for a period of under one year.

These programs and others, such as the SP-100 program, the ROVER/NERVA, Project Timberwind programs, and the TOPAZ program, created high-temperature fuels (uranium nitride and carbide fuels), materials and other technologies that form the nucleus of any future space nuclear-power development program. In addition, a large number of study and evaluation programs funded by the U.S. Department of Energy (DOE), NASA, and Department of Defense (DOD) have resulted in numerous plausible designs for a range of missions and suggested many mission-enhancing or enabling features of nuclear systems.

The proposed JIMO mission and other robust space-exploration-related missions require a significant extrapolation from the demonstrated fission reactor capability in space. A power level of 200–2000 kWt is envisioned for an operational life of around 10 years. The required coolant temperatures could be as high as 1350 K. This is a challenging task. Fortunately, there has been considerable progress in ground-based and sea-based nuclear reactor development and implementation over the past four decades. This coupled with the just mentioned space nuclear program database gives us a wealth of information and conceptual design options to choose among as a starting point for the JIMO space reactor development.

This next series of sections describe the following aspects of the reactor module design, development, and implementation: 1) top-level requirements for the reactor module, 2) a comparison of system masses for the three reactor types, 3) reactor operations and dynamic behavior, 4) discussion of nuclear safety issues and approaches to handling them, 5) technology readiness levels and overall assessment, 6) interface considerations with the rest of the spacecraft, and 7) summary and conclusions.

II. Reactor Requirements

After extracting initial JIMO requirements, analytical efforts approached the space reactor and power-conversion-system design process from the following perspective: 1) nuclear safety must be ensured for all mission phases; 2) power requirements are 50–300 kWe; 3) lifetime requirements and capability of achieving mission with EP; 4) reactor fueling is optimal—before or at launch site; 5) reactor integration is optimal—before or at launch site; and 6) launch assumptions—several launch vehicle configurations considered.

To perform the trade studies in a consistent manner, the high-level requirements were translated to a set of detailed requirements that are necessary for design and trade studies. Table 1 presents the detailed set of requirements. A number of the numerical values of the requirements necessary for a detailed design were to be determined at this stage of the work, but will need to be settled prior to start of serious designs.

A cumulative lifetime of 10 full power years was considered necessary to meet the projected mission life and required duty cycle of the reactor. Several constraints

on the reactor performance dictated a set of key requirements (see Table 1). They are as follows:

1) **Operational constraint**: The need to remain critical at end of life (EOL), accounting for uncertainty, sets the key requirements of k_{eff} (the reactivity coefficient: see also Sec. III. B.2) at EOL at 1.000 (+0.005 − 0.00).

2) **Safety constraint**: To ensure subcriticality under the worst credible accident scenario, the reactors are designed to have a $k_{\text{eff}} = 0.985$ under those conditions. Accident conditions included immersion in water or wet sand and burial in dry sand. The k_{eff} value of 0.985 is appropriately conservative given the low probability of the event, the detailed analyses that are performed to satisfy the requirement, and the test program that is planned to confirm the level of subcriticality for

Table 1 Reactor requirements

Category	Requirement	Spec value
Reactivity	Lifetime/mission assurance	10 full power years
	Provide starting function	
	K_{eff} (EOL)	1.000 + 0.005/−0.000
	K_{eff} (BOL) = K_{eff} (EOL) + Burnup reactivity + Temperature reactivity + Margins	TBD
Safety	K_{eff} for maximum credible accident bounding case, i.e., reflectors gone, wet sand surrounding the reactor, internals flooded with pure water, fuel pin internals not flooded	<0.985
	Ensured safety for all mission phases	TBD
	Minimum shutdown element speed	TBD
	Safety monitoring parameters	TBD
Control	Operational for 10 yr at full power with one stuck control element	
	Maximum control element speed	TBD
	Autonomous control system	
	Leakage control strategy (avoid in-core rods)	
	Max rod worth of one element	TBD
	K_{eff} of all elements in least reactive configuration	<0.9
	Control monitoring parameters	N flux, T, P, position
Fuel	Peak central temperature (UN)	<1450 K (TBR)
	Peak clad temperature (UN)	<1375 K (TBR)
	Enrichment	93%
	Burn-up	<4%
Operational	Power coefficient over mission life	Negative, all powers
	Number of scheduled shutdowns	TBD
	Restart time after unscheduled shutdown	<TBD days
Shield	Lifetime dose at 30 m	<25 krad
	Lifetime fluence at 30 m	$<10^{11}$ n/cm^2
	Shadow angle	5 × 10 deg

simulated submersion configurations. It has been determined that reactor impacts can result in considerable reactor core deformation, leading to large reactivity swings. These can be more safety significant than a simple "intact impact with original core geometry" into either water, wet sand, or dry sand.

3) **Resource constraint**: Past designs and the various reactor systems have used different fissile fuel enrichment values. To ensure a level playing field for all reactor configurations studied, the fissile enrichment of the fuel was set at 93%.

4) **Technology constraint**: Recognizing the interest in avoiding significant fuel qualification, the peak fuel burn-up was set at 4% (atom). This is well below the peak value demonstrated for SP-100. The data at the higher burn-up values, however, were sparse, and for reasons of conservatism, the 4% value was chosen for our design. At the low power densities anticipated, larger diameter pins could be effective in reducing system mass without loss of performance. A tradeoff analysis will need to be performed to decide if the mass savings warrants the extra fuel qualification expense; for the purpose of early studies, reliance on the SP-100 fuel database has been assumed, and a 4% burn-up constraint imposed.

The other requirements reflect the standard constraints on shutdown reactivity, negative power coefficient over entire power range, dose levels at payload, etc. It is anticipated that the reactor will not need to be shut down (and subsequently restarted) once it attains initial criticality. Finally, the results of transient accident analysis will develop requirements on the rate of movements of the control blades (moderating fission) in order to ensure safety.

III. Reactor and Power Conversion—Mass Comparison

A model for reactor module mass was developed and used to compare the reactor types and to perform parameter studies of power and shield design and later was incorporated in the overall power train model.

A trade study was performed for three reactor types: 1) liquid-metal cooled reactor (LMR), 2) heat-pipe-cooled reactor (HPR), and 3) gas-cooled reactor (GCR). This trade study took into consideration coupling these reactors to three conversion systems: 1) Brayton, 2) Stirling, and 3) thermoelectric (TE). A trade study should consider performance, cost, schedule, and risk. This section concentrates on performance; later sections describe technical readiness, ease of testing, versatility, scalability, development concerns, and other characteristics, all of which influence cost, schedule, and risk. Because the trip time to Jupiter is dictated most strongly by the thrust-to-mass ratio of the vehicle and because thrust scales with the electrical power, the dominant measure of performance is the system dry mass for a given electrical power level available to the thrusters.

A. Earlier Work and Reactor Descriptions

Past studies have compared various combinations of reactor type and conversion type. The trades have traditionally looked at performance first (as indicated by system mass for a given power) and then tempered the conclusions with qualitative features such as versatility, growth potential, or technological readiness. During the early days of the SP-100 program (1983), Rockwell performed a technology assessment followed by a power system trade study. That study concluded

that the gas-cooled reactor directly coupled with a Brayton power conversion system had the highest overall figure of merit for the originally specified requirement set. But when the requirements and weightings were adjusted, the liquid-metal-cooled reactor (LMR), with lithium coolant and a fairly high-temperature Brayton system, was the combination selected, with an LMR and thermoelectric option as backup. Later the LMR-thermoelectric combination became the basis for the SP-100 program. The requirement change that led to this had a very strong emphasis on minimum mass and an additional emphasis on ability of the reactor to drive various conversion systems that might be developed later [1].

The more recent report by the Special Purpose Fission Technology (SPFT) program of the U.S. DOE from the NASA/DOE Interagency Space Reactor Power System Concept Screening Committee concluded that the preferred combination of reactor and power conversion system changed as the power regime and allowed the development time to change. The regime consistent with the JIMO requirements was dubbed Level 3 and called for 100 to 250 kWe, coolant exit temperature $>$1200 K, launch by 2015, power system specific mass of 25 to 35 kg/kWe, and scalability to multimegawatts. For these conditions, the plausible combinations were reduced to 1) LMR with Brayton, 2) LMR with Rankine, and 3) GCR with Brayton (direct drive). Figure 1 shows the summary result of voting by the committee members. There was clearly a strong difference between the favored three combinations and the remaining options, The committee did not offer GCR driving Rankine, Stirling, or thermoelectric as favorable options.

The present study follows upon the earlier work and focuses on LMRs, HPRs, and GCRs. Configurations for these three reactor types were developed in the DOE SPFT program, and these were chosen as the basis for the comparisons in this study. Alternative configurations (such as the SP-100 Generic Flight System

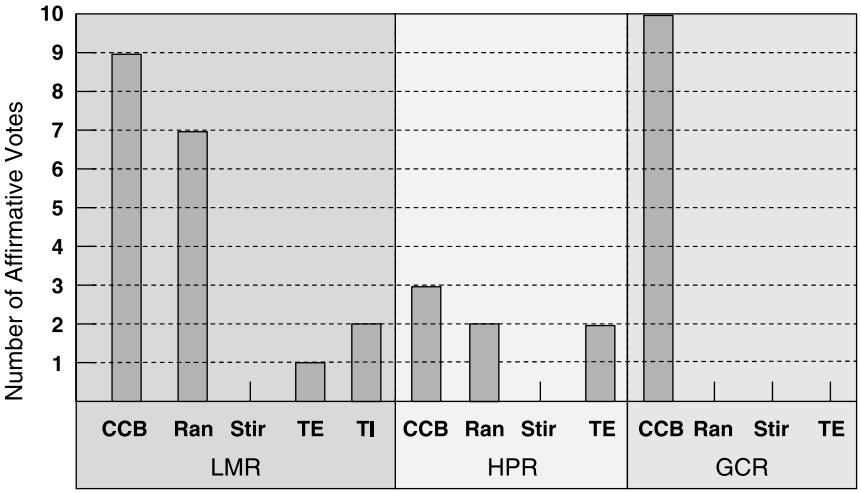


Fig. 1 Results for Level 3 system comparison from DOE-SPFT program screening study.

for the LMR, or the NERVA-derived GCR) were also considered but did not appear as attractive for this mission set.

A brief overview of the three reactor types is shown in Fig. 2. All three reactor types use uranium-nitride (UN) fuel pellets with a Nb1Zr clad containing a Re (rhenium) liner. It is also feasible for these reactors to use UO_2 fuel, but its lower density and thermal conductivity make UO_2 less attractive. The LMR uses pumped lithium to remove the heat from the reactor to a heat exchanger where it is transferred to the power conversion system. The HPR uses sodium-filled heat pipes to transfer the heat from the reactor to a heat exchanger. The GCR uses a flowing helium-xenon gas mixture to transfer the heat from the reactor to the power conversion system. With a Brayton conversion system, the GCR does not use an intermediate heat exchanger. Rather the Brayton working fluid passes through the core, and the reactor heat is transferred directly to the gas from the fuel pins.

All three systems control the reactor with external neutron reflectors rather than internal neutron absorbers, similar to the SNAP-10A approach, as opposed to the SP-100 approach. For larger reactor systems, internal control rods will be needed, and so they might be needed for thermoelectric options, which tend to have low conversion efficiency. This difference in control approach did not have a strong effect on the trade comparisons.

A detailed discussion of the various characteristics, pros, and cons of the three systems will be discussed in a later section. But briefly, the LMR draws upon extensive LMR experience with NaK and Na reactors (albeit at lower temperatures), is compact because of the excellent heat-transfer capability of liquid metals, and is versatile in working with different conversion systems. The HPR draws upon extensive design work and electrically heated testing, has passive heat

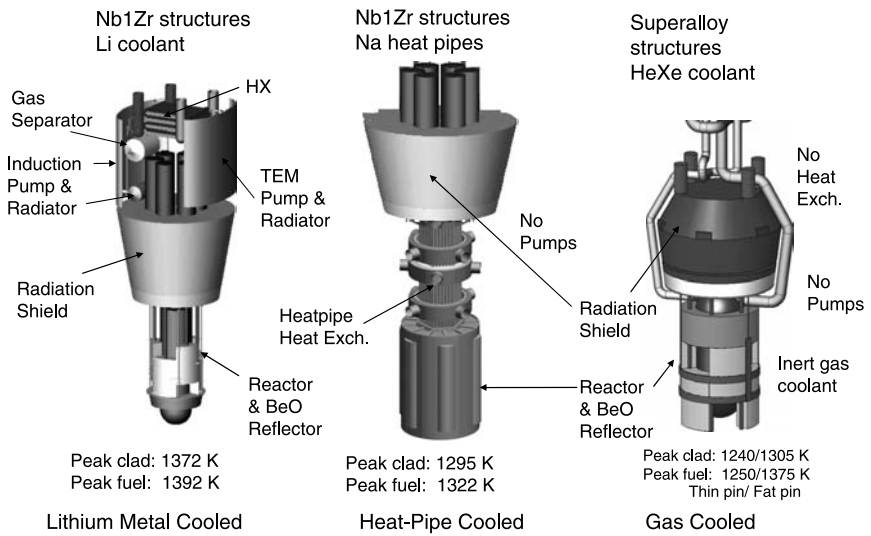


Fig. 2 Reactor options (all with external control elements).

removal from the core via numerously redundant heat pipes, and has an accessible core (no pressure vessel). The GCR draws upon the high-temperature test reactor experience (in Japan) with prototypic temperature and pressure levels, has no freeze–thaw issues and few material interaction concerns (because of the inert-gas coolant), and in the direct-drive configuration employs all super-alloy outer boundaries (which simplifies testing and integration).

B. Static Model Development and Validation

1. Model Basis and Overview

To compare the three reactor types across a broad range of conditions that included various power levels, power conversion schemes, and shielding requirements, a simplified model for the reactor module mass was developed. The reactor module was defined as including the reactor element (sometimes called the core and reflectors), radiation shield, primary heat-transport system, reactor instrumentation and controls, reentry shield, and superstructure. A model was developed to estimate the mass of all of these components as a function of reactor type, power-conversion type, reactor thermal power, radiation dose requirements, shield half-angle, and other parameters. The heat exchanger between the reactor and the power conversion system was included in the primary heat transport system for the Brayton system, but not for the Stirling or thermoelectric systems (because those systems include the heat exchanger as an integral part of their hardware).

The reactor model was based on the RSMASS-D model by Al Marshall [1]. This model takes into account criticality, fuel burn-up, heat transfer, and numerous other constraints to estimate the mass of space reactor. It was developed for LMRs, but it was extended easily to GCRs and HPRs by a judicious choice of input parameters. The shield model within RSMASS-D was replaced with a similar model that could be solved in a closed form rather than iteratively. RSMASS does not include in its calculations the primary heat transport system, and so a model for its mass was inserted. Updated values for the instrumentation and controls, and for the reentry shield, from the DOE SPFT Program (as reported in the DOE space reactor design data packages provided to this contract) were used to update the models for those items. Finally, the superstructure was assigned with an estimated mass of 5% of the other masses.

The dominant input and outputs that can be passed between the reactor module model and the other modules of the overall system model are listed here: primary inputs; power conversion type; reactor type; reactor thermal power (MW); time at full power (yr); number of full-power heat exchangers; desired lifetime n fluence (n/cm^2); desired lifetime gamma dose (rad); distance from reactor to payload (m); time averaged xenon propellant mass (kg); xenon propellant ave diameter (m); shield cone half-angle, x axis (degrees); mass of reactor element (kg); mass of radiation shield (kg); mass of primary heat transport (kg); mass of I&C (kg); mass of reentry shield (kg); mass of super-structure (kg); mass of the reactor module (kg); electrical power for pumps (kW). Additional input parameters can be found within the model. Many of these additional parameters are dependent on the type of reactor and on the type of power conversion system to which the reactor is connected.

2. Specific Design Anchor Points—Level Field

This model includes several internal adjustable coefficients. Most of these are based on actual physical parameters, but the fine tuning of these parameters depends on the assumptions made for operational and safety requirements. To anchor this general mass model, a set of specific designs was developed for the three reactor types at two different power levels, 400 and 1500 kWt. These designs were offshoots of the SPFT design development process (DDP) designs, but were adjusted to have consistent modeling assumptions because the mass of a reactor system depends on the design assumptions and constraints.

For this study, the dominant assumption or constraint was that all of the reactors would be designed to be equally safe, to first order. As will be discussed in later sections, the dominant hazard involving the reactor is release of radiation to the public during a launch accident. Because a space reactor is not very radioactive before it is operated, this hazard is greatly mitigated by designing the reactor so that it remains subcritical for all credible launch accidents. Previous studies have shown that one of the most challenging credible launch accident conditions for a reactor to remain subcritical under water immersion conditions is for all of the internal coolant channels to be flooded with pure water and the outside to be surrounded by wet sand. Fuel compaction under impact can be even more challenging. Water slows down (thermalizes) the neutrons within the reactor and makes them more prone to induce fission; flooding the core with pure water maximizes this effect without adding absorption by water impurities (such as are actually present in sea water or pond water). Surrounding the reactor with wet sand rather than water is a worse case because wet sand reflects the neutrons back into the core better and without as much absorption.

The scenario assumed was that the reactor falls into the ocean after a failed launch event and either buries itself in the sand in the ocean bottom or is covered over by sand after settling to the bottom. For this trade study, the internal geometry is assumed to remain intact for all reactor types considered. Experiments during the SNAP-10A development showed that external reflectors are easily stripped off during most impact scenarios with water, and so it was assumed for all of these cases that the external reflectors were removed. The reactor would be launched with the external reflectors locked in their most open configuration, and so this also was an expedient means to remove fine differences in the amount of openness of the reflectors. Any neutron-absorbing block that might be placed in the reflector gap for launch also was assumed to be stripped off.

A final design requirement was that the reactor remains operable to the end of life. This means that the core must remain critical in spite of the burn-up of some of the uranium fuel, and in spite of the reactivity reduction that occurs when the reactor heats from room temperature to operating temperature. So, specifically, the design condition for reactivity (or "*k*-effective," or "k_{eff}") for the accident condition of water flooded and surrounded by wet sand was taken to be $k_{\text{eff}} = 0.985$ for all reactor types. Here $k_{\text{eff}} = 1$ is critical; $k_{\text{eff}} = 0.985$ gives some margin; a k_{eff} change of 0.015 is substantial for a reactor, but not excessive. The exact value of the level of subcritically is subject to some debate. However, we believe that our chosen value is the optimum number based on conservatism and design and is adequate for a trade study because it would be applied to all of the reactors being considered. The reactivity loss during heat-up (or "temperature defect") was

determined to be about 1.5%, and this amount was added to the calculated fuel burn-up for a given power level, amount of fuel, and trip time (in full-power years) to determine the required k_{eff} at startup when cold. Typically, a reactivity swing needed between the wet-sand, water-flooded condition and beginning of life cold-startup condition was about 5%.

A very significant difference between the reactors designed during the DOE SPFT program and the SP-100 program was the ability to meet these conditions without the use of internal safety rods to absorb neutrons before startup. This simplifies the design and eliminates penetrations of "thimbles" into the hot reactor core and drive shafts through the radiation shield into the core center (see Chapter 2 in this book). This design approach was used for all reactor types in order to be consistent. (All three types could also use in-core safety rods if desired or needed.) Finally, the same reflector type was used for all three reactor types. This consisted of sliding reflectors made of BeO to maximize reflection with some neutron production and also to withstand high temperature. (BeO was actually slightly better than just Be.)

Summarizing the design conditions for the anchoring points, the following criteria were imposed:

1) Uranium enrichment is 93.15% U-235 (which is generally more available than 97% enriched fuel used for SP-100).
2) External sliding reflectors for control use BeO as the reflecting material.
3) Reflectors extend axially to the midplane of the top and bottom axial BeO reflectors within the pins, which were approximately 4 cm long.
4) Pressure drop of helium/xenon gas flowing through reactor or reactor heat exchanger is about 3.5% of the absolute pressure (for the Brayton conversion system).
5) Reactivity at startup while cold is 1.015 plus projected burn up for 10 full-power years.
6) Reactivity at beginning of life when submerged under wet sand with no reflectors and flooded internally with water (and inside heat pipes but not inside the fuel pins) is 0.985.
7) Pressure vessel creeps less than 2% in 10 years at operating temperature and pressure.
8) Clad creeps less than 2% in 10 years at operating temperature and pressure.
9) Peak clad temperature is less than 1400 K.

For all reactor concepts, the particular version of the Sandia code called FEPSIM was used to model the gas flow pressure drop through the core or heat exchanger, the peak clad temperature, and the vessel and clad creep. The number of fuel pins, size of fuel pins, size of coolant passages, and pitch of pins were varied until a near-minimum mass was achieved consistent with the requirements just listed. To expedite meeting the reactivity requirement, the coolant volume fraction in the core was adjusted to be about 16%, because experience with neutronics calculations has shown that void fractions much higher than this causes excessive problems keeping the reactor subcritical under water immersion (and smaller void fractions result in excessive pressure drops). An additional constraint that arose recently is the need to keep the turbomachinery shaft speed at about 45,000 rpm or less. This imposes limitations on the gas pressure and helium content. The GCR

design was adjusted to meet this requirement also. The impact on the HPR and LMR is expected to be smaller than for the GCR, provided the pressure is around 200 psi or greater.

The LMR version of FEPSIM was used to tally masses for the LMR case but was not used to optimize the heat transfer and pressure drops in the flowing lithium. Rather, the various sizing runs listed in the LMR design data package, developed during the DOE SPFT program by using the Lockheed Martin code COROPT from the SP-100 program, were used and extrapolated to 1500 kWt. The extrapolated reactor geometry was then adjusted to meet the reactivity requirements.

The HPR version of FEPSIM was used to tally masses for the HPR case, but it does not handle the heat-transfer limitations of the HPR (which are a combination of axial limitations within the heat pipes and transverse conduction for a loss-of-heat-pipe scenario). However, there were comments on scaling in the HPR design data package that were used to estimate the geometry for the 1500-kWt case. The extrapolated reactor geometry was then adjusted to meet the reactivity requirements.

Table 2 shows a summary of the point-design reactor geometries and masses for the GCR, HPR, and LMR at 400 and 1500 kWt using the SP-100–sized fuel pins. The GCR masses are very high. That is because in this figure the fuel pins are forced to be close to the SP-100 pin diameters. The SP-100 pins were sized for liquid-metal-cooled reactors. Liquid metal has a considerably higher density

Table 2 Summary of the point-design reactor geometries and masses with SP-100–sized fuel pins

Reactor type	GCR	GCR	HPR	HPR	LMR	LMR
Enrichment, %	93	93	93	93	93	93
Thermal power, Brayton cycle, kW	400	1500	400	1500	400	1500
Inlet pressure, MPa	1.50	3.00	1.50	1.50	1.50	1.50
Number of fuel pins	757	757	381	610	673	727
Diameter of UN pellet, cm	0.72	0.80	0.79	0.79	0.63	0.61
Diameter of pressure vessel, cm	38.67	45.11	24.00	30.30	24.95	26.55
Outer diameter of radial reflector, cm	56.67	63.11	45.18	52.25	44.60	42.98
Reflector material	BeO	BeO	BeO	BeO	BeO	BeO
Length of active fuel in reactor, cm	52.00	52.00	56.00	56.00	43.00	56.00
Length of the pressure vessel, cm	104.17	110.61	64.00	64.00	65.09	97.04
Mass of the UN pellets, kg	219	273	142	228	121	164
Reactor, kg	867	1040	554	795	420	586
Radiation shield, kg	739	1155	515	610	444	672
Primary heat-transport system, kg	41	58	228.0	328.35	148.9	428.8
Reactor I&C, kg	140	140	140	140	140	140
Reentry shield, kg	65	80	57	57	40	50
Superstructure, kg	82	113	65	87	51	84
Reactor module, kg	1935	2586	1559	2018	1244	1961

and higher thermal conductivity than a helium-xenon gas mixture, and so a LMR does not need as thick a coolant boundary around the pins as the GCR does. So a GCR with SP-100–sized pins will have a larger total diameter than an LMR. The shield also would be larger and heavier. That is why a GCR has higher system mass with SP-100–sized fuel pins. In addition, any reactor that uses larger pins will have a larger fuel-pellet-to-clad ratio (if the clad thickness stays the same); consequently, the reactor can be made smaller in diameter because of less dilution of the uranium. The DOE SPFT team realized this and adjusted the pin size upward to a more appropriate value. The baseline case in the DOE SPFT DDP for GCR has 313 pins with a pin diameter of 1.06 cm for the 400-kWt case. With that pin diameter, the reactor module mass is 1567 kg.

This round of analyses showed that the GCR will pay a substantial mass penalty if it is forced to use fuel pins that were sized for a liquid-metal-cooled reactor. Larger pins are better. This makes better use of the high thermal conductivity of the UN fuel and allows a smaller void fraction, which helps maintain submerged subcriticality. It was later determined that the use of larger pins also reduces the mass of the LMR (while still meeting the other system requirements). The HPR also could likely be improved by this change at low powers, but at higher powers it might run up against another constraint. For the failed-heat pipe scenario, the HPR depends on thermal conduction of heat through the pin and along the clad to transport heat from the fuel pins surrounding the failed heat pipe to adjacent modules. Larger pins might exacerbate this problem and lead to unacceptable clad temperatures and thermal stresses.

The UN fuel pellet diameter for the SP-100 general flight unit design was 6.48 mm. The DDP LMR design assumed this UN pellet diameter, but the DDP designs for the HPR and GCR assumed larger diameters, so that already there was some assumed deviation from the established SP-100 designs. Further mass reductions could be achieved with even larger diameters, as much as two or three times the SP-100 size. This raises the question of the validation level of the larger pin sizes. Fortunately, the UN fuel is very good at retaining fission gases without much damage. Comparison of micrographs of indicated UO_2 fuels (1 atom percent burn-up) and UN fuel (6 atom percent burn-up) shows the marked superiority of the UN fuel. This comparison suggests that the large-diameter pins should perform well, especially at the expected burn-up of 4% or less. No matter what diameter pellet is chosen (even the established SP-100 size), it will need to be revalidated by an irradiation test because the fabrication line that makes those pellets will not be the same one that produced the pellets that were tested. (The original process line was dismantled at the end of the program.) This leaves open the possibility of validating two or more pellet sizes in parallel. (The database for the SP-100 baseline configuration with Nb1Zr clad and Re liner is fairly limited.) It is recognized that this approach will increase the fuel requalification time and cost, but it is anticipated that the perturbation will not be very large.

Figure 3 shows a comparison of the cross sections of the original 313-pin GCR DDP design and the smaller lower-mass version that uses only 85 pins with larger diameters. The larger-diameter fuel (1.67 cm diam) is smaller than the SNAP-10A fuel (3.1 cm diam). SNAP-10A used UZrH fuel rather than UN. Larger pins can be attractive from a handling and monitoring point of view.

FEPSIM-GCR is an Excel-based model that can be used to calculate the reactor characteristics of temperature, pressure drop, material creep, system masses, fuel

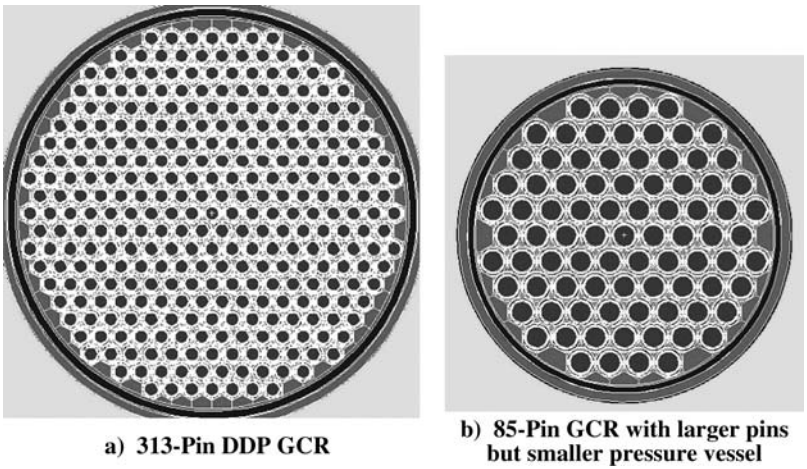


Fig. 3 Comparison of original GCR DDP and the lighter-weight option with larger pins.

burn-up, etc. But separate neutron transport calculations with the MCNP (Monte Carlo Neutronics Program) code must be performed to determine k_{eff} for every proposed geometry. This was awkward and severely limited the number of designs that could be considered. So numerous MCNP reactor criticality runs were performed to systematically vary the key GCR parameters and establish a data set of k_{eff} for various GCR configurations. From this set, we determined a multivariable quadratic formula for k_{eff}. This formula was inserted into FEPSIM, and with it we were able to create plots of reactor module mass vs number of pins in the reactor, as well as fuel pin diameter, Reynolds number, and peak clad temperature.

Figures 4–6 show the results of parameter scans for a 400-kWe direct-drive gas-cooled reactor system. Figure 4 shows the UN pellet diameter vs number of pins. With fewer pins, the pellet must have a larger diameter in order to have enough U-235 to go critical. Figure 7 shows the resulting peak clad temperature. SP-100 clad has been validated up to 1400 K, and there were some in-reactor tests run at 1500 K clad temperature without failure. The figure shows that acceptable clad temperatures are ensured for high system pressures. But for lower pressures (where the heat transfer is not as good), one must move to a greater number of smaller diameter pins. Figure 6 shows the Reynolds numbers. The Reynolds number approaches laminar regime for a large number of pins and small resulting channels. Figure 7 shows the resulting reactor module masses (including shield, controls, etc.). The large red circles show the cases that keep the clad temperature at around 1300 K (to leave 100 K of margin) for lower pressures. Figure 8 shows how the reactor module mass scales with pressure in the reactor. The red circles indicate the points that keep the clad temperature below 1300 K. It is not too sensitive until the mass approaches a cliff at about 150 psi. Figures 9 and 10 show similar plots for various reactor power levels.

Table 3 shows how the GCR system parameters vary for different pin diameters and number of pins.

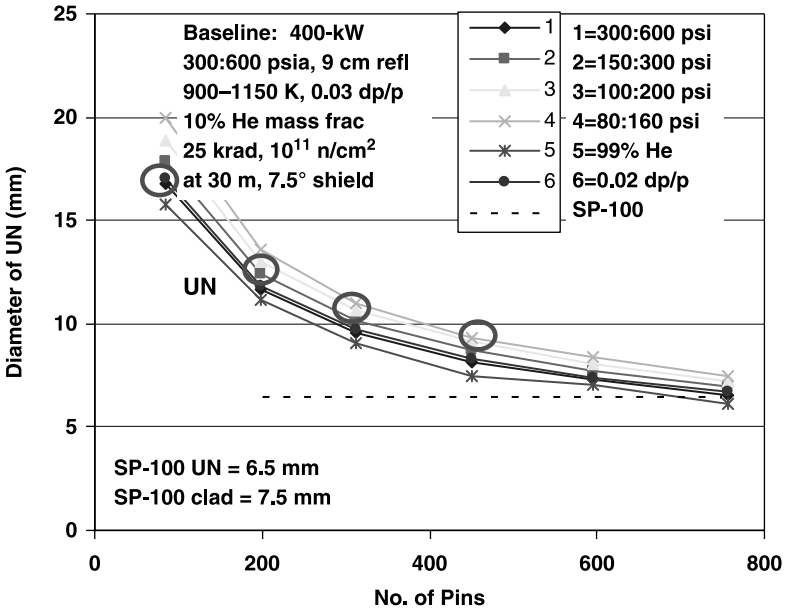


Fig. 4 Diameter of UN fuel pellet vs number of pins.

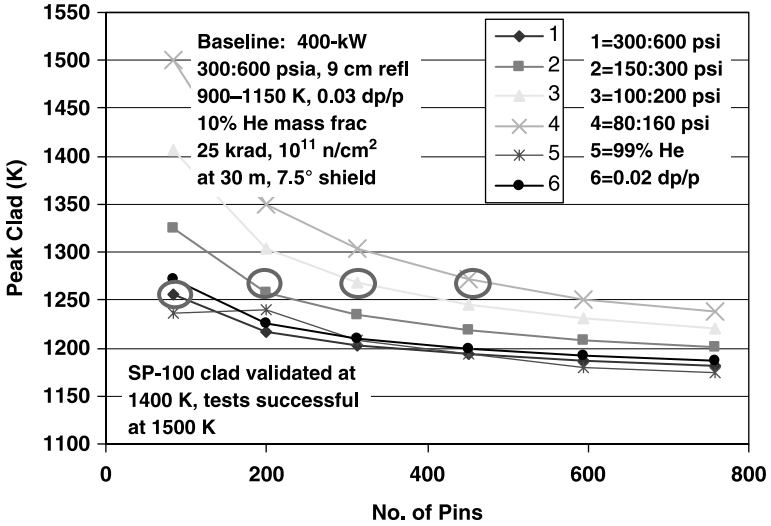


Fig. 5 Peak clad temperature vs number of pins.

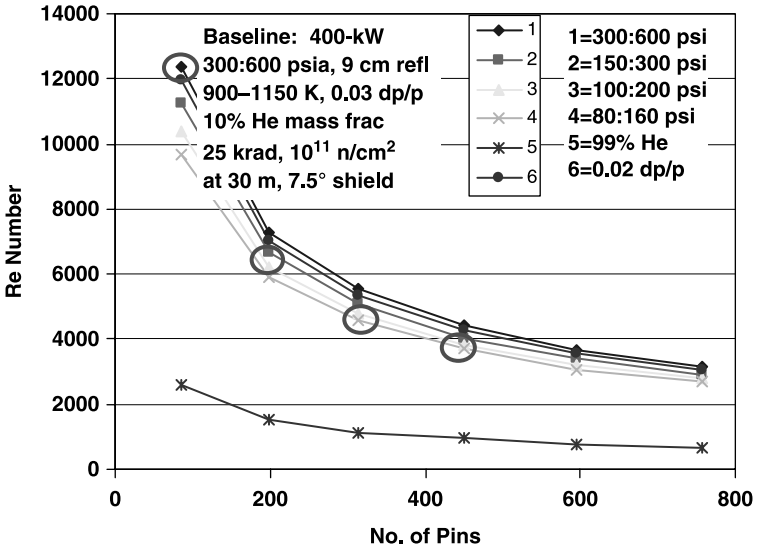


Fig. 6 Reynolds number vs number of pins.

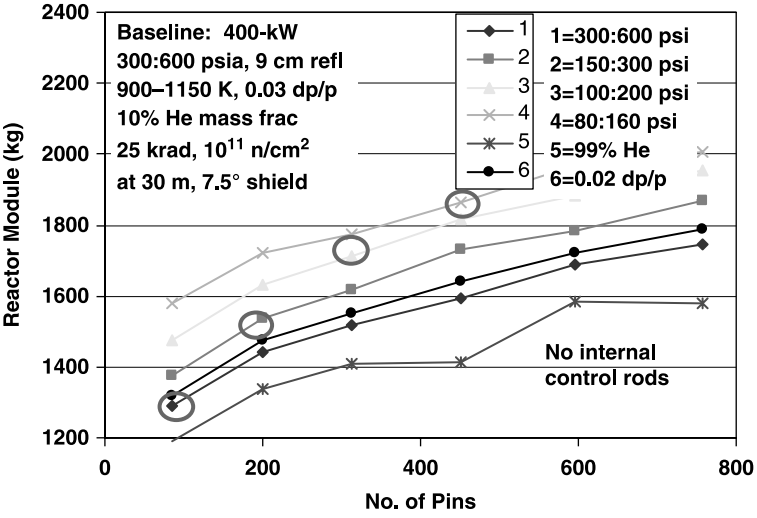


Fig. 7 Reactor module mass vs number of pins.

3. Model Validation and Results

Historic SP-100 design data were obtained to help validate the model for the LMR. In addition, detailed designs at 400 and 1500 kWt were developed using the DOE SPFT designs as starting points to anchor the model at those power levels for

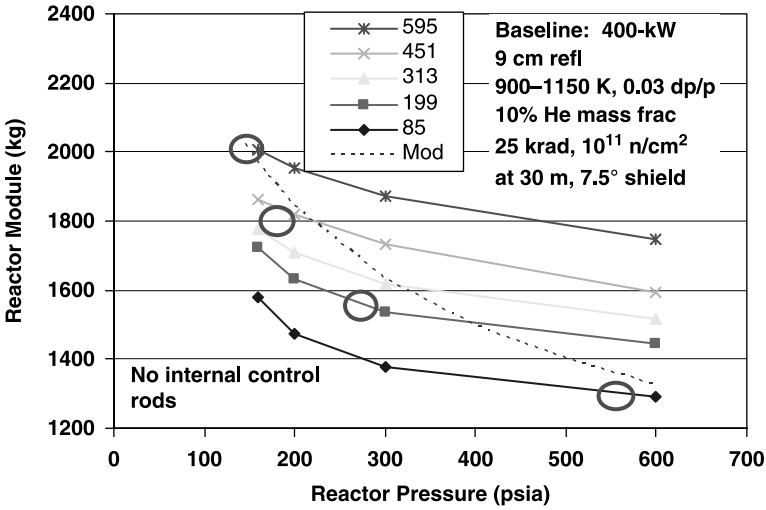


Fig. 8 Reactor module mass vs number of pins and pressure.

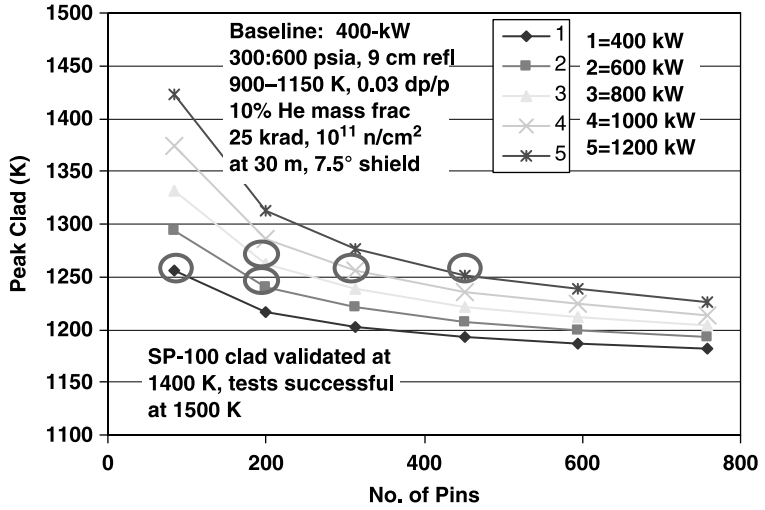


Fig. 9 Peak clad temperature vs number of pins and power.

all three reactor types. Figure 11 shows a comparison of the reactor model for the LMR with the historical SP-100 design data. Only the reactor is compared because often the mass of the primary heat transport system was not reported in the literature, and the mass of the shield is strongly dependent on the radiation design requirement and shield angle. Also shown are the four design points listed in the SPFT design data package for the LMR.

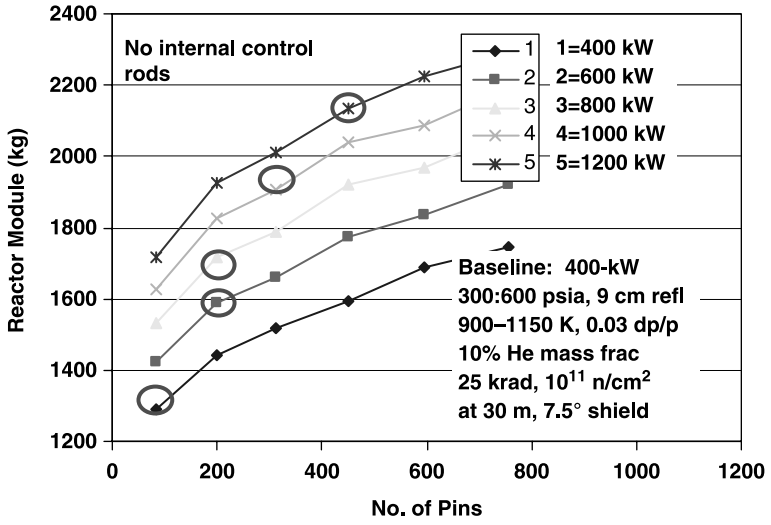


Fig. 10 Reactor module mass vs number of pins and power.

Figure 12 shows the reactor module mass (reactor, shield, heat transport, I&C, reentry shield, and superstructure) vs reactor thermal power for the three reactor types, assuming a Brayton power conversion system, that is, the reactor heat transport system includes a heat exchanger suitable for passing the heat to the working fluid of the Brayton system for the LMR and HPR. The GCR is directly coupled to the Brayton working fluid. Also included are the detailed design points for the three systems at 400 and 1500 kWt. For all of these systems, there is

Table 3 Summary of GCR parameters for different fuel pin sizes

	757-pin	313-pin	85-pin
Thermal power, kW	400	400	400
Helium fraction, mass %	10.0	10.0	10.0
Pressure, MPa	2.06	2.06	2.06
Pellet diameter, mm	7.0	10.2	17.8
Clad diameter, mm	9.2	12.7	21.1
Channel width, mm	0.64	0.92	1.56
Coolant volume fraction, %	16.7	18.0	19.3
Pressure drop fraction, %	3.0	3.0	3.0
Pressure vessel diameter, m	0.373	0.332	0.290
Reflectors diameter, m	0.555	0.514	0.472
Gas-clad temp diff, K	61.7	101.5	209.9
Peak clad temperature, K	1200.9	1234.0	1324.4
Peak fuel temperature, K	1213.4	1257.5	1387.1
Reactor module mass, kg	1870	1620	1377

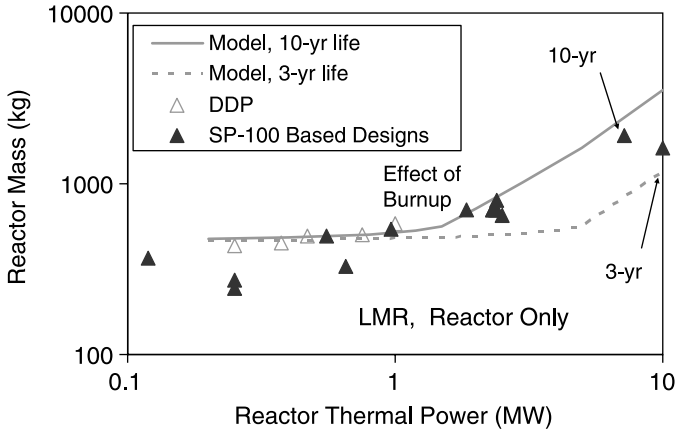


Fig. 11 Comparison of reactor element masses for historic SP-100 published calculations, SPFT DDP numbers, and present model.

assumed to be only one full-power heat exchanger (or equivalent). To support multiple rotating units, valving is used to connect the backup rotating unit flow into the heat exchanger. This minimizes the mass impact of using spare units. This is not the approach that we finally adopted; rather, we went to three separate heat exchangers. So that results in higher masses than what is shown here, except for the GCR direct drive system.

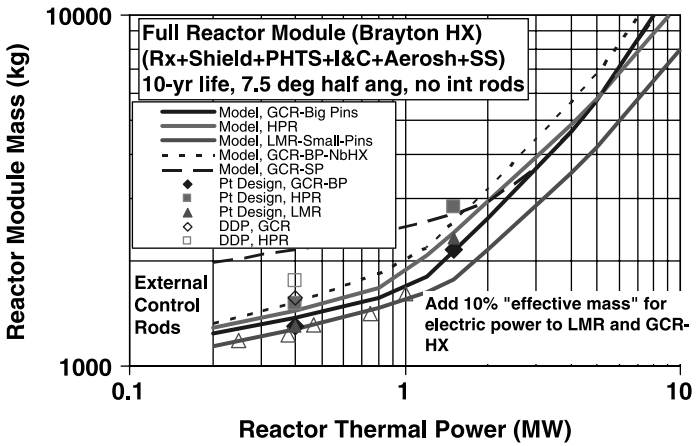


Fig. 12 Comparison of reactor module masses for Brayton conversion and various configuration options.

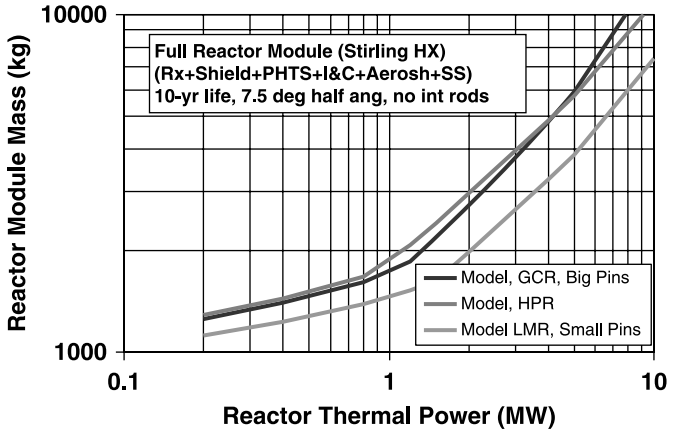


Fig. 13 Comparison of reactor module masses for Stirling conversion and various configuration options.

The module mass increases slowly with power for all systems up to about 1 MW. The reactor mass is essentially fixed because it is initially criticality limited, and the slow increase is caused by increasing heat-transfer requirements. Beyond 1 MW the reactor is burn-up limited. The requirement of 10 full-power years of reactor operation causes about 5% burn-up at about 1.5 MWt. This is about the limit of the fuel-validated database. For higher powers, the reactor fuel mass must increase linearly with power to keep the burn-up from exceeding the demonstrated 4% (6% has been demonstrated in fuel with W clad). This results in a nearly linear increase in module mass with power. Demonstrating higher burn-up capability in

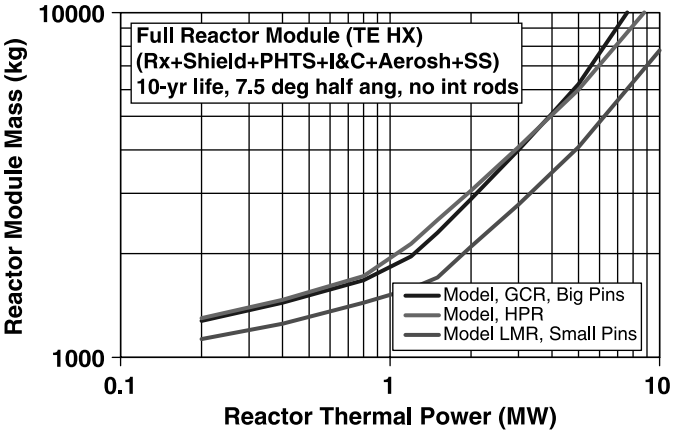


Fig. 14 Comparison of reactor module masses for thermoelectric conversion and various configuration options.

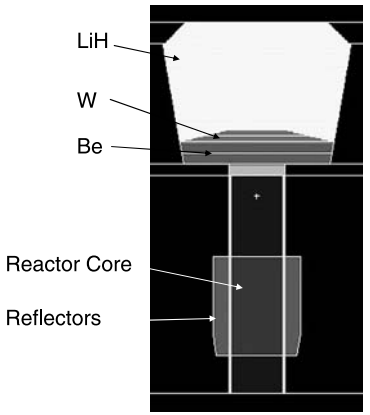


Fig. 15 Shield configuration for the dose model.

the fuel could push this limitation back. But one would still need to consider whether the resulting reactivity decrease with time could be accommodated with external control elements.

Figures 13 and 14 show similar results for the Stirling and thermoelectric conversion systems. The GCR uses large pins in these plots; for small pins options, consult previous plots and adjust accordingly.

C. Simple Shield Model

The Monte Carlo reactor and shield neutronics code MCNP was run numerous times for various configurations of shield materials. Figure 15 shows the fundamental configuration. From this database a simple formula was developed to model the amount of gamma dose and neutron fluence attenuation that would result from a given shield configuration. This, combined with mass formulaes based on geometry, yields a model for shield mass vs radiation attenuation and cone angle for the zone of protection. The coefficients are summarized in Table 4. They can be used to estimate the thicknesses of the Be, W, and LiH.

Table 4 Attenuation lengths, 1/*e*, for fast neutron fluence and gamma dose[a]

Material	Neutron attenuation, cm	Gamma attenuation, cm	Density, g/cc
Be	5.8	35	1.850
W	5.2	2.0	19.30
LiH	5.6	33	0.757

[a]Knowing the effective attenuation coefficient allows development of a simple shield model.

The attenuation lengths (where the flux falls by a factor of e), combined with the fact that the flux falls off with distance squared, yield a simple formula for the fluence and dose behind a conical shield if there are no other structures outside the shadow of that shield:

$$F_n = A_n \exp\left(\frac{-L_{\mathrm{Be}}}{\lambda_{\mathrm{nBe}}} + \frac{-L_{\mathrm{LiH}}}{\lambda_{\mathrm{nLiH}}} + \frac{-L_W}{\lambda_{\mathrm{nW}}}\right)\frac{P_r t_i}{L_p^2} \tag{1}$$

$$D_\gamma = A_\gamma \exp\left(\frac{-L_{\mathrm{Be}}}{\lambda_{\gamma\mathrm{Be}}} + \frac{-L_{\mathrm{LiH}}}{\lambda_{\gamma\mathrm{LiH}}} + \frac{-L_W}{\lambda_{\gamma W}}\right)\frac{P_r t_i}{L_p^2} \tag{2}$$

where A_n and A_γ are the fluence and dose coefficients (8.1×10^8 n/J and 0.30 rad cm^2/ J); λ_{nBe}, λ_{nLiH}, and λ_{nWe} are the attenuation lengths ($1/e$) for neutrons in Be, LiH, and W; λ_γBe, λ_γLiH, and $\lambda_\gamma W$ are the attenuation lengths for gammas in Be, LiH, and W; P_r is the reactor power; t_i is the reactor operation time; and L_p is the distance from the reactor to the payload.

If L_{Be} is fixed and known and the desired neutron fluence and gamma dose are specified, then these equations can be inverted to determine the length of LiH and W needed. Let C_n and C_γ be defined as follows to include the attenuation effect of the Be and of distance, plus the conversion from dose to full-power years of the reactor:

$$C_n = A_n \exp\left(\frac{-L_{\mathrm{Be}}}{\lambda_{\mathrm{nBe}}}\right)\frac{P_r t_i}{L_p^2} \tag{3}$$

$$C_\gamma = A_\gamma \exp\left(\frac{-L_{\mathrm{Be}}}{\lambda_{\gamma\mathrm{Be}}}\right)\frac{P_r t_i}{L_p^2} \tag{4}$$

Then the needed thicknesses of LiH and W are

$$L_{\mathrm{LiH}} = \lambda_{\mathrm{nLiH}}\lambda_{\gamma\mathrm{LiH}}\frac{\left[-\lambda_{\mathrm{nW}}\lambda\nu\left(F_n/C_n\right) + \lambda_{\gamma W}\lambda\nu\left(D_\gamma/C_\gamma\right)\right]}{\lambda_{\mathrm{nW}}\lambda_{\gamma\mathrm{LiH}} - \lambda_{\gamma W}\lambda_{\mathrm{nLiH}}} \tag{5}$$

$$L_W = \lambda_{\mathrm{nW}}\lambda_{\gamma W}\frac{\left[-\lambda_{\mathrm{nLiH}}\lambda\nu\left(F_n/C_n\right) - \lambda_{\gamma\mathrm{LiH}}\lambda\nu\left(D_\gamma/C_\gamma\right)\right]}{\lambda_{\mathrm{nW}}\lambda_{\gamma\mathrm{LiH}} - \lambda_{\gamma W}\lambda_{\mathrm{nLiH}}} \tag{6}$$

From this information, and the assumed angle of divergence, a first estimate of the mass of the shield can be made. Additional correction factors can be made for tapering the outer edges of the W or LiH, but this requires guidance from two-dimensional modeling.

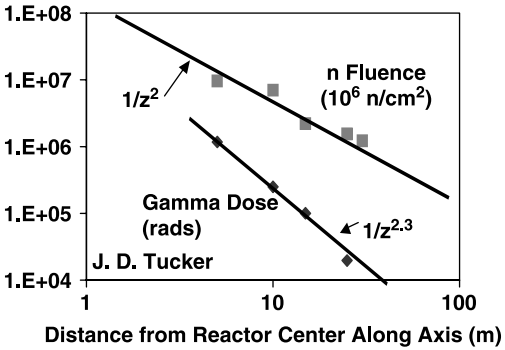


Fig. 16 Dose fall-off with distance.

More MCNP calculations were run to explore the dose around the spacecraft. To simplify things in these early stages, no credit was taken for the various structures in the spacecraft and science package body. The shielding benefit of spacecraft parts will not be too strong because neutrons and 1-MeV gammas from the reactor penetrate materials fairly readily. It was determined that beyond the shield the lifetime neutron fluence fell of with the inverse of distance from the reactor center to the second power, and that gamma dose fell off with the inverse of distance to the 2.3 power (because of view factors and the tapered gamma shield). It was also determined that at the edges of the shadow projected by the shield the dose and fluence changed strongly with radial position, and the rate of change was approximately exponential with radial distance (or angle). With these insights a simple radiation dose model was developed. Figure 16 shows the fall off of dose with distance from the reactor for a 400-kWt reactor. Figure 17 shows a plot for lifetime gamma dose (10 full-power years). Figure 18 shows the neutron fluence map. The maps show that the radiation shield reduces the neutron fluence by a factor of 30,000 and the gamma dose by a factor of 100.

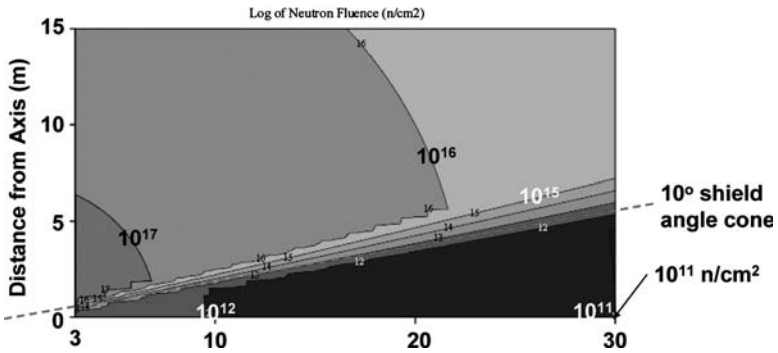


Fig. 17 Map of lifetime gamma doses.

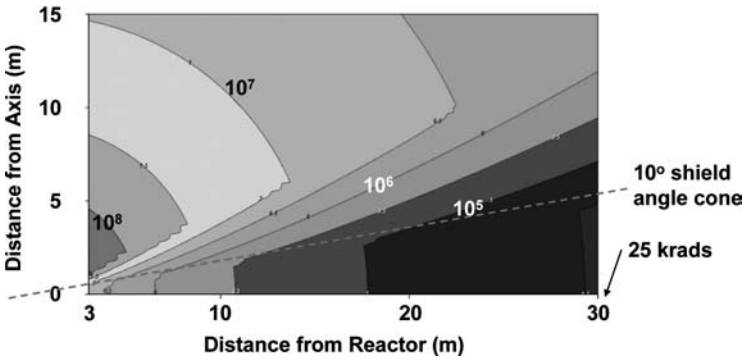
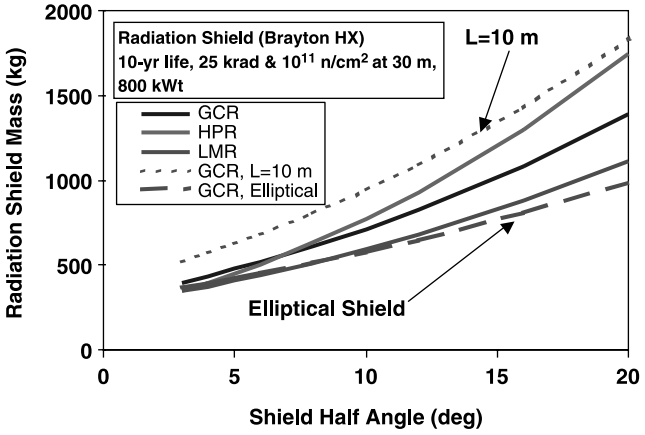


Fig. 18 Map of lifetime neutron fluences.

D. Shield Parametrics

The shield model was converted to Excel and included in the reactor module system model. The model was exercised to determined trends. Figure 19 shows the shield mass vs cone half-angle for 800-kW thermal reactors with Brayton conversion. Each reactor concept exhibits various virtues or liabilities associated with its particular design. The GCR is slightly larger, so that the shield mass is somewhat heavier. The reverse is true for the LMR. The HPR requires that the heat exchangers be between the reactor and shield. This increases the distance



Includes effect of HX helping to attenuate radiation
Assumes one 100% HX with valvingto spare converter
HPR has largest shield to accommodate HX between reactor & shield

Fig. 19 Shield mass for various configurations.

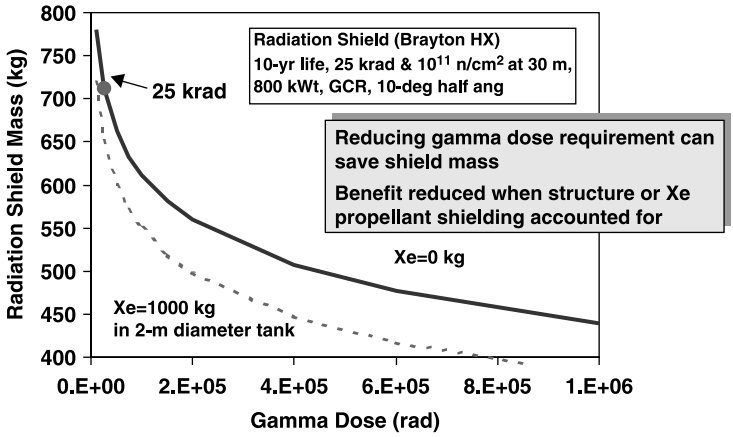


Fig. 20 Shield mass for different dose limits.

between the reactor and shield necessitating a larger shield in order to achieve the desired shielded protection area. Moving sensitive payloads closer to the shield makes the shield thicker and more mass. Using an elliptical shield (with half the angle transversely) reduces the mass slightly. Shield mass reduces when reducing the gamma dose (see Fig. 20).

Xenon or ammonia, both electric thruster propellants, can be used to augment the reactor radiation shield. A simple model was developed to determine the integrated dose or fluence vs time for a shield augmented by a tank of propellant in which the propellant was consumed at a constant rate. Figure 21 shows the resulting dose either with or without such an augmentation. The horizontal axis is in full-power years, so that it is assumed that the propellant consumption rate is proportional to the system power. The case is for an 800-kWt reactor, a 30-m

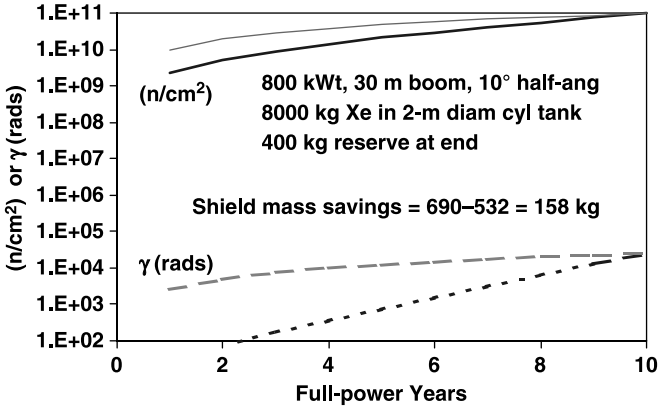


Fig. 21 Time-dependent dose and fluence behind xenon propellant tank.

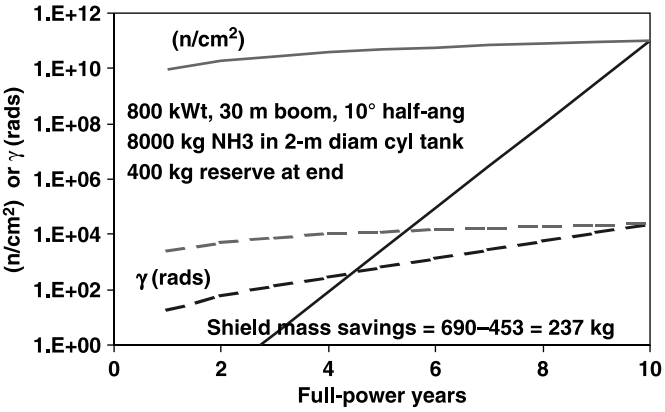


Fig. 22 Time-dependent dose and behind ammonia propellant tank.

boom, and 8000 kg of xenon initially in a 2-m-diam cylindrical tank. The xenon attenuation coefficient was taken from the shield model. The blue lines are for the augmented shield, and the magenta curves are for a shield without using propellant. The two fixed shields were adjusted so that the final doses were 25 krad and 10^{11} n/cm^2 at the end of 10 full-power years. The propellant consumption rate was assumed to be such that 400 kg of xenon would remain at the end of 10 years (reserve). Under these assumptions, the fixed shield would be 158 kg less mass for the augmented case.

The attenuation coefficient for neutrons and gammas through ammonia propellant was determined via MCNP runs. These coefficients were used to determine the integrated dose for shields augmented with ammonia shielding. The results are shown in Fig. 22. The mass savings in the fixed shield for this case is 237 kg. The extremely low neutron fluences at early times probably will not be achieved in reality because of leakage and scattering paths, but the final results at high fluences are approximately correct.

IV. Reactor Operation Startup

Accurate modeling of reactor transient behavior during operations and off-nominal conditions is essential to obtain a detailed understanding of performance. This, in turn, is important in ensuring public safety and mission assurance. Dynamic modeling also will lead to the design of safe and reliable modes of operation. Development of a dynamic model was performed using Next Generation of Space Transportation (NGST) Internal Research and Development funds; the details of that development are reported in a separate report on those internal research and design (IR&D) efforts. What is reported here is the application of that model to the three reactor types to help in the trade study comparisons. Detailed results for dynamic operations are not shown here; however, Fig. 23 shows the results of detailed startup models on the time required to achieve full-power operations with each reactor concept, assuming a Brayton conversion system.

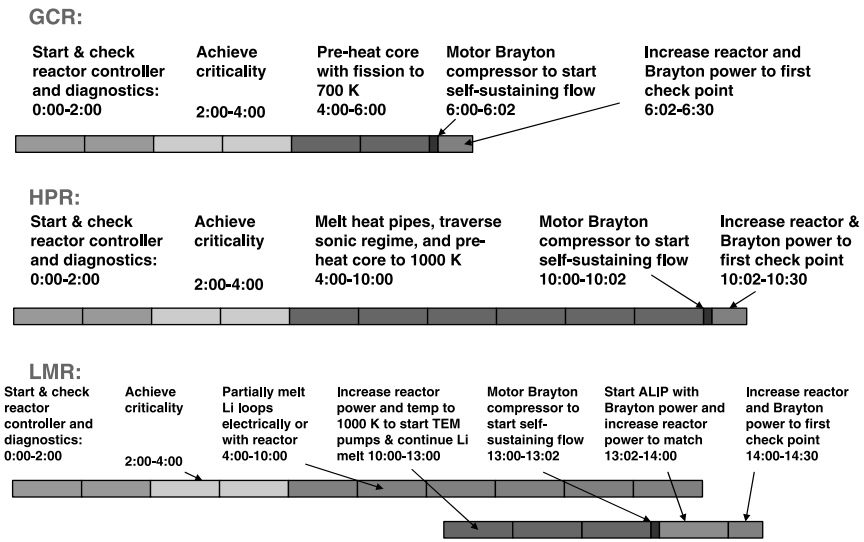


Fig. 23 Approximate startup timelines.

The dynamic modeling suggests that the Brayton system can start up very rapidly if the structures are preheated with a temperature difference between the turbine inlet structures (e.g., the reactor, or reactor heat exchanger and ducts, and the radiator heat exchanger). Operational experience with Brayton units (such as auxiliary power systems) supports this suggestion. The characteristic timescale is that needed to establish a pressure difference with the compressor and to start cooling the gas locally. If the structures are preheated, it is expected that the Brayton system will become self-sustaining in less than a minute of motoring the compressor (via the alternator).

So, the proposed startup sequence for the reactor and turbomachinery is as follows:

1) Bring the reactor to a critical state but at a very low power level such that any heat generated can be removed by conduction and radiated to space. Nominally this is less than a kilowatt of thermal power.
2) For an LMR, use this low power to help melt the lithium in the system. This must be done slowly, over a period of hours, to prevent damage of the piping and vessel during melt expansion.
3) Slowly raise the reactor temperature to suitable temperature for Brayton startup. This is around 500 K or 600 K, and let the reactor and heat exchanger reach thermal equilibrium. Again, the reactor power is fairly low at this point, nominally about a kilowatt.
4) Motor the Brayton compressor (via the alternator) to begin Brayton flow and simultaneously start the flow in the radiator coolant pumps. Keep the load to the PMAD (Power management and distribution) as low as possible at first, and adjust as needed to keep the turbomachinery from overspinning. The

turbomachinery should become self-sustaining in a minute or less. If the system fails to start, stop motoring, recharge the startup batteries via the solar arrays, and try again. Increase reactor power and temperature if needed.

V. Conclusions

Based upon detailed work for the JIMO (the NASA Jupiter Iced Moon Orbiter) program, it is likely that any of the reactor configurations can be engineered. Depending upon the concept evaluation figures of merit, for example, the things that evaluators deem to be important, one concept can be easily selected above another. No space reactor in this thermal or electric power range has been ever operated before; consequently, it would appear prudent to select a concept with the fewest unresolved risks in order to achieve operations within a feasible time frame. For this reason, the GCR appears to hold an advantage. It was straightforward to meet all known safety criteria, although there remain some uncertainties regarding impact criticality. Achieving most safety requirements necessitated a modest increase in mass for the reactor system. However, to put this in context, it can be estimated that the reactor and power conversion system could weigh perhaps 2200 kg. This is to be compared to a nearly equivalent mass for the radiator and associated plumbing and to a very significant mass for electrical power conditioning equipment and electric thrusters. It would not be unreasonable to force the reactor design team to work very hard to achieve a 200-kg mass reduction, whereas simply changing the radiator topology could reduce mass by several hundreds to perhaps a thousand kilograms. Ultimately, this becomes a very involved systems engineering process, the results of which might be highly dependent upon the end application (mission).

There appears to be no reason why a nuclear reactor–based power system in the 100–1000 kWe class could not be built, deployed, and operated. A more significant issue will be maintaining the necessary funding support to carry the project through fruition. Although not prescient, after the initial draft of this report was written, NASA terminated the JIMO. This occurred for a variety of reasons, but most likely was the large demand upon agency funding for projects such a shuttle return to flight, ISS assembly completion, shuttle retirement, Hubble repair, ongoing exploration demands, the crew exploration vehicle, and the crew launch vehicle. Several commercial firms are interested in pursuing nuclear electric propulsion for commercially viable missions.

Reference

[1] Marshall, A. C., "RSMASS-D Models: An Improved Method for Estimating Reactor and Shield Mass for Space Reactor Applications," Sandia National Lab., Rept. SAND91-7826, Albuquerque, NM, 1997.

Copyrighted Materials
Copyright © 2008 AIAA Retrieved from www.knovel.com

Chapter 6

Nuclear Safety: Legal Aspects and Policy Recommendations

Roger X. Lenard*
Little Prairie Services, Edgewood, New Mexico

I. Finding 1: Space Nuclear Power and Energy Have Important Historic and Pivotal Future Roles in Space Exploration

MANY missions that have been carried out owe their very existence to the availability of nuclear energy. There is little doubt that the information from Galileo, Cassini, Magellan, and the Pioneer probes has been of inestimable scientific and even social value. In the case of the Pioneer probes, a whole new regime of data has been opened by the so-called anomalous acceleration effect. These probes all enjoy the use of the nearly inexhaustible energy of nuclear fuel, which is most useful in areas deficient in solar flux, but utilitarian under other extremes as well. Although solar energy has played a major role in the development of space, there are certain areas where the utility of solar power has achieved its limit, for example, in the cases of Mars Exploration Rovers (MER). These devices are performing magnificiently, but their utility is limited by the available power and sensitivity to dust; hence, the next generation of rovers, the Mars Science Laboratories (MSL) will employ small radioisotope thermoelectric generators (RTG) as a source of electricity and thermal energy in order to significantly expand their utility envelope. Further, the Space Exploration Initiative announced by President Bush will require surface nuclear-power, almost certainly nuclear electric propulsion (NEP) and potentially nuclear thermal propulsion (NTP). NASA's Project Prometheus, although with reduced funding, is completing phase A, reaching toward a NEP spacecraft capable of navigating and orbiting the icy moons of the Jovian system.

The material presented in this chapter is updated from the paper published in *Acta Astronautica*, "Nuclear Safety, Legal Aspects and Policy Recommendations for Space Nuclear Power and Propulsion Systems," Vol. 59, No. 1–5, 2006, pp. 398–412, and is reproduced with permission. Copyright © 2008 by the author. Published by the American Institute of Aeronautics and Astronautics, Inc., with permission.

*Chief Technical Manager.

The space exploration program, for example, might involve the employment of surface nuclear-power systems for enabling an exploration-rich lunar or Mars exploration program because of the surfeit of solar energy in many locations, but also as a cost-effectiveness gesture. The many competing factors in any exploration enterprise typically are traded against cost of the project. The human and robotic space exploration effort in the United States is hampered in the early years by a set of infrastructural and exploration-related budgetary demands, which include shuttle return to flight, the crew exploration vehicle, and its return to the moon initiative, International Space Station assembly complete, Hubble robotic repair, the ongoing Mars robotic exploration initiative, as well as a large array of NASA Center support requirements. Thus, only a small amount of funding will be available to support new exploration venues. What should the investment profile be? What are the technical aggregates with the highest leverage in terms of safety and cost? How are these factors to be weighed? These overarching systems-architecture issues can enable the implementation of an exploration-rich venue if correct investments in power technologies are made. The seminal question is: why nuclear-power systems for an exploration-rich venue? The answer itself is many faceted, but a few examples can be fashioned in the main. We have many competent analyses indicating that the cost of a given crewed lunar mission can be reduced by ~50% (uplift costs) if in situ resources are used for only replacing the return propellant oxygen. This reduction is possible because for a cryogenic system, approximately 85% of the propellant mass is oxygen, and the mass necessary to get the payload off the moon and on the return leg to Earth must be carried from the surface of the Earth all of the way to the lunar surface. The mass multiplier is significant, yet it could be even more compelling for Mars transportation. This considerable reduction applies only to round-trip payloads, and for one-way missions other avenues must be investigated. A second area is that of replenishing life-support gases such as oxygen and nitrogen. Oxygen is used at the rate of almost 1 kg per day per crew member, not including airlock or extraventricular-activity (EVA) losses. A crew of six on a 600-day mission consumes substantial, ~3600 kg oxygen. Additionally, each crew member consumes approximately 3–4 kg of food and substantial quantities of water each day. These resources must either be carried to the target world or generated in situ. At the moon and Mars, copious quantities of water are bound up in various mineral formations; on Mars, subsurface water might be abundant. In all cases, whether because of propellant production, food generation, life-support replenishment, or normal system losses, large amounts of power are essential if for no other reason than cost reduction. Thus, it appears that nuclear-power must be used if cost-effective surface exploration is to become a reality [1–3].

The utility of nuclear electric propulsion has been analyzed for cost reduction of commercial satellite transportation and more recently for support of the lunar Mars exploration project. The use of a commercially viable NEP system could reduce costs for transporting the cargo segment by ~50%; this is as significant a cost reduction for one-way payloads as the use of in-situ resource utilization (ISRU) lunar oxygen is for round-trip payloads. Nuclear thermal propulsion has similar advantages in crew safety by dramatically reducing transportation time to

Mars for a given initial mass in low Earth orbit (IMLEO), a commonly employed metric for cost, because one of the most costly segments of the exploration enterprise is in Earth-to-orbit transportation.

II. Finding 2: To Implement Space Nuclear Power and Propulsion It Must Be Perceived to be Safe by the General Population

The utility of nuclear-power is almost axiomatic; however, nuclear-power has a slightly blemished reputation; only a very small fraction of this impeachment is deserved or justified. These blemishes on an otherwise impressive history have created a perception among a small group of antinuclear aficionados that all nuclear-power in space is either unsafe or has some clandestine military function. As with the introduction of many new technologies, nuclear-power has experienced a learning curve. Early in its infancy, the totality of nuclear system hazards was not well understood, and some operational, administrative, design bases, and implementation procedures did not appreciate the potential risks associated with its early use. Over time, and, in some respects, as a consequence of some high-profile accidents, more well-defined procedures began to be developed. The United Nations Committee on the Peaceful Uses of Outer Space (COPOUS) generated the statement of principle [4] that has codified the world body's consensus on this subject. The United States has a well-established set of regulations and policy guidelines including NSC/PD-25 [5], the National Environmental Policy Act, and the Interagency Nuclear Safety Review Panel (INSRP) as mechanisms to ensure from a design basis and from an independent administrative and operational safety review that the space systems are safe. Typically, the INSRP employs an approach where are credible accidents are analyzed and the risks enumerated. Other international treaties and principles also apply, including the Outer Space Treaty [6], United States Space Policy [7], Return of Astronauts and Objects from Outer Space [8], The Registration Convention [9], the Non Proliferation Treaty [10], and the Liability Treaty [11]. All of these have some bearing on what a state's party can or cannot do with respect to their activities in outer space. Some, such as the Outer Space and Liability Treaty, are actual treaties, and in the United States carry force of law when ratified by the United States Senate; some, such as the Astronaut Return are codified as agreements; others, such as the Principle 3, are only conventions and are not ratified and are therefore considered as guidelines. Finally, still other documents, such as the nefarious Moon Treaty, have only a few signatories and are almost never recognized. Noncredible incidents with high potential consequence are also assessed to ascertain if some consequence or frequency limiting factor can be applied to the mission without compromising science objectives.

The policies in the United States have led to a very impressive array of safe, highly successful missions powered by nuclear RTG missions. Although not all of the United Nation's COPOUS principles are met by the letter, they are met in the spirit of the U.S. policy approach. For this reason, it is useful to review the applicable policies and principles.

III. Finding 3: Existing Policies and Procedures are Adequate for Achieving Requirements of Public Safety and Environmental Compliance

A. History, Perspectives, and Objectives

A total of 44 U.S. radioisotope power sources were deployed into space between 1961 and 1997. The United States has experienced a few failures with RTGs; however, some of the their plutonium sources have been recovered, and the radioisotope containment system has worked as designed, preventing the release of the radioisotope fuel. The United States also launched the SNAP-10A reactor into space in 1965. Although the United States has carried out a number of space reactor programs since 1965, none of these subsequent programs led to a space-deployed reactor system, and none completed the launch safety review process. The former Soviet Union (SU) developed and flew approximately 38 nuclear reactors for a variety of defense-related programs. Two of these missions resulted in an accidental reentry as a result of failure of the end-of-life boost rocket engine. The former SU also deployed a number of RTGs, one of which ended in a failure to achieve desired orbit, namely, the Mars 96 probe. The final impact site for this mission is not known, although it is conjectured to have landed either in Chile or the south Pacific Ocean. In total, there have been many more RTG-powered missions than reactor missions worldwide. As a consequence, particularly in the West, the safety approach is not as well established for space reactors as it is for space-based radioisotope sources. Space nuclear safety considerations for reactor systems differ significantly from those for radioisotope sources.

The principal safety issue for a radioisotope source is the possibility of accidental release of the highly radioactive fuel. For reactors, however, the radioactive inventory at launch is typically very small, and the principle safety concern is the possibility of an inadvertent criticality. The low radioactive inventory is a consequence of the requirement that no preflight operation of the flight reactor at substantial power should be accomplished; consequently, no fission product inventory will be contained in the fuel at launch. Zero-power critical operation is allowed to calibrate the reactor, if necessary. Zero-power operations produce effectively no fission product inventory.

Safety considerations for space reactors are also very different from those for terrestrial reactors. For terrestrial reactors, much attention is given to the possibility of fission product and actinide release into Earth's biosphere following a postulated accident. A space reactor does not, in general, pose a threat to Earth's biosphere after deployment in high orbit. Operations of a reactor in lower Earth orbits do present a risk, and mitigating effects should be followed in cases where the reactor might be operated in lower Earth orbits. Additionally, a significant safety advantage can result if space reactors are required to remain subcritical (with no previous high-power operation) until safely deployed in space. On the other hand, terrestrial reactors have not been subject to postulated propellant fires and explosions or high-speed impact, although these scenarios are now being investigated as the potential for terrorist threats has increased. Herein we propose some recommendations that will assist in clarifying the meaning of some existing procedures, principles, and policies, and will also aid in space systems engineering where nuclear power sources may be involved.

It is imperative that whatever complexion the space nuclear mission might assume, the program makes a clear distinction between space-related safety considerations and other important considerations. Here the scope of space nuclear safety is defined to include protection of the public, workers, astronauts, and Earth's environment from radiation or radioisotopes produced by or contained in the space reactor system or components following the delivery of the reactor system to the launch processing location. Although in the United States, the Interagency Nuclear Safety Review Panel (INSRP) does not address nonradiological safety issues for space nuclear systems, these issues are included in this discussion as well as an additional point to be considered in promulgating the benefits of space nuclear systems. Reactor system operational failures must be prevented to ensure mission success; however, an operational failure that does not threaten Earth's biosphere or its inhabitants is not considered a safety issue. In the recent past, several highly visible Mars probe failures have led to a mistaken focus of mission success and safety: this must be avoided because it will lead to completely unnecessary and highly expensive mission assurance features being raised to safety proportions. Safeguarding special nuclear materials and threats to the space environment, and, if surface nuclear systems are deployed, adequate precautions to protect the celestial surface are also important considerations that must be addressed by the program. Some of these issues are discussed later. Nonetheless, neither safeguards nor space environment protection issues are or should be included as safety issues. It is necessary to make these distinctions to ensure that safety standards are not applied to programmatic manifestations that do not directly affect safety and to ensure that all safety activities are focused on safety issues.

Great care must be used to ensure that the nuclear safety program addresses the unique safety issues and approaches appropriate for space reactors. In addition to the safety guidance provided by the mission sponsor, basic guidance has been established by an interagency Nuclear Safety Policy Working Group (NSPWG) [12] that can be adapted to many space reactor programs. The original NSPWG guidelines were developed for a piloted nuclear propulsion mission to Mars; consequently, the guidelines have been somewhat modified to apply to the overall space exploration mission, including noncrewed civil space and commercial space missions that might eventuate. These guidelines, summarized here, will serve as an overarching guideline for nuclear safety planning, as a recent example, a JIMO (Jupiter Iced Moon Orbiter) space reactor system.

B. Safety Guidelines and Implementation

The following recommendations should be considered to effectively implement a nuclear reactor safety program that is perceived by the public to be rigorous. Some of these are codified by the Nuclear Safety Policy Working Group but are modified in some ways in these recommendations to be more transparent and utilitarian to the space-system architect. Others have been added to clarify more adequately parameters that might aid in mission design. These recommendations are primarily for space reactors because there is widespread acceptance of RTG safety requirements and policies.

Recommendation 1: The reactor shall not be operated prior to space deployment, except for low-power testing on the ground, from which negligible radioactivity is produced.

The purpose for low-power testing is to make sure that the reactor critical configuration is within design and safety limits and to calibrate the control system. This guidance is already part of the existing operating framework.

Recommendation 2: The reactor system shall be designed to remain shut down prior to the system achieving its planned orbit.

This guideline is part of the presently proposed operating protocols. Administratively, dual-fault-tolerant criticality inhibitions will be used for the reactor system. These can take various forms, including positive control drive lock-outs and reflector drive blocks, for example. Consideration should be given to providing some form of authenticated, two-man control logic with encryption key firewalls to prevent hacking into the systems' control scheme. Further, the same two-man authentication logic ought to also be applied to overall spacecraft commands so that no potential for unauthorized commands to change orbits, reenter or cause collision potential can be performed.

Recommendation 3: Inadvertent criticality shall be precluded for credible accident conditions. Inadvertent criticality can be ensured through passive features (poisons and safety rods) or through active disassembly as part of the launch system's flight termination system.

Design requirements and design features must be implemented to meet this criterion. During a launch, a number of accident scenarios appear to be credible. The most credible accident is a launch-system failure. These occur at a rate of ~0.05–0.1 of launches. During a launch-system accident, details discussed later, the reactor power system can be subjected to fireballs, overpressures, propellant fires, impacts with hard surfaces, and immersion in water or burial in wet or dry sand. Each of these possibilities must be adequately analyzed and designed so that the reactor remains subcritical during these insults. A preliminary analysis suggests the possibility that for some highly contrived compaction accidents the reactor can quickly pass through a supercritical condition with no significant consequences. If further analysis demonstrates that momentary criticality does not compromise safety, the basic guidelines can be modified to include this possibility.

Another, more important approach to resolving both safety and safeguards related concerns would be to install conventional dismantlement approaches to the reactor system as part of the launch vehicle's flight termination system (FTS). This concept was investigated fairly thoroughly by Sandia National Laboratories as part of the JIMO program for the Naval Reactors Prime Contract Team. The FTS has a demonstrated reliability of 0.99999995 for the first stage and 0.99999992 for the second stage. The concept here is that the reactor would be energetically, but not in a nuclear sense, dismantled as part of the FTS operations for a failed launch. Launch vehicles are already considered a very hazardous practice, and the FTS is designed to preclude a highly hazardous system from impacting areas where any damage could result. If the reactor is split into two or more fragments (depending upon the amount of uranium present), it simply cannot become critical.

This approach would most likely address safeguards concerns because there is insufficient highly enriched uranium to provide an attractive target for diversion. Active disassembly eliminates any feasible concerns that the reactor could become critical during a launch accident. It is important to understand that the unique features of a reactor (near-zero radioactive source term at launch) enable this feature. This approach is not applicable to RTGs, which contain a very high source term at launch, and every effort must be made to prevent the spread of the radioactive heat source.

Recommendation 4: Radiological release from the spacecraft during normal operation shall have an insignificant effect on Earth.

No credible mechanism that can result in radiological consequences on Earth as a result of operations in space has been identified. This safety guideline has been expanded to include no radiological release as a consequence of normal startup, operations, or shutdown whether the reactor is in space or on the surface of another celestial body. Consideration to expanding this to include contamination of other celestial bodies should be discussed.

Recommendation 5: The consequence on Earth of a radiological release from an accident in space shall be insignificant.

Mission operation and mission planning for the proposed space program shall be performed to analyze credible accident scenarios that could result in a radiological release to Earth from an accident in space. The approach to this requirement is to minimize the potential for unplanned reentries to an extremely low probability through orbit selection and highly reliable spacecraft propulsion, emergency orbit-raising capabilities, and the spacecraft's attitude control system. To assist the spacecraft design process, consideration to stating definitive frequency of failure, for example, that the probability of an unplanned reentry be $<10^{-7}$, would dramatically assist in the space-system design process. Such a minimal probability is likely adequate for all cases except those involving the most grave of consequences. It is also necessary to carefully plan flybys past the moon on the departure leg because the moon's gravitational influence could dramatically perturb the spacecraft's trajectory. The latter condition is primarily a consideration for nuclear electric propulsion systems with attendant low acceleration levels.

Recommendation 6: Safe disposal of spent nuclear systems shall be explicitly included in mission planning.

Until the present time, all space nuclear reactor systems have been operated in Earth orbit. The space exploration program will present the possibility of space reactor systems departing Earth orbit on a variety of mission scenarios, and also with sample return missions, the potential for nuclear systems to reenter Earth orbit from lunar or interplanetary space missions. Because of the experience with the former Soviet Union "Cosmos" satellites reactor systems leaking cesium and NaK coolant resulting in substantive debris formation, disposal outside Earth orbits should be considered if possible. Deep-space disposal should be accompanied by detailed orbital analyses to ensure that Earth orbit crossings are highly

unlikely. Detailed orbit analyses should be performed to ensure that gravitational anomalies from other planetary bodies, the moons of any planet that the nuclear-power system is orbiting, and the tidal forces of the celestial body being orbited or flown by would not force the departure of the space reactor system out of from its orbit or depart significantly from its intended flyby trajectory.

Recommendation 6a: Disposal beyond Earth orbit in non-Earth crossing orbits should be considered where feasible.

Recommendation 6b: The probability of Earth vicinity return of any disposed asset should be of a time frame consistent with the decay of fission products to about the level of the actinides. This terminology is more well defined in recommendation 6c.

Recommendation 6c: The total body burden source term of the in-space decayed fission products should not exceed the approximate actinide body burden of the reactor.

The term "to about the level of the actinides" contained in United Nations Principle 3 is an important guideline but is a vague recommendation; we recommend that the TEDE (total effective dose equivalent) burden of the fission products be no greater than the reactor's initial actinide TEDE inventory.

Recommendation 6d: Disposal by active dismantlement should be considered as a mission option.

Recommendation 7: Planned or intentional Earth reentry shall be precluded from mission profiles at this time.

Planned Earth reentries of a space nuclear reactor system are proscribed from mission planning at this time. The benefits of a planned reentry must clearly outweigh the associated risks.

Recommendation 8: Both the probability and the consequences of an inadvertent reentry shall be made as low as reasonably achievable.

Careful design, detailed deterministic analysis, risk analysis, and testing will be conducted to meet this guideline. As a consideration, defense in depth to preclude any high probability reentry should be applied. The inadvertent reentry condition applies primarily to either a fresh reactor, whose reentry represents no radiological, but a safeguards consequence, or a previously operated reactor, which represents little safeguards consequence, but potentially high radiological consequence. To minimize risk, the probability for inadvertent reentry should be minimized. The probability of inadvertent reentry is a function of many factors, including operating orbit, mission scenarios, potential for MMOD damage, and defense in depth. The following recommendations should be used as a guide to designers and mission planners:

Recommendation 8a: A reactor that is operated in or above a sufficiently high orbit (SHO) (approximately 800 km) should be configured to remain in that orbit for approximately the lifetime of the fission products to decay in accordance with recommendation 6c. If such an orbital lifetime cannot be achieved through spacecraft configuration control, then a reliable system (failure probability $\Pi_f < 10^{-5}$) should be installed to boost the orbit to an orbit whose lifetime is consistent with recommendation 6c.

Recommendation 8b: A reactor power system operated below a SHO but above the 50% of the SHO lifetime shall have a highly reliable emergency orbit raising system whose integrated Π_f, such that $\Pi_f < 10^{-.6}$.

Recommendation 8c: A reactor power system operated below a 50% SHO lifetime, but above 5% SHO lifetime, shall have a highly reliable emergency orbit-raising system whose integrated probability of failure Π_f *is such that* $\Pi_f < 10^{-7}$.

This reliability level can be generated through multiple independent systems

Recommendation 8d: Routine operation of a space nuclear-power system below 300 km should be avoided if operationally feasible; periodic operations to 300 km might be justifiable if risk is well controlled.

Recommendation 9: For inadvertent reentry through the atmosphere, the reactor shall be analyzed to ascertain the highest likelihood reentry condition. It is desirable for the reactor to remain essentially intact or an essentially full dispersal of radioactive materials at high altitude will result unless this consideration results in lower reliability or compromises safety or operations in other ways.

This criterion might be required to cover a multitude of design, administrative, and operational considerations. The primary concern is of a space reactor utilizing a highly enriched uranium core, reentering, and becoming a safeguards issue. This consideration, post-9/11, dominates almost every other administrative and operational concern. Many different approaches are being considered to address this issue, including the use of lower enrichment uranium reactors for space missions in order to make the reactor less attractive regarding diversion. Of course, the longer the reactor has operated, the less attractive as a diversion item it becomes; on the other hand, it represents a greater safety hazard. The employment of active disassembly to guarantee dispersal at high altitudes should be a serious consideration because this approach would eliminate the uncertainties associated with the reentry of the reactor as compromised by mission-specific equipment. Studies of this approach have been made in the past (see recommendation 11). Under such scenarios where safeguards are not an issue, other requirements could render this condition of substantially lower importance.

Recommendation 10: The reactor shall remain subcritical throughout an inadvertent reentry and Earth impact.

This design requirement is design specific but is an important space nuclear system design requirement. A preliminary analysis suggests the possibility that for some highly contrived compaction accidents the reactor can quickly pass through a supercritical condition with no significant consequences. If further analysis demonstrates that momentary criticality does not compromise safety, the basic guidelines can be modified to include this possibility. Again, energetic disassembly as part of the flight termination system should be considered as a design option (see recommendation 11).

Recommendation 11: For any credible Earth impact scenario, radioactivity should be confined to a local area to limit radiological consequences. A variety of passive, active, or a combination of features can be employed to achieve this result.

To meet mission design requirements, accidental reentries of a nuclear reactor should be kept to ~10^{-7} or below if the system contains a fission product inventory

that is substantially greater than the TEDE of the contained at-launch actinides. If the reactor remains intact throughout the reentry, care should be applied to limit the spread of radioactivity. There exist a number of approaches to meeting the preceding criteria along with launch accident subcriticality and other major safety and nuclear safeguards concerns. The NERVA program postulated the explosive disassembly, into small fragments, of the NERVA rocket engine, should a hot reentry be a mission potential [13]. From a safety and safeguard perspective, the envelope of an intentional disassembly should be considered seriously for all phases of flight. During the launch phase, active disassembly precludes unintended criticality no mater how prone to criticality the reactor might be in a given accident outcome condition. Further, a highly dispersed core represents no safeguards threat because the enriched uranium is too highly diluted in the environment. During reentry conditions, the JIMO program agonized over how to ensure an intact reentry without jeopardizing other aspects of launch safety or compromising operational performance. Further, it became apparent that there was little control over the initial reentry configuration. These uncertainties combined to result in a staggeringly large number of possible reentry accident initiating conditions, each with a dramatically different and highly unpredictable outcome condition. The problem was how to comply with recommendations 10 and 11 in a rigorous fashion. The independent assertion that active disassembly is a feasible option was a watershed moment in the initial concept design cycle. A high-altitude explosive disassembly could likely guarantee virtual complete dispersal into very small fragments that represent little to no public risk. In essence, a completely independent variable has not been introduced into the design parameter space. Design tools for explosive packages have achieved a high degree of fidelity, and test facilities exist to validate the code results; consequently, the system can be designed to result in any degree of dispersal of radioactive material from a reentering reactor system that might be required.

Recommendation 12: For surface-power reactor systems, the reactor shall not be operated at significant power prior to landing on the surface of another celestial body unless the mission planning cannot be readily accomplished otherwise.

Surface nuclear reactor power systems can be landed on celestial objects where human presence is extant or planned. To preclude potential for exposure to radiation or contamination by fission products or other isotopes, the surface power reactor should not be operated prior to landing.

Recommendation 12a: Surface-power reactors where humans are or will be present should be adequately shielded prior to operation so that radiation dose to individuals routinely habiting the site is ~1 mrem/h. This is well below the annual dose limit to astronauts of 50 rem/year, but still leaves margin for other sources of dose. (Approximately 2-m lunar regolith shielding should be sufficient for most cases; 3-m thickness is entirely adequate.) The space program should also thoroughly review the data available on radiation hormesis to ascertain what optimum shielding levels might be for space systems.

Recommendation 12b: Surface-power reactors should be located remotely from the site of routine habitation to enhance shielding and to preclude adverse

consequences of a landing accident at the reactor site that releases radiation. (A nominal distance of 1 km has been used in most analyses.)

Recommendation 12c: A rover-mounted radiation sensor should be included in a regolith mover that maps the radiation fields at low reactor power levels and supplementary shielding added to locations of inadequate neutron or gamma shielding.

Recommendation 12d: A well-delineated no-occupancy zone should be enforced for habitats, rovers, or EVAs that will prevent inadvertent incursion into a reactor generated radiation area.

Recommendation 12e: If a nuclear reactor system is operated on the surface of another celestial body where humans are not or will not be present, operations and end-of-life disposal consideration should minimize the insult to the celestial system where feasible.

Recommendation 12f: Initial surface nuclear reactors should be made as reliable as possible; however, if maintenance is required, the combination of robotic, telepresence, or direct human intervention might be necessary. However, dose levels should apply the ALARA principle during such situations.

Recommendation 13: Any in-space nuclear-power or-propulsion system shall not enter within a keep-out zone of any inhabited structure so that astronauts, crew, or workers will not be exposed to an enhanced radiation environment.

The preceding is intended as an administrative control over space nuclear systems operations. If close proximity to a radiation source is unavoidable for abbreviated periods of time, then specific approval will be required by the mission commander or other authority.

Recommendation 14: Any space nuclear system returning to Earth orbit shall have positive two-man, authenticated control established over the reactor and spacecraft with secure communications links established. Any space nuclear system returning to Earth orbit shall have all main and backup propulsion systems operational, and there shall be no system or component failures that could compromise a highly reliable SHO or above maintenance and control capability.

Recommendation 15: Disposal of a space nuclear system that is operating on the surface of another world shall be decommissioned and entombed to adequately comply with planetary protection objectives.

IV. Finding 4: The Existing Processes for Design, Fabrication, and Test, Including Safety Analysis are Adequate for Pre-Launch Safety and Environmental Compliance

The terrestrial nuclear-power industry in the West is well established, with well-understood design, fabrication, test, and transportation procedures. During recent studies and analyses, it was determined that most, if not all of the design, fabrication, test, and transportation to the launch site scenarios are adequately covered by existing rules, regulations, policies, and requirements. However, there exist new areas of risk once the reactor system has arrived at the launch site. For this reason, we here investigate potential postshipment scenarios an perform an initial screening as to probability and consequence of that scenario. Potential

postshipment accidents that could lead to the release of radiation or nuclear material are addressed in this section. The basic safety issues for a space reactor mission are fresh fuel dispersal and accidental criticality. The probability of accidental criticality is expected to be very small, and with active dispersal mechanisms can be made virtually nonexistent through all flight phases; nonetheless, the potential consequences of an inadvertent criticality are expected to be far more significant than accidental fresh fuel dispersal; consequently, the active dispersal approach is preferred. This, of course, will result in dispersal of fresh fuel during a launch-phase accident. Although dispersal of fresh fuel does not entail a high risk, the issue must be addressed in detail. Scenarios relating to radiologically hot fuel dispersal are not expected to be credible; however, these scenarios must be studied to ensure that their probability is extremely low and that active dispersal techniques are included in the scenario analysis. The sequences will be divided into prelaunch, a series of launch and deployment scenarios, and postdeployment situations including surface activities. Because credible accident scenarios for the launch and deployment into Earth orbit are similar for both nuclear electric and nuclear thermal propulsion, as well as for surface nuclear-power systems, all will be treated in an equivalent way through these phases of flight. Surface-power systems will be differentiated during the landing and operations phases.

Recommendation 16: The space nuclear reactor program should concentrate on major postshipment activity and accident categories.

Figure 1 depicts the general sequence of events for a space system once it has arrived at Cape Canaveral Air Force Station (CCAFS) or other launch site.

For these sequences, the principal types of possible accidents can be categorized as follows: 1) fresh fuel dispersal consisting of impact accidents with fuel or reactor assembly, explosion-driven fuel dispersal, and overheating in fire environment; and 2) accidental criticality consisting of compaction accidents, flooding/reflection accidents, movement of control/safety elements, and fuel loading accident.

The scenarios for these postulated accident categories are discussed by mission phase in the following.

A. Arrival at Launch Site: Possible Scenarios

After the reactor system arrives at the launch site, the system must be moved to a processing facility, removed from the shipping container, and installed at the facility for checkout and postarrival integration and testing. Possible accident scenarios that could lead to fuel dispersal or accidental criticality during these manipulations are summarized in the following: 1) fresh fuel dispersal consisting of transportation accident; dropping while handling with crane, forklift, or manual handling; impact by vehicle or heavy equipment, such as a forklift or falling heavy equipment; storage facility or nearby vehicle explosion or fire; terrorist activities; or impacts as a result of natural disasters (tornadoes, hurricanes, earthquakes); 2) accidental criticality—compaction accidents consisting of transportation accident; dropping while handling with crane or forklift; impact

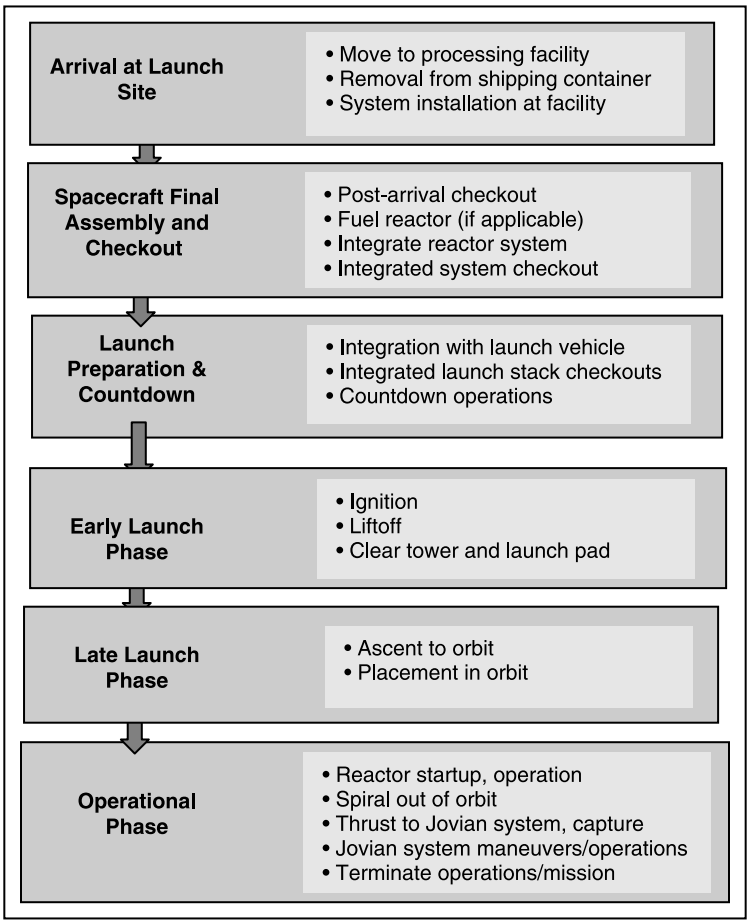


Fig. 1 Sequence of events at the launch site.

by vehicle or heavy equipment, such as a forklift or falling heavy equipment; storage facility or nearby vehicle explosion or fire; terrorist activities; or impacts as a result of natural disasters (tornadoes, hurricanes, earthquakes); and 3) accidental criticality—flooding/reflection accidents consisting of fuel falling into moderating fluid as a result of transportation or handling accident or natural disaster; assembled unsealed reactor accidentally flooded by moderating fluid; impact accident breaches pressure vessel followed by flooding; accidental criticality—movement of control/safety elements; impact as a result of transportation or handling accident or natural disaster causes movement of control/safety elements; explosion or fire causes movement of control/safety elements; or terrorist activities.

B. Spacecraft Final Assembly and Checkout: Possible Scenarios

Possible scenarios for this phase are similar to the preceding phase. Additional scenarios must be considered if fuel loading takes place at the launch site: 1) fresh fuel dispersal consisting of transportation accident; dropping while handling with crane, forklift, or manual handling; impact by vehicle or heavy equipment, such as a forklift or falling heavy equipment; terrorist activities; or impacts as a result of natural disasters (tornadoes, hurricanes, earthquakes); 2) accidental criticality—compaction accidents consisting of transportation accident; dropping while handling with crane or forklift; impact by vehicle or heavy equipment during assembly; storage facility or nearby vehicle explosion or fire; terrorist activities; or impacts as a result of natural disasters (tornadoes, hurricanes, earthquakes); 3) accidental criticality—reactor fuel loading accident (if performed at launch site) consisting of improper fuel loading; fuel elements dropped on fully loaded reactor; or control element withdrawn beyond critical during $1/\mu$ (neutron lifetime measurements in approach to critical experiments) measurements or criticality testing; 4) accidental criticality—flooding/reflection or compaction accidents consisting of assembled unsealed reactor accidentally flooded by moderating fluid (if not sealed during preceding phase); impact accident breaches pressure vessel followed by flooding; or reactor dropped or heavy load falls on reactor; and 5) accidental criticality—movement of control/safety elements consisting of assembly mistake causing movement of control/safety elements; explosion or fire causes movement of control/safety elements; spurious or unintentional signal causing control or safety element movement; or terrorist activities.

C. Launch Preparation and Countdown: Possible Scenarios

In addition to many of the scenarios present for the preceding phases, propellant fire and explosion scenarios must be considered for launch preparation: 1) fresh fuel dispersal consisting of dropping while handling with crane, forklift, or manual handling; impact by vehicle or heavy equipment, such as a forklift or falling heavy equipment; propellant explosion impact with launchpad; propellant explosion shrapnel impact; propellant fire, pressure vessel and fuel integrity loss, dispersal of fresh fuel; or propellant fire, collapse of launch vehicle, impact with launchpad; 2) accidental criticality—compaction accidents consisting of propellant explosion impact with launchpad; reactor dropped or heavy load falls on reactor; or propellant fire, collapse of launch vehicle, impact with launchpad; 3) accidental criticality—flooding/reflection accidents consisting of propellant explosion impact with launchpad, breach pressure vessel, subsequent flooding by water or propellant; or propellant fire, collapse of launch vehicle, impact with launchpad, breach pressure vessel, subsequent flooding by water or propellant; and 4) accidental criticality—movement of control/safety elements consisting of impact with launchpad causing movement of control/safety elements; propellant explosion, subsequent impact, or fragment impact causes movement of control/safety elements; propellant fire, collapsing impact causes movement of control/safety elements; propellant fire, thermally induced movement of control/safety elements; other types of explosions or fires causing movement of control/safety elements; or spurious or unintentional signal causing control or safety element movement.

D. Early Launch Phase: Possible Scenarios

The early launch phase (assumed from the United States) begins with launch-vehicle ignition and ends when the projected impact point passes from land to ocean water: 1) fresh fuel dispersal consisting of propellant explosion impact with launchpad; propellant explosion shrapnel impact; propellant fire, pressure vessel and fuel integrity loss, dispersal of fresh fuel; propellant fire, collapse of launch vehicle, impact with launchpad; launch-vehicle fall-back or tip-over impact; command destruct and impact; or launch failure, sand impact; 2) accidental criticality—compaction accidents consisting of propellant explosion impact with launchpad; propellant fire, collapse of launch vehicle, impact with launchpad; launch-vehicle fall-back or tip-over impact; command destruct and impact; or launch failure, sand impact, water impact; 3) accidental criticality—flooding/reflection accidents consisting of propellant explosion impact with launchpad, breach pressure vessel, subsequent flooding by water or propellant; propellant fire, collapse of launch vehicle, impact with launchpad, breach pressure vessel, subsequent flooding by water or propellant; or launch-vehicle fall-back or tip-over impact, breach pressure vessel, subsequent flooding by water or propellant; and 4) accidental criticality—movement of control/safety elements consisting of impact with launchpad causing movement of control/safety elements; or propellant explosion, subsequent impact, or fragment impact causes movement of control/safety elements.

E. Late Launch Phase: Possible Scenarios

This phase begins after clearing land and includes ascent as well as placement into orbit: 1) fresh fuel dispersal consisting of propellant explosion shrapnel impact; deployment failure, ocean impact; deployment failure, land impact; or deployment failure, reentry heating dispersal; 2) accidental criticality—flooding/reflection accidents consisting of deployment failure, ocean impact, subsequent flooding by ocean water; deployment failure, land impact, subsequent flooding by water; or deployment failure, land or water impact compaction reactivity increase; and 3) accidental criticality—movement of control/safety elements consisting of deployment failure, impact, causing movement of control/safety elements.

V. Finding 5: The Safety and Operations Phase for NEP or NTP Systems Should Be Developed so as to Maximize Possible Scenarios for Space Nuclear Reactor Employment

Flight operations include reactor startup, rise to full-power operation, electric propulsion or direct thermal propulsion, departure from Earth orbit, in-flight operations, celestial system capture, transfer trajectories, maneuvering, operations, return trajectories (if performed), Earth orbit capture (if performed), subsequent mission performance, and final disposal and decommissioning. Because all activities subsequent to Earth orbit represent effectively no risk to Earth's biosphere unless a return trajectory is involved, we will not regard them as a safety issue. The possible scenarios for NEP are shown in Fig. 2, whereas operational scenarios for NTP are shown in Fig. 3.

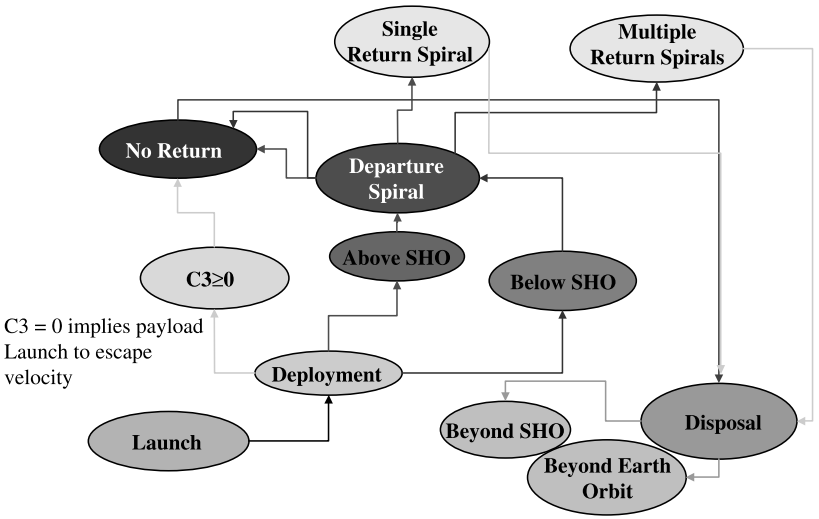


Fig. 2 Possible operational modes for NEP.

The distinction between the two systems is inherent in the difference between high-thrust and low-thrust systems. Generally, NTP systems are considered high thrust, and NEP systems are considered low-thrust systems. For purposes of this distinction, any total space system with a thrust-to-weight ratio $>10^{-1}$ g can be considered high thrust, in that the time over which ΔV added to perform the thrusting maneuver is small compared to the time of an orbit. However, at this time, no

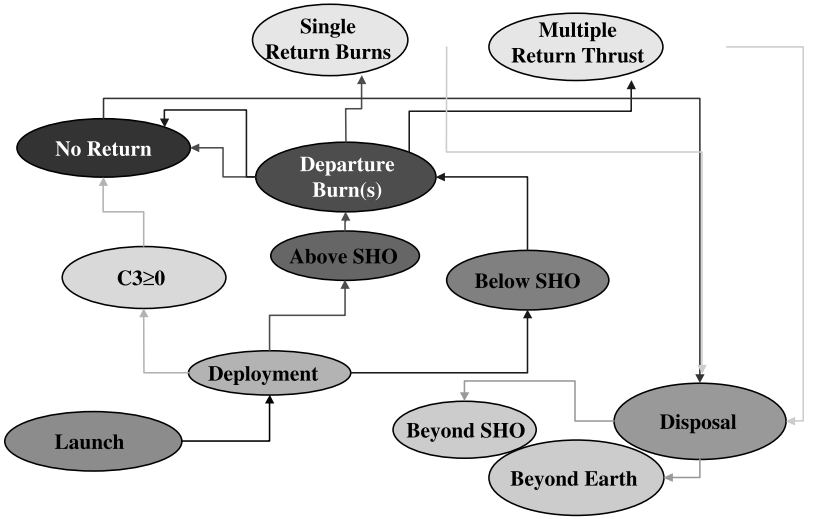


Fig. 3 Possible NTP operational modes.

known electric propulsion systems fall into a high-thrust category. It is also possible for an NTP system to operate below 10^{-1} g; consequently, to reduce gravity losses, multiple perigee burns might be necessary. These distinctions are reflected in Fig. 3.

Recommendation 17: Hazards and risks definitions should be presented in a consistent fashion throughout the space nuclear reactor program.

Ultimately, independent safety reviewers and the public are the consumers of safety and environmental compliance documentation; therefore, these documents should have a common format that is readily comprehensible. To the reader familiar with the Cassini Final Safety Report Analysis (FSAR) format, we have initially listed our definitions in the Cassini FSAR format. For example, the Cassini FSAR has apportioned pad/postlaunch credible scenarios into the major event bins and configurations shown in Fig. 4. Although this division is an acceptable approach, it is not completely commensurate with the hazards tables that have been generally defined; however, we employ this format as a transition to the hazards tables format that has been used thus far. First, we define vehicle codes that represent the various phases of vehicle assembly and operations through payload deployment (see Table 1).

A. Scenario Bins from Cassini FSAR Format

From the preceding generic binning, we establish a set of failures that can appear to result in release of radiation or nuclear material as shown in Table 2. The failures and formats are those used in the Cassini FSAR. Although this particular division of activities will not be used in our final hazards assessment format, it is indicative of our process. This table relates the preceding activity bins with launch-vehicle configurations so that a credible risk analysis can be performed.

From the preceding, certain credible events can occur that could result in the release of radiation or nuclear material. From the hazards tables already submitted, we take the general category series LV-XX-YY (covering nuclear spacecraft integration with launch vehicle to cover all pad accidents and scenarios including accidental destruct under configuration 0 or 1).

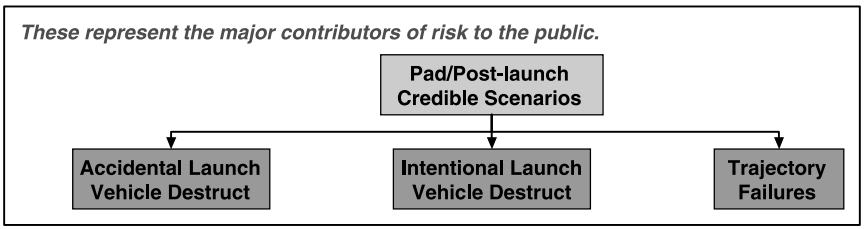


Fig. 4 Division of scenarios.

Table 1 Launch-vehicle and spacecraft configuration codes

Vehicle code	JIMO system configuration
−2	Launch vehicle, no propellants [first-stage main first-stage strap-ons (if used)], upper stage(s), SP/NEP/NTP[a] vehicle (fueled) separate from launch vehicle no payload fairing)
−1	Launch vehicle, no propellants [first-stage main first-stage strap-ons (if used)], upper stage(s), SP/NEP/NTP vehicle (fueled) separate from launch vehicle in payload fairing)
0	Launch vehicle, no propellants [first-stage main first-stage strap-ons (if used)], upper stage(s), SP/NEP/NTP vehicle (fueled, payload fairing)
1	Launch vehicle, fully fueled [first-stage main first-stage strap-ons (if used)], upper stage(s), SP/NEP/NTP vehicle (fueled, payload fairing)
2	Launch vehicle, fully fueled [first-stage, upper stage, SP/NEP/NTP vehicle (Fueled), Payload Fairing], post strap-on separation
4	SP/NEP/NTP spacecraft (fueled, first and upper stage, payload fairing separation)
5	SP/NEP/NTP spacecraft and upper stage only
6	SP/NEP/NTP spacecraft only

[a]SP = surface power; NEP= nuclear electric propulsion; NTP = nuclear thermal propulsion.

Under the general hazards tables category series LV (just mentioned) and LA (launch, ascent, and on-orbit activities prior to reactor startup), vehicle configurations 1 through 6 are germane under both accidental and intentional launch-vehicle failure/destruct, and trajectory failures are covered. The hazards tables cover additional scenarios, including on-orbit and in-space activities. We prefer covering activity bins in the hazards tables format because the end scenario is reasonably independent of the pathway to the failure-analysis pathway, although the probabilities associated with the failure might be different in the case of accidental vs intentional launch-vehicle destruct. Also, the scenarios as just listed are not independent, in view of the fact that when a trajectory failure occurs, once the failure propagates beyond a given point, either an auto-destruct or a manual destruct is initiated. Further, trajectory failures will likely have markedly different failure probabilities for the launch, ascent, and orbital deployment phase vs the on-orbit/in-space portion of the activities. Therefore, we rewrite the Table 2 in the hazards format formulation.

B. Conversion of Hazard Categories from Cassini FSAR Format to Hazards Table Format

This alternative binning process results in fewer bins to assess and appears to document a more operationally realistic approach. These scenarios/hazard bins represent JIMO system activities until the vehicle is in orbit around the Jovian system. From a safety perspective, we stop the hazards-analysis process at that point because the JIMO system cannot return to Earth in any credible scenario. In each of the preceding scenarios, a category of failures can occur. These are listed in Table 3 with respect to launch-vehicle/spacecraft configuration.

Table 2 Failure modes in Cassini FSAR format for JIMO configurations: radiation or nuclear material release scenarios

	System configuration	
Scenario bin	2	1
Accidental spacecraft/launch-vehicle failure		
Intentional spacecraft/launch-vehicle destruct		
Trajectory failure		

C. Failure Events That Could Result in Release of Radiation/Nuclear Material

For each of the hazard bins, we now categorize a set of failures that could result in a release of radiation or nuclear material (Tables 4 and 5). In these cases, the initiating events are listed in a nomenclature of LV-XX-YY, where the XX is a two-letter designator for such incidents as inadvertent criticality, or radiation exposure or fission product/isotope release, and the YY is the numerical identifier of independent initiators.

During integration activities with the launch vehicle, only configurations 0 and 1 are feasible, and certain impact scenarios are eliminated because of CCAFS restrictions and limitations on where integration activities are performed. Each of the preceding scenarios will have a group of initiating events that must be analyzed separately.

VI. Finding 6: Safety Assessment for Additional Risks Posed by Lunar and Mars Base Mission Scenarios Indicates That Space Reactor Systems Can Be Used Safely and Effectively on the Surfaces of Other Celestial Bodies

Table 6 identifies hazards by activity for the lunar and Mars base power system. The scenarios could apply in an equivalent way to other celestial bodies. Although the nuclear-power subsystem from a NEP system could be used, including the

Table 3 Hazards table and SP/NEP/NTP space-system configuration codes: Conversion of Cassini FSAR to hazards tables format

	System configuration								
Scenario/hazard bin	−2	−1	0	1	2	3	4	5	6
LV-XX-YY: JIMO integration with launch vehicle	**X**	**X**	**X**	**X**					
LA-XX-YY: launch, ascent and orbit insertion prior to reactor startup				**X**	**X**	**X**	**X**		
OO-XX-YY: on-orbit and in-space activities after reactor startup									**X**

Table 4 Credible scenarios during SP/NEP/NTP spacecraft/ launch-vehicle integration phase

LV-XX-YY: JIMO integration with launch vehicle failure Mode	System Configuration						
	−2	−1	0	1	2	3	4
Reactor hard surface impact	**X**	**X**	**X**	**X**			
Reactor water impact				**X**			
Reactor ground impact	**X**	**X**	**X**	**X**			
Reactor dry sand impact							
Reactor wet sand impact							
On-pad explosion				**X**			
JIMO propellant explosion	**X**	**X**	**X**	**X**			
Accidental criticality	**X**	**X**	**X**	**X**			

reactor, controls, payload shield, primary heat transport and power conversion system in a fashion essentially unchanged, there are several additions, primarily to compensate for the impact of lunar or Mars dust and materials as well as atmospheric constituents on exposed high-temperature materials. Also, there are numerous other activities that can result in problems. There are differences between the lunar base power systems in that although the lunar base system might only need to be singly contained or, with a superalloy system, simply contained to prevent lunar dust from contacting reactor moving parts, while on Mars the system might (depending upon materials the system is made from) be hermetically sealed. According to design considerations, the power system is to be located approximately 1 km from the central base complex to reduce potential radiation levels. Routine human activity, rover activity, and regularly scheduled take and landing activities will occur. These activities represent initiating events for safety incidents. The selected groups form areas that are new types of activities based on an enumeration of potential hazardous actions.

Table 5 Credible scenarios during launch, ascent (JIMO system configuration vs prelaunch scenarios)

LA-XX-YY; launch, ascent and on-orbit activities prior to reactor startup failure mode	System configuration						
	−2	−1	0	1	2	3	4
Reactor hard surface impact				**X**	**X**	**X**	**X**
Reactor water impact				**X**	**X**	**X**	**X**
Reactor ground impact				**X**	**X**	**X**	**X**
Reactor dry sand impact				**X**	**X**	**X**	**X**
Reactor wet sand impact				**X**	**X**	**X**	**X**
JIMO propellant explosion				**X**	**X**	**X**	**X**
Accidental criticality				**X**	**X**	**X**	**X**
Suborbital reentry				**X**	**X**	**X**	**X**
Orbital reentry							**X**

Table 6 Lunar or Mars base nuclear-power station hazards

	Mars base power system landing	Mars base NPS startup	Mars base NPS operations	Mars base standby/ dormancy	Decommission-ing/ disposal
Fission product/ isotope release	**X**	**X**	**X**	**X**	**X**
Contamination of personnel			**X**	**X**	**X**
Radiation exposure			**X**	**X**	**X**
Inadvertent criticality	**X**	**X**	**X**	**X**	**X**
Inadvertent reentry	**X**				
Damage to spacecraft	**X**	**X**	**X**	**X**	
Damage to facilities	**X**				

Recommendation 18: Serious and competent design studies for the use of a nuclear reactor for base-load power at a lunar and Mars base should begin immediately to ascertain the power levels and duty factors that might be required for such a system.

There are many studies present about power requirements for a lunar and Mars base. For the human exploration of space to become viable, it must be more cost effective as well as scientifically productive. The use of in situ resources for life-support closure and propellant production can well lead to dramatic cost reductions while maintaining a high level of science return. However, such practices will require substantial levels of surface power in locations where solar energy is not the most viable candidate. Determining the requirements for a nuclear-power system so competent design studies can process is a necessity.

VII. Finding 7: Definable Surface Nuclear Power System Hazards Can Be Defined and Associated Risks Can Be Mitigated

A. Primary Differences Between Cargo and Robotic Payload NEP System and a Moon or Mars Base Power System That Can Impact Safety

1) Routine human activity in the local area is different.

2) Routine crew of robotic activity in the area is non-existent or very different from nuclear electric propulsion systems.

3) A portion of the reactor shield is composed of Mars soils via burial at the power station location; the quality and uniformity of the lunar regolith or Mars

soils used shielding are unknown and could be highly variable, impacting the shielding quality factor.

4) Regularly scheduled takeoffs and landing events are needed to support the Mars base.

5) A vertical mast and radiator boom assembly is needed to eliminate waste heat on the moon and to incorporate a forced Mars convection radiator for power production on Mars.

1. Potential Safety Issues Associated with the Mars Base Power System

Once the moon or Mars base power system has safely landed on the surface of the desired celestial bodys, it represents no hazards to Earth or its biosphere. All hazards are localized to the immediate environs of the moon or Mars, or any other world where the nuclear-power system is located, activities that can be conducted by humans in the vicinity of the power system, activities of crewed or remotely controlled rovers in the vicinity of the power system, and potential for impacts from routine takeoffs and landings of moon or Mars ascent/descent vehicles. For purposes of this assessment, a safety issue is only some activity, risk, or consequence that actually represents an increase in concerns respecting the moon's or Mars' future use by humanity or the potential risk to persons or to astronauts working at the base, in rovers or at other locations on the Mars surface. To this end, Table 4 is modified to include risk incorporating the aforementioned restriction.

Probabilities for some accidents are increased as a result of the potential failure of the landing system. Some consideration should be given to the failure probability of moon or Mars landers. The success rate for lunar landings is quite high, >95%; however, to date the Mars entry and landing sequence failure rate is ~50%.

The conditional probabilities in Table 7 should be referenced as follows. A green stoplight should be interpreted that the hazard will probably occur at most once during the lifetime of the moon base or Mars base power system. A yellow stoplight means this activity will probably occur at least once during the lifetime of the Mars base power system. An orange stoplight means this hazard could occur more than once in the lifetime of a Mars base power system. Because routine landing and takeoff activities will be occurring, potential for a misguided landing or an aborted takeoff that impact the moon or Mars nuclear-power system are at least feasible, although of extremely low probability. The more remote the power system is located, the more remote is this possibility, however, the more challenging the setup of the power station

2. Initiating Events for Mars Base Power System

Potential initiating events associated with the Mars power system include the following:

1) fission product/isotope release—rover or ascent/descent vehicle accident ruptures pressure vessel and fuel cladding; reactor overtemperature, or power transient, ruptures fuel cladding and breaches pressure vessel/ducting; loss of coolant accident; loss of flow accident; unauthorized human activities; reactor power system landing vehicle accident; corrosion of reactor; and erosion of components by sand or dust; 2) contamination of personnel/Mars environment

Table 7 Probability of an initiating scenario for different hazard categories

Hazard	Mars base power system landing	Mars base NPS startup	Mars base NPS operations	Mars base standby/ dormancy	Decommissioning/ disposal
Fission product/ isotope release	a	b	c	b	b
Contamination of personnel	b	b	c	b	b
Radiation exposure	b	c	b	b	b
Inadvertent criticality	c	b	b	b	b
Inadvertent reentry	a				
Damage to spacecraft	c	c	c	b	b
Damage to facilities	c	b	c	c	b

[a]Failure or event occurs more than once during lifetime of system or for single events a high probability of his failure occurring.
[b]Failure or event occurs at most once during lifetime of system.
[c]Failure or event occurs at least once during lifetime of system.

pressure vesse land fuel cladding by the moon or Mars environment—core pressure vessel and fuel cladding breach; mars power system landing incident; and improper decommissioning; 3) radiation exposure—crewed operations in and around operating reactor facility; unplanned ascent/descent operations within 1 km of Mars power system in greater does rate zones; shielding breach by rover, ascent/descent vehicle, or unauthorized human activity near Mars power system; radiation shine from Mars soil or atmosphere; and inadvertent contact with improperly decommissioned reactor; 4) inadvertent criticality—unplanned control input; landing incident with core compaction; and violation of criticality limitations; 5) inadvertent reentry (on Mars surface)—Mars power system lands in wrong location; and Mars power system crashes after unplanned reentry; 4) damage to Spacecraft (Mars power system) by external source—hard landing or crash; rover impact; another landing spacecraft or an aborted takeoff land on Mars power system; and severing of power cables by EVA or rover activity; and 7) damage to facilities (other than Mars base power system)—cooling fan blades break up and hits Mars base or personnel.

Based on the preceding scenarios, there are feasible conditions where astronauts or personnel could be exposed to radiation or become contaminated. EVA situations would presume the astronaut or crew member to be in a space suit; therefore, the contamination would likely be able to be removed in a straightforward fashion, although special provisions would have to be made for such an event. Radiation exposure is a more serious concern because an astronaut or crew

member will experience increasing exposure as the person gets closer to the power station within the 1-km keep-out zone. It would appear prudent to have some form of audible and visual alarm that would be activated whenever personnel get within 1 km of the power station while it is operating, to adequately warn the individual or group that radiation levels are hazardous within this zone. Because there is a possibility that a crewed lander could land accidentally within the keep-out zone, this radiation exposure condition could result in some serious consequences if the reactor is not shut down and the lander is close to an operating reactor.

Mars power system decommissioning is an important issue from a long-term radiation protection perspective. Unlike the lunar counterpart, where no wind or water is present, on Mars it is now known it there exists significant dust storms, and there is a very high likelihood of at least stagnant water. This water is expected to be a richly briny solution (at least in some locations) with sulfate and bromide salts. This poses a longer-term environmental compatibility problem with extended entombment than the lunar system would likely pose. Proper entombment will allow the system to remain in place with sufficient shielding to minimize radiation dose to any individual who enters the area. Even with the potential for chemical attack during entombment, because of the relatively short half-life of most of the fission products, there should be no unusual safety concerns with long-term disposal on the surface of either the moon or Mars.

VIII. Finding 8: There Appears to Be No Reason That a Space Nuclear Reactor Power System Cannot Be Safely Deployed and Operated on the Surface of Another World While Maintaining Standards of Planetary Protection

A space nuclear-power system appears to be adaptable in a technical and risk-abatement fashion for use in crewed activities on the Mars surface. However, there could be substantial changes to a design adapted for in-space operations, and other design modifications might be necessary. Some of these changes are from a safety perspective; others are from an operational perspective. We assume that the shielding levels postulated in our shielding analysis using Mars or Lunar soils can be achieved. We further assume that the logistics of drilling a hole in Moon or Mars regolith into which a modified reactor assembly can fit is able to be performed, and a precision landing over this hole can be accomplished. Further, we assume that a mechanism for filling regolith around the reactor assembly can be successfully developed. All of this must be accomplished on Mars without benefit of human presence, whereas on the lunar surface it is envisioned that crew members will already be in place to assist in the preparation of the lunar surface for the power system. Depending on the deployment architecture, it is possible that lunar deployment could occur without human presence as well. The primary risks with either the Moon or Mars nuclear-power station would appear to be procedures violations of some form. The violations would most likely include violation of the radiation-area exclusion boundaries by EVA crew members or crewed rovers. Other risks such as reactivity excursions would likely be extremely rare given the autonomous nature of the reactor control system. With a properly designed reactor power system, overall risks should be quite small.

IX. Finding 9: A Space Reactor System Enables Effective Design Options in Mitigating Potential Radiation Releases

The International Academy of Astronautics (IAA) recommends that a space nuclear mission place paramount importance on safety. The inclusion of careful safety planning at an early stage and throughout all mission activities is vital to ensure that the space nuclear system mission profiles will be conducted in a manner that clearly demonstrates an impeccable safety program. The guiding philosophy for the space nuclear-power and propulsion program is to maintain a high profile for safety throughout concept development and design such that a safety mentality is established as an integral aspect of design and operations. Inherent in a safety-based effort is the imperative to periodically review operations and administrative considerations to ascertain if any of these might result in diminished risk.

X. Finding 10: A Transparent and Systematically Traceable Space-System Safety Test and Analysis Program Must Be Conducted to Ensure Crew and Public Safety

This section discusses the safety test and analysis program for the space reactor system. Although the focus is on nuclear safety associated with the launch of the JIMO reactor system, some discussion is provided on the additional safety testing required for the ground reactor test program. Safety activities associated with the conduct of the reactor ground test need to be integrated into the overall safety plan; nonetheless, safety requirements, testing, analysis, and implementation for the ground test must be clearly differentiated from the safety associated with the launch of the space reactor system.

A. Safety Testing

Zero-power critical testing will be performed during the fueling operation. Following zero-power testing, the reactor will be shut down and will not be taken critical again until it is placed in its intended operational orbit. This approach presents a major safety advantage in that no safety impact on Earth's biosphere or its inhabitants is predicted to result from any postulated reactor system accident after deployment in high orbit. A careful analysis is required to ensure that postulated operational accidents do not present safety issues; nonetheless, this basic approach limits reactor system radiological safety considerations to postulated accidents that could lead to accidental criticality or lead to the dispersal of essentially fresh nuclear fuel. The radioactive content of the essentially fresh uranium fuel is very low, however, and is not expected to present a major radiological risk. Nonradiological safety issues associated with the reactor system include nonradiological consequences of liquid metal fires and explosions and the dispersal of toxic materials, such as beryllium and beryllium compounds.

Given this limitation on types of postulated accidents resulting in safety issues, safety-testing requirements for a space reactor are quite limited. Safety testing for the space reactor systems falls potentially into two major categories: system disruption tests and criticality tests, as shown in Table 8, and possible complete ground test of the reactor power system.

Table 8 Possible types of safety tests

System disruption tests	Criticality tests
Propellant explosions	Normal configurations
Propellant fires	Water-flooded configuration
Shrapnel impacts from explosions	Compacted geometries (including water immersion)
Reactor system impact with surfaces or objects	Various reflector configurations
Reentry effects	Sand reflection
Normal launch environments	Reconfigured core geometries
Impact launch environments	Compacted or reconfigured geometries postlaunch environment
Explosive disassembly of reactor core	Test benchmarked code predictions using surrogate materials for uranium

At this stage it is difficult to predict if all of the subcategories of testing will be required, and the detailed requirements for these tests are difficult to forecast. Nonetheless, some basic features of the required safety tests are outlined here. The test facilities at Sandia National Laboratories are used in the following as examples of the kind of facilities that are available for safety testing; however, the proposed test plan will examine all possible test facilities and select those facilities best suited to the safety test program.

B. Propellant Explosion and Fire Tests

The range of possible environments resulting from a postulated propellant fire or explosion is likely to be very large. Detailed computer modeling will be used to determine the effect of these environments on the reactor system. The principal concern is the possibility of reactor system reconfiguration that could result in an inadvertent criticality. The possibility of dispersion of nuclear fuel materials and toxic substances will be examined as well. Some propellant fire and explosion testing will be required to validate computer models and to provide parameters required by these models. More accurate equations of state for propellants might be required. These tests will require a mock-up of the reactor system, reactor components, or both. Mockups will include relevant design features and either actual materials or surrogate materials. Analysis of the design and potential propellant fire and explosion environments can identify specific issues that require additional testing. Facilities for conducting fire and explosion tests are well established. Figure 5 shows a nuclear container fire test at the Coyote Canyon Test Facility.

C. Impact Tests

Fragments produced and propelled by a propellant explosion can impact the reactor system. Although liquid-fueled rockets (such as the Delta-IV/H) exhibit more benign fire and explosion scenarios than solid rocket systems, realistic environments must be modeled. Further, in an international space exploration program, it is considered feasible that a space nuclear system will be launched on



Fig. 5 Nuclear container fire testing at the Coyote Canyon test facility [at Sandia National Laboratories (SNL)].

a system containing solid propellants. A launch abort or failure to achieve orbit could result in high-speed impact of the reactor system with solid surfaces or water. Other possible incidents, such as dropping the reactor system during mating with the launch vehicle, can result in reactor impact. The consequences of these postulated accidents will be assessed using computer modeling. Actual impact testing using a mock-up reactor with simulated fuel will benchmark the codes. As for propellant fire and explosion assessments, some shrapnel or fragment impact tests will be required to validate computer models and to provide parameters required by these models. Also, an analysis can identify specific issues that require additional testing. Some of the presently existing facilities for impact testing include drop test facilities, pull-down test facilities (Fig. 6), rocket-sled impact facilities (Fig. 7), shock test facilities, water impact facilities, and large centrifuge facilities.

D. Reentry Tests

The geometry of the reentry shield (if used) and the materials of potentially exposed components have been well studied. Established computer analysis tools will be used to examine postulated reentry accidents. If more detailed analysis identifies a need for testing, wind-tunnel facilities can be used to perform the required tests.

E. Launch Environment Tests

For a normal launch, the rector system will be subject to dynamic *g*-loads, staging shocks, and vibration. Testing will be required to ensure that safety



Fig. 6 Nuclear container pull-down impact testing (at SNL).



Fig. 7 Nuclear container rocket-sled impact test facility at SNL.

systems will not be compromised by these environmental insults. Shaker tables and shock test facilities will be required to verify the integrity of safety features for the space reactor system for the expected launch environment.

F. Criticality Tests

The neutronic analysis methods needed to determine the reactor multiplication factor for possible accident geometries are well established. Typically, advanced transport theory or Monte Carlo computer codes are used to determine whether core reconfiguration, core flooding, or other possible environments can lead to an inadvertent reactor criticality. However, these computer codes require accurate neutron cross sections. (Neutron cross sections are related to the probability of neutron interactions with specific materials.) Inaccuracies in neutron cross sections for some reactor materials can introduce uncertainties into the neutronic analysis. Thus, critical tests might be required to reduce uncertainties resulting from cross-section inaccuracies or unusual geometries.

Criticality testing mock-ups should use the actual reactor materials and use dimensions and geometries similar to those expected for the actual flight reactor system. Criticality mock-ups are only tested at very low power levels (often called zero-power testing). As a consequence, many details of the actual reactor design (coolant system, pressure boundaries) are not required for the criticality mock-up. The simplified design of the mock-up permits relatively inexpensive, early verification of cross sections and analysis methods. If criticality predictions do not accurately predict test findings, alternative cross sections might be required, or the analysis predictions might be benchmarked to the results obtained from criticality testing. The use of a criticality mock-up also permits rapid change-out of materials and components such that a variety of postulated accident configurations, geometries, and environments can be studied. Some alternative configurations can include reflector reconfigurations, alternative reflecting materials (e.g., wet sand), water flooding, and distorted or compacted geometries. Criticality testing capabilities are less widespread today than they were several decades ago. Criticality testing requires not only the appropriate equipment and expertise, but it also requires a facility approved for carrying out a fairly wide scope of criticality tests. Several of the national laboratories and other facilities should be capable of performing the required criticality tests.

XI. Finding 11: Prior Space Reactor Programs Expended Resources on Destructive Disassembly Testing for Low-Probability Incidents—System-Level Testing Should Be Reserved for More Likely Scenarios

Safety testing and analysis should be integrated into planning for the reactor system ground test program. Sharing of facilities and test results will optimize program resources and minimize development time. For example, some of the critical facility test results obtained for the flight reactor will be essential to reactor designers and will be applicable to the ground reactor safety program. Reactivity temperature coefficient measurements obtained for ground-test safety assessments are also needed for understanding the performance of the space reactor system. Reentry safety analysis and (possibly) testing can provide information needed for

safeguards issues relating to recovery of the nuclear fuel. Testing of the ground reactor cooling system can provide needed performance information for the flight reactor. Other types of tests and analysis might be required for reliability, mission success, operational performance, safeguards, and space environmental protection. These testing considerations should be included in an overall test plan.

The early space reactor programs postulated reactor accidents, such as core-flooding accidents, that resulted in reactivity excursions sufficiently rapid to cause fuel vaporization and destructive disassembly. Much effort was directed toward the study of reactivity-induced destructive disassembly accidents for space reactors. Full-scale disruptive disassembly tests were carried out for both the SNAP-10A and the NERVA reactors. In retrospect, however, the emphasis placed on reactivity-induced disassembly accidents is questionable. Scenarios required to induce accidents of this type were not highly plausible, and if the space nuclear system meets the aforementioned safety requirements and recommendations, they should be precluded by the design. Much of the emphasis on reactivity-induced destructive disassembly accidents was motivated by the absence of a requirement for subcriticality during postulated accident scenarios for SNAP-10A. This type of testing should not be justified for the presently understood space nuclear missions; consequently, reactivity-induced destructive disassembly tests are not recommended.

A. Safety Analysis

Safety analysis for the JIMO space reactor program will be extensive. Test-validated safety analysis is essential to the overall safety assessment and flight approval and plays a key role in the guidance of the safety program. For the most part, existing computer models will be used to carry out the safety analysis. Some modifications to these tools and development of additional analysis tools might be required to address the special needs of the JIMO program. Although the test program discussed in the preceding will be required to validate much of the analysis, many of these analysis tools have been validated by previous testing. Some of the important types of safety analysis planned for the space reactor mission include neutronies, shielding, fires and explosions, and international disassembly.

1. Neutronics

Well-established Monte Carlo and transport theory computer codes (e.g., MCNP—Monte Carlo N-Particle Transport code, which was initially developed and is fastidiously maintained by Los Alamos National Laboratory, is widely used in reactor design, radiation transport, and radiation shielding problems) will be used to explore the reactivity effects of various reactor configurations and environments for postulated accident scenarios.

2. Shielding

Monte Carlo and transport theory computer codes will be used to determine possible radiation exposure doses resulting from postulated inadvertent criticality scenarios.

3. Fires and Explosions

A number of established computer codes can be used to perform an analysis of postulated propellant fire (e.g., the Sandia Fireball Code) and explosion environments. Structural response codes will be used to determine system response to explosions and the consequences of fragments impact on the reactor system. Some code modifications might be required to couple the system thermal and structural response analysis with the predictions of the postulated accident environments, including possible sequential or multisource events.

4. Intentional Disassembly

A number of codes will be necessary to characterize intentional disassembly to prevent accidental criticality and to ensure dispersal in the event of an accidental reentry. These codes include CTH, PRONTO3D/SPH (single particle hydrodynamic) and, under the latest version for the advanced simulation multiple processor efforts, ALEGRA. These will be used in conjunction with reactivity codes such as MCNP to ensure that the reactor will not become critical during an intentional disassembly sequence. (CTH is a large-scale structural deformation code originally developed by Sandia National Laboratories. Although still used by Sandia and other laboratories, it is no longer supported in favor of more advanced structrual codes such as PRONTO3D and ALEGRA.)

B. Reentry Analysis

Trajectory analysis tools are well developed. For example, the Trajectory Simulation and Analysis Program (TSAP) is well written and documented. The Heating and Analysis Done Interactively (BLUNTY) code can be used to perform reentry-heating calculations and to generate output in a format suitable for standard thermal response codes.

C. Coupled Impact/Reactivity Analyses

A number of established impact analysis computer codes are available to analyze impact of complex geometries. An example of a recent impact is presented here. Sandia National Laboratories recently carried out an analysis of a postulated vertical drop of a JIMO space reactor from 100 m onto a hard surface, resulting in a 100-m/s impact. The analysis was carried out under internal research and development funding from NGST [1–3] using the PRONTO-3D/SPH hydrodynamic code. Some preliminary results are shown in Fig. 8. Two cases are shown, one with the lower grid plate weakly attached to the vessel and one with it firmly attached to the vessel. The analysis indicates that the frozen lithium absorbs some of the shock; nonetheless, significant distortion of the reactor vessel is predicted. When the grid plate is attached to the vessel, the impact causes the fuel pins to splay outward slightly; consequently, attaching the grid firmly to the vessel can aid in the reduction of reactor criticality. In any case, wide swings in reactivity were noted (Fig. 9). Placing a wedge at the base of the lower head might help drive the pins further apart for this impact scenario. The predicted distorted geometry will be used in an MCNP neutronics analysis to determine the effect on

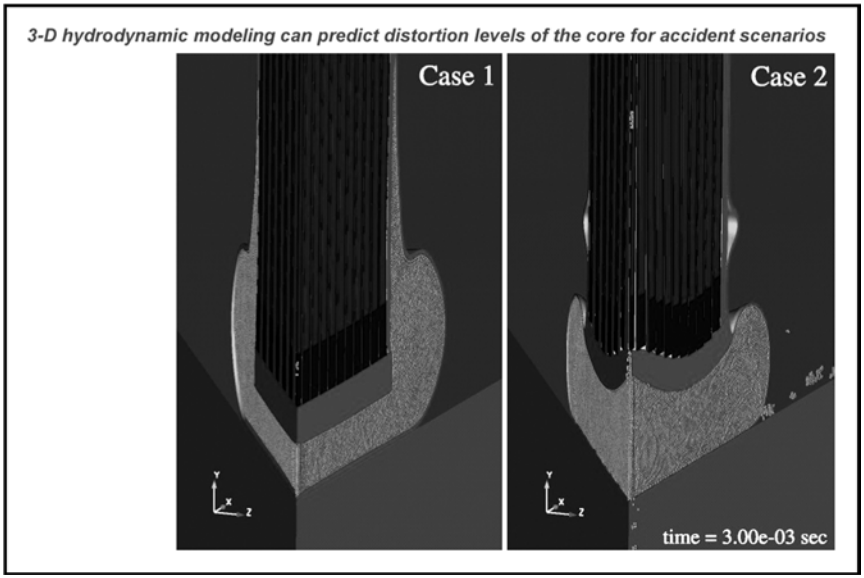


Fig. 8 Impact of bare reactor on concrete at 44 m/s (100-m drop).

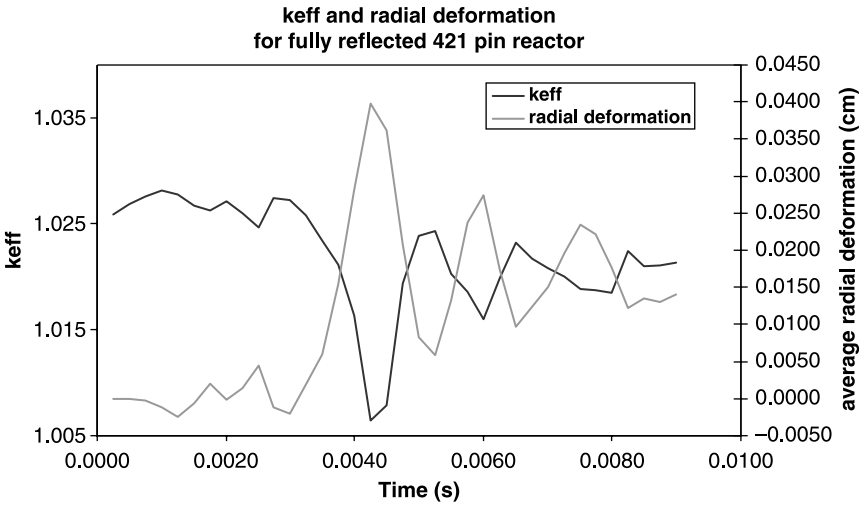


Fig. 9 Induced reactivity swings during 100-m/s impact.

reactivity [14, 15]. Although it is not possible to assess every possible accident scenario, analysis of this type can provide useful insights and envelop the realm of possible accident conditions.

D. Risk/Consequence Analysis

Established methods will be used to perform a risk/consequence analysis for the JIMO space reactor mission. Part of the analysis will provide source terms for various postulated accident scenarios. The analysis will also examine the possibility of atmospheric dispersion of radioactive materials, possible inhalation and ingestion of radioactive materials, environmental contamination, cloud shine and ground shine, and projected collective doses for various scenarios. Risks and projected consequences associated with various scenarios will be tabulated and discussed. Event-tree and fault-tree methods will be used to guide and elucidate the analysis and to identify issues or components that require further study or modifications to reduce mission safety risk. This analysis will take a graded approach as shown in Fig. 10 [14, 15]. Such an approach precludes involving large effort on scenarios with minimal risk and concentrates effort on areas of high risk.

E. Other Analysis

Other types of analyses will be used to assess and guide the safety program for the ground reactor test and to provide performance predictions. Example analyses include reactor kinetics and burn-up analysis, fission product inventory

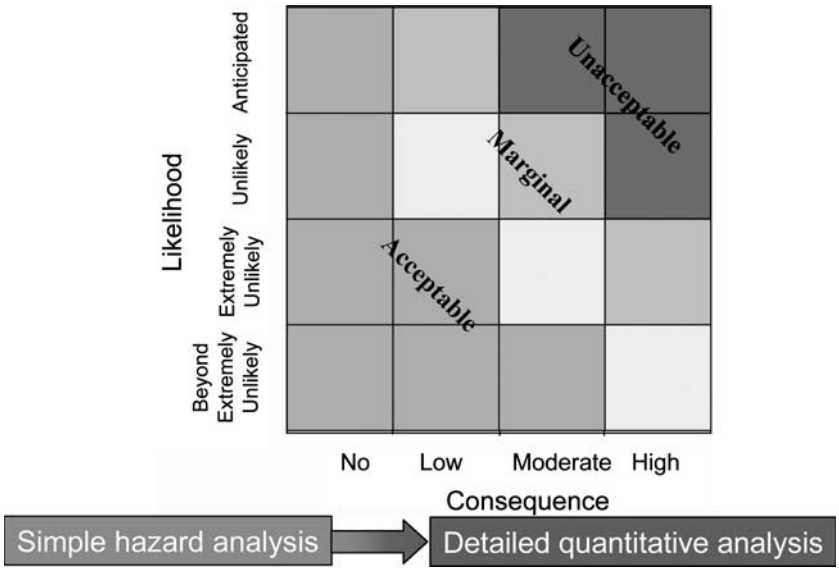


Fig. 10 Graded risks assessment and analysis approach.

Table 9 Accident scenario probability estimates for prelaunch ($t < 0$ s)

Failures and initiators		Estimated probability of occurrence			
Initiators	Accident type	Accident	Release of fresh fuel	Induced criticality[a]	Release of fission products
Hoisting failure	Dropped reactor	10^{-5}	$<10^{-5}$	$<10^{-6}$	$<10^{-6}$
Spurious signal	Accidental startup	$\sim 10^{-9}$	<N/A>	$\sim 10^{-9}$	$<10^{-9}$
Spurious signal	Command destruct	$\sim 10^{-9}$	$\sim 10^{-9}$	$\sim 10^{-9}$	$\sim 10^{-9}$
Propellant spill or leak	Propellant fire/explosion	10^{-4}	$<10^{-4}$	$<10^{-6}$	$<10^{-6}$

[a]Includes subsequent reactor surface impact and immersion in water or wet sand

predictions, reactor cooling analysis, and predictions of system response to postulated accidents. These analyses, however, do not directly address safety as applied to the launch of the JIMO reactor system.

Recommendation 19: The space nuclear reactor program should prioritize test and analysis programs based on engineering judgment of failure probabilities.

The proposed safety test and analysis program should not proceed independently of failure scenario probabilities. Although launch-vehicle data books might not be available, a basis for what likely failures might include can be based on historic data and engineering judgment. To that end, the IAA study team has identified potential failure scenarios and has performed an initial screening of events and matched realistic probabilities of failure (based on the Cassini FSAR in some cases) coupled with probability of a release of nuclear material, fission products, or an inadvertent criticality. The potential failure probabilities are matched with different phases of flight from the time the reactor module arrives at the launch site until reactor startup occurs. The results are shown in Tables 9–12 [16].

Table 10 Accident scenario probability estimates for early launch phase ($t < 20$ s)

Failures and initiators		Estimated probability of occurrence			
Initiators	Accident type	Accident	Release of fresh fuel	Induced criticality[a]	Release of fission products
Fall-back or tip-over	Launchpad impact	$<10^{-6}$	$<10^{-6}$	$<10^{-6}$	$<10^{-6}$
Trajectory failure	Command destruct	6.6×10^{-4}	~ 1[a]	$<10^{-7}$[b]	$<10^{-7}$[b]
In-flight explosion	Land impact	$\sim 10^{-4}$	$\sim 10^{-4}$	$<10^{-7}$[b]	$<10^{-6}$

[a]Assumes external environment reactivity enhancement, impact, or control failure.
[b]Assumes explosive disassembly.

Table 11 Accident probability estimates for late ascent phase and orbit circularization ($t = 20 - 4800$ s)

Failures and initiators		Estimated probability of occurrence			
Initiators	Accident type	Accident	Release of fresh fuel	Induced criticality[a]	Release of fission products
Trajectory failure	Command destruct	$\sim 10^{-2}$	~1	$<10^{-7}$[b]	$<10^{-7}$[b]
Suborbital reentry	Land impact	$\sim 10^{-4}$	~1	$<10^{-7}$[b]	$<10^{-7}$[b]
	Ocean impact	$\sim 10^{-3}$	~1	$<10^{-7}$[b]	~1[b]
Orbital reentry	Land or ocean impact	$\sim 10^{-7}$[c]	~1	$<10^{-7}$[b]	~1[b]

[a]Assumes external environment reactivity enhancement, impact, or control failure.
[b]Assumes explosive disassembly and complete dispersal.
[c]Requirement.

XII. Finding 12: An Integrated Approach for Performance and Safety Analysis and Testing Is Critical to a Cost-Effective Development Program

This section describes a "recommended approach for integrated performance and safety analysis, compliant with Atomic Energy Act requirements." We interpret this to mean following a launch approval process similar to that used by previous launches of radioisotopic power systems, following all Department of Energy (DOE) orders and Environmental Protection Agency (EPA) rules for safe handling of radioactive materials, and integrating these processes with the traditional launch process. An integrated safety program will be established to address all mission-related safety issues in a coordinated manner. In the following, the safety program organizational structure is discussed along with a discussion of the basic steps required to secure launch approval.

Table 12 Accident scenario probability estimates for reactor operational phase ($t > 4800$ s)

Failures and initiators		Estimated probability of occurrence			
Initiators	Accident type	Accident	Release of fresh fuel	Induced criticality[a]	Release of fission products
Trajectory failure	Reentry	$<10^{-7}$	~1[a]	$<10^{-7}$	~1[a]
Flyby trajectory malfunction	Reentry	$<10^{-7}$	~1[a]	$<10^{-7}$	~1[a]

[a]Assumes explosive disassembly and complete dispersal.

A. Safety Program Organization

The space nuclear reactor safety program will ensure that the mission will be conducted safely and that launch approval will be obtained. The safety program will foster a safety culture among all program participants. This philosophy makes safety everyone's responsibility, rather than assuming that all safety issues are only the safety team's concern. Making safety an integral aspect of the program also enhances safety communication and teamwork. A preliminary safety program has been initiated during the phase A design effort and will continue through system development and deployment. Addressing safety issues during system development ensures that the design can either be changed to eliminate the hazard or appropriate controls can be incorporated. An example of this is the launch-accident impact safety effort that was started during task 2. This has enabled us to ascertain methods to internally mount the reactor that enhances safety during hard surface impacts. The designed-in-safety approach should be required by space reactor system standard practice and should ensure a cost-effective safety approach by dictating that safety is not implemented postdesign.

An integrated organizational structure of the space nuclear reactor safety program will need to be developed jointly with all of the relevant parties. An integrated safety program manager will be responsible for ensuring the integration and proper functioning of all program safety activities. The program manager is the recipient for safety reporting and is the ultimate authority within the program for all safety decisions. Traditionally, an independent nuclear safety team is established and reports directly to the program manager to provide independent assurance that nuclear safety issues are properly addressed. Where possible, the analysis and testing program that is associated with system validation and performance is employed to support safety analysis or to verify safety functions and safety margins.

A reactor design-safety team performs the primary safety functions and provides safety findings to the reactor project manager and the integrated safety program manager. To provide an additional measure of independence, the design-safety team is sometimes funded by and reports to a line organization different from the reactor design team. The reactor design-safety team functions include 1) interfacing with the project and program offices on safety matters, 2) developing a safety program plan, 3) identifying applicable safety guidance and requirements, 4) identifying safety documentation and approval requirements, 5) interpretating safety guidance, 6) developing detailed safety specifications, 7) contributing to safety component design, 8) performing in-depth safety analysis, 9) performing safety testing, 10) developing safety procedures, 11) preparing safety analysis reports for the program office, 12) presenting safety findings to INSRP and defending findings, 13) interfacing with design team and quality assurance team on safety matters, 14) conducting internal safety audits and reviews, 15) preparing much of the environmental impact statement (EIS), 16) preparing other safety documentation (e.g., for range safety), and 17) serving as public interface on safety matters.

A comprehensive, ongoing operational safety program is an essential aspect of the integrated safety program. The operational safety program is needed to ensure safe operation for the protection of workers, the public, and the environment. The operational safety program is conducted in compliance with DOE orders relating to radiation safety, occupational safety, and environmental protection.

The operational safety program includes an operational safety analysis, a quality assurance program, a radiation protection plan and radiation protection program, operational reviews and surveys, a contractor self-appraisal program, provisions for DOE reviews surveys and approvals, and readiness reviews for each specific facility. A separate safety program will be established, in compliance with appropriate DOE orders, for the Ground Reactor Test Program. DOE orders and Department of Transportation (DOT) regulations will be followed for packaging and transport of special nuclear materials and nuclear systems.

XIII. Finding 13: The Ultimate Objective of All Programmatic Activities Is to Obtain Launch Approval for the Space Reactor System—the Program Should Be Structured to Attain the Goal

A number of review processes have addressed launches of RTGs in the past, and one would expect essentially identical processes to be used to for review and approval of a space reactor launch. The principal review processes in the past have included the INSRP as well as reviews for the environmental protection, range safety, range operations, and orbital safety. Other safety review and approval processes include approvals for transportation of nuclear materials to the launch site and launch-site safety approval. An approximate sequence for the INSRP review and approval process is presented in Fig. 11. The figure also presents the approximate sequence for the EIS, range safety, range operations, and orbital safety. For any U.S. space mission involving the use of nuclear-energy systems with significant quantities of radioactive or fissile material, INSRP review is required, and launch approval must be obtained from the Office of the President.

The launch decision is based on a consideration of the projected benefits and risks of the mission and on a safety analysis and evaluation that includes both the program's analysis and an independent characterization of mission safety by an interagency nuclear safety review panel. The process includes several increasingly detailed safety analysis reports (SARs) prepared by the JIMO program office and participating contractors, review and evaluation of those SARs by INSRP, and characterization of the mission radiological risks by INSRP in a safety evaluation report (SER). The SER is provided to the Office of Science and Technology Policy (OSTP) and the National Security Council (NSC) within the Office of the President. The Office of the President grants (or denies) final approval for launch.

The National Environmental Policy Act (NEPA) EIS process is entirely separate from the INSRP review. Typically, the NEPA process is completed early in the program cycle; preliminary data and analysis can be used. In addition, the NEPA process differs in that it involves the public and a large number of federal, state, and local agencies. The EIS provides a general understanding of how the action will be implemented and what potential environmental impacts could result. It is also designed to inform decision makers and the public of a reasonable range of alternatives that are compatible with the purpose and need of the action. These alternatives must be compared with the proposed action in terms of their potential environmental impacts. An EIS for the JIMO nuclear mission must provide a detailed analysis of the impact of a normal launch on the air, water, plants, etc. of

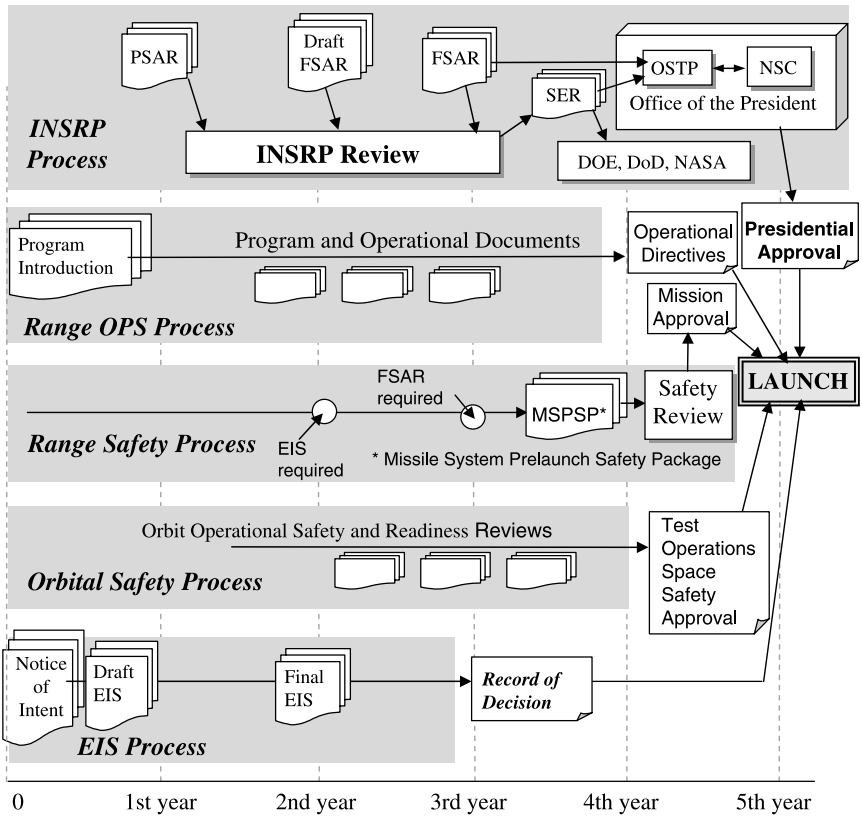


Fig. 11 Notional timeline of events for launch approval.

the launch area. It must also discuss a reasonable range of postulated accidents and their potential impact.

An emergency response plan is also required. Emergency preparedness plans are required for all sites and situations involving the utilization, handling, transporting, or storing special nuclear materials. Contingency plans and emergency response resources are also required for the launch aborts and for other postulated scenarios that could result in reentry of the system. Unique features of launch abort and reentry emergency response include plans for nuclear source or nuclear system recovery and long-term postcontingency assessments and recovery.

Recommendation 20: The U.S. INSRP process has ensured a rich legacy of safety radioisotope launches—the same (for U.S. launches) or a similar practice (for foreign launches) should be adopted for space reactors.

A number of documents have been needed in the past as part of the launch approval process for RTGs; the list needed for a reactor launch might be very similar. The list of important safety documentation for RTG launches that has

traditionally been provided by the mission program office includes the following:

1) Launch-vehicle data book
2) Space nuclear safety documentation
3) Safety program plan
   a) Flight safety requirements documents
   b) Safety analysis reports (PSAR, draft FSAR, and FSAR)
   c) Radiological protection plan
   d) Emergency preparedness and response plan
   e) Safety analysis report for packaging (SARP)
   f) Ground safety analysis report (GSAR)
4) Range documentation
   a) Program introduction plan (PI)
   b) Statement of capabilities document (SOC)
   c) Program requirements document (PRD)
   d) Operational requirements (OR)
   e) Operational directive (OD)
   f) Missile system prelaunch safety package (MSPSP)
5) Orbital safety documentation
   a) Test operational risk assessment (TORA)
   b) Preliminary hazards list (PHL)
   c) Test operations space safety approval (TOSSA)
   d) Orbital readiness space safety review (ORSSR)
4) Environmental protection documentation
   a) Notice of intent
   b) Environmental impact statement (draft and final)
   c) Notice of availability

XIV. Conclusions

The International Academy of Astronautics (IAA) staunchly endorses the use of reliable and safe space and surface nuclear-power and propulsion systems in areas where they can provide distinct advantages. The IAA recognizes there are a number of venues under which space nuclear systems can be implemented. There are commercial space transportation and asset recovery missions that appear to be profitable only under implementation with space nuclear-power. There are science missions such as the Jupiter Icy Moons Orbiter Program, where large payload, massive payload radiation protection (from the Jovian radiation field), and data transmission requirements are enabled by space nuclear-power and propulsion. Human transportation to Mars is made demonstrably more safe by nuclear thermal propulsion, and using nuclear electric power on the surface of the moon and Mars can dramatically reduce the costs of human exploration programs.

Other systems concepts have recently surfaced where nuclear fission power systems, either through advanced technologies in an electric propulsion mode or through such concepts as MiniMag Orion (see Chapter 2 in this book) coupled with macro-particle accelerators, can enable one-way accelerations to $0.1c$ to $0.15c$ (c is the speed of light) and can retain the ability to rendezvous with star systems four to five light years distant within a human life span. This is an astounding although

futuristic concept. However, the fact that known extensions to existing and operational technologies can provide the basis for initial interstellar rendezvous flights is significant, and nuclear energy is the enabling capability.

It is for the preceding reasons, to mention a few, that the IAA has reviewed the wide body of safety and policy literature and has made some recommendations to improve their utility to the space-systems design community where appropriate. The existing safety and environmental compliance process employed in the United States appears appropriate for other countries as modified to meet their own internal requirements, while still remaining in compliance with international norms.

We have reviewed the issue regarding use of reactors in Earth orbit and found that the abnormally large advantages to using $I_{sp} > 4000$ s to accelerate large payloads from lower Earth orbits to their destination and to rapidly and cost effectively transport humans to the moon or Mars cannot be dismissed or ignored. To this end, we have clarified some ambiguities in the meaning of decay times, hence the implications of a sufficiently high orbit (in United Nations parlance), and we further have provided some proposed guidance regarding the design approaches to what highly reliable orbit-raising systems might mean. Although the term *highly reliable* might have been employed to allow some states parties to create their own design approaches, consistent with internal criteria, we note that ambiguous requirements do not enhance public confidence. Nuclear systems are not like other technologies, at least not in the opinion of the public, which in many cases has been highly sensitized by antinuclear activists whose agenda is not to enhance the use of nuclear-power systems, regardless of the operational or scientific justification. To cope properly with this issue, where, in many cases, objective truth and physical reality have been overtaken by rhetoric and ideology, we cannot overstate the importance of a rigorous, transparent, and highly safe space reactor program.

References

[1] Lipinski, R. J., Wright, S. A., Lenard, R. X., Metzinger, K., Humberstone, M., Beard, S. G., Potter, D. L., Rollstin, L. R., Helmick, P. H., Nygren, R. E., Youchison, D. L., Viswanathan, S., Hanson, D., Berry, D., Vehar, D., and Young, M. F., "IRAD-Supported Activities for the Jupiter Icy Moons Orbiter," Sandia, National Lab., Rept. Albuquerque, NM, 23 Nov. 2004.

[2] National Aeronautics and Space Administration, Project Prometheus Final Report, Jet Propulsion Laboratory, California Institute of Technology, 982-R120261, Pasadena, CA, Oct. 2005.

[3] Lipinski, R. J., Wright, S. A., Lenard, R. X., Suo-Antilla, A. J., Vernon, M. E., Marshall, A. C., Jablonski, J. A., and Helmick, P. H., "CRADA SC03/01673 Final Report: Space Reactor Trade Studies and Conceptual Design," Sandia National Lab., Albuquerque, NM, Nov. 23, 2004.

[4] "Principles Relating to the Peaceful Uses of Nuclear Power Systems in Outer Space," COPOUS, Resolution 47/67, United Nations Committee on the Peaceful Uses of Nuclear Power in Outer Space, Vienna, Austria, 14 Dec. 1992, http://www.unvienna.org/SpaceLaw/Gares/html/gares_47_0067.html.

[5] "Presidential Directive: Science and Technology Experiments with Possible Large Scale Adverse Environmental Effects and Launch of Nuclear Systems into Outer

Space," National Security Council Memorandum NSC/Presidential Directive-25, Washington, D.C., Dec. 1977.

[6] "Treaty on the Principles Governing the Activities of States in the Exploration and Use of Outer Space, Including the Moon and Other Celestial Bodies," United Nations, 10 Oct. 1967, http://www.state.gov/t/trt/5181.htm.

[7] Presidential Decision Directive PDD-NSC-49/NSTL-48 National Space Policy of 1996, National Security Council Memorandum, Washington, D.C., Sept. 14, 1996.

[8] "Agreement on the Rescue of Astronauts and the Return of Astronauts and the Return of Objects Launched into Outer Space," United Nations, Dec. 3, 1968, http://www.unoosa.unvienna.org/ SpaceLaw/rescuetxt.htm.

[9] "Convention on Registration of Objects Launched into Outer Space," United Nations, Jan. 14, 1975, http://www.unoosa.unvienna.org/SpaceLaw//SORregistry/registxt.htm.

[10] "Treaty on the Non Proliferation of Nuclear Weapons, (NPT)," United Nations, ratified 1970, extended indefinitely May 11, 1995, http://document2.un.org/wmd/not/index.htm.

[11] "Convention on the International Liability for Damage Caused by Outer Space Objects," United Nations, March 29, 1972, http://www.unoosa.unvienna.org/SpaceLaw/liabilitytxt.htm.

[12] Marshall, A. C., Bari, R. A., Brown, N. W., Cullingford, H. S., Hardy, A. C., Lee, J. H., McCulloch, W. H., Remp, K., Niederauer, G. F., Rice, J. W., Sawyer, J. C., and Sholtis, J. A., "Nuclear Safety Policy Working Group Recommendations," NASA Technical Memorandum 105705, April 1993.

[13] Wackerle, J., "A Feasibility Study of the Disposal of a Rover Reactor with High Explosive," Los Alamos National Lab., Rept. LAMS – 2688, Los Alamos, NM, March 1962.

[14] Lenard, R. X., "Launch Impact Reactivity Analysis," Oral Paper at Space Technology Applications International Forum (STAIF), Univ. of New Mexico, Albuquerque, NM, Feb. 2005.

[15] Lenard, R. X., and Robinson, D., "Objectives, Scenarios and Approach to JIMO Safety and Safeguards," Sandia National Labs., Briefing to Naval Reactor Prime Contract Team, Albuquerque, NM, Oct. 22, 2005.

[16] Lenard, R. X., and Marshall, A. C., "Jupiter Icy Moons Orbiter Derivative Mission Analysis for Lunar Mission Scenarios," Sec. 1.3.6.2, Sandia National Labs., Albuquerque, NM, Dec. 22, 2004.

Copyrighted Materials
Copyright © 2008 AIAA Retrieved from www.knovel.com

Acronyms and Abbreviations

accel = accelerator grid
AF-MPD = applied-field magnetoplasmadynamics
AM = atomic mass
ASI = Italian Space Agency
AU = astronomical unit
CCAFS = Cape Canaveral Air Force Station
COPOUS = Committee on the Peaceful Uses of Outer Space
CTR = controlled thermonuclear reactor
DC = direct current
decel = decelerator grid
DOD = U.S. Department of Defense
DOE = U.S. Department of Energy
DS-1 = Deep Space 1 (mission)
ECR = electron cyclotron resonance
ETS = environmental impact system
EMF = electromagnetic force
EOL = end of life
EP = electric propulsion
EPS = electric propulsion system
EVA = extravehicular activity
FCU = flow control unit
FF = fission fragments
FTS = flight termination system
GCR = gas-cooled reactor
GEO = geosynchronous Earth orbit
GIE = gridded ion engine
GNP = gross national product
GTO = geostationary transfer orbit
HAT = hot anode thruster
HEDM = high-energy density matter
HET = Hall-effect thruster
HIPARC = high-power arcjet
HiPEP = high-power electric propulsion
HPR = heat-pipe-cooled reactor
HT = heat transfer
IAA = International Astronautical Academy
IAC = International Astronautical Congress
ICBM = intercontinental ballistic missile
IMLEO = initial mass in low Earth orbit
INSRP = Interagency Nuclear Safety Review Panel
IPS = ion propulsion system

IR & D = internal research and design
JIMO = NASA's Jupiter Icy Moons Orbiter
JPL = Jet Propulsion Laboratory
KE = kinetic energy
LANTR = liquid-oxygen augmented NTR
LASL = Los Alamos Science Laboratories
LEO = low Earth orbit
LHS = left-hand side
LMR = liquid-metal-cooled reactor
LRE = liquid rocket engine
MAI = Moscow Aviation Institute
MCNP = Monte Carlo Neutronics Program
MER = Mars Exploration Rover
MESC = magnetoelectrostatic containment
MHD = magnetohydrodynamics
MITEE = Miniature Reactor Engine
MMO = Mini-MagOrion
MMS = Matra Marconi Space, Ltd.
MPD = magnetoplasmadynamics
MSL = Mars Science Laboratories
NEP = nuclear electric propulsion
NEPA = National Environmental Policy Act
NEPSTP = Nuclear Electric Space Test Program
NERVA = Nuclear Engine for Rocket Vehicle Applications
NEXIS = nuclear electric xenon ion system
NEXT = NASA evolutionary xenon thruster
NGST = Next Generation of Space Transportation
NP = nuclear propulsion
NRDS = Nuclear Rocket Development Station
NSC = National Security Council
NSPWG = Nuclear Safety Policy Working Group
NSSK = north-south stationkeeping
NTP = nuclear thermal propulsion
NTR = nuclear thermal rocket
OTV = orbital transfer vehicle
PBR = particle bed reactor
PCU = power conditioning unit
PMAD = power management and distribution
PPT = pulsed plasma thruster
q-s = quasi-steady
RF = radio frequency
RIT = radio-frequency ionization thruster
RMT = radio-frequency with magnetic field thruster
ROM = rough order of magnitude
RTG = radioisotope thermo-ionic generators
SAR = safety analysis report
SC = superconducting
SDIO = Strategic Defense Initiative Organization

SER = safety evaluation report
SF-MPD = self-field magnetoplasmadynamics
SHO = sufficiently high orbit
SI = specific impulse
SNL = Sandia National Laboratories
SNTP = U.S. Air Force Space Nuclear Thermal Propulsion Program
SPFT = Special Purpose Fission Technology Program
SPT = stationary plasma thruster
SSTO = single stage to orbit
TAL = thruster with anode layer
TE = thermoelectric
TEDE = total effective dose equivalent
T/P = thrust/power
UN = United Nations
UN = uranium nitride
USAF = U.S. Air Force
VASIMR = variable-specific-impulse magnetoplasma rocket
VHF = very high frequency
XIPS = xenon ion propulsion system

Copyrighted Materials
Copyright © 2008 AIAA Retrieved from www.knovel.com

Appendix A

Radioactivity, Doses, and Risks in Nuclear Propulsion

Alessio Del Rossi*
Technip Italy, Cinisello Balsamo, Italy
and
Claudio Bruno†
University of Rome "La Sapienza," Rome, Italy

I. Introduction

"RADIATION" and "nuclear" are words that tend to spread fear among people. Even in technologically developed countries, the public has little or no knowledge of radiation, and when they do, they usually associate it with weapons, accidents, fallout, and cancer. Only specialists know about natural background exposure or about medical use of radiation. In this context the use of nuclear energy for rockets might encounter strong resistance.

The purpose of this Appendix is to inform the nonspecialist about what radiation and dose are, about effects of radiation on humans, and about sources of radiation, including estimates of the dose from nuclear propulsion systems.

II. Radioactivity

Radioactivity is the process undergone by unstable nuclei (radionuclides), as well as nuclei in excited states, causing spontaneous changes, or transformations, in composition and/or internal energy of the nucleus. This means that, unlike in chemistry, radioactivity can change a chemical element into another ("transmutation"), releasing or absorbing energy in the process. The mass numbers of nuclei are often shown as top-left indices on the element symbol. The most common transformations are three: alpha decay, beta decay, and gamma decay.

Copyright © 2008 by the American Institute of Aeronautics and Astronautics, Inc. All rights reserved.
*Engineer.
†Professor, School of Aerospace Engineering.

A. Alpha Decay

In alpha decay the nucleus of an element with mass number A_1 and atomic number Z_1 emits an alpha particle. Alpha particles are made of two protons and two neutrons, that is, a helium nucleus. The original nucleus is replaced by a new nucleus whose mass number A_2 is equal to A_1-4 and atomic number Z_2 is Z_1-2, and an alpha particle.

For instance, ^{222}Rn ($A_{\mathrm{Rn}} = 222$, $Z_{\mathrm{Rn}} = 86$) decays into ^{218}Po, meaning that the nucleus of ^{222}Rn emits an alpha particle ($A_\alpha = 4$, $Z_\alpha = 2$), leaving as remainder a nucleus whose mass number is 218 (222 − 4) and atomic number (86 − 2) = 84, that is, ^{218}Po.

The mass (energy) of the parent nucleus must exceed the sum of the masses (energies) of the daughter nucleus and alpha particle emitted. The condition for α decay to occur can be expressed as follows [1]:

$$M(A, Z) > M(A\text{-}4, Z - 2) + M(\mathrm{He}^4)$$

B. Beta Decay

Beta decay is the spontaneous transformation of an unstable nucleus into a new nucleus with charge differing by $\Delta Z = \pm 1$ because of the emission of an electron (β^- decay) or a positron (β^+ decay) or the capture of an electron (*e*-capture). A positron is simply a *positive* electron, the electron antiparticle.

In the first case (β^- decay) one of the neutrons of the nucleus emits an electron and becomes a proton. The mass number A does not change, while the new nucleus has an atomic number higher by 1.

Tritium (^{3}H, often indicated by a T), $A_T = 3, Z_T = 1$, β^- decays into ^{3}He ($A_{\mathrm{He}} = 3$, $Z_{\mathrm{He}} = 2$), meaning that one of the two neutrons of the tritium nucleus emits an electron and becomes a proton; the mass number does not change, that is, $A_T = A_{\mathrm{He}}$, while the positive charge of the new nucleus increases by 1, $Z_{\mathrm{He}} = Z_T + 1$.

The energy condition is that the mass (energy) of the parent nucleus is higher than the sum of the masses (energies) of the daughter nucleus and the electron and is expressed by [1]

$$M(A, Z) > M(A, Z + 1) + m_e$$

In the β^+ decay the unstable nucleus emits a positron β^+. The β^+ decay can be treated as the transformation of a proton into a neutron because also in this case the parent nucleus and the daughter nucleus have the same mass number A, while the atomic number Z of the daughter is lower by 1. The proton mass is lower than the neutron mass (or energy, see Chapter 1). The transformation of the proton into a neutron is possible because the proton is bonded to a nucleus and the excess energy to become a neutron is supplied by the nucleus itself. The energy condition can be expressed in analogy with the β^- case [1]:

$$M(A, Z) > M(A, Z - 1) + m_e$$

For instance, ^{11}C ($A_C = 11$, $Z_C = 6$) β^+ decays into ^{11}B, $A_B = 11$, $Z_B = 5$, and the missing charge of Boron-11 is that of the positron emitted.

The third type of beta decay is the electron capture: it consists of the capture of an electron by a nucleus from its own electron shell. For heavy nuclei with the *K*-shell close to the nucleus, this phenomenon (also called *K*-capture) is quite common; captures from *L* shell (*L*-capture), *M* shell (*M*-capture), etc. have also been observed. After the capture, the nucleus has the same mass number *A*, but its atomic number *Z* decreases by 1: the electron captured and one of the protons of the nucleus become a neutron in the daughter nucleus.

For instance, ^{7}Be, $A_{\mathrm{Be}} = 7$ $Z_{\mathrm{Be}} = 4$, after capturing an electron from its *K* shell, becomes ^{7}Li, $A_{\mathrm{Li}} = 7$ $Z_{\mathrm{Li}} = 3$; the mass number does not change: $A_{\mathrm{Be}} = A_{\mathrm{Li}} = 7$, while the atomic number *Z* of the lithium is lower by 1.

The mass (energy) condition is that the sum of the masses (energies) of the captured electron, and the parent nucleus is higher than the mass (energy) of the daughter nucleus [1].

$$M(A, Z) > M(A, Z + 1) + m_e$$

Because of the vacancy created in the electron shell, there is the transition of one of the shell electrons to that vacancy, accompanied by the photon emission in the x-ray band.

C. Gamma Rays

Unstable nuclei going from an excited energy state down to a less energetic, eventually stable, state can emit energy quanta in the γ rays wavelength ($10^{-8} \geq \lambda \geq 2 * 10^{-11}$ cm). There can be single transitions, where the nucleus goes directly from an excited state to the ground, or stable, state following the emission of a single γ quantum, or there can be multiple transitions, that is, a cascade of transitions bringing the nucleus to the ground state and involving multiple emissions of γ quanta. The energy of the γ quantum emitted is determined by the difference in energy of the two energy levels between which the transition has occurred.

There are different mechanisms responsible for exciting nuclei and leading to gamma radiation. In fact, quite commonly alpha and beta decays can leave the nucleus in an excited state. An alpha decay is usually followed by the emission of low-energy γ quanta ($<$0.5 MeV), while after a beta decay higher γ quanta are emitted (energy up to 2–2.5 MeV) [1].

III. Radiation, Dose, and Their Units

An ad hoc set of quantities and related units required to describe radiation decay and its effects has been introduced since the effects of nuclear radiation were discovered and gradually understood. A list of them follows.

A. Activity (Bq)

Given any radiation decay (α, β, γ, etc.), the **activity** of an element is the rate at which any and all transitions (i.e., emission of α, β, γ rays) occur. It is said that a radionuclide has an activity of 1 **becquerel** (Bq) when it undergoes one transition

per second. An older unit, going back to Madame Curie, is the curie (Ci), equivalent to $3.7 * 10^{10}$ transitions per second. This is "the quantity of emanation in equilibrium of 1 gram of radium" (Madame Curie said: "la quantité d'émanation en équilibre avec un gramme de radium"), that is, that quantity of Radon-222 in equilibrium with one gram of its parent Radium-226, see NIST Laboratory, http://physics.nist.gov/GenInt/Curie/1913.html. Not only for activity but also for all other quantities, both Système International (SI) units and old ones, partly deriving from the centimeter-gram-second (CGS)-system, are in current usage.

$$1\ \text{Bq} = 1\ \text{transition/s}$$

$$1\ \text{C}_1 = 3.7 * 10^{10}\ \text{Bq}$$

Activity is *not* a synonym of power or energy and has *nothing to do* with the effects of radiation on matter, living or not.

B. Half-Life (s)

The **half-life** is the time period over which half the nuclei of a given radionuclide decay. The half-life varies depending on the radionuclide considered, for example, ^{214}Po has 164 µs. An example might help: ^{214}Pb has a half-life of 26.8 min, which means that if there are N nuclei of ^{214}Pb at time zero, after 26.8 min there will be $N/2$ nuclei (the $N/2$ remaining have become ^{214}Bi because of beta decay), after 53.6 min there will be $N/4$ nuclei of ^{214}Pb ($3/4N$ have become ^{214}Bi), and so on.

C. Absorbed Dose D (Gy)

When radiation passes through matter, it deposits energy. The **absorbed dose** is the energy deposited by radiation inside matter per mass unit. Its SI unit is the **gray** (Gy), equivalent to 1 joule deposited per kilogram of absorbing "target" material (1 J/kg). The older unit is the rad (radiation absorbed dose), defined as the deposition of 100 erg per **gram** of material [2].

$$1\ \text{Gy} = 100\ \text{rad}$$

D. Equivalent Dose H (Sv)

Biological effects caused by radiation are not only dependent upon the dose absorbed (that is, on the amount of Gy) but also, and above all, by **the kind** of radiation. "Sparsely" ionizing radiations such as gamma, x ray, or beta rays are less effective in damaging than "densely" ionizing radiation such as alpha particles or fission fragments. To account for this difference, a weighing factor dependent on the kind of radiation and energy has been introduced. The weighing factor goes from 1 (for photons or electrons) to 20 (for alpha particles) and is dimensionless (see Table A.1) [2].

The sum of the total radiation doses D combined with the proper weighing factor w_r gives the **equivalent dose H** [2]:

$$\text{H} = \sum w_r * D$$

Table A.1 Weighing factors for different types of radiation

Radiation and energy	Weighing factor w_r
Photons, all energy	1
Electrons, all energy	1
Neutrons	
<10 KeV	5
10–100 KeV	10
100 KeV–2 MeV	20
2 MeV–20 MeV	10
>20 MeV	5
(see also Fig. A.1)	
Protons, all	1
Protons, (ART recoil) >2 MeV	5

Because w_r is dimensionless, the equivalent dose H has the same dimensions as the absorbed dose D, that is, joule per kilogram. Its SI unit is the **sievert** (Sv). The older unit is the **REM** (or rem); (roentgen equivalent man), whereby

$$1 \text{ Sv} = 100 \text{ rem}$$

E. Effective Dose E (Sv)

The consequences of radiation on the human body depend on the particular organ or tissue hit by radiation, as different organs have different responses to

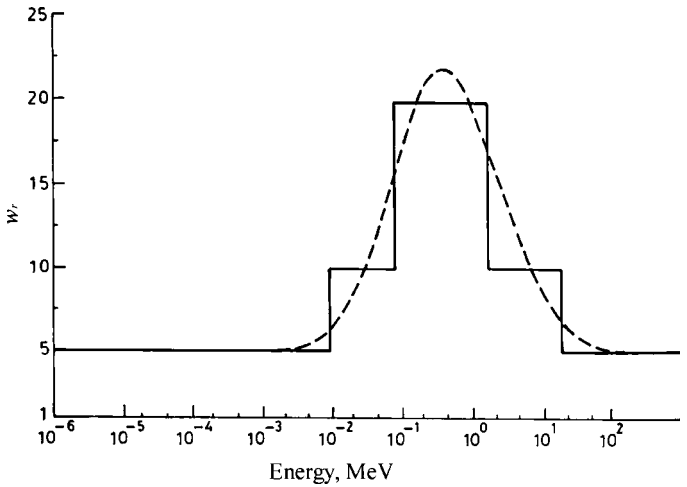


Fig. A.1 Weighing factor for neutrons.

Table A.2 Weighing factors for tissue/organ

Organ or tissue	Weighing factor W_T
Gonads	0.20
Red bone marrow	0.12
Colon	0.12
Lung	0.12
Stomach	0.12
Bladder	0.05
Breast	0.05
Liver	0.05
Oesophagus	0.05
Thyroid	0.05
Skin	0.01
Bone surfaces	0.01
Remainder	0.05

radiation exposure. This is the reason why another weighing factor w_T must be introduced (see Table A.2) [2]:

The sum of the equivalent dose D with the tissue weighing factor gives the **effective dose *E*** [2]:

$$E = \sum W_T * \mathrm{H}$$

The dimensions of the effective dose are **the same** as absorbed dose and equivalent dose, joule per kilogram. Its SI unit is the same as that of the equivalent dose: **sievert**.

F. Collective Dose (man Sv)

Absorbed, equivalent, and effective doses apply to **individuals** or average individuals. To assess the dose received by a **group** or **population**, it is more practical to introduce the **collective dose**. It is obtained by summing up the individual doses of each person of the group considered. Its SI unit is **man Sv**. A collective dose of 1000-man Sv corresponds to 1000 people receiving each 1 mSv or 10 people receiving 100 mSv. This quantity is defined for a specific source of radiation or for a specific practice causing exposure and is convenient when considering nuclear accidents [3].

G. Dose Commitment (Sv)

Some events, such as weapon tests, release radioactivity directly into the environment and cause a continuous exposure over a long time period, which can include several generations. To account for the dose committed to a typical, though hypothetical, individual from a given moment into the future, the so-called "dose commitment" has been defined. This quantity is the integral over a specified time

period (typically 250 or 10,000 years) of the average dose rate, per person, to a specified group (even the whole world population) after the event considered. Its SI unit is the sievert [3]. If an event delivers a dose commitment of 1.4 mSv for 250 years, a hypothetical individual, born at the moment of the event and dead 250 years old, would receive a dose of 1.4 mSv during his entire life.

IV. Effects of Ionizing Radiation

Ionizing radiation interacts with matter, changing the state of atoms and molecules. In cells there are two types of consequences after radiation interaction: the cell can die or can be modified. These two different outcomes have different implications for the whole body: in fact, there can be deterministic and stochastic effects.

A. Deterministic Effects

Radiation can kill cells of a tissue or organ. If the numbers of cells killed is low, the tissue keeps functioning without serious consequences. If the number of cells killed is sufficiently large, the tissue is harmed and can lose its function; eventually, the tissue or even the organ itself might die.

It is clear that with increasing number of dead cells there is more and more serious damage to the tissue. The specifics of the outcome depend on the fact that cell depletion is a dynamic process, in competition with proliferation of unaffected cells. If the loss of cells is low, it can be quickly compensated by repopulation (with no damage or short-time effects). If the loss is large, there is a drastic noncompensated reduction of tissue cells (resulting in serious damage and/or death). The fraction of cells killed depends on dose; therefore, the severity of effects depends on dose as well. These effects are defined as deterministic and have dose thresholds.

Some deterministic effects are temporary or permanent sterility, depression of the blood-forming system, skin reddening, desquamation, skin loss, lens inflammation, and cataract. A peculiar case of deterministic effect is the radiation syndrome from acute and whole-body irradiation. If the dose is high enough, the strong cell depletion in vital organs (blood-forming organs, gastrointestinal tract, etc.) causes death. An acute whole-body exposure dose **between 3 and 5 Gy**, without any specific medical treatment, causes the death of 50% of the people exposed.

Table A.3 shows some thresholds for deterministic effects. The thresholds, like all thresholds for deterministic effects, apply to people in normal health [3].

B. Stochastic Effect

If a cell is not directly killed by radiation but somehow modified, the outcome will be different from those included among deterministic effects. In-vitro cellular research shows that damage from radiation to deoxyribonucleic acid (DNA) causes the most detrimental effects. There are two mechanisms by which radiation can damage DNA: direct or indirect interaction.

In the first case, ionizing radiation directly damages a gene; in the second, radiation produces active chemical radicals near the DNA. The radicals can

Table A.3 Threshold for deterministic effects

Deterministic effect	Threshold, Gy
Male temporary sterility	
Acute exposure	0.15
Chronic exposure (per year)	0.4
Male permanent sterility	
Acute exposure	3.5–6
Chronic exposure (per year)	2
Female permanent sterility	
Single exposure	2.5–6
Chronic exposure (per year)	0.2
Depression of blood formation	
Acute bone marrow exposure	0.5
Long-term exposure (per year)	0.4
Lens opacities (sparsely ionizing radiation)	2–10
Lens opacities (densely ionizing radiation)	1–2
Lens opacities (chronic exposure to sparsely ioniz. rad. per year)	0.15
Dry skin desquamation (3 weeks after exposure)	3–5
Moist desquamation (blistering after 1 month)	20
Tissue necrosis	50

diffuse and interact with DNA, inducing chemical changes. Very efficient mechanisms exist (enzyme actions) that repair DNA, whatever the cause of harm. For instance, if only one of the two symmetric strands forming the DNA is damaged, information on the other strand makes the repair process highly probable and successful, though **not always error free**. *It is this repair process, activated and energized by radiation, that is the basis for a field of radiation effects called radiation* ***hormesis***. Radiation hormesis is actually beneficial to organisms, as will be discussed later. If both strands are damaged at the same location, information is lost forever: the repair process is more difficult, and genetic changes are likely. Such changes are defined genetic mutations. The very nature of this damage/repair process causes effects that are random and statistical, called *stochastic*. Stochastic effects can be somatic (i.e., inducing cancer), that is, they occur in the individual exposed, or they can be hereditary, when the cells damaged are those whose function is to transmit genetic information to offspring. There is increasing evidence that below a certain dose the repair process is highly effective, reversing even effects of chemical oxides, peroxides, and superoxides within cells. This process is in direct opposition to the linear no-threshold concept. However, because stochastic effects might have no dose lower bound, there is no threshold in this case [3].

1. Radiation-Induced Cancer

There is substantive evidence that almost all cancers originate from a single cell. However, single changes in the cell genetic code are usually insufficient to initiate a cancer. Several cell mutations (two to seven) are required in

carcinogenesis to go from preneoplasia (cancer precursors) to cancer. Radiation can act at several stages of this process, but it seems to have a major role in the initial conversion of the cell to a preneoplastic state. A preneoplastic cell is immersed in an environment of normal cells, which tend to suppress and constrain preneo-plastic properties. Overcoming these constraints results in cancer.

Cancer can be triggered by many factors, such as smoke, chemical agents, and others, and it is therefore impossible to determine whether radiation is the cause of a particular type of cancer or not. The only way to ascertain a correlation between radiation and cancer induction is statistical. Epidemiology is the study of the distribution of diseases among people and is still an observational rather then experimental science: bias or confounding factors are highly probable.

In the present context, the so-called life span study (LSS), an ad hoc study of survivors of Hiroshima and Nagasaki, has produced a significant amount of data on effects of exposure to radiation on humans. Studies of people partially exposed to radiation as a result of medical investigations or treatments are another source of data, together with information available from studies of occupational exposures, that is, in the Mayak facility in Russia and the Chernobyl accident (see Appendix B and [4]).

From a general point of view, linear (or linear-quadratic) no-threshold dose response is to be expected, even though for certain cancers and at low doses correlations are less reliable.

Some interesting results are those for solid cancers obtained by the LSS, where ERR (excess relative risk) (Fig. A.2) and EAR (excess absolute risk) (see Fig. A.3) are estimated. ERR and EAR represent the increased cancer rate in an exposed group relative to an unexposed group, measured on relative and absolute scales. An ERR of 1 corresponds to a doubling of the cancer rate. EAR can be expressed as

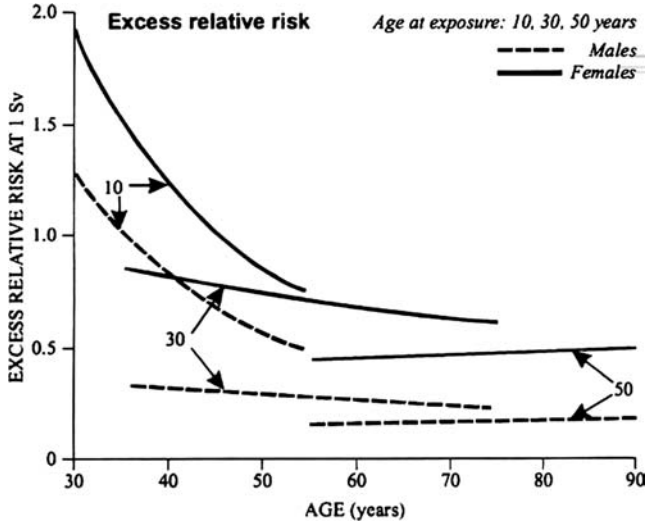


Fig. A.2 ERR at 1 Sv.

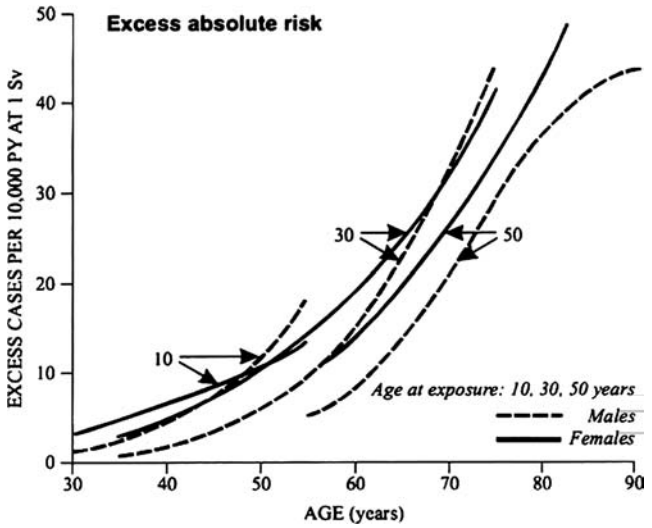


Fig. A.3 EAR at 1 Sv.

the number of excess cases of cancers per, for example, 10,000 persons. They can be expressed per unit dose or per a specific dose (i.e., 1 Sv) [5].

2. Radiation Hormesis Considerations

The Hiroshima/Nagasaki data clearly dispute the linear no-threshold (LNT) hypothesis as shown in Fig. A.4.

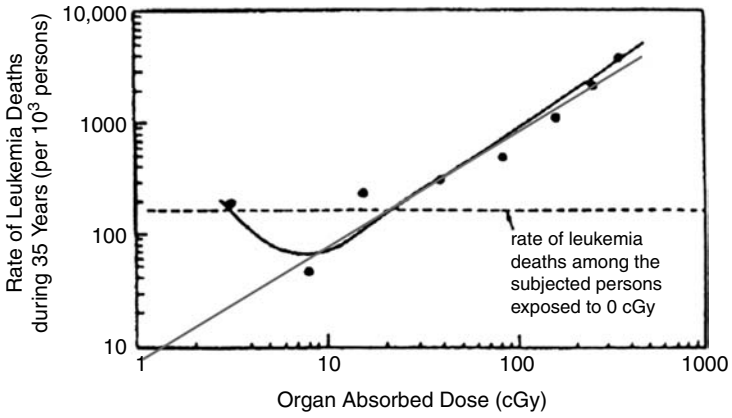


Fig. A.4 Radiation hormesis data from Hiroshima and Nagasaki survivors.

These data indicate that the actual leukemia deaths do not follow the LNT hypothesis, whose intersection at zero dose is shown in the overlay straight line. The problem with the LNT hypothesis is that it ignores realities of dose in other circumstances. This, when coupled with a no minimum dose, can become very problematic. For example, it is well known that 100 aspirin in a single dose can kill. If we follow the LNT concept, it means that a person taking one aspirin a week for 100 weeks will die, or out of 100 persons taking a single aspirin, one will die [5]. In fact, there exist more recent data besides Hiroshima and Nagasaki, for instance, those for U.S naval nuclear shipyard workers [6, 7] as shown in Fig. A.5.

Figure A.5 reports statistical data concerning workers at the naval shipyard at Portsmouth, New Hampshire in the United States, and a control group of 20,419 unexposed workers. That and the more recent study in [7] indicated a reduced mortality rate at a given age with respect to unexposed workers. The same effect is observed to be true for U.S. nuclear weapons workers. These data and others (for instance, see [9]) have suggested that at low doses radiation stimulates the biological defenses against cancer and other diseases that instead might be triggered at much higher doses [10, 11]. In fact, restricted to other disease-causing agents, this hypothesis was put forward and called *hormesis* by Arndt and Schultz in the late 1880s [12]. The statistical studies reported, for example, in [6, 7, 13], as well as many other studies, seem to confirm hormesis is real, although still hotly denied by many, likely because of the principle of caution. The data cited in [12] imply that doses less than a few cSv might in fact be beneficial. See also the literature cited in the site http://www.ans.org/pi/ps/docs/ps-41tb.pdf.

In the context of space propulsion, it should be a priority for space organizations such is AIAA and the International Academy of Astronautics (and the United Nations as well) to establish the importance to cost and risk reduction of adopting the radiation hormesis approach to radiation protection.

3. Hereditary Effects

No radiation-induced hereditary disease has been demonstrated in humans so far. However ionizing radiation is recognized as mutagenic (i.e., capable of

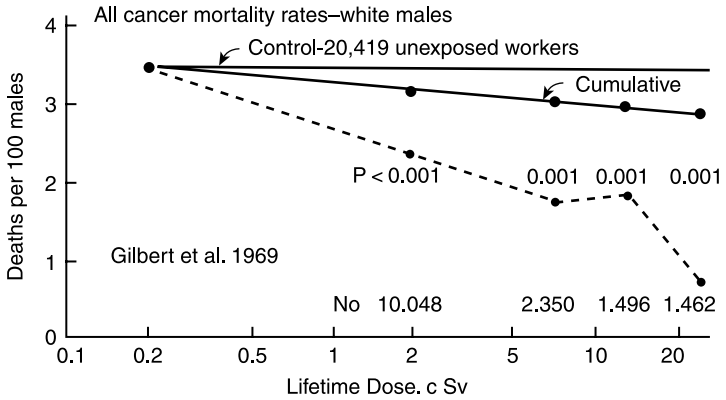


Fig. A.5 U.S. nuclear naval shipyard workers [8].

changing hereditary traits). Experiments on plants and animals have clearly shown that radiation can cause genetic effects, and there is no reason to believe that humans are an exception.

It has been estimated that, for a population exposed to radiation in one generation, the risk, expressed as number of cases per million people per Gy, in the progeny of the first postradiation generation is 750–1500 autosomal-dominant and X-linked diseases; 250–1200 chronic multifactorial diseases; and 2000 congenital abnormalities. The total radiation-induced cases are 3000–4700 per Gy per million and constitute 0.41–0.67% of the total 738,000 cases per million [14].

V. Sources of Radiation Exposure

Radiation to which humans are exposed comes from various sources. It can be natural radiation or can be produced by human activities.

A. Natural Radiation Exposure

Natural radiation, also defined as **background radiation**, has always existed in nature. Life on Earth has developed and keeps proliferating in a naturally radioactive environment. There are different sources of background radiation, responsible for either internal or external exposure.

Table A.4 shows the doses from natural sources. The **worldwide annual effective dose is 2.4 mSv**, and, considering a 5.3 billion world population, the collective dose is $13 * 10^6$ man Sv [4].

1. Cosmic Rays

Cosmic rays are a source of external exposure. They can be divided into primary and secondary radiation. Primary radiation can be further divided, depending on its origin, into galactic and solar, the second being less significant on the Earth's ground. Outside the Earth's atmosphere the main components of cosmic radiation are positively charged particles, mostly protons, of energy between 10^2 and 10^5 MeV; they constitute the so-called primary radiation (galactic and solar). When these particles approach Earth, they are deflected by the terrestrial magnetic field

Table A.4 Mean dose value for background radiation

Source	Worldwide average annual effective dose, mSv	Typical range, mSv
External exposure		
Cosmic rays	0.4	0.3–1.0
Terrestrial gamma rays	0.5	0.3–0.6
Internal exposure		
Inhalation (mainly radon)	1.2	0.2–10
Ingestion	0.3	0.2–0.8
Total	2.4	1–10

according to their momenta. In their travel toward the ground, primary radiation particles interact with the atmosphere, producing many particles such as electrons, photons, mesons, protons, and neutrons: these are called secondary radiation.

Secondary radiation particles themselves can interact with the atmosphere, or decay, producing so-called avalanche ionization: from a single-particle starting event up to 10^8 particles can be generated. In the atmosphere below 20 km, cosmic radiation is constituted almost exclusively of its secondary component [15]. The typical range of effective dose per person per year is 0.3–1.0 mSv, with average effective dose ~0.4 mSv [4]. For locations high above the sea level, very large doses are received, for example, in La Paz, Bolivia (sea-level altitude 3600 m), the average dose from cosmic rays is 2.02 mSv per year. Flying at 8000-m altitude results in a dose rate of 2.8 μSv h^{-1} [15]. Cosmic rays and their shielding will be a key issue in future interplanetary travel [16, 17].

2. *Terrestrial Radiation*

Inside the Earth there are radionuclides whose half-life ($T_{1/2}$) is comparable with Earth's age. **In fact the Earth's core is still hot thanks to the energy released by radionuclides in their decay processes**. The most significant, for dose computation are ^{40}K ($T_{1/2} = 1.28 * 10^9$ y), ^{232}Th ($T_{1/2} = 1.41 * 10^{10}$ y), ^{238}U ($T_{1/2} = 4.47 * 10^9$ y); of secondary importance are ^{87}Rb ($T_{1/2} = 4.7 * 10^{10}$ y) and ^{235}U ($T_{1/2} = 7.04 * 10^8$ y). Most radionuclides belong to one of the three families of uranium, thorium, and actinium (see Figs. A.6–A.8) [16]. In all three families radon (Rn) is formed as a decay product. Radon appearance is the clearest evidence that the Earth's crust is radioactive, and can be responsible for internal or external exposure.

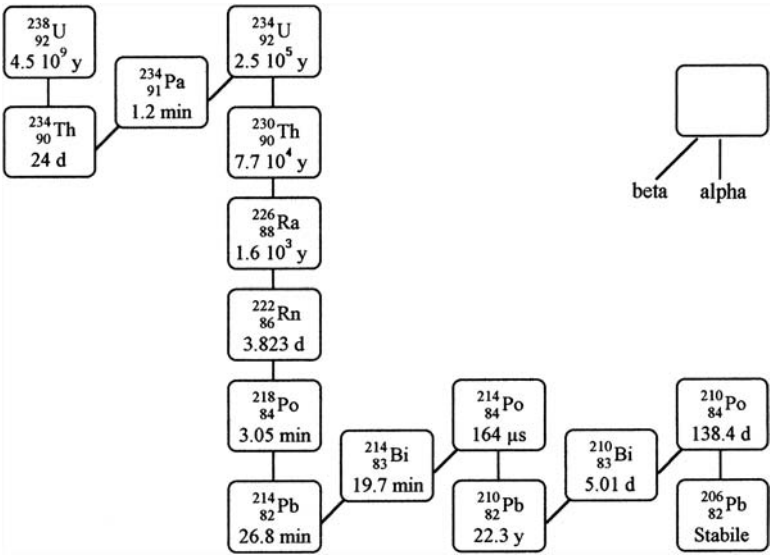


Fig. A.6 Uranium-238 decay chain.

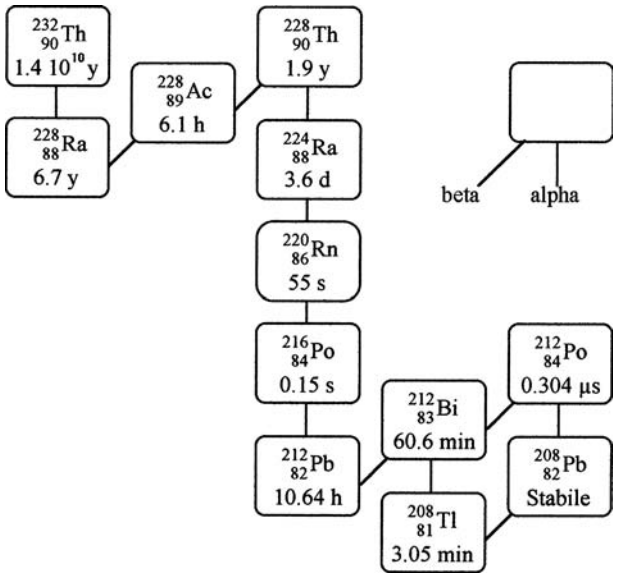


Fig. A.7 Thorium-232 decay chain.

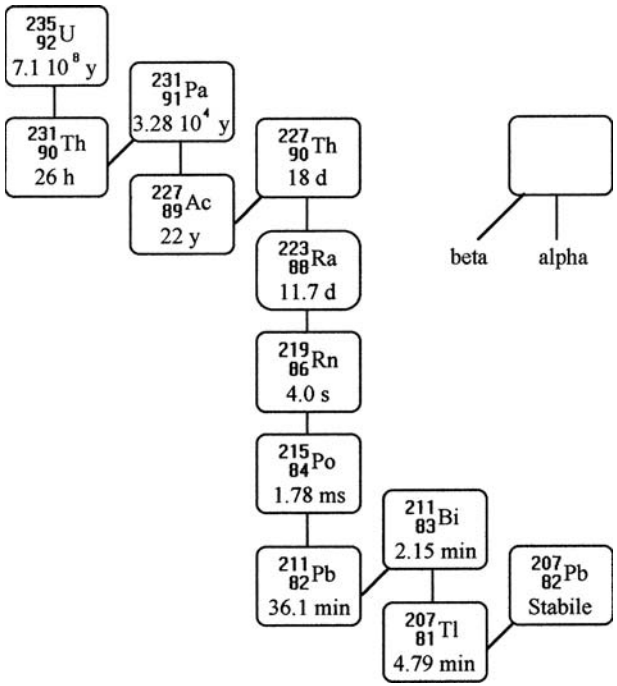


Fig. A.8 Uranium-235 decay chain.

External exposure from terrestrial radiation. External exposure to gamma rays from natural radionuclides can occur both outdoors, because radionuclides are present in the Earth crust, and indoors, as they might be present in construction material or seep through building foundations. Combining outdoor and indoor exposure, for a person spending 80% of time indoor, a range of **0.3–0.6 mSv per person per year is typical**. Worldwide-averaged annual effective exposure is estimated ~0.5 mSv [4].

Internal exposure from terrestrial radiation. Potassium isotopes are present in the human body with a weight percentage 0.18%; the isotope ^{40}K has an isotopic abundance $1.18 * 10^{-4}$, and its main decay mechanism is beta. The annual dose from ^{40}K is estimated 0.165 mSv. Some isotopes (the most significant are ^{210}Pb and ^{210}Po) can be ingested through food and water. The typical range of the annual effective dose is **0.2–0.8 mSv**, but higher values are detected in South America (because of the large quantity of ^{210}Po present in "yerba mate," a popular herb used in drinks) and arctic and subarctic areas (where ^{210}Po and ^{210}Pb tend to accumulate in moose meat). The worldwide-averaged annual effective dose is 0.3 mSv.

Some radioisotopes can be inhaled, the most significant in this case being ^{222}Rn and, much less importantly, ^{210}Po (smoking 10 cigarettes a day doubles ^{210}Po introduction). Typical range of inhaled dose is **0.2–10 mSv**. The range is so wide because the contribution is mainly given by radon and thus depends on its indoor accumulation. The worldwide-averaged annual effective dose as a result of inhalation is **1.2 mSv**. The summary of background radiation sources is in Table A.4 [4].

B. Medical Radiation Exposure

Ionizing radiation for medical purposes, both in diagnosis and in treatment, is widely used. Most of these procedures are carried out in countries where only one-quarter of the world population lives. World health care has been divided into four qualitative levels, depending on the number of physicians available.

Diagnostic exposures are characterized by low doses to individuals, whereas therapeutic exposure is usually much larger. High doses are used to treat diseases, especially cancer. The number of diagnostic procedures is much larger than treatment procedures (the ratio is about 450 to 1): this is because of the widespread use of x rays. (They contribute to 78% of collective dose.)

The worldwide-averaged annual effective dose is **0.4 mSv**; the total collective dose estimated is $2500 * 10^6$ man Sv. Table A.5 shows effective doses reported for each health-care level [4]. Table A.6 [15] shows the effective dose for some diagnostic examinations.

C. Exposure from Atmospheric Nuclear Testing

Until the Treaty Banning Nuclear Weapon Tests in the Atmosphere, in Outer Space and Under Water, signed in Moscow on August 5, 1963, almost all nuclear explosions to test weapons (fissions and fusions) were carried out in the northern-hemisphere's atmosphere. For instance, in the former Soviet Union at Semipalatinsk, in Kazakhstan, 456 tests were carried out between 1949 and 1989 [18]; after the treaty almost all tests have been conducted underground. The two time periods of most intense atmospheric tests were 1952–1958 and 1961–1962

Table A.5 Average dose from medical use

Health-care level	Population per physician	Annual number of examinations per 1,000 persons	Average annual effective dose to population, mSv
I	<1,000	920	1.2
II	1,000–3,000	150	0.14
III	3,000–10,000	20	0.02
IV	>10,000	<20	<0.02
Worldwide average	——	330	0.4

(see Fig. A.9). The total number of atmospheric tests is 543, and the total yield estimated is 440 megatons (189 megatons from fission) [4].

The total collective effective dose resulting from weapon tests to date is $3 * 10^7$ man Sv; of these $7 * 10^6$ man Sv will be delivered within the first 250 years (until 2200); the remainder, because of the long life of the C^{14} radionuclide produced, will be delivered in the next 10,000 years. The annual average effective dose varies both with time (decreasing thanks to the ban treaty) and with location: in the northern hemisphere the dose is higher than in the southern. The average effective dose estimated for the year 1999 is 5.87 μSv in the northern hemisphere, 2.68 μSv in the southern, and 5.51 globally (see Table A.7).

D. Nuclear-Power Generation by Utilities

Today about 17% of electricity produced worldwide, that is, about 250 GW, is from nuclear-power plants. Assuming that this practice continues over the next 100 years, the maximum collective dose can be estimated from the cumulative dose over the period of practice. The normalized 100-year collective dose is 6-man Sv per GW and per year. The annual dose is 1500-man Sv (6×250), resulting in a maximum annual dose per person of 0.2 μSv [5].

E. Exposure from Major Accidents

There have been accidents in using nuclear energy or radioactive elements. In medical and diagnostic practice accidents can occur (a few hundreds of all types

Table A.6 Doses from some examinations

Examination	Effective dose per examination, mSv
Chest radiography	0.14
Mammography	0.5
Angiography	12
Urography	3.7
Dental	0.03

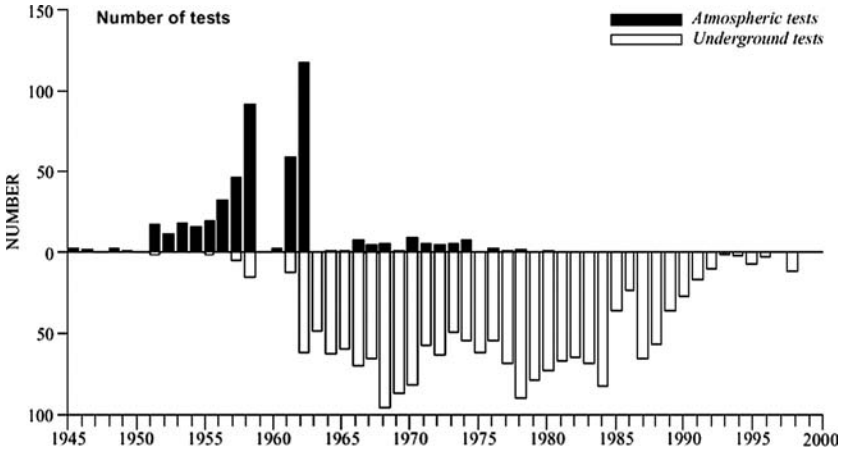


Fig. A.9 Number of weapons tests vs time.

each year) and usually have serious consequences. The probability that any member of the public would be involved is, however, very small, and, by and large, the consequences do not affect the public.

Weapons production and transportation have resulted in several accidents, but the collective dose committed is small. The two most serious accidents in nuclear weapons production were at Kyshtym, in the former Soviet Union, and at the Windscale plant at Sellafield, in the United Kingdom, both in 1957. The first accident caused a collective dose of 2500-man Sv over the next 30 years. The

Table A.7 Doses from weapons tests

	Average annual effective dose μSv		
Year	Northern hemisphere	Southern hemisphere	World
1945	0.64	——	0.57
1955	16.8	3.34	15.4
1965	48.7	11.7	44.6
1975	14.8	5.01	13.7
1985	8.98	2.78	8.30
1995	6.61	2.55	6.20
1996	6.42	2.57	5.97
1997	6.23	2.59	5.85
1998	6.05	2.63	5.63
1999	5.87	2.68	5.51
1945–1999	1076	328	994
1999–2099	264	157	253
2099–2199	63	53	62
2200	2181	2180	2181
1945	3580	2720	3490

Sellafield accident caused a total collective dose in Europe (including England) of about 2000-man Sv.

The two most important accidents in power plants were those at Three Mile Island, in the United States, and Chernobyl, in the Ukraine, although the Chernobyl installation produced energy only as a byproduct, the plant being chiefly a plutonium-producing facility. Additionally, what happened can hardly be defined an accident. At Three Mile Island the containment system, missing at Chernobyl, prevented a large amount of fission fragments from spreading to the environment: the total collective effective dose was $\leq$40-man Sv, with the maximum dose to nearby individuals $\leq$1 mSv. The Chernobyl accident (see its detailed account in Appendix B) had much more serious consequences. It caused the death of 30 people among the rescue workers within a few weeks, at least 1800 cases of thyroid cancer in the children exposed, and a total of 56 fatalities to date. The worldwide average annual effective dose per person because of the Chernobyl accident, estimated for the year 2000, is 0.002 mSv, down from its peak 0.04 mSv in 1986 [4].

F. Occupational Exposure

There are jobs in which workers are routinely exposed to radiation, both because of man-made sources (i.e., medical practice, people employed in nuclear fuel cycle facilities, etc.) and because of enhanced levels of natural radiation (i.e., airplane crews flying at a height of 8000 m receive a dose of 2.8 μSv per hour). This kind of exposure does not affect other members of the public, but it is interesting to see the dose (see Table A.8) that these workers receive in order to have a better understanding of the issue [4].

G. Exposure from Future Nuclear Propulsion Systems

A new source of dose could in principle result because of future nuclear propulsion systems. The Rubbia's engine and MITEE (see Chapters 1 and 2) are two of the most promising systems [19, 20]: an assessment of the dose committed to the public arising from their use is necessary in order to show the impact they could have.

To set to rest a very old misconception, there is literally no way a nuclear reactor, whether for power generation or propulsion, could trigger a nuclear explosion: the reason is the impossibility of reaching the proper conditions of confinement time and critical mass.

However, what could happen is that because of coolant loss, or other reasons, "runaway" fission in a reactor can heat the reactor core too much, eventually melting it down. This effect is called a loss of coolant accident (LOCA). When this happens (like in the case of Chernobyl), high-temperature chemical reactions can occur, especially if water or graphite moderators are present. Water could be dissociated by the high temperatures, producing hydrogen and oxygen and possibly burning or exploding, and graphite could burn in an oxygen or hydrogen atmosphere. Besides, excessive heat-release rates can also cause explosions simply as a result of rapid thermal expansion of the nuclear "fuel" or other reactor

Table A.8 Occupational exposure

Source/practice	Number of monitored workers (thousands)	Average annual effective dose, mSv
Man-made sources		
Nuclear fuel cycle (including uranium mining)	800	1.8
Industrial uses of radiation	700	0.5
Defence activities	420	0.2
Medical uses of radiation	2320	0.3
Education/veterinary	360	0.1
Total from man-made sources	4600	0.6
Enhanced natural sources		
Air travel (crew)	250	3.0
Mining (other than coal)	760	2.7
Coal mining	3910	0.7
Mineral processing	300	1.0
Above ground workplaces (radon)	1250	4.8
Total from natural sources	6500	1.8

material. LOCAs are most serious in nuclear reactors. In the absence of a containment structure, radionuclides from the core can be ejected by the chemical or thermal explosion and contaminate the nearby environment.

This said, it should be clear that this type of accident is in fact caused by chemistry, not fission. (The use by the popular press of the words "nuclear explosion" in this context is due to factual ignorance and is misleading.) In space, it is highly unlikely that there will be the necessary constituents available to cause the spectacular failures such as those seen in Chernobyl.

To test the effects of an actual meltdown caused by runaway fission, during the NERVA program a test was performed at Los Alamos in which a KIWI nuclear reactor was deliberately let to explode by excluding the cooling system. (This was the so-called KIWI-TNT test.) The results are reported in [21, 22]. The reactor was totally destroyed, but contamination was limited to a relatively small area of order 100-m radius. After clearing appropriately the site from debris, activities could be resumed. This test did much to allay fears that a NERVA-type core meltdown and explosion could in any way produce a large-scale catastrophe. A nuclear rocket reactor must be inherently far smaller than that in powerplants, and so the outcome of the KIWI-TNT test is not surprising.

A specific and more serious concern in propulsion applications, a nuclear reactor must be orbited, that is, lifted through the Earth atmosphere, perform its interplanetary mission starting from LEO or MEO, and (possibly) be parked again in Earth orbit at the end of its mission. The question is, what could happen during each of these three legs. Chapter 6 describes in detail possible scenarios; here is a synthetic dose evaluation analysis.

Any reactor will contain fissile fuel, of the order $\mathcal{O}(1)$ to $\mathcal{O}(10)$ kg depending on fuel type. Of course, no reactor will be operated while being lifted off, but the

danger exists of an accident, such as that of the *Challenger*, in which the conventional launcher could explode, damaging the reactor to be orbited and spreading fissile material from the damaged reactor stored in the payload bay either to the atmosphere or to the ground.

During the interplanetary trajectory, instead, no accident would affect Earth. The most dangerous occurrence would be if the reactor, containing all of the (new) radionuclides produced during its space operation, would for some reason reenter the Earth's atmosphere accidentally. No space agency is considering deliberate reentering of nuclear reactors, so that such an event would have to be unplanned, unwanted, and therefore accidental.

The consequences would be the spreading of many radionuclides families in the atmosphere, at a height that can be estimated roughly between 40 and, say, 10 km, that is, near the peak of aerodynamic heating. The total mass of radionuclides spread would be approximately the same of the original fuel, that is, $\mathcal{O}(1)$ to $\mathcal{O}(10)$ kg. Additional contamination would come from secondary radioactivity, that is, induced in the reactor structural materials.

Insofar as to the actual consequences, this event is similar to what happens during an atomic explosion in the atmosphere, where fissionable material and bomb structure are vaporized and released. Data from atmospheric atomic tests that can effectively estimate these effects exist. In any event, the quantity of radionuclides in an atomic explosion is many times larger than that in any nuclear reactor at this time envisaged for space missions; accordingly, radioactive contamination is expected to be smaller, as estimated next.

1. Nuclear Accidents in a Rubbia's Engine

Like all other nuclear-propulsion concepts, the Rubbia's engine is not planned to fission while in the atmosphere. The dose to the public would be the highest in a hypothetical accidental reentry, for instance, at the end of a Mars mission. For each kilogram of americium fuel loaded, it is estimated that the total collective dose committed for the following 250 years is 9.5-man Sv. The individual dose commitment over the following 250 years would be $1.8 * 10^{-6}$ mSv. In the case of an americium stockpile of 15 kg, typical of a manned Mars mission using the Rubbia's engine, the total collective dose committed for the first 250 years would be 140-man Sv, whereas the individual value would be $3 * 10^{-5}$ mSv [23].

In addition, the fuel considered in Rubbia engine (Am-242 m) was purposely chosen because of its neutron cross section sharply decreasing with temperature. This feature means that any hypothetical runaway fission in Am 242 m would automatically stop above a certain temperature, and the reactor regime would be brought back to a stable state.

2. Nuclear Accidents in a MITEE Engine

Also in the case of MITEE, the most catastrophic accident could be the total destruction of the vehicle accidentally reentering the atmosphere after a mission. Like Rubbia's engine, MITEE is planned not to fission while in the Earth's atmosphere, so that also in this case a prompt criticality accident (explosion caused by overheating) would have less considerable consequences than the total

destruction for a chemical explosion or unwanted reentry in the atmosphere after returning from a mission to Mars. The average dose commitment over the following 250 years would be about $1.6 * 10^{-8}$ mSv for each kg of uranium loaded, and for a typical MITEE configuration the average dose commitment for 250 years would be therefore about $4 * 10^{-7}$ mSv (Maise, G., personal communication) [4, 20, 21].

3. Safety in Ground Testing of Future Nuclear Rockets

A key worry in planning nuclear propulsion revolves around the issue of ground testing. In the past, KIWI, NERVA, and PHOEBUS reactors were all tested at Los Alamos in the open air.

A recent book recounts details of those tests and the safety measures employed; no accidents involving loss of life or damage to people took place during the entire U.S. program [21, 22].

Nevertheless, planning future ground tests is a concern. However, at least in the case of the type of reactor envisaged by C. Rubbia and investigated by the Italian Space Agency (ASI) under Project P 242 (see Chapter 1), the following considerations apply.

The Rubbia engine is modular, each module being a self-standing generator of hot hydrogen gas. About 30 to 40 modules may compose the engine.

For a manned Mars mission the thrust F required is of order 10^3 N, while the specific impulse I_{sp} is about 2500 s. Comparison with the NERVA thermal engine tested at Los Alamos ($F = 334{,}000$ N; $I_{sp} = 825$ s; mass flow rate $= 40$ kg/s) shows that the single module of the Rubbia engine to be tested in an appropriate test facility will process a mass flow rate of hydrogen of order 2.5 g/s. So, the scale factor between a module of Rubbia engine and NERVA is about 16,000. The amount of hydrogen, and therefore of fission fragments deposited inside the hydrogen used as propellant, will be exceedingly small.

As a consequence, testing a single module of the Rubbia engine can be performed in a closed loop, and this appears also feasible for all nuclear rockets of comparable thrust, therefore also MITEE, or nuclear-electric rockets. In fact, ways of efficiently separating fission fragments from hydrogen have already been described in the proprietary Final Report of ASI P 242 Phase A [24]. Closed-loop tests can be performed in any reasonably self-contained facility and building, thus ensuring no radiation can escape.

H. Comparison of Exposures

The doses received by an individual from the main different sources in year 2000 are summarized in Table A.9. Their values are given in annual per caput effective dose (mSv). The values are averaged, meaning that there are significant variations in exposure to individuals, depending on location, diet, personal habits, and so forth.

The largest contribution to total dose is from the natural background: 2.4 mSv, but typical values can range from 1 up to 10 mSv, with large groups of population receiving a dose of 10–20 mSv. The second most important source, 0.4 mSv, comes from the medical use of radiation. It has an increasing trend, thanks to

Table A.9 Annual per capita doses in the year 2000

Source	Worldwide annual per caput dose, mSv	Range or trend
Natural background	2.4	Typical range 1–10 mSv; sizeable population also 10–20 mSv
Diagnostic medical use	0.4	Typical range 0.04–1.0 mSv at lowest and highest level of health care
Atmospheric nuclear testing	0.005	Has decreased from a maximum of 0.15 mSv in 1963; higher in northern hemisphere and lower in southern hemisphere
Chernobyl accident	0.002	Has decreased from a maximum of 0.04 mSv in 1986; higher in locations near the accident area
Nuclear-power production	0.0002	Has increased with expansion of plants but decreased thanks to improved practice

increasingly available medical radiation facilities. The third cause is the fallout from past weapons tests, that is, 0.005 mSv. The value has been decreasing thanks to the Treaty Banning Nuclear Weapon Tests, the maximum value being reached in 1963, when it was 7% of the natural background. Other man-made sources, like the Chernobyl accident and nuclear-power production, are much smaller, 0.002 and 0.0002 mSv, respectively.

VI. Conclusions

The individual dose commitments for 250 years arising from a rather improbable total "crash" of Rubbia's engine, $1.8 * 10^{-6}$ mSv, and MITEE, $1.6 * 10^{-8}$ mSv, are insignificant compared to other sources of exposure. Should the Rubbia's engine crash, a hypothetical individual born in the year of the crash and dying at age 250 would have received all along his life a dose of $3 * 10^{-5}$ mSv, much lower than the dose imparted by a dental examination (0.03 mSv); the same would be true for a MITEE accident of the same type. The average dose from natural background to each individual is 2.4 mSv in one single year. Table A.10 shows contribution to dose compared to other sources.

The contribution to individual average dose from the crash of Rubbia's engine or MITEE is therefore not a reason of concern to public health. It would take an accident involving a nuclear engine a million times more powerful to start approaching the dose humans receive while living on Earth.

As a more general conclusion, we note that nuclear thermal propulsion and nuclear electric propulsion are exceptional enablers to space exploration; doses from nuclear reactors in space, provided they are adequately shielded, will be insignificant compared to the space environment itself. In fact, the reduced trip times enabled by nuclear propulsion will enhance safety as a result of reduced exposure to zero gravity and the cosmic radiation background. There are extensive data supporting the radiation hormesis approach to radiation health effects, as opposed to the linear no-threshold hypothesis. That should guide the radiation

Table A.10 Comparison of doses from different sources

Source	Effective dose/dose commitment, mSv	Comment
Rubbia's engine accident → Catastrophic LEO reentry	$1.8 * 10^{-6}$	Dose committed for 250 years (per kg fuel)
MITEE accident → catastrophic LEO reentry	$1.6 * 10^{-8}$	Dose committed for 250 years (per kg fuel)
Natural background	2.4	Average effective dose in 1 year
Dental x-ray examination	0.03	Average effective dose from a single examination
Flying at 8 km for 10 h	$2.8 * 10^{-8}$	1 h gives $2.8 * 10\,\mu$Sv

safety doctrine for space nuclear-power and -propulsion systems, including ground testing. It is likely that no single event will assist the technical development of nuclear power and propulsion more than the reduction in costs and regulatory burdens generated by eliminating the linear no-threshold hypothesis as the basis for radiation health effects.

References

[1] Mukhin, K. N., *Physics of Atomic Nucleus,* Vol. I, Mir, Moscow, 1987, Chap. 1–4.
[2] "Recommendations of the International Commission on Radiological Protection (ICRP)," *Annals of the ICRP*, Vol. 21, No. 1–3, 1991; also ICRP Publication 60.
[3] "Sources and Effects of Ionizing Radiation," United Nations Scientific Committee on the Effects of Atomic Radiation, UNSCEAR 1993 Report to the General Assembly, with Scientific Annexes, United Nations, New York, Sept. 1993.
[4] "Sources and Effects of Ionizing Radiation," United Nations Scientific Committee on the Effects of Atomic Radiation, UNSCEAR 2000 Report to the General Assembly, with Scientific Annexes, United Nations, New York, Sept. 2000.
[5] Whithlock, J., "When Menes Collide," *Canadian Nuclear Society Bulletin*, Vol. 20, No. 3, 1999.
[6] Stern, F. B., Waxweiler, R. A., and Beaumont, J. J., "A Case Control Study of Leukemia at a Naval Nuclear Shipyard," *American Journal of Epidemiology*, Vol. 123, 1986, pp. 980–992.
[7] Sponsler R., and Cameron, J. R., "Nuclear Shipyard Worker Study (1980–1988): a Large Cohort Exposed to Low-Dose-Rate Gamma Radiation," *International Journal Low Radiation*, Vol. 1, No. 4, 2005, pp. 463–478.
[8] Matanowski, G. M., Breysse, P. N., and Elliott, E. A., "Electromagnetic Field Exposure and Male Breast Cancer," *Lancet*, Vol. 337, 1991, pp. 737–746.
[9] Shimizu, Y., Kato, H., Schull, W. J., and Mabuchi, K., "Dose Response Analysis Among Atomic-Bomb Survivors Exposed to Low-Level Radiation," *Low Dose Irradiation and Biological Defense Mechanisms*, edited by T. Sugahara, L. Sagan, and T. Aoyama, Excerpta Medica Publishers, Amsterdam, 1992, pp. 71–74.
[10] Calabrese, E. J., and Baldwin, L. A., "Hormesis as a Biological Hypothesis," *Environ. Health Perspectives*, Vol. 106 (Supplement 1), Feb. 1998, pp. 357–362.
[11] Luckey, T. D., *Radiation Hormesis*, CRC Press, Boca Raton, FL, 1991.

[12] Luckey, T. D., "Radiation Hormesis," *Signals and Images, Selected Topics from the 7th and 8th GIRI (Group International de Recherches sur l'Infinitesimal)*, edited by M. Bastide, Kluwer Academic Publishers/Springer, Dordrecht, 1997, pp. 31–40.

[13] Gilbert, E. S., Wilkinson, G. S., and Dreyer, N. A., "Leukemia Among Nuclear Workers with Protracted Exposure to Low-Dose Ionizing Radiation," *Epidemiology*, Vol. 3, No. 3, 1992, pp. 275, 276.

[14] "Hereditary Effects of Radiation," United Nations Scientific Committee on the Effects of Atomic Radiation, UNSCEAR 2001 Report to the General Assembly, with Scientific Annexes, United Nations, New York, Sept. 2001.

[15] Galli, G., and Mancini, C., "Esposizione alla Radioattività Ambientale," *Ingegneria Nucleare e Tecnologie Energetiche*, Vol. 38, No. 1–4, 1996. See also Batistoni, P., personal communication, 2002. Data on nuclear decays can be found at http://www.webelements.com/webelements/elements/text/periodic=table/key.html, http://atom.kaeri.re.kr/, or http://www2.bnl.gov/ton/, and also at http://sutekh.nd.rl.ac.uk/CON/

[16] Parker, E. N., "Shielding Space Travellers," *Scientific American*, Vol. 294, No. 3, 2006, pp. 22–29.

[17] Simonsen, L. C., Wilson, J. W., Kim, M. H., and Cucinotta, F. A., "Radiation Exposure for Human Mars Exploration," *Health Physics*, Vol. 79, No. 5, 2000, pp. 515–525.

[18] NATO Science Information site, http://www.nato.int/science/e/grants.

[19] Powell, J., Maise, G., and Paniagua, J., "MITEE: An Ultra Lightweight Nuclear Engine for New and Unique Planetary Science and Exploration Missions," International Astronautical Congress, IAF-98-R.1.01, Sept–Oct. 1998.

[20] Powell, J., Maise, G., and Paniagua, J., "The MITEE Family of Compact, Ultra Lightweight Nuclear Thermal Propulsion Engines for Planetary Space Exploration," International Astronautical Congress, IAF-99-5.6.03, Oct. 1999.

[21] Dewar, J. A., "The Story of The Nuclear Rocket: Lessons for The Future," International Astronautical Congress, Paper IAC-02-IAA.2.4.06, Oct. 2002.

[22] Dewar, J. A., *To the End of the Solar System: The Story of the Nuclear Rocket*, Univ. Press of Kentucky, Lexington, KY, 2002.

[23] Rubbia, C., *Fission Fragments Heating for Space Propulsion*, European Organization for Nuclear Research, Geneva, 2000.

[24] Augelli, M., Bignami, G., Bruno, C., Calligarich, E., De Maria, G., Mulas, M., Musso, C., Pellizzoni, A., Piperno, W., Piva, R., Procacci, B., Rosa-Clot, M., and Rubbia, C., "Report of the Working Group on a Preliminary Assessment of a New Fission Fragment Heated Propulsion Concept and its Applicability to Manned Missions to the Planet Mars (Project 242)," ASI Internal Report, Rome, March 15, 1999 (Proprietary).

Copyrighted Materials
Copyright © 2008 AIAA Retrieved from www.knovel.com

INDEX

Index Terms **Links**

A

Absorbed dose D (gy) 248
Activity (Bq) 247
Alpha decay 246
Ammonia 134
Annihilation 8
Anode cooling 153
Anode erosion 151
Atmospheric nuclear testing,
radiation exposure from 259 261
Atom bonds 5
Attenuation factor 12

B

Background radiation. *See* natural
radiation exposure.
Becquerel 247
Beta decay 246
Bi-exit nozzle 131
Bimodal NERVA derivative 39
Blowing forces 139
Bq. *See* Becquerel.

This page has been reformatted by Knovel to provide easier navigation.

Index Terms	Links
C	
Cancer, radiation-induced	252
Cassini FSAR	219
Hazards table format	220
scenarios	219
Cathode cooling	152
Cathode erosion	151
CERMET	42
advantages of	44
reactor	43
Charged particles movement	158
Chemical potential	5
Chemical propulsion, nuclear thermal rockets vs	24
Chemical rockets	
hybrid nuclear thermal	45
nuclear thermal vs	33
Chernobyl accident	269
casualties	273
reactor design	269
flaws	269
void coefficient	270
released radioactivity	273
time line	270
Coaxial applied field, MPD thruster and	154
acceleration mechanism	155
charged particles movement	158

This page has been reformatted by Knovel to provide easier navigation.

Index Terms	Links	
Coaxial applied field, MPD thruster and (*Cont.*)		
current distribution	156	157
experimental evidence	161	
Hall parameter	155	
numerical simulation	164	
plasma rotational frequency	159	
propellants	162	
thrust	159	
Cold (neutral) gas injection	143	
Cold gas thruster	32	
Collective dose (man Sv)	250	
Commercial satellites	204	
Control rods	36	
Controlled thermonuclear-reactor (CTR)	94	
Coolant flow paths	36	
Cosmic rays	256	
Criticality tests	231	
CTR. *See* controlled thermonuclear reactor.		
Curium	46	
Current density	99	
Current distribution	156	157

D

Deterministic effects	251	252
Discharge chamber	100	

This page has been reformatted by Knovel to provide easier navigation.

Index Terms	Links
Discharge initiation, magnetoplasmadynamic thrusters and	67
Discharge voltages	132
constrictor diameter	132
cooling system	132
mass flow	132
propellant	132
DLR Stuttgart, X-16 and	165
Dose commitment (Sv)	250
Dual-cone nozzle	131
E	
Early launch phase accident scenario probability	236
ECR. *See* electron-cyclotron resonance.	
Effective dose E (Sv)	249
Electric propulsion (EP)	54
efficiencies of	57
gridded ion engine	54
rocket equation	57
specific impulse	57
velocity increments	60
system parameters	58
specific impulse	59
thrusting duration	59

This page has been reformatted by Knovel to provide easier navigation.

Index Terms	Links
Electricity generation, radiation exposure from	260
Electrode design	147
Electrode erosion	150
anode	151
cathode	151
Electrode voltage drops/losses	147
anodes	153
cathodes	152
electrode erosion	150
MPD thruster cathode phenomenology	147
propellants	153
thruster anode phenomenology	148
Electron volts	5
Electron-cyclotron-resonance (ECR)	70
Electroweak force	2 4
EP. *See* electric propulsion.	
Equivalent dose H (Sv)	248
ESA-XX RF thruster	82
Exhaust velocity	97
Explosion environments, safety analysis and	233
External exposure, terrestrial radiation and	259

F

Failure events	
Cassini FSAR	219
radiation release and	221

This page has been reformatted by Knovel to provide easier navigation.

Index Terms	Links		
Fire tests, safety and	228		
Fission	7	31	
release	224		
Fixed power	17		
Forces in nature	2		
electroweak	2		
gravitation	2		
nuclear force	2		
Fuel element assembly	36		
Fuel mass	16		
Fusion	7		

G

Gamma rays	247		
Gas core nuclear thermal rockets	20		
Rubbia	21		
Gas-cooled reactor (GCR)	180		
GCR. *See* gas-cooled reactor.			
GIE. *See* gridded ion engine.			
Gravitation	2		
Gravitational energy	4		
Gray (Gy)	248		
Gridded ion engines (GIE)	54	61	69
current capabilities	91		
ESA-XX RF thruster	82		
HiPEP MESC thruster	89		
ionization mechanisms	69		

This page has been reformatted by Knovel to provide easier navigation.

Index Terms	Links
Gridded ion engines (GIE) (*Cont.*)	
magnetoplasmadynamic thrusters	66
NAL/NASDA/Toshiba BBM-2 MESC thruster	86
NASA 30-cm beam diameter thrusters	86
neutralizer	61
NEXIS MESC thruster	87
NSTAR MESC thruster	85
plasma production mechanism	63
RIT-15	78
RIT-22	80
RIT-35 RF thruster	86
RIT-XT	80
SERT II	79
space plasma	62
T5 thruster	77
T6 Kaufman-type thruster	81
thrusters	63
very large diameter	90
Tokyo Metropolitan Institute of Technology 30-cm MESC thruster	87
UK-25 Kaufman-type thruster	83
XIPS-25 MESC thruster	83
Ground testing safety	265
Gy. *See* Gray.	

This page has been reformatted by Knovel to provide easier navigation.

Index Terms	Links
H	
Half-life	248
Hall parameter	155
Hall-effect thruster (HET)	63
propellant, xenon	65
specific impulse	65
thrust	66
thruster temperatures	66
Hazards table format	220
Heating and Analysis Done Interactively code	233
Heat-pipe-cooled reactor (HPR)	180
HEDM. *See* high energy density matter.	
Hereditary effects	255
HET. *See* Hall-Effect thruster.	
High energy density matter (HEDM)	
propellants	6
High power hybrid ATTILA thruster	168
High specific impulse	101
HiPEP (hi-power electric propulsion)	
MESC thruster	89
Hi-power electric propulsion. *See* HiPEP.	
Hormesis	252
HPR. *See* heat-pipe-cooled reactor.	
Hybrid nuclear thermal chemical	
rockets	45
Hydrazine	134
Hydrogen	134

This page has been reformatted by Knovel to provide easier navigation.

Index Terms	Links	

I

Impact analyses	233	
Impact tests, safety and	228	
Inert mass	16	
Intentional disassembly, safety analysis and	233	
Internal exposure, terrestrial radiation and	259	
Ion thrusters	53	
gridded ion engines	61	69
Hall-effect thruster	63	
high power operation	101	
lifetime predictability	114	
megawatt level operation	107	
parametric variations	101	
perveance increase	106	
specific impulse increase	104	
systems required	114	
technological limitations	107	
thruster diameter	103	
high specific impulse	101	
magnetoplasmadynamic thrusters	55	
scaling process	93	
current density	99	
discharge chamber	100	
exhaust velocity	97	
grid design options	94	
perveance	99	
power density	99	

This page has been reformatted by Knovel to provide easier navigation.

Index Terms	Links	
Ion thrusters (*Cont.*)		
specific impulse	97	
thrust densities	99	
thermal design	115	
throttling capability	114	
types and capabilities of	68	
variable-specific-impulse magnetoplasma rocket	67	69
Ionization mechanisms, radiofrequency discharge thrusters	70	
Ionizing radiation	251	
deterministic effects	251	252
stochastic effect	251	
Isotope release	224	

K

Kaufman-type direct current discharge thrusters	73	
KE. *See* kinetic energy.		
Kinetic energy (KE)	3	

L

Late ascent accident scenario probability	237	
Launch accident scenario probability		
early launch phase	236	
late ascent	237	

This page has been reformatted by Knovel to provide easier navigation.

Index Terms	Links
Launch accident scenario probability (*Cont.*)	
orbit circularization	237
prelaunch	236
reactor	237
Launch environment tests	229
Launch site safety	213
scenarios	
arrival at site	214
countdown	216
early launch	217
late launch	217
launch preparation	216
spacecraft final assembly	216
Linear no-threshold (LNT)	254
Liquid-metal cooled reactor (LMR)	180
LMR. *See* liquid-metal cooled reactor.	
LNT. *See* linear no-threshold.	
Lunar based nuclear power, hazards	221

M

Magneto-electrostatic containment (MESC) dc thrusters	75		
Magnetoplasmadynamic (MPD) thruster	55	66	138
cathode phenomenology	147		
coaxial applied field	154		
acceleration mechanism	155		
charged particles movement	158		

This page has been reformatted by Knovel to provide easier navigation.

Index Terms	Links	
Magnetoplasmadynamic (MPD) thruster (*Cont.*)		
current distribution	156	157
experimental evidence	161	
Hall parameter	155	
numerical simulation	164	
plasma rotational frequency	159	
propellants	162	
thrust	159	
design of	66	
discharge initiation	67	
history of	164	
NASA	165	
Russia	167	
X-16	165	
self-field	138	
test facilities	168	
MagOrion	45	
man Sv	250	
Mars-based nuclear power		
hazards	221	
safety issues	224	
contamination	224	
fission release	224	
inadvertent reentry	225	
isotope release	224	
radiation exposure	225	
Mars exploration projects	203	
oxygen	204	

This page has been reformatted by Knovel to provide easier navigation.

Index Terms	Links		
Mass	16		
fixed power	17		
fuel	16		
inert	16		
propellant mass	16		
Massless nuclear propulsion	25		
Medical radiation exposure	259	260	
Megawatt level operation, ion thrusters and	107		
actual designs	110	111	
parameter ranges	113		
peak thruster performance	110	111	112
propellant selection	112	113	
MESC. *See* magneto-electrostatic containment.			
Mini-MagOrion (MMO)	45		
curium	46		
MITEE engine, radiation exposure from	264		
MMO. *See* Mini-MagOrion.			
Moderator	36		
Mono-atomic gases	135		
MPD. *See* magnetoplasmadynamic thrusters.			

N

NAL/NASDA/Toshiba BBm-2 MESC thruster	86		
NASA 30-cm beam diameter thrusters	86		

This page has been reformatted by Knovel to provide easier navigation.

Index Terms	Links	
NASA evolutionary xenon thruster. *See* NEXT.		
NASA thruster, superconductive magnet	165	
Natural isotopes	8	
Natural radiation exposure	256	
cosmic rays	256	
mean dose value	256	
terrestrial	257	
NEP. *See* nuclear electric propulsion.		
NERVA (Nuclear Engine for Rocket Vehicle Applications)	37	
NERVA derivative	37	
bimodal	39	
history of	38	
reactor problem	38	
test results	38	39
Neutralizer	61	
Neutronics	232	
Newton's Third Law	2	9
NEXIS (nuclear electric xenon ion system) MESC thruster	88	
NEXT (NASA evolutionary xenon thruster) MESC thruster	87	
Nominal power	14	
NP. *See* nuclear propulsion.		
NSTAR MESC thruster	85	
NTP systems	217	
NTP, development of safety	217	

This page has been reformatted by Knovel to provide easier navigation.

Index Terms	Links		
NTR. *See* nuclear thermal rockets.			
Nuclear electric propulsion (NEP)	23	203	217
development of safety	217		
Nuclear electric xenon ion system. *See* NEXIS.			
Nuclear Engine for Rocket Vehicle Applications. *See* NERVA.			
Nuclear force	2		
Nuclear isomers	8		
Nuclear potential	6		
Nuclear power in space	203		
commercial satellites	204		
failures	219		
radiation release	221		
launch site safety	213		
Mars exploration projects	203		
NEP systems	217		
NTP systems	217		
nuclear electric propulsion	203		
nuclear thermal propulsion	203		
public safety concerns	206		
accidental fuel release	206		
safety guideline recommendations	207		
space stations, hazards	221		
Nuclear powered systems			
adaptability of	226		
criticality tests	231		
launch environment tests	229		

This page has been reformatted by Knovel to provide easier navigation.

Index Terms	Links		
Nuclear powered systems (*Cont.*)			
radiation mitigation	227		
safety testing	227		
fire tests	228		
impact tests	228		
propellant explosions	228		
reentry	229		
Nuclear propulsion (NP), origins of	1		
massless	25		
pulsed	1		
strategies	19		
nuclear thermal rockets	19		
systems			
ground testing safety	265		
MITEE engine	264		
Rubbia engine	264		
Nuclear thermal propulsion (NTP)	203		
Nuclear thermal rockets (NTR)	10	19	31
chemical type vs	24		
chemical vs	33		
cold-gas thruster	32		
concepts	37		
CERMET	42		
hybrid nuclear thermal/chemical	45		
NERVA	37		
particle-bed reactor	41		
fission	31		
gas-core	20		

This page has been reformatted by Knovel to provide easier navigation.

Index Terms	Links	
Nuclear thermal rockets (NTR) (*Cont.*)		
MagOrion	45	
mini-MagOrion	45	
nuclear electric propulsion	23	
Orion	45	
Project Prometheus	49	
pulsed	21	
radiation exposure	33	34
radiation safety	47	
Plutonium-238	47	
solid-core	20	
specific impulse	33	
system configuration	34	
control rods	36	
coolant flow paths	36	
fuel-element assembly	36	
moderator	36	
radial reflector	34	36
reactor pressure vessel	36	
type comparisons	45	

O

Occupational radiation exposure	262	263
Orbit circularization accident scenario probability	237	
Orion project	45	
Oxygen	204	

This page has been reformatted by Knovel to provide easier navigation.

Index Terms	Links		
P			
Particle-bed reactor (PBR)	41		
advantages of	42		
development of	42		
PBR. *See* particle-bed reactor.			
Peak thruster performance	110	111	112
Perveance	99		
increase of	106		
Photonic propulsion. *See* massless nuclear propulsion.			
Physics, fundamentals of	2		
forces in nature	2		
potential energy	2		
Plasma production mechanism	63		
Plasma rotational frequency	159		
Plutonium-238, safety issues	47		
acute radiation effects	48		
radiation skin dosage limits	48		
Point-design reactor			
geometries	186		
masses	186		
Postulated propellant fire	233		
Sandia Fireball Code	233		
Potential energy	2		
atom bonds	5		
chemical	5		
electroweak force	4		

This page has been reformatted by Knovel to provide easier navigation.

Index Terms	Links	
Potential energy (*Cont.*)		
gravitational	4	
Power	14	
mass	16	
nominal	14	
Power density	99	
Prelaunch accident scenario probability	236	
Project Prometheus	49	
Propellants		
coaxial applied field and	162	
explosions, safety testing and	228	
fire, safety analysis	233	
influence of	134	
ion thruster high power operation and	112	113
mass	16	
self-field-MPD thrusters and	153	
xenon	65	
Propulsion	9	
Newton's Third Law	9	
power	14	
specific impulse	10	
thrust	12	
Pulsed nuclear propulsion	1	21
Pumping forces	139	

This page has been reformatted by Knovel to provide easier navigation.

Index Terms	Links	

R

Radial reflector	34	36
Radiation decay	247	
absorbed dose D (Gy)	248	
activity (Bq)	247	
collective dose (man Sv)	250	
dose commitment	250	
effective dose E (Sv)	249	
equivalent dose H (Sv)	248	
half-life	248	
Radiation effects	48	
Radiation exposure	225	256
atmospheric nuclear testing	259	261
comparison of	265	
electricity generation	260	
major accidents	260	
medical exposure	259	
natural	256	
nuclear propulsion systems	262	
nuclear thermal rocket and	33	34
occupational	262	263
Radiation hormesis considerations	254	
Radiation mitigation	227	
Radiation release	221	
failure events scenario	221	

This page has been reformatted by Knovel to provide easier navigation.

Index Terms	Links
Radiation safety	
mission time	49
Plutonium-238	47
Radiation skin dosage limits	48
Radiation-induced cancer	252
Radioactive fuel release, public safety concerns and	206
Radioactivity	245
alpha decay	246
beta decay	246
gamma rays	247
ionizing radiation	251
radiation decay	247
radiation exposure	256
Radiofrequency (RF) discharge thrusters	70
high frequency operation	72
magnetic field thruster	72
Kaufman-type direct-current discharge thrusters	73
magneto-electrostatic containment dc thrusters	75
radiofrequency ionization thruster	70
Radiofrequency ionization thruster (RIT)	70
Radiofrequency magnetic field thruster (RMT)	72
Reactivity analyses	233
Reactor accident scenario probability	237
Reactor pressure vessel	36

This page has been reformatted by Knovel to provide easier navigation.

Index Terms	Links
Reactor requirements	178
operational constraints	179
resource constraints	180
safety constraints	179
technology constraints	180
Reactor safety	
program organization	238
safety documentation	240
ultimate goals	239
Reactor testing	231
impact analyses	233
reactivity analyses	233
reentry analysis	233
risk/consequence analysis	235
safety analysis	232
explosion environments	233
intentional disassembly	233
neutronics	232
postulated propellant fire	233
shielding	232
Reactor transient behavior, modeling of	200
Reactor type comparison	180
early studies	180
modeling	183
dominant inputs and outputs	183
point-design reactor geometries and masses	186
shield materials	195

This page has been reformatted by Knovel to provide easier navigation.

Index Terms	Links
Reactor type comparison (*Cont.*)	
specific design anchor points	184
validation	190
types	180
gas-cooled reactor	180
heat-pipe-cooled	180
liquid-metal cooled	180
Reentry, Mars-based nuclear power safety issues and	225
Reentry analysis	233
Heating and Analysis Done Interactively code	233
Trajectory Simulation and Analysis Program	233
Reentry tests, safety and	229
Regenerative cooling	131
RF. *See* radiofrequency.	
Risk/consequence analysis	235
RIT. *See* radiofrequency ionization thruster.	
RIT-15	78
RIT-22	80
RIT-35 RF thruster	86
RIT-XT	80
RMT. *See* radiofrequency magnetic field thruster.	
Rocket equation	57

This page has been reformatted by Knovel to provide easier navigation.

Index Terms	Links
Rubbia engine	21
radiation exposure from	264
Russia, magnetoplasmadynamic thrusters and	167

S

Safety issues, nuclear power in space and	205
Safety testing	227
Sandia Fireball Code	233
Satellites, commercial	204
Scaling down of thrust	13
Scaling up of thrust	13
Self-field (SF)-MPD thruster	138
blowing forces	139
cold (neutral) gas injection	143
electrode design	147
electrode voltage drops/losses	147
pumping forces	139
SERT II	79
SF. *See* self-field.	
Shield modeling	195
augmentation to	199
reactor types	198
Shielding	232
SI. *See* specific impulse.	
Sievert (Sv)	249

This page has been reformatted by Knovel to provide easier navigation.

Index Terms	Links			
Simulation development, magnetoplasmadynamic thrusters and	164			
Solid core nuclear thermal rockets	20			
Space plasma	62			
Specific impulse (SI)	57	10	33	59
	65	97		
attenuation factor	12			
increase	104			
velocity increments	60			
Spiral motion	18			
Stochastic effect	251			
hereditary	255			
hormesis	252			
radiation hormesis considerations	254			
radiation-induced cancer	252			
Superconductive magnet, NASA thruster and	165			
Sv. *See* Sievert.				

T

T5 thruster	77			
T6 Kaufman-type thruster	81			
Terrestrial radiation	257			
external exposure	259			
internal exposure	259			
Theory of Special Relativity	2	3		

This page has been reformatted by Knovel to provide easier navigation.

Index Terms	Links
Thermal arcjets	127
compared to other propulsion types	136
existing technology	136
Germany	136
United States	136
mono-atomic gases	135
numerics	132
operating principles	129
bi-exit nozzle	131
discharge voltage	132
dual-cone nozzle	131
efficiency	130
regenerative cooling	131
operational lifetime	135
propellants	134
ammonia	134
hydrazine	134
hydrogen	134
system description	132
theory	132
Thermal design, ion thrusters and	115
Throttling capability, ion thrusters and	114
Thrust	12
coaxial applied field and	159
densities	99
scaling down	13
scaling up	13

This page has been reformatted by Knovel to provide easier navigation.

Index Terms	Links	
Thrusters	63	
anode phenomenology	148	
diameter	103	
duration	59	
temperatures	66	
Tokyo Metropolitan Institute of Technology 30-cm MESC thruster	87	
Trajectory Simulation and Analysis Program (TSAP)	233	
TSAP. *See* Trajectory Simulation and Analysis Program.		
U		
UK-25 Kaufman-type thruster	83	
V		
Variable-specific-impulse magnetoplasma rocket (VASIMR)	67	69
concepts	67	
VASIMR. *See* variable-specific-impulse magnetoplasma rocket.		
Velocity increments	60	
Very large diameter thrusters	90	
Void coefficient	270	

This page has been reformatted by Knovel to provide easier navigation.

Index Terms	Links
X	
X-16	165
DLR Stuttgart	165
Xenon	65
XIPS-25 MESC thruster	83

This page has been reformatted by Knovel to provide easier navigation.